COPY NO. 64

UNITED AIRCRAFT CORPORATION
RESEARCH LABORATORIES

EAST HARTFORD, CONN.

Report R-1624-5

Investigation of Control and Stability
Augmentation Requirements for Tandem
Tilting Ducted Propeller VTOL Transports

UNCLASSIFIED

Department of the Navy
Bureau of Naval Weapons
Contract No. NOw 61-0848-d

REPORTED BY James W. Clark
James W. Clark
David P. Miller
David P. Miller
Robert A. Gallant
Robert A. Gallant

APPROVED BY Frank S. Owen
Frank S. Owen
Chief, Aerophysics Section

NO. OF PAGES 207

DATE July 1963

Report R-1624-5

Investigation of Control and Stability Augmentation Requirements for Tandem Tilting Ducted Propeller VTOL Transports

TABLE OF CONTENTS

TABLE OF CONTENTS (Cont'd.)

TABLE OF CONTENTS (Cont'd.)

Report R-1624-5

Investigation of Control and Stability Augmentation Requirements for Tandem Tilting Ducted Propeller VTOL Transports

I. SUMMARY

Theoretical and analog computer investigations were conducted to determine the control and stability augmentation requirements for tandem tilting ducted propeller VTOL transports. The type of aircraft considered had performance capabilities similar to those required for the Tri-Service VTOL Transport.

Initial studies were directed toward establishing representative aerodynamic characteristics for the aircraft. Calculated handling qualities were then compared with existing handling qualities criteria to evaluate the performance of constant-gain, programmed-gain, and adaptive control and stability augmentation systems. Estimates were made of the relative cost and weight of each of these systems. On the basis of these studies a relatively simple programmed-gain system was selected as most suitable for this application. Detailed calculations of the stability and control characteristics of the aircraft with the selected system were made, and a six-degree-of-freedom, fixed-base, piloted analog computer simulation was conducted using the Sikorsky V/STOL Aircraft Simulator with a contact analog display. Typical operational flight conditions were simulated in order to investigate the handling qualities of the aircraft with and without the programmed-gain system.

The results of this investigation indicate that the control and stability augmentation requirements of tandem tilting ducted propeller aircraft are influenced primarily by the following stability and control problems: (1) unstable or lightly damped Dutch roll characteristics which vary widely with changing flight conditions and which are basically attributable to the large side-force-curve slopes of the ducted propellers; (2) large changes in pitching moment required to trim due to the effect of changes in velocity on the pitching moments on the ducted propellers; and (3) difficulty in obtaining an acceptable level of maximum yaw control power at hover and low speeds primarily due to the marginal effectiveness of the control vanes in the exits of the ducted propellers. For aircraft having widely varying unstable Dutch roll characteristics, a relatively simple stability augmentation system in which the roll rate damping gain is programmed as a function of duct incidence angle is the least complex, lightest weight, and lowest cost system which will provide satisfactory handling qualities. A constant-gain system should be adequate if the tendency for Dutch roll instability is alleviated in the design

of the aircraft. Due to the Dutch roll problem a triplicated stability augmentation system may be required, rather than a duplicated system with pilot reset, in order to assure that a safe landing could be made following a partial stability augmentation failure during take-off or landing.

The results of the flight simulator studies indicated that equivalent first-order time lags up to 0.20 or 0.25 sec in the collective pitch control system, up to 0.20 or 0.30 sec in the longitudinal control system, and up to 0.10 sec in the lateral-directional control system will result in satisfactory handling qualities. Increases in the speed stability derivative $M_u g/I_y$ were found to require increases in pitch rate damping M_q/I_y and longitudinal control sensitivity M_{δ_s}/I_y. Cross-wind landing approaches in the presence of gusts were found to be difficult because of the Dutch roll tendency and the low maximum yaw control power at low speeds. The presence of lateral-directional control coupling due to incorrect phasing or mixing of differential collective pitch and vane deflection was found to be quite noticeable but not objectionable for transition flight conditions; further research is recommended to determine criteria for the maximum amount of control coupling which is acceptable.

This program was performed under Contract NOw 61-0848-d with the Department of the Navy, Bureau of Naval Weapons. The program was administered by Mr. William Koven, Chief of Aircraft Stability and Control Unit, Airframe Design Division.

II. INTRODUCTION

The wide ranges of speed and altitude at which V/STOL aircraft operate are accompanied by large and rapid changes in their configuration and aerodynamic characteristics. As a consequence, critical stability and control problems are experienced, particularly at flight conditions near the aerodynamic limitations of the aircraft (e.g., in high-power take-offs and decelerating descents). The results of flight tests of V/STOL research aircraft have indicated that control and stability augmentation systems having constant gains may not provide satisfactory handling qualities at all flight conditions. It is probable, therefore, that more complex systems in which provisions are made to vary the gains either manually or automatically will be required in order to realize the full operational value of advanced V/STOL aircraft.

The investigation reported herein was conducted to determine the control and stability augmentation requirements for tandem tilting ducted propeller VTOL transports and to determine the least complex, lowest cost, and lightest weight system which will provide satisfactory handling qualities at all flight conditions.

III. RESULTS AND DISCUSSION

A. Description of Aircraft and Aerodynamics

A sketch of a tandem tilting ducted propeller aircraft in the hovering and forward flight configurations is shown in Fig. 1. At hover the four ducted propellers are oriented such that their thrust axes are vertical. Pitching and rolling control moments at hover are provided by differential collective pitch of the four peopellers; yawing control moments are provided by vanes located in the two aft ducts. To accelerate the aircraft to forward flight, the ducts are tilted towards the horizontal (Fig. 1). In forward flight pitching moments are provided by combinations of differential collective pitch and vane deflections; rolling and yawing moments are obtained by phasing or mixing differential collective pitch and vane deflections to minimize lateral-directional control coupling. Static stability in forward flight is derived from the horizontal tail panels located outboard of the rear ducts (fixed with respect to the fuselage) and from the vertical stabilizer.

The general arrangement of the hypothetical transport aircraft which was used as a basis for this study is shown in Fig. 2. This configuration was scaled up from a wind tunnel model for which unpublished aerodynamic data were obtained from the NASA Langley Research Center (most of the data used have recently been published in Ref. 1). The data were analyzed and modified to include simulation of variable pitch propellers and several sizes of horizontal tails with and without elevators, and were scaled up to represent a 35,000-lb aircraft (the model was assumed to be 1/7 of full scale).

A detailed description of the aerodynamic characteristics of the aircraft and the techniques used in programming the aerodynamics for the analog computer is presented in Appendix A. The stability derivatives for steady level flight which were later calculated using the analog computer are presented in Tables I and II for reference.

The significant aerodynamic characteristics of tandem tilting ducted propeller configurations which were apparent in the data were high lift-curve and side-force-curve slopes of the ducted propellers, large changes in pitching moment on the aircraft with changes in forward speed, and widely varying aerodynamic interference effects between the fore and aft ducted propellers at angles of attack and yaw. The side-force-curve slope Y_v of the complete aircraft as determined from the NASA data was of the same order of magnitude as the lift-curve slope Z_w due to the large contribution of the symmetrical ducted propellers. The subsequent stability analysis indicated that the high side-force-curve slope did not in itself adversely affect stability but for this configuration caused the roll-due-to-sideslip derivative L_v to be excessively large; because of the large L_v, the Dutch roll mode tended to be very lightly damped or unstable. The high side-force-curve slopes of

the ducted propellers also resulted in the directional static stability N_v being very sensitive to aerodynamic interference or blocking by the fuselage and vertical tail. As shown in Table II, the configuration described in the NASA data was directionally unstable above speeds of about 160 ft/sec for the nominal location of the center of gravity (Fig. 2) at zero angle of attack. Changes in aerodynamic interference caused the directional stability to vary considerably with angle of attack and duct incidence angle (N_v was found to be greatest at negative angles of attack, i.e., in take-off transitions).

The large changes in pitching moment on the aircraft with changes in forward speed are attributable to variation of the moments on the ducted propellers and also to changes in the aerodynamic interference between fore and aft ducted propellers. Values of the speed stability derivative $M_u g/I_y$ which were later calculated on the analog computer ranged from +0.08 at hover to a maximum of +0.25 at some transition flight conditions.

In analyzing the NASA data preparatory to programming the aerodynamics for the analog computer, reference was made to the large amount of ducted propeller data presented in Ref. 2, and also to Ref. 3 which presents data for a three-duct flying platform model which was constructed using three of the four ducted propeller units later used on the tandem tilting ducted propeller aircraft model. It was found from these analyses that the lift and drag characteristics of each of the four ducted propellers could be simulated individually by means of performance maps which were constructed using polynomials and trigonometric functions. Empirical multiplying factors determined from wind tunnel data for the tandem duct aircraft were used to describe the combined effects of propeller hub moments and aerodynamic interference between the ducted propellers. Since each of the ducts were simulated individually, the forces and moments on the aircraft due to pitching, yawing, and rolling rotation rates (i.e., the damping forces and moments) could be calculated directly by the computer. This simulation technique is described in detail in Appendix A.

B. Calculation of Representative Flight Profiles

Representative flight profiles for take-off and landing transitions and for constant-altitude transitions were calculated using an unpiloted three-degree-of-freedom analog computer simulation. The use of an unpiloted simulation permitted successive calculations by the analog computer to obtain flight variables and aircraft dynamics at specific points along each flight path. To achieve repeatability of each flight profile, constant duct tilt rates were used. High-gain control circuits were utilized to restrain certain of the flight variables while permitting the others to vary freely according to the unbalanced forces on the aircraft. Block diagrams of the high-gain control circuits are shown in Figs. 3 and 4. The

values of the control loop gains K_1 through K_4 were selected as high as possible (limited only by values that drove the circuit unstable) in order to obtain repeatability. The high-gain control circuits were used only in calculating the representative flight profiles and hence had no influence in the subsequent evaluation of the dynamics of the aircraft. For example, constant-altitude accelerations from hover were calculated using constant duct-tilt rates and the high-gain control circuits shown in Fig. 3; differential collective pitch was used to maintain horizontal pitch attitude of the fuselage while collective pitch was used to maintain constant altitude. Variations in the flight profiles were obtained by varying duct tilt rate, instant of initiating duct rotation, terminal duct angle, and for the decelerating descent profile, the initial altitude and variation of programmed rate-of-descent with altitude (see altitude program block in Fig. 4). Aircraft accelerations, flight path, and the control inputs which would have been required had a pilot been flying the aircraft were factors considered in selecting the representative transition profiles. Pertinent data for the basic profiles are tabulated in Table III.

1. Steady Level Flight

The variation of duct incidence angle, collective pitch angle, and pitching moment required to trim with velocity for steady level flight are shown in Fig. 5. The small change in duct incidence angle with velocity at high speeds illustrates the necessity for providing low duct-tilt rates at high speeds. Since constant-speed propellers were assumed, the variation of collective pitch angle with velocity provides an indication of the power required for steady level flight. It should be noted that since the hypothetical 35,000-lb aircraft was equipped with a propeller having three blades (the same as the wind tunnel model), the variation of collective pitch angle with velocity shown in Fig. 5 is probably somewhat greater than would be experienced in practical designs of full-scale airplanes which would employ a larger number of blades of higher activity factor. The variation of pitching moment required to trim with velocity shows a reversal in slope during transition which results from the combined effects of thrust rotation, thrust modulation, and changes on the pitching moments on the ducted propellers.

2. Accelerating Ascent Flight Profiles

Two basic accelerating ascent flight profiles having static thrust-to-weight ratios of 1.05 and 1.35 were studied. Figure 6 shows the flight path of each profile with velocity and time from initiation of transition marked at several points. The variations of duct incidence angle, angle of attack of the fuselage, and pitching moment required to trim with flight velocity are shown in Fig. 7. The effects of increasing the static thrust-to-weight ratio and decreasing the duct tilt rate on

the take-off flight path shown in Fig. 8. The maximum average duct tilt rate was limited at high thrust-to-weight ratios by large longitudinal accelerations (nearly 1 g at 8 deg/sec for T/W = 1.35) resulting from power that otherwise would have been used for increasing the potential energy of the aircraft at low tilt rates. The maximum duct tilt rate was limited at low thrust-to-weight ratios by the failure of the aircraft to gain altitude (on the T/W = 1.05 profile with a duct tilt rate of 8 deg/sec the aircraft actually settled below the initial hovering level). Settling of the aircraft occurred when the ducts had been rotated so far that the lift on the shrouds plus the lift component of thrust was less than the weight of the aircraft for a moderate length of time.

Since pilots usually prefer to have a high duct tilt rate available and then actually use a lower effective tilt rate by tilting the ducts intermittently rather than continually, several of the profiles were calculated using twice the nominal duct tilt rate. An average tilt rate equal to the nominal value was then maintained by successive rotation and holding of the ducts for two-second intervals. Flight profiles calculated using this method of rotating the ducts, which would be more like actual pilot technique, were in close agreement with profiles calculated using a constant duct tilt rate.

3. Decelerating Descent Flight Profile

The flight path of a representative decelerating descent profile, shown in Fig. 9, was initiated from steady level flight at an altitude of 800 ft and a velocity of 180 ft/sec, and utilized a constant duct tilt rate of 2 deg/sec. In addition to maintaining level attitude of the fuselage, the unpiloted aircraft was forced to fly a programmed variation of rate of descent with time from initiation of transition. Level attitude was maintained by means of differential collective pitch (fore and aft), while the programmed rate of descent was controlled by means of collective pitch of all four propellers. The block diagram of the high-gain control circuit used to maintain the programmed rate of descent is shown in Fig. 4. Variations of duct incidence angle, pitching moment required to trim, and collective pitch angle with velocity for this flight profile are shown in Fig. 10. In order to obtain an immediate sink rate of the aircraft from steady level flight, the high lift-curve slope of the ducts necessitated delaying the rotation of the ducts towards the hovering position until after the speed of the aircraft was reduced. In addition, by decreasing the speed of the aircraft before the ducts were rotated, the large positive pitching moments produced by the ducts at high angles of attack and high speeds were avoided.

The low value of deceleration and the associated large horizontal distance traveled in conversion from high-speed flight to hovering (Fig. 9) are characteristic of the tilting ducted propeller aircraft. VTOL aircraft capable of rotating

their thrust vector rearward, such as helicopters, readily obtain deceleration levels of 0.25 g or greater. The thrust vector of the tilting ducted propeller aircraft could be directed rearward by rapidly rotating the ducts beyond the position for hovering (i.e., beyond a duct incidence angle of 90 deg); however, the large forces and moments developed on the ducts in the transition process would tend to make the aircraft climb.

4. Constant Altitude Flight Profiles

Constant altitude transition flight profiles were calculated using the same technique with the exception that the collective pitch angle controller maintained constant altitude rather than a programmed rate of descent. Variation of duct incidence angle, pitching moment required to trim, and horizontal distance from the point at which the transition was initiated are shown in Figs. 11 and 12 for accelerating and decelerating transitions, respectively. The horizontal distance required to bring the aircraft to a hovering condition for the constant altitude deceleration profile was about 60% less than for the decelerating descent flight profile.

C. Calculation of Stability Derivatives

The total force and moment stability derivatives were calculated directly using the analog computer at frequent intervals along the representative flight profiles (usually at velocities 20 ft/sec apart). This was accomplished by setting as initial conditions on the computer the instantaneous transition flight variables previously recorded and, with the computer in the "initial condition" mode, varying the rotational and linear velocity components in the body axis system and the control deflections by small amounts. The changes in the forces X and Z and the pitching moment M due to these variations in q, u, w, δ_β, and δ_v were recorded on an x-y plotter and their slopes measured to obtain the longitudinal stability and control derivatives. In a similar manner, the stability derivatives for the lateral and directional degrees of freedom were obtained by measuring the variation of the side force Y and moments L and N due to v, p, r, $\Delta\delta_\beta$, and $\Delta\delta_v$. Results showing the variation of longitudinal and lateral-directional stability derivatives with velocity during steady level flight for the nominal location of the center of gravity are shown in Tables I and II. The values of the derivatives L_v/I_x and N_v/I_z as altered by moving the center of gravity of the aircraft forward 0.55 ft and up 0.40 ft are also shown in Table II.

D. Preliminary Analyses of Handling Qualities and Stability Augmentation Requirements

Using the calculated flight profiles and the corresponding stability derivatives preliminary analyses were made to determine the factors which influence selection of the control and stability augmentation system and to compare the theoretical performance of constant-gain and variable-gain systems. The objectives of these studies was to select the least complex type of system likely to provide satisfactory handling qualities for more thorough investigation in the flight simulator program. The results are presented in this section; detailed descriptions of the analytical techniques used, including derivations of the characteristic equations and transfer functions, are presented in Appendixes B and C.

1. Longitudinal Mode

a. Dynamic Characteristics Without Stability Augmentation

Figure 13 summarizes the stick-fixed dynamic characteristics of the aircraft without stability augmentation in steady level flight. The variation of the roots of the longitudinal characteristic equation with flight velocity are shown for velocities from -50.6 ft/sec (hovering in a 30-knot tail wind) to 423 ft/sec (250-knot cruise) at altitudes of sea level and 20,000 ft. Also shown are the acceptance boundary of the current military Instrument Flight Rules specifications for helicopters (Ref. 4), the Bureau of Naval Weapons requirements for aircraft in the cruise configuration, and a suggested boundary for the short period mode of VTOL aircraft at high speeds (Ref. 5). The two sets of roots are referred to herein as the short-period mode and the phugoid mode according to their root locations at high speeds, even though at low speeds the period of the phugoid mode is shorter than that of the short-period mode.

Considering first the phugoid mode, the aircraft was unstable at speeds from -50.6 ft/sec to approximately +35 ft/sec. At hover the time to double amplitude was 7.54 sec and the frequency of oscillation was 0.37 rad/sec (the period was 17.0 sec). Figure 14 presents an enlargement of the portion of the s-plane plot of Fig. 13 near the origin, and includes the IFR acceptance boundary of MIL-H-8501A. As shown in Fig. 14, the unstable phugoid characteristics of the tandem tilting ducted propeller aircraft at hover are similar to those of many operational helicopters and do not in themselves indicate unacceptable handling qualities for contact flight conditions. However, as is the case with many operational helicopters, the tandem tilting ducted propeller aircraft would not meet the requirements of MIL-H-8501A for IFR flight without stability augmentation. Note also in Fig. 14 that the addition of attitude stabilization alone would not satisfy the military specifications; at least a small amount of pitch rate stabilization would be required. Figure 13 indicates that with increasing speed the phugoid became more stable and

the period increased (the phugoid roots approached the origin, as is the usual case with fixed-wing aircraft).

The short-period mode in reverse flight and in hover was nonoscillatory but became oscillatory and increased in frequency as speed increased (Fig. 13). At high speeds at sea level the short-period roots approached but did not fall within either the BuWeps Configuration P,CO boundary or the boundary proposed in Ref. 5, primarily because both the frequency of oscillation ω and the damping ratio ζ were low due to the high moment of inertia in pitch I_y. At an altitude of 20,000 ft, the reduced dynamic pressure caused the roots to be even further from the acceptable boundary.

Figure 15 presents a summary of the longitudinal dynamic characteristics of the aircraft on the three most critical transition flight profiles. The longitudinal root locations are shown for velocity increments of 20 ft/sec for high-power take-off (initial thrust-to-weight ratio of 1.35), constant altitude acceleration, and decelerating descent. For all three flight profiles the short-period mode was stable. The phugoid mode was stable, although lightly damped, for the constant altitude acceleration and decelerating descent flight profiles. The thrust-to-weight ratio 1.35 take-off flight profile resulted in the most unstable longitudinal dynamics of all flight conditions. At speeds between 60 and 90 ft/sec the time to double amplitude was approximately 3.5 sec and the period ranged between 11.5 and 15.0 sec.

b. Effects of Varying Stability Derivatives and Control Lags

An IBM 7090 digital computer program which was prepared for calculating the roots of the longitudinal characteristic equation was also used to investigate the effects of the individual stability derivatives and stability augmentation lags on the stick-fixed dynamics. Figure 16 shows the effects of halving and doubling the stability derivatives X_u, M_q, and M_u on the unstable phugoid root of the basic aircraft at hover. Note the strong destabilizing effect of increasing the speed stability derivative M_u. Also note that changes in the derivatives X_u (a measure of the change in drag of the aircraft with change in velocity) and M_q (the pitch rate damping) have nearly identical effects on the location of the phugoid root. The equivalence of X_u and M_q at hover can be readily seen from an inspection of the characteristic equation for hover:

$$\lambda^4 + \left[-\frac{X_u}{m} - \frac{M_q}{I_y}\right]\lambda^3 + \left[\frac{X_u}{m}\,\frac{M_q}{I_y}\right]\lambda^2 + \left[\frac{M_u g}{I_y}\right]\lambda = 0 \qquad (1)$$

Since the parameters X_u/m and M_q/I_y are approximately equal for tandem tilting ducted propeller aircraft, examination of Eq. (1) reveals that similar changes in either parameter will change the coefficients of the λ^3 and λ^2 terms by the same amount.

For the tandem tilting ducted propeller aircraft the damping in pitch derivative M_q/I_y was lower and the speed stability derivative $M_u g/I_y$ was higher than the corresponding derivatives of most helicopters. However, the destabilizing effects attributable to the differences in these derivatives were largely alleviated by the stabilizing effect of the much larger drag of the tandem tilting ducted propeller aircraft as represented by the derivative X_u/m. Thus, the high drag which is characteristic of this and other VTOL aircraft such as the tilt-wing or deflected slip-stream configurations at low forward speeds is actually helpful in stabilizing the phugoid mode, although it may be a hindrance as far as the ability to hover accurately over a spot in gusty conditions is concerned.

Figure 17 illustrates the effects of changes in the derivatives M_q, M_θ, M_u, and M_w on the phugoid and short-period roots at approximately the most critical flight condition (a velocity of 80 ft/sec on the $T/W = 1.35$ take-off flight profile). The derivatives M_u and M_w can be controlled to some extent in the design of the aircraft; the derivatives M_q and M_θ cannot be altered appreciably except by the addition of stability augmentation. Note particularly the strong destabilizing effect of the speed stability derivative $M_u g/I_y$ on the phugoid mode; at this flight condition $M_u g/I_y$ was several times its value at hover and was the primary contributor to instability. The important effect of the static stability derivative $M_w g/I_y$ is also shown in Fig. 17. Since increases in $M_w g/I_y$ are derived from the horizontal tail, the favorable effect of an unstalled horizontal tail is evident. At this particular flight condition the aircraft was statically stable in pitch (the center of pressure was located 1.24 ft aft of the center of gravity, resulting in a value of $M_w g/I_y$ of -0.087). The root locations are shown in Fig. 17 for increments in $M_w g/I_y$ of -0.14. An increase in static stability which resulted in an increment in $M_w g/I_y$ of -0.14 at this flight condition was equivalent to moving the center of gravity forward by 2.0 ft or alternately increasing the horizontal tail area by 135% of its basic value (see Fig. 2 for dimensions of the tail). Also shown are the root locations for the aircraft without a horizontal tail. Thus, the stabilizing effect of an unstalled horizontal tail of varying area may be judged from Fig. 17.

The poor stability characteristics of the aircraft on the high-power take-off flight profile were traced to the adverse effect of high negative angles of attack on the stability derivatives. A series of analog computer experiments were performed which indicated that in general: (1) minimum damping in pitch M_q/I_y occurred when the free-stream velocity vector was directed approximately straight into the ducts (i.e., along the propeller shaft axes); (2) minimum static stability

$M_w g/I_y$ occurred at angles of attack greater than ± 30 deg (the approximate stall limits of the horizontal tail); and (3) the speed stability derivative $M_u g/I_y$ decreased only slightly with increasing negative angle of attack. Therefore, the destabilizing influence on damping in pitch and static stability caused by the high negative angles of attack encountered during the take-off greatly overpowered the small stabilizing effect caused by the slight decrease in speed stability. The angles of attack encountered during the decelerating descent were not as large, with the result that the aircraft remained stable during that maneuver.

Due to the destabilizing effect of stall on the horizontal tail panels at the high local angles of attack which are encountered during transition, the question of whether the tail panels should rotate with the ducts or whether they should be fixed with respect to the fuselage must be examined. On the aircraft considered in the present study, the panels were fixed with respect to the fuselage. Figure 18 shows the variation with velocity of the average angle of attack of the horizontal tail for this configuration during the three transition flight profiles which are the most critical from the stability standpoint (the angles of attack shown do not include corrections for downwash). The lightly shaded areas indicate the range of speeds over which the aircraft is unstable for each flight profile with the horizontal tail fixed with respect to the fuselage. Also shown are the approximate stall boundaries for the particular airfoil (NACA 0015) used as the horizontal tail on the NASA wind tunnel model. Note that the tail is unstalled through these maneuvers except at speeds below 60 ft/sec on the high thrust-to-weight ratio take-off. Since the most unstable of all longitudinal stability conditions occur on this flight profile at speeds between 40 and 80 ft/sec, it appears that it would be advisable to eliminate stall in this region, thereby increasing the static stability of the aircraft. As shown in Fig. 18, stall could be eliminated entirely on the high thrust-to-weight ratio take-off by attaching the tail panels to the ducts so that they rotate with the ducts. However, this would result in unacceptable stall on the tail panels at all other transition conditions. Thus it may be concluded that taking only aerodynamic considerations into account, it is advisable to have the horizontal tail panels remain fixed with respect to the fuselage as the ducts rotate and to supply the additional stability which is required on the high thrust-to-weight ratio flight profile by means of pitch rate stabilization.

The effects on the stick-fixed dynamics of first-order lags in the longitudinal control and stability augmentation system were investigated using the control system model shown in Fig. 19. Calculations of the roots were made for values of time constant $\tau_p = 0$, 0.03 and 0.20 sec for several levels of pitch rate stabilization and attitude stabilization. Typical results for steady level flight at 40 knots are shown in Fig. 20. In general, the lags were found to have a negligible effect on the phugoid mode. The lags had a stabilizing effect on the short-period mode when only pitch rate stabilization was used. With increasing level of attitude stabilization M_θ the lags tended to drive the short-period mode unstable. Figure 20 indicates

that the latter instability could be counteracted if this problem should arise by increasing the level of artificial pitch rate stabilization M_q.

In summary, these analyses indicated that the longitudinal stick-fixed dynamics of tandem tilting ducted propeller aircraft are most sensitive to changes in the speed stability derivative M_u, and to a lesser extent the static stability derivative M_w. Since the natural aerodynamic damping in pitch of the aircraft is small, large changes in M_q are required to appreciably affect the dynamics of the aircraft (these large changes are readily obtainable through stability augmentation, however). The derivative X_u is considerably larger than for helicopters and has a moderately stabilizing effect on the dynamics. In addition, the effects of lags up to 0.20 sec in the longitudinal control and stability augmentation system should not adversely affect the stick-fixed dynamics unless large amounts of attitude stabilization are used.

c. Comparison of Theoretical Performance of Constant-Gain and Variable-Gain Systems

Calculations were made to determine stick-fixed dynamics, pitch rate damping, and longitudinal control sensitivity with each of several constant and programmed-gain control and stability augmentation systems. The theoretical performance of these systems were then compared with existing handling qualities criteria in an effort to select the most promising system for more thorough study in the flight simulator program. Figure 19 shows the control and stability augmentation system model which was used as a basis for these calculations.

Considering first the stick-fixed dynamics of the aircraft, it was found that a constant-gain pitch rate stability augmentation system (i.e., K_p and K_{δ_β} constant, (Fig. 19) would result in stick-fixed stability at all flight conditions provided the initial level of pitch rate damping at hover was greater than about $M_q/I_y = -1.0$. Thus, the minimum specifications of MIL-H-8501A for IFR flight shown in Fig. 14 could be satisfied with a simple constant-gain system. Since definitive optimum criteria for the stick-fixed dynamics of VTOL aircraft in the transition region have not been determined as of this time, further theoretical calculations to determine an "optimum" gain program from the standpoint of stick-fixed dynamics are not possible.

There have been a number of studies reported in the literature which have defined handling qualities criteria for hover and low speeds in terms of pitch rate damping vs longitudinal control stick sensitivity (see, for example, Refs. 6 through 10). A comparison of the more pertinent of these criteria is shown in Fig. 21 along with points indicating pitch rate damping and control sensitivity of seven operational helicopters. As indicated in Fig. 21 the criteria are not in agreement. This lack of agreement is believed to be caused primarily by wide differences in the stick-fixed dynamics and the speed stability characteristics

of the various aircraft which were used in establishing the criteria. In the study of Ref. 6, which was conducted using a variable-stability HUP-1 helicopter, it was determined that the stability derivative $M_u g/I_y$ had a strong influence on the amount of control sensitivity and damping desired by the pilot. It was concluded that the pilot ratings were dependent more on the longitudinal control stick displacements required to trim gusts and changes in forward speed than on the longitudinal dynamics. A similar result was obtained in the flight simulator program of the present study for the range of dynamics investigated in Ref. 6, although for times to double amplitude less than about 4.0 sec the unstable dynamics were judged to be increasingly important (the minimum time to double amplitude was 3.0 sec in the study of Ref. 6 and about 1.4 sec in the present study). Thus, it is apparent that handling qualities criteria which do not take into account the stick-fixed dynamics and the speed-stability characteristics will not be generally applicable to all types of VTOL aircraft.

It will be noted in Fig. 21 that the various criteria exhibit a similarity in that the Cooper Pilot Opinion Rating 3.5 boundaries tend to be concave upward around "optimum" lines which are nearly vertical. In order to provide a basis for comparing the theoretical performance of the various control systems it was assumed that the "optimum" lines would be indicative of the desired handling qualities of an aircraft throughout most of the transition speed range. Calculations were made to determine the manner in which M_q and M_{δ_s} varied relative to an assumed "optimum" line for each transition flight profile. Initial calculations were performed for minimum levels of pitch rate damping at hover of $M_q/I_y = -0.430$ per sec (the minimum requirement for IFR flight in MIL-H-8501A; see Fig. 21) and $M_q/I_y = -5.53$ per sec. These calculations were later repeated for the level of pitch rate damping found to be desirable in the flight simulator study ($M_q/I_y = -2.20$ per sec). Principal results are shown in Figs. 22 through 24.

Figure 22 shows the manner in which damping and control power varied for the high-power take-off, constant-altitude acceleration, and decelerating descent flight profiles for the aircraft without stability augmentation (i.e., $K_p = 0$ in Fig. 19). For this set of calculations the gain K_{δ_β} (Fig. 19) followed its final program, which is shown in Fig. 25, so that it was constant at -1.33 deg/in. at all but the highest transition speeds. Figure 23 shows the manner in which damping and control power varied for a constant pitch rate gain system ($K_p = 7.50$ in.-sec/rad) which resulted in a value of artificial pitch rate stabilization of approximately $M_q/I_y = -2.0$ per sec at hover with the same K_{δ_β} program as was used in Fig. 22. Note in Fig. 23 that with increasing speed the damping and control power decrease in a direction which is in general parallel to the "optimum" line. Thus, if the "optimum" line was truly indicative of the desirable performance of the aircraft, the system illustrated in Fig. 23 would be expected to give reasonably satisfactory performance. Figure 24 shows the performance of a system in which a more involved gain program for K_{δ_β} was used; in this system, K_{δ_β} was programmed as a function of the sine of duct incidence angle i_D and the reciprocal of square of propeller

rotational speed $1/n^2$:

$$K_{\delta_\beta} = \frac{1}{n^2}\left[A + B \sin i_D\right] \qquad (2)$$

Note in Fig. 24 that all three curves tend to stay closer to the "optimum" line (particularly the curve for the decelerating descent flight profile which was calculated for 84% of the propeller rotational speed used for the other two profiles). However, the advantages of this more complex system over the one for which performance is shown in Fig. 23 are not very prominent. Use of the more complex system cannot be justified without first experimentally investigating the adequacy of the simpler system using the flight simulator. The stick-fixed dynamics of the aircraft were stable for both of these gain programs, and there was little difference in the root locations.

As part of this analysis, duct incidence angle, velocity, and dynamic pressure were also investigated as parameters against which gains could be programmed. Duct incidence was found to be appreciably superior because the pitching moment effectiveness of differential collective pitch of the ducted propellers is affected little by changes in the free-stream conditions but is strongly dependent upon duct incidence angle. Both longitudinal control moments and artificial pitch rate stabilization are derived from differential collective pitch. Since the final level of artificial pitch rate stabilization selected was an order of magnitude greater than the natural aerodynamic pitch damping of the aircraft, both control sensitivity and total pitch rate damping (small natural damping plus large artificial damping) varied in a manner which was very closely related to duct incidence angle (i.e., practically independent of free-stream conditions). In view of this close relation, one would expect that if a variable-gain system is required at all, then a programmed-gain system should provide handling qualities almost as good as an adaptive control system.

2. Lateral and Directional Modes

a. Dynamic Characteristics Without Stability Augmentation

Figure 26 presents a summary of the stick-fixed lateral-directional dynamic characteristics of the aircraft without stability augmentation in steady level flight. The variation of the roots of the lateral-directional characteristic equation with velocity are shown for flight conditions from hover to 250 knots at sea level, and at the high altitude cruise conditions.

The most predominant feature of the lateral-directional dynamics was the unstable Dutch roll mode. This type of instability is likely to be a characteristic problem

of tandem tilting ducted propeller aircraft. The instability arises primarily from the large dihedral effect associated with the large side-force-curve slopes of the ducted propellers and from the marginal static directional stability. The NASA wind tunnel model which was used as a basis for this study was slightly directionally unstable towards the end of transition and at high speeds, even with the largest vertical stabilizer for which data were available (Fig. 2). The spiral stability mode was stable at all flight conditions, with the stability increasing as velocity increased (Fig. 26). The roll convergence mode was also stable and is not of particular concern in the design of the aircraft as long as sufficient roll control power is available to provide adequate roll control response characteristics.

The lateral-directional dynamics for two take-off flight profiles (thrust-to-weight ratios of 1.05 and 1.35) are shown in Fig. 27. As would be expected from the results for steady level flight, the Dutch roll instability was also predominant during transitions. The greatest instability occurred at low speeds on the high-power ($T/W = 1.35$) take-off flight profile at approximately the flight conditions at which the longitudinal stability problems were also most serious.

b. Effects of Varying Stability Derivatives and Control Lags

In view of the apparent importance of the Dutch roll problem for tandem tilting ducted propeller aircraft, the effects on the stick-fixed dynamics of changes in the individual aerodynamic stability derivatives were analyzed using the root locus technique. The principal results are presented in this section of the report; a detailed discussion of the method of analysis is presented in Appendix C.

A typical root diagram showing the effects of changes in the basic stability derivatives of the aircraft without stability augmentation is shown in Fig. 28 (the particular flight condition shown is steady level flight at 40 knots). Table IV presents a general summary of the effects of these changes throughout the transition flight range. In this Table, arrows indicate the direction in which each root moves as a given stability derivative is increased in value. Inspection of Table IV indicates that the most significant derivatives are the effective dihedral L_v/I_x , the directional static stability N_v/I_z , the roll rate damping L_p/I_x , and to a lesser extent the yaw rate damping N_r/I_z . The large dihedral effect L_v/I_x is shown to be the most important contributor to the Dutch roll instability and can be counteracted most effectively by means of artificial roll rate stabilization. Reduction of the dihedral effect and improvement of the directional static stability should of course be carefully considered in the design of the aircraft. It is interesting to note that increasing the side-force-curve slope Y_v/m actually had a small stabilizing effect on the Dutch roll mode. Therefore, it may be concluded that the high side-force-curve slope of the ducted propellers did not contribute directly to the Dutch roll instability but contributed indirectly by increasing the effective dihedral.

The effects of changes in the moments of inertia in roll I_X and yaw I_Z on the lateral-directional dynamics are shown in Fig. 29. Increasing I_X decreased the frequency of the Dutch roll oscillation and slightly increased the time to double amplitude. Increasing I_Z had little effect on the frequency and decreased the time to double amplitude. Thus it appears that the Dutch roll instability would tend to be alleviated by an increase in moment of inertia in roll and a decrease in moment of inertia in yaw. Unfortunately these two conditions are probably incompatible in the design of the tandem tilting ducted propeller aircraft. As would be expected, the influence of I_X on the roll convergence root was large while its influence on the spiral stability root was small. The influence of I_Z on the roll convergence and spiral stability roots was large. Note that as I_Z was decreased to half its nominal value so that I_Z approached I_X, these two roots formed a coupled oscillatory pair. This coupling, which would result in unsatisfactory responses to control inputs, is only of academic interest since it is improbable that such a large reduction in I_Z would result from design changes in the case of the tandem tilting ducted propeller aircraft. The effect of changes in the product of inertia I_{XZ} were found to be negligible and were not included in Fig. 29.

Examination of the root diagrams which were obtained indicated that the dihedral effect L_V/I_X was the principal cause of the greater Dutch roll instability on the high-power take-off flight profile (Fig. 27). In the flight speed range from 20 to 80 ft/sec the derivative L_V/I_X was consistently higher on this profile than on all other flight profiles. The NASA wind tunnel data for roll and yaw, which admittedly were limited, indicated that the side-force-curve slopes of the rear ducts (which were mounted high on the fuselage) increased with increasing angle of attack at constant duct incidence angle. It was also noticed from the aerodynamic data that the decrease in directional stability during all transitions to forward flight seemed to be attributable to the forward travel of the center of pressure of the ducted propellers as the ducts rotated down. This forward travel of the center of pressure occurred more rapidly than the vertical stabilizer effectiveness increased due to increasing dynamic pressure. It was further evident that directional static stability decreased less during the high-power take-off, probably because of less aerodynamic interference between the ducts at high negative angles of attack. Therefore it might tentatively be concluded, pending the acquisition of more complete lateral-directional wind tunnel data, that the high negative angles of attack experienced in high-power take-offs result in substantial changes in the aerodynamic interference between the front and rear ducts, with the net result that the destabilizing effect of angle of attack on dihedral effect is more powerful than the stabilizing effect of angle of attack on directional static stability. Due to the high side-force-curve slope of the ducted propellers, the derivative L_V/I_X was found to be very sensitive to the vertical location of the center of gravity of the aircraft. This implies that vertical travel of the center of gravity should also be considered carefully in the design of the aircraft.

The effects of first-order control lags on the lateral-directional stick-fixed dynamics were also calculated using a modified lateral-directional characteristic equation (see Section VIII. C. 4. of Appendix C). The control and stability augmentation system model shown in Fig. 30 was used; combined lags of τ_Y and τ_R from 0.1 to 0.5 sec were used with the final levels of stability augmentation. As shown in Fig. 31, the addition of lags resulted in two additional roots which formed an oscillatory pair. The principal result of importance is that the lags actually had a very small stabilizing effect on the critical Dutch roll mode. Therefore, as long as the lag time constants remain lower than the value above which the new oscillatory pair is driven unstable, lags should not have a serious effect on the stick-fixed dynamics. This result was later confirmed in the flight simulator program where it was apparent that lags influenced the response to control inputs considerably more than they influenced the stick-fixed dynamics of the aircraft.

c. Requirements for Gain Programs

In view of the general lack of lateral-directional handling qualities criteria for VTOL aircraft, the analyses of the theoretical performance of possible lateral-directional control systems were concerned primarily with the stick-fixed dynamics, and to a limited extent with control power and damping at hover.

As discussed previously, studies of the longitudinal dynamics indicated that the level of artificial pitch rate damping required for stick-fixed longitudinal stability at all flight conditions was an order of magnitude higher than the natural aerodynamic pitch damping, and that the longitudinal control effectiveness (and hence the artificial pitch rate damping) varied in a manner which was closely related to duct incidence angle. A similar result was found for the case of artificial roll rate damping. Figure 26 illustrates the manner in which the Dutch roll roots varied with increasing speed for steady level flight; note that as speed increased in transition to approximately 180 ft/sec the time to double amplitude increased, after which the time to double amplitude decreased with further increases in speed. It was found that a minimum value of artificial roll rate stabilization of approximately $(L_p/I_x)_{SAS} \doteq -3.0$ per sec would result in a stable system at the high speed flight conditions. However, this value was considerably greater than that required at speeds near 180 ft/sec. Since the burden of roll control and roll stability augmentation shifts from differential collective pitch to the relatively ineffective vanes as speed increases from hover, it seemed advisable to devise a gain program which would gradually decrease roll stability augmentation as speed increased in transition up to the point at which increasing augmentation was required for stability of the system. This scheme would tend to minimize the use of vanes for roll stability augmentation, thereby making increased vane travel available for roll and yaw control.

E. Description of Basic Control and Stability Augmentation System

Using the results of the analyses reported in the preceding section, a basic programmed-gain control and stability augmentation system was devised for the initial piloted six-degree-of-freedom flight simulator studies. Provisions were made to allow adjustment of the gains in the initial system and the form of the gain programs, if required. The so-called "final" system which evolved from the flight simulator program differed from this basic system primarily in the levels of the gains; therefore, a brief description of the basic system is presented herein while a detailed description of the final gain programs is presented in Appendix E.

1. Longitudinal Mode

A block diagram of the basic longitudinal control and stability augmentation system is shown in Fig. 32. This diagram includes the longitudinal pitch attitude control stick, the collective pitch control stick and beeper switch, the duct incidence angle beeper switch, and the pitch rate stabilization loop.

A schematic of the initial longitudinal control and stability augmentation system investigated, which differed from the final system only in the magnitude of the gains K_p and K_{δ_v}, is shown in Fig. 33. In accordance with the results of the calculations of the theoretical performance, the longitudinal control stick gains K_{δ_β} and K_{δ_v} were programmed against duct incidence angle and the pitch rate stabilization gain K_p was held constant. Also shown in Fig. 33 are the corresponding initial levels of maximum longitudinal control power M_{MAX}/I_y and total pitch rate damping M_q/I_y for steady level flight (the dashed and solid curves show the minimum and maximum pitch rate stabilization studied using the flight simulator).

Initial values of the other gains shown in Fig. 32 were: collective pitch gain $K_c = 4.0$ deg/in., which resulted in a collective stick sensitivity of $Z_{\delta_c}/W = -0.25$ g/in. and which would be expected to be a desirable height control sensitivity according to the criteria of Ref. 11; collective beeper switch gain $K_{CP} = 0.5$ deg/sec; and duct incidence beeper switch gain linearly proportional to duct incidence angle according to $K_{i_D} = 0.08\, i_D$ deg/sec (chosen to provide a duct tilt rate of approximately 8 deg/sec at hover). All of these gains were also varied in the flight simulator program.

2. Lateral and Directional Modes

Using the model shown in Fig. 34 a programmed-gain system was developed for initial investigations in the flight simulator program. A schematic of this system showing the initial gain programs, maximum lateral and directional control powers, and total

roll rate and yaw rate damping is shown in Fig. 35. The principal characteristics of the system were: (1) lateral control stick gain $K_{\Delta\delta_\beta}$ and pedal gain $K_{\Delta\delta_V}$ were programmed against duct incidence angle; (2) control phasing or mixing gains G_{V_L} and G_{β_P} were programmed against duct incidence angle; and (3) roll rate stabilization gain K_R was programmed against duct incidence angle, and yaw rate stabilization gain K_Y was held constant at a small value. In addition, the initial maximum roll control power and total roll rate damping at hover were chosen as $L_{MAX}/I_x = 1.2$ rad/sec^2 and $L_p/I_x = -2.10$ per sec, respectively, which results in a point within the acceptable region of the criteria of Ref. 9 (these levels were later approximately doubled during the flight simulator program). In view of the low effectiveness of the vanes, the initial yaw control power was set at the maximum available level (vane deflection angles of ± 30 deg) of $N_{MAX}/I_z = 0.25$ rad/sec^2 and the total yaw rate damping was set at $N_r/I_z = -0.50$ per sec. This combination of control power and damping corresponds to a Cooper Pilot Rating of about 5 or 6 according to the criteria of Ref. 9. Control power was later judged in the flight simulator study to be too low by perhaps a factor of two.

F. Results of Flight Simulator Program

A six-degree-of-freedom, piloted, fixed-base analog computer simulation was conducted to verify that the programmed-gain control and stability augmentation system would provide satisfactory handling qualities for the tandem tilting ducted propeller aircraft. The gain levels which had been calculated on the basis of the theoretical analyses were adjusted to provide satisfactory stick-fixed dynamics and control response over a wide range of flight conditions. Additional studies were conducted to determine the effects on handling qualities of lags in the control system, of incorrect phasing of the lateral-directional controls, and of increases in the stability derivative $M_u g/I_y$.

A description of the Sikorsky V/STOL Aircraft Simulator and contact analog display is presented in Appendix F. Table V presents a summary of the training and experience of the pilots participating in this program. It must be emphasized that the purpose of the flight simulator program was to verify that a programmed-gain control and stability augmentation system would provide satisfactory handling qualities for this type of aircraft, rather than to establish optimum handling qualities criteria. The results discussed herein are based primarily on the work of Pilot A, who was principal investigator on the project; Pilots B and C participated to a limited extent at the end of the program and tended to confirm the earlier findings. Where the Cooper Pilot Opinion Rating System (Table VI) was applied, the intention was to aid in the discussion of the effects of particular variables on the handling qualities and not to establish optimum criteria.

1. Limitations of Aircraft Simulated

During the early phases of the program it was evident, as had been expected, that the effectiveness of the two vanes in the aft ducts was not sufficient to meet the combined requirements for control and stability augmentation about all three axes. Several tandem tilting ducted propeller VTOL designs have been proposed which included two additional vanes in the forward ducts. Consequently, in order to provide sufficient control power for the aircraft simulated in the present study, four vanes were simulated. Full deflection of two vanes was used for pitch control, and full deflection of the other two was used for lateral and directional control and stabilization. The total vane deflection due to longitudinal control stick deflection was limited to $\delta_v = \pm 30$ deg. The total vane deflection due to combined lateral control stick, pedals, and roll and yaw rate stabilization was limited to $\Delta\delta_v = \pm 30$ deg.

Rough estimates of the lateral-directional control system authorities which might be required were made by examining analog computer traces for maneuvering flight at hover, low speeds, and transitions. These estimates indicated that for the particular aircraft which was simulated, between 25 and 30% of the total travel of the vanes and differential collective pitch would be required by the lateral-directional stability augmentation system. At higher speeds, it is probable that greater stability augmentation system authorities would be required in view of the fact that the relatively ineffective vanes are used to supply the roll rate damping needed for stabilizing the Dutch roll mode (time did not permit investigation of the authorities required at high speeds).

2. Longitudinal Handling Qualities

A series of three-degree-of-freedom runs were made to evaluate levels of total pitch rate damping between $M_q/I_y = -0.20$ and -5.53 per sec, longitudinal control sensitivity between $M_{\delta_s}/I_y = 0.18$ and 0.32 rad/sec^2-in., and collective stick sensitivity between $Z_{\delta_c}/W = -0.09$ and -0.25 g/in. (all values at hover). The task for these runs included hovering, climbing transitions, constant altitude transitions, and approaches at 40 knots (flight path angle of 8.5 deg) followed by a flare and VTOL-type landing.

The value of pitch rate damping which was finally selected was $M_q/I_y = -2.2$ per sec, and the corresponding value of longitudinal control stick sensitivity was $M_{\delta_s}/I_y = 0.27$ rad/sec^2-in. (these values are at hover; values at other steady level flight conditions are shown in Figs. 36 and 37, and the corresponding maximum longitudinal control power is shown in Fig. 38). The longitudinal control stick sensitivity selected as most satisfactory fell very close to the "optimum" line which had been selected for the theoretical analyses (the left-hand "optimum" line in Fig. 21).

The values which were found to be satisfactory compare favorably with the results of a flight simulator study of a similar tandem tilting ducted propeller aircraft reported in Ref. 12 (see Fig. 39). The slightly higher pitch rate damping preferred for the aircraft studied in Ref. 12 is probably required by a shorter time to double amplitude (T_2 of 2.0 sec at hover according to calculations made by the authors, as contrasted to T_2 of 3.6 sec for the aircraft simulated in the present study). The results of the present study and the study of Ref. 12 indicate that considerably more control sensitivity and damping is required than the minimum specified in MIL-H-8501A.

The locations of the roots of the longitudinal characteristic equation for the aircraft with the final stability augmentation in steady level flight are shown in Fig. 40. Both the phugoid and short-period modes were stable at all flight conditions. Note that for the level of pitch rate stabilization which was found to be satisfactory (total Mq/I_y of -2.2 at hover) the short-period mode was more than critically damped at flight speeds up to approximately 130 ft/sec. Calculations made by the authors indicate that a similar situation must have existed for the levels of damping which were selected as optimum in Ref. 12. Under these conditions, the angle of attack response to a longitudinal control stick input consists of the sum of two decaying exponentials (i.e., the response would be nonoscillatory), and the aircraft seems to lag a stick input. This effect was noted in the present study at higher levels of damping than that finally selected; it was particularly noted that the longitudinal acceleration of the aircraft following a given longitudinal control stick input decreased with increasing damping due to the increased time required to achieve changes in pitch attitude.

The longitudinal root locations for the aircraft with stability augmentation on the critical $T/W = 1.35$ take-off flight profile are shown in Fig. 41. The effect of the stability augmentation system may be seen by comparing Figs. 41 and 15.

At all flight conditions a forward input to the longitudinal control stick was required to increase speed. The stick position required for trim exhibited a reversal during transitions due to the combined effects of thrust rotation, thrust modulation, and changes in the pitching moments on the ducted propellers. This reversal, which is common in helicopters, was not found to be objectionable.

The initial collective stick sensitivity at hover of $Z_{\delta_c}/W = -0.25$ g/in. was found to be too high; a collective stick sensitivity of $Z_{\delta_c}/W = -0.093$ g/in. permitted more precise altitude control in hover in the presence of simulated gusts. As shown in Fig. 42, the altitude damping of this type of VTOL aircraft is considerably lower than that of helicopters, which have much lower disc loadings. Nevertheless, the hovering characteristics were satisfactory, indicating that the criteria proposed in Refs. 11 and 13 for floor-mounted altitude controllers may not be generally applicable to all classes of VTOL aircraft. Changes in the gain of the beeper switch on the collective stick, which was used to change the range of

collective pitch angles over which the stick had authority, were found to have little effect on the handling qualities; the initial gain for K_{CB}, which resulted in a blade angle change rate of 0.5 deg/sec, was satisfactory. Similarly, the beeper switch for duct incidence angle resulted in satisfactory transitions with the initial linear gain program in which the duct tilt rate was equal to $0.08\, i_D$ deg/sec (a duct tilt rate of half this value was also judged to be acceptable, but was not as satisfactory as the higher tilt rate).

The longitudinal handling qualities at the high-speed cruise conditions at sea level and an altitude of 20,000 ft were evaluated for steady level flight and two-minute turns. The maneuvering performance of the aircraft seemed to be satisfactory despite the fact that the longitudinal short-period dynamic characteristics, particularly at the high altitude conditions, were not within the acceptance boundaries shown in Fig. 40. One would suspect therefore that these criteria may be more applicable to aircraft which are required to have high maneuvering performance, and may be overly restrictive for transport configurations. As a matter of interest, the increases in static stability and damping which would be required to offset the high moment of inertia I_y and thereby bring the roots into the satisfactory regions as defined by these criteria were calculated. The abscissa $-\zeta\omega_n$ in Fig. 40 is directly proportional to M_q/I_y, while the undamped natural frequency ω_n is proportional to the square root of $M_w g/I_y$. Thus, forcing the short-period root at the 250-knot (423 ft/sec) cruise condition at 20,000 ft to fall within the boundaries would require a 400% increase in static stability and a 30% increase in damping.

3. Lateral and Directional Handling Qualities

With the longitudinal control and stability augmentation system gains set at their selected levels, a series of runs were made to select the most satisfactory levels of lateral and directional control sensitivity and rate damping. Levels of lateral stick sensitivity from $L_{\delta_L}/I_x = 0.20$ to 0.80 rad/sec^2-in., total roll rate damping from $L_p/I_x = -2.10$ to -8.40 per sec, pedal sensitivity from $N_{\delta_p}/I_z = 0.08$ to 0.16 rad/sec^2-in., and total yaw rate damping from $N_r/I_z = -0.29$ to -1.00 per sec (all values at hover) were investigated.

The levels of lateral and directional control sensitivity and the corresponding maximum control power and rate damping which were finally selected are shown in Figs. 43 through 48 for steady level flight conditions. For duct incidence angles corresponding to hover and transition flight ($30 \leq i_D \leq 90$ deg) it was found that approximately twice the initial lateral control sensitivity and roll rate damping was required (i.e., twice the gain $K_{\Delta\delta\beta}$ in Fig. 34). The initial pedal sensitivity at these duct angles was judged to be adequate, but the maximum yaw control power of $N_{MAX}/I_z = 0.243$ rad/sec^2 in hover which resulted from full deflection of two

vanes (30 deg) was estimated to be too low by a factor of two. Thus, to obtain adequate maximum yaw control moments in hover of perhaps $N_{MAX}/I_Z = 0.50$ or 0.60 rad/sec^2, would require the use of larger vanes and probably the addition of vanes in the forward ducts as well as in the aft ducts. Because of the marginal effectiveness of the vanes, it was difficult to observe the effects of changes in the yaw rate damping gain K_R on the handling qualities except near hover. Nevertheless, it was found that the presence of at least a small amount of artificial yaw rate damping helped alleviate pilot-induced motions of the aircraft during low-speed maneuvers.

Figure 49 shows Cooper Pilot Opinion Ratings (Table VI) for flight at airspeeds from hover to 180 ft/sec (106 knots) with and without the lateral-directional stability augmentation system operative for several locations of the center of gravity of the aircraft. The center of gravity was moved forward and aft by 0.55 ft and vertically by 0.40 ft from its nominal position (Fig. 2) in order to examine its effect on the lateral-directional handling qualities. The pilot ratings were based on a task which included continuation of flight at the indicated speed, maneuvering and turns to a heading, transitions, and VTOL-type landings. For the aircraft with the nominal location of the center of gravity, the pilot rating increased (became less acceptable) with increasing velocity because of an increasing tendency to oscillate and overshoot when rolling out of turns. Additionally, in the region from 140 to 180 ft/sec the Dutch roll mode could be excited easily by normal control inputs in steady level flight. By moving the center of gravity forward and up, the dihedral effect was reduced and the directional static stability increased, thereby alleviating the Dutch roll somewhat. As discussed previously, the roll rate stabilization which was available decreased with decreasing duct incidence angle since the source of roll control moment shifted from differential collective pitch to the less effective vanes. It is apparent, therefore, that tandem ducted propeller configurations which rely heavily on roll rate stabilization for adequate Dutch roll damping would have marginal handling qualities for continuous flight at speeds near the end of transition. However, the simulator studies indicated that these handling qualities were satisfactory for transitions where the marginal areas were encountered as transients during normal operation, rather than in prolonged flight.

Pilot ratings for the aircraft without roll rate and yaw rate stability augmentation are also shown in Fig. 49 for the most favorable location of the center of gravity (forward and up). At low speeds the Dutch roll instability could be controlled, but extreme difficulty was experienced in controlling heading and lateral airspeed. As speed increased the frequency of the Dutch roll mode increased rapidly, and although its time to double amplitude also increased the aircraft would become uncontrollable after about five cycles at 40 knots. At high speeds the frequency decreased with increasing airspeed but the aircraft could not be controlled in turns. In view of these chracteristics, it is doubtful that the aircraft which was simulated could be landed safely following failure of the lateral-directional

stability augmentation system. A triplicated stability augmentation system would have to be provided since a complete failure during a take-off or landing would result in dangerous flight conditions. A dual channel system in which the pilot could test and re-engage the channel which was still operative would be adequate for this type of aircraft if the Dutch roll instability could be alleviated in the design of the aircraft (see discussion of dual and triplicated systems in Appendix G).

Figure 50 shows the lateral-directional root locations with the final stability augmentation system in steady level flight. Due to the combined effects of roll rate and yaw rate stabilization, the Dutch roll mode was at least lightly damped at all flight speeds. In addition, comparison of Figs. 26 and 50 shows that the net effect of roll rate and yaw rate stabilization was to increase the stability of the roll convergence and spiral stability roots. Increasing the stability of the spiral mode is not always desirable since it tends to reduce the performance of the aircraft in entering turns.

The lateral-directional dynamics with stability augmentation for the critical high-power take-off flight profile are shown in Fig. 51. The Dutch roll mode was stable throughout the transition with the levels of roll rate and yaw rate stabilization which was selected for the stability augmentation system.

The lateral-directional dynamics of the aircraft at the high-speed cruise condition at both sea level and an altitude of 20,000 ft were found to be satisfactory after the lateral control stick sensitivity and the roll rate damping were increased to the levels shown in Figs. 43 and 44 (i.e., after the gain $K_{\Delta\delta\beta}$ had been doubled). The rolling parameter $(1/\sqrt{\sigma})\,|\phi/v|$, which provides a measure of the ratio of roll angle to sideslip velocity, was calculated for steady level flight conditions and is shown plotted against the reciprocal of the number of cycles required to damp to half amplitude in Fig. 52. Although at the high altitude flight conditions the points did not fall within the boundaries specified in MIL-F-8785 (ASG), the pilots did not object to the magnitudes of the Dutch roll oscillations.

Runs were made at the high speeds at sea level with the phasing gains which were finally selected and also with the exact gains required to eliminate control coupling at sea level (see Figs. 53 and 54, and the discussion in Section VIII. C. 3. of Appendix C). With the final gain program, considerable coupling existed at these conditions and cross-controlling was required during maneuvers, although the amount required was not believed to be objectionable. Insufficient time was available to examine the coupling problem in detail; further research is recommended to establish the maximum amount of cross-coupling which is tolerable under transition and cruise flight conditions.

4. Additional Handling Qualities Results

Several additional studies were conducted using the flight simulator to investigate factors which might be expected to affect the design of the control and stability augmentation system and to explore changes which might improve its performance. Although none of these studies produced results which would alter the basic conclusion that a programmed-gain system would be adequate for this type of aircraft, the results are presented in this section since they are believed to be of general interest in the design of tandem tilting ducted propeller aircraft.

a. Effect of Speed Stability Derivative $M_u g/I_y$

As shown in Section II.D.1.b., the effect on the stick-fixed dynamics of increasing the stability derivative $M_u g/I_y$ at hover and low speeds is to decrease the time to double amplitude and to decrease the period of the phugoid oscillation. In the flight test program reported in Ref. 6 it was found that increasing $M_u g/I_y$ increased the levels of pitch rate damping and longitudinal control stick sensitivity required for optimum handling qualities. Accordingly, a series of runs were made in the present study to observe the effect of increasing $M_u g/I_y$ on the longitudinal dynamics and control response with and without simulated gusts. The results are shown in the form of pilot ratings for hover and low speed flight in Fig. 55.

For the runs without gusts, increasing $M_u g/I_y$ from its basic value of +0.077 resulted in no adverse change in the dynamics until a value of approximately +0.40 was reached; however, the large changes in stick position required to trim with changing velocity became objectionable at values as low as +0.20. Increasing $M_u g/I_y$ above +0.40 resulted in a noticeable shortening of the time to double amplitude, but the period remained long enough that the oscillations could be controlled. Clearly, more longitudinal control sensitivity would be required and increased damping would be helpful for acceptable handling qualities at large values of $M_u g/I_y$.

The variation of pilot rating with $M_u g/I_y$ for the runs with simulated gust disturbances are also shown in Fig. 55. The gust disturbances were simulated by the superposition of two sine waves on a steady wind of 20 ft/sec. The low frequency sine wave had an amplitude of $\pm$12 ft/sec and a period of 6 sec, while the high frequency sine wave had an amplitude of $\pm$2.8 ft/sec and a period of 1 sec. The gusts caused the aircraft to pitch considerably, and the additional control motions which were required had the side effect of exciting the lateral-directional modes. As would be expected, the large control motions required to control the aircraft were more objectionable when hovering in gusts than in still air. From these results and the results of Ref. 6, it is inferred that handling qualities criteria expressed in terms of pitch rate damping vs longitudinal control stick sensitivity are not generally applicable to all aircraft since the speed stability derivative $M_u g/I_y$ and the dynamic characteristics of the aircraft are not taken into consideration,

and that criteria of this type which are obtained in flight test programs and simulator studies under still air conditions will result in an underestimation of the levels of damping and control sensitivity which are required for a given aircraft.

b. Effect of Lag in Pitch Control System

The effect of a first-order lag in the pitch control system on the handling qualities of the aircraft was investigated. A theoretical analysis of the effect of a lag on the stick-fixed longitudinal dynamics is presented in Section VIII.B.3. of Appendix B. In the flight simulator program the lag was in the forward loop, as shown in Fig. 19, so that both longitudinal control stick input and pitch rate stabilization were affected.

The variation of over-all pilot ratings with the lag time constant for flight in the speed range from hover to 106 knots is shown in Fig. 56. Values of the lag time constant τ_p from 0 to the extreme value of 1.0 sec were used. For these runs only the three longitudinal degrees of freedom were simulated. The task included hovering, transitions, and constant speed approaches followed by flares. At all values of the lag, no adverse effects on the stick-fixed dynamics were noted (this observation is in agreement with the theoretical analysis which showed that in the absence of artificial pitch attitude stabilization, the effect of a lag is actually slightly stabilizing; see Fig. 20). The lag in the response of the aircraft to a longitudinal control stick input became objectionable for values of the time constant above about 0.20 or 0.30 sec. Since the longitudinal control system for this type of aircraft would have an equivalent time constant of perhaps 0.05, it does not seem as though lag will present a serious problem.

c. Effect of Lags in Lateral and Directional Control Systems

A similar investigation was conducted to determine the effect of first-order lags in the lateral-directional control system on the handling qualities of the aircraft. As in the case of the longitudinal control system, the lags were in the forward loop (see Fig. 30) so that the lateral control stick and pedal inputs as well as roll rate and yaw rate stabilization were affected.

Results of the flight simulator investigation are shown in Fig. 57. The task for these runs was similar to that for the study of lags in the longitudinal control system and also included six-degree-of-freedom maneuvering at hover and turns to a heading. Values of the lags τ_R and τ_Y from 0 to 0.5 sec were used, with both lags having the same value during a run. At low values of the lags (up to about 0.2 sec) the lags in the response to lateral control stick and pedal inputs were noticeable but were not objectionable. The aircraft was more difficult to control for precision hovering, but as speed increased the adverse effect of the lags seemed to diminish. At the extreme value of 0.5 sec large roll oscillations built up when attempting to control lateral airspeed at hover. As speed increased it became increasingly

difficult to control heading, and the lightly damped Dutch roll mode was more difficult to damp out with the lateral control stick (the applied rolling moments tended to become in phase with the Dutch roll motion of the aircraft).

The results of this brief study indicated that first-order lag time constants less than about 0.1 sec would not have a significant effect on the lateral-directional handling qualities of the aircraft.

d. Effect of Lag in Collective Pitch Control

The effect of a first-order lag in the collective pitch control on the handling qualities at hover was also investigated. Values of the lag time constant up to 1.0 sec were used with a collective stick sensitivity of $Z_{\delta_c}/W = -0.093$ g/in. The ability of the pilot to control altitude precisely in hover was found to deteriorate with increasing value of the lag time constant as indicated in Fig. 58, and some difficulty was experienced in setting power for cruise in a partially converted configuration. No difficulty was encountered due to lagging changes in longitudinal pitch trim associated with the lagging thrust changes. The results indicated that lags in the collective pitch control of less than about 0.20 or 0.25 sec are acceptable for the low value of altitude damping of the tandem tilting ducted propeller aircraft.

e. Effect of Crosswind on Approaches

In view of the apparent lateral-directional stability problems of this type of aircraft, a brief study was conducted to determine the effects of a crosswind and gusts on the handling qualities during approaches and STOL-type landings. The approaches were at airspeeds of 40 and 20 knots at a rate of descent of 600 ft/min., which resulted in flight path angles of 8.5 and 16.5 deg, respectively. A steady wind of 20 ft/sec from 0 deg (north) was used with simulated gust disturbances having peaks of ± 6 and ± 12 ft/sec superimposed. The aircraft was flown over true courses of 0, 45, and 90 deg. The results of the study are shown in Fig. 59.

Approaches at a speed of 40 knots without gusts were found to be affected very little by the crosswind. Under these same steady wind conditions, approaches at 20 knots became less satisfactory as the component of crosswind increased because of the large crab angles required (the lateral angle between fuselage centerline and direction of flight required to compensate for drift), and because the maximum directional control power was barely sufficient to remove the crab angle prior to touchdown. At this low speed and large crab angle it was found more expedient to turn into the wind and land across the runway at a ground speed of 8 knots rather than to remove the crab angle and land along the runway.

For the 40-knot approaches with gusts (Fig. 59), increasing the crosswind component resulted in a rapid deterioration of pilot rating. At a true course of

90 deg it was possible to maintain the approach path, but the pilot was constantly required to use large control motions to damp out the Dutch roll mode which was excited by the gusts. Although no quantitative results could be obtained, this study indicated that normal operations under gusty conditions may be difficult for VTOL aircraft having a lightly damped Dutch roll mode.

f. Miscellaneous Flight Simulator Results

The six-degree-of-freedom simulation also provided an opportunity to evaluate various modifications to the basic control system. The principal results of these modifications are discussed in the following paragraphs.

As a possible means of improving the handling qualities of the aircraft in hovering turns, the longitudinal control stick was given limited authority to change the duct incidence angle. Thus, when turning into the wind, the duct incidence angle could be decreased by pushing the longitudinal control stick forward rather than by actuating the duct incidence beeper switch. Several runs were made at a gain of 2.5 deg of duct incidence angle per inch of longitudinal control stick deflection. It was found that variation of pitch attitude of the aircraft during hovering turns was reduced. Although the results were not fully conclusive, it is believed that such a modification merits further investigation.

The effect of a first-order lag in duct tilt rate on handling qualities was investigated for a lag time constant of 0.5 sec. The only flight condition at which the lag was apparent was during the flare following a constant speed approach. The lag was successfully compensated for by initiating the flare at a slightly higher altitude.

Various levels of pitch attitude stabilization from $M_\theta/I_y = 0$ to -10.0 per sec^2 were also investigated. Attitude stabilization corresponding to $M_\theta/I_y = -4.5$ per sec^2 in conjunction with the level of pitch rate damping which was finally selected ($M_q/I_y = -2.2$ per sec) was found to result in a very slight improvement in pitch attitude control during transitions. The pitch attitude stabilization reduced the disturbances induced by changes in collective pitch. However, pitch attitude stabilization appears to be unnecessary for aircraft of this type.

The effects of incorrect phasing on the handling qualities during transition were investigated by setting the phasing gains G_{VL} and $G_{\beta P}$ at 50% of their correct values. Decreasing G_{VL}, i.e., decreasing the amount of vane deflection to approximately 50% of that required to eliminate yawing moment due to a lateral stick input, resulted in no degradation of performance at hover and at very low speeds since the phasing gains are small at large duct angles (both G_{VL} and $G_{\beta P}$ are zero at a duct incidence angle of 90 deg). With increasing speed the amount of cross-control required to maneuver increased. A similar effect was noticed for the runs during

which $G_{\beta P}$ was reduced to one-half of its correct value. At the higher speeds the cross-control was quite apparent (right pedal caused left roll). Incorrect $G_{\beta P}$ appeared to be more objectionable than incorrect G_{VP}, but the pilot ratings for all runs were no worse than for the basic configuration with correct phasing (see shaded area between 160 and 180 ft/sec in Fig. 49). It is believed that the amount of control coupling which may be acceptable during transitions is considerable; further research should be conducted, using qualified test pilots, to determine criteria for the amount of roll-yaw coupling which will be acceptable.

5. Summary of Principal Results of Flight Simulator Program

The flight simulator program indicated that a relatively simple programmed-gain control and stability augmentation system should provide satisfactory handling qualities (pilot rating 3.5 or better) for the tandem tilting ducted propeller type of aircraft. The same type of system should also be satisfactory for aircraft of this type having less severe lateral-directional stability problems with the exception that programming of the roll rate stabilization gain might not be required. Because of the flexibility which is available in the design of a programmed-gain system, further improvements in handling qualities which might result from use of an adaptive control system would be expected to be small and unnecessary.

The Dutch roll instability of the basic aircraft which was simulated resulted in unacceptable dynamic characteristics for emergency landings following a stability augmentation system failure. A triplicated stability augmentation system with automatic disengagement of the channel which failed, rather than a dual channel system with pilot test and reset, would be required to insure against a complete loss of stability augmentation during take-offs and landings. A dual channel system would be adequate if the Dutch roll instability could be alleviated in the design of the aircraft.

G. Comparison of Relative Weights and Costs of Alternate Stability Augmentation Systems

A brief study of alternate systems for fulfilling the stability augmentation requirements of tandem tilting ducted propeller aircraft was conducted. Estimates were made of the relative cost and weight of the basic programmed-gain system which was found to provide adequate handling qualities, of a similar system in which the pilot could manually adjust the level of roll rate damping, and of a rate-command adaptive control system. In view of the Dutch roll handling qualities problem of this type of aircraft following a stability augmentation failure, both duplicated systems (in which the pilot would manually test and reset the operative channel) and triplicated systems (in which the one failed channel would automatically be

disengaged) were considered. A detailed description of the methods used and block diagrams of the systems studied are presented in Appendix G.

The principal results are shown in Figs. 60 and 61. As shown in Fig. 60, a triplicated programmed-gain system was estimated to weigh approximately 1.37 times as much as the basic duplicated programmed-gain system (the least complex type of system capable of providing adequate handling qualities). Note also that a duplicated adaptive control system would weigh 1.60 times as much, and a triplicated adaptive control system 2.19 times as much, as the basic duplicated programmed-gain system. Figure 61 shows that the triplicated programmed-gain system was estimated to cost 1.48 times as much as the basic duplicated programmed-gain system. The corresponding cost factors for duplicated and triplicated adaptive control systems were 1.30 and 1.92, respectively. The programmed-gain system with manual pilot adjustment of roll rate gain was estimated to be slightly lower in weight and cost than the basic system; however, it is improbable that such a system would be more desirable than the basic programmed-gain system in view of the added workload on the pilot.

IV. CONCLUSIONS AND RECOMMENDATIONS

On the basis of the results of theoretical analyses and flight simulator studies of the tandem tilting ducted propeller VTOL transport, the following conclusions may be drawn:

A. The control and stability augmentation requirements of this type of aircraft are influenced primarily by the following stability and control problems: (1) unstable or lightly damped Dutch roll characteristics which vary widely with changing flight conditions, and which are basically attributable to the large side force-curve-slopes of the ducted propellers; (2) large changes in pitching moment required to trim, due to the effect of changes in velocity and duct incidence angle on the pitching moments on the ducts; and (3) difficulty in obtaining an acceptable level of maximum yaw control power at hover and low speeds, primarily due to the marginal effectiveness of the control vanes in the exits of the ducted propellers.

B. The natural aerodynamic rate damping of this type of aircraft is small compared with the levels of artificial rate damping which must be added to achieve satisfactory handling qualities. The longitudinal stability of the aircraft at low speeds is similar to that of many operational helicopters; handling qualities may be improved by the addition of pitch rate stabilization. The Dutch roll stability may be improved most effectively by increasing the static directional stability and decreasing the effective dihedral in the design of the aircraft, and by the addition of roll rate stabilization.

C. Relatively simple variable-gain control and stability augmentation systems are required for tandem tilting ducted propeller transports having unstable Dutch roll characteristics which vary widely with changing flight conditions. Systems in which the control gains and roll rate stabilization gain are programmed as functions of duct incidence angle have the least complexity, lightest weight, and lowest cost of those types of systems which will provide satisfactory handling qualities. Constant roll rate stabilization gain should be satisfactory if the Dutch roll damping is improved in the design of the aircraft.

D. Due to the Dutch roll problem, a triplicated stability augmentation system may be required, rather than a duplicated system with pilot reset, in order to assure that a safe landing could be made following a partial stability augmentation failure during take-off or landing.

E. Equivalent first-order time lags up to 0.20 or 0.25 sec in the collective pitch control system, up to 0.20 or 0.30 sec in the longitudinal

control system, and up to 0.10 sec in the lateral and directional control system will result in satisfactory handling qualities.

F. For aircraft of this type, cross-wind landing approaches in the presence of gusts may be difficult because of the Dutch roll tendency and the low maximum yaw control power at low speeds.

G. An analytical and flight simulator or flight test program should be conducted to determine the maximum amount of lateral-directional control coupling which may be tolerated during transitions and in cruise. The maximum levels of roll and yaw control power and the maximum levels of artificial roll rate and yaw rate stabilization which can be used are dependent on the amount of coupling which is acceptable.

V. REFERENCES

1. Newsom, W. A., Jr.: Aerodynamic Characteristics of Four-Duct Tandem VTOL-Aircraft Configurations. NASA Technical Note D-1481, January 1963.

2. Theodorsen, T.: Theoretical Investigation of Ducted Propeller Aerodynamics. U. S. Army Transportation Research Command, Technical Report, crd 3860, Vol. II, August 1960.

3. Smith, C. C., Jr.: Wind-Tunnel Investigation of a Small-Scale Model of an Aerial Vehicle Supported by Tilting Ducted Fans. NASA Technical Note D-409, August 1960.

4. Anon.: Military Specification - Helicopter Flying and Ground Handling Qualities; General Requirements for MIL-H-8501A, September 7, 1961.

5. Anderson, S. B.: An Examination of Handling Qualities Criteria for V/STOL Aircraft. NASA Technical Note D-331, July 1960.

6. Seckel, E., J. J. Traybar, and G. E. Miller: Longitudinal Handling Qualities for Hovering. Princeton University, Department of Aeronautical Engineering, Report No. 594, December 1961.

7. Isca, J. A., and J. Patierno: Instrument Flight Simulator Study of the VTOL Controllability-Control Power Relationship. Institute of the Aerospace Sciences Paper No. 61-118-1812, presented at the National IAS-ARS Joint Meeting, Los Angeles, June 13-16, 1961.

8. Madden, J., J. Kroll, and D. Neil: A Study of VTOL/STOL Flying Qualities Requirements. Bell Aircraft Corporation Report No. 203-917001, August 10, 1960.

9. Faye, A. E., Jr.: Attitude Control Requirements for Hovering Determined Through the Use of a Piloted Flight Simulator. NASA Technical Note D-792, April 1961.

10. Lynn, R. R.: New Control Criteria for VTOL Aircraft. Institute of the Aerospace Sciences Paper No. 62-63, presented at the 30th Annual Meeting, New York January 22-24, 1962.

11. Gerdes, R. M. and R. F. Weick: A Preliminary Piloted Simulator and Flight Study of Height Control Requirements for VTOL Aircraft. NASA TN D-1201, February 1962.

12. Henderson, C., J. Kroll, and A. Hesby: Control Characteristics of V/STOL Aircraft in Transition. Bell Aerosystems Company Report No. 2023-917002, July 1, 1962.

13. A'Harrah, R. C. and S. F.Kwiatkowski: A New Look at V/STOL Flying Qualities. Institute of the Aerospace Sciences Paper No. 61-62, presented at the IAS 29th Annual Meeting, New York, January 23-25, 1961.

14. Grose, R. M.: Wind Tunnel Tests of Shrouded Propellers at Mach Numbers from 0 to 0.60. WADC Technical Report 58-604, December 1958.

15. O'Hara, F.: An Analysis of the Longitudinal Stability and Control of a Single-Rotor Helicopter. Great Britain Aeronautical Research Council R. & M. No. 2958, July 1954 (issued 1957).

16. Schultz, E. R.: The Determination of Helicopter Longitudinal Stability Derivatives from Flight Test Data. Part III: An Analog Computer Study of Flight Measured Longitudinal Transient Motions of a Single Rotor Helicopter. WADC Technical Report 55-438, Part III, September 1959.

17. Curtiss, H. C., Jr.: Some Basic Considerations Regarding the Longitudinal Dynamics of Aircraft and Helicopters. Princeton University, Department of Aeronautical Engineering, Report No. 562, July 1961.

18. Anon.: Military Specification - Flying Qualities of Piloted Airplanes. MIL-F-8785 (ASG), Amendment 4, April 17, 1959.

19. Anon.: Tri-Service VTOL Research Aircraft. Bell Aerosystems Company Report No. D2127-953001, Vol. 4, Stability and Control, March 1962.

VI. LIST OF SYMBOLS

A	Constant in Eq. (2), deg $(rev/sec)^2/in.$
$A_0 - A_4$	Coefficients of longitudinal characteristic equation without first-order lag
$A'_0 - A'_5$	Coefficients of longitudinal characteristic equation with first-order lag
b	Spanwise distance between centerlines of ducts, ft
b_{REF}	Lateral reference length, 58.3 ft
B	Constant in Eq. (2), deg $(rev/sec)^2/in.$
$B_0 - B_4$	Coefficients of lateral-directional characteristic equation without first-order lags
$B'_0 - B'_6$	Coefficients of lateral-directional characteristic equation with first-order lags
$C_1 - C_2$	Aerodynamic parameters in Eq. (42)
$C_{1/2}$	Number of cycles to damp to half amplitude
C_2	Number of cycles to amplify to double amplitude
C_D	Drag coefficient, drag force/$q_0 S$
C_{ℓ_β}	Rolling-moment-coefficient slope of ducted propellers, rolling moment per deg/$q_0 S b_{REF}$
C_L	Lift coefficient, lift force/$q_0 S$
C_{L_α}	Lift coefficient slope, lift force per deg/$q_0 S$
$C_{L_{\alpha_{TAIL}}}$	Lift coefficient slope of horizontal tail, lift force per deg/$q_0 S$
$C_{Y_{\beta_{FIN}}}$	Side-force-coefficient slope of vertical tail, side force per deg/$q_0 S$
d_F	Distance from center of gravity of aircraft to axis of rotation of front ducts, ft
d_R	Distance from center of gravity of aircraft to axis of rotation of rear ducts, ft

d_{SP}	Distance along propeller shaft from axis of rotation of duct to propeller plane of rotation, ft
D_P	Diameter of propeller, ft
e_m	Empirical function of duct incidence angle in Eq. (8), ft
f_1, f_2	Fractions of correct lateral-directional control phasing gains in Eq. (47)
$F(s)$	Laplace transform of a function $F(t)$
g	Gravitational constant, 32.2 ft/sec^2
g_1, g_3	Empirical functions of local advance ratio J_{O_i} in Eqs. (4) and (5)
g_2	Empirical function of effective duct incidence angle $i_D+\alpha_i$ in Eq. (5)
G_{VL}	Lateral-directional control phasing gain, degrees differential vanes per degree differential collective pitch
G_{β_P}	Lateral-directional control phasing gain, degrees differential collective pitch per degree differential vanes
h	Altitude above sea level, ft
h_0	Initial altitude in transitions, ft
$h_{1,2}$	Vertical distance from horizontal reference line through center of gravity of aircraft to axis of rotation of forward ducts, ft
i_D	Duct incidence angle with respect to horizontal reference line of aircraft, deg
I_x	Moment of inertia in roll, slug-ft^2
I_y	Moment of inertia in pitch, slug-ft^2
I_z	Moment of inertia in yaw, slug-ft^2
I_{xz}	Product of inertia, slug-ft^2
j	Imaginary number, $\sqrt{-1}$
J_{O_i}	Advance ratio at ducted propeller i, V_i/nD_p

K_C	Collective stick gain, degrees of collective pitch per inch of collective stick deflection
K_{CB}	Gain of collective pitch beeper switch, deg/sec
K_{D_i}	Nondimensional drag coefficient of ducted propeller i , Drag/$\rho n^2 D_p^4$
K_{i_D}	Gain of duct incidence angle beeper switch, deg/sec
K_{L_i}	Nondimensional lift coefficient of ducted propeller i , Lift/$\rho n^2 D_p^4$
K_P	Pitch rate stabilization gain, in.-sec/rad
K_R	Roll rate stabilization gain, in.-sec/rad
K_T	Nondimensional thrust coefficient of one ducted propeller, Thrust/$\rho n^2 D_p^4$
K_Y	Yaw rate stabilization gain, in.-sec/rad
K_{Y_i}	Nondimensional side-force coefficient of ducted propeller i , Side-Force/$\rho n^2 D_p^4$
$K_{\Delta\delta_v}$	Pedal gain, degrees of differential vanes per inch of pedal deflection
$K_{\Delta\delta_\beta}$	Lateral control stick gain, degrees of differential collective pitch per inch of lateral control stick deflection
K_{δ_v}	Longitudinal control stick gain, degrees of vanes per inch of longitudinal control stick deflection
K_{δ_β}	Longitudinal control stick gain, degrees of differential collective pitch per inch of longitudinal control stick deflection
K_θ	Pitch attitude stabilization gain, in./rad
$K_1 - K_4$	Gains in attitude and altitude analog control circuits
$\ell_{1,2}$	Distance along horizontal reference line from center of gravity of aircraft to axis of rotation of forward ducts, ft
L	Rolling moment, ft-lb
L_{MAX}	Maximum rolling moment due to full lateral control stick deflection, ft-lb
m	Mass of aircraft, slugs

M	Pitching moment, ft-lb
M_{MAX}	Maximum pitching moment due to full longitudinal control stick deflection, ft-lb
n	Propeller rotational speed, rev/sec
N	Yawing moment, ft-lb
N_{MAX}	Maximum yawing moment due to full pedal deflection, ft-lb
p	Roll rate, rad/sec
q	Pitch rate, rad/sec
q_e	Dynamic pressure at duct exit, lb/ft^2
q_0	Dynamic pressure in free stream, lb/ft^2
r	Yaw rate, rad/sec
s	Distance along ground from initial point in transition, ft; also, Laplace transform variable
S	Reference area (total planform area of the four ducted propellers at $i_D = 0$, including adjacent fuselage area between ducts 1 and 2, and between ducts 3 and 4), 305 ft^2
t	Time, sec
T	Thrust, lb
T_t	Total time of transition, sec
$T_{1/2}$	Time to damp to half amplitude, sec
T_2	Time to amplify to double amplitude, sec
u	Velocity perturbation along x-axis (stability-axis system), ft/sec
v	Velocity perturbation along y-axis (stability-axis system), ft/sec
V	Velocity of center of gravity, ft/sec
V_i	Instantaneous velocity at ducted propeller i, ft/sec

V_e	Initial velocity, ft/sec
V_{et}	Instantaneous velocity at horizontal and vertical tails, ft/sec
w	Velocity perturbation along z-axis (stability-axis system), ft/sec
W	Weight of aircraft, lb
x	Stability axis pointing in direction of initial velocity vector (Fig. 75)
X	Force in direction of x stability axis, lb
X_2	Force in direction of x stability axis for right forward duct, lb
y	Stability axis pointing out right side of aircraft, normal to x and z stability axes (Fig. 78)
$\bar{y}_t$	Length of the roll moment arm of horizontal tail, 18.5 ft
Y	Force in direction of y stability axis, lb
z	Stability axis pointing downward from aircraft, normal to x and y stability axes (Fig. 75)
$\bar{z}_{FIN}$	Vertical component of distance from the center of gravity to center of pressure of vertical tail, 7.63 ft
Z	Force in direction of z stability axis, lb
α	Instantaneous angle of attack of fuselage, deg
α_e	Initial angle of attack of fuselage, deg
α_i	Local angle of attack at ducted propeller i , deg
α_t	Local angle of attack of horizontal tail, deg
β	Instantaneous sideslip angle of fuselage, deg
β_c	Collective blade pitch angle, deg
β_{et}	Instantaneous sideslip angle of vertical tail, deg
β_i	Local yaw angle at ducted propeller i , deg

$\Delta\alpha_i$	Roll-induced change in local angle of attack at ducted propeller i, deg
$\Delta\delta_v$	Differential vane deflection angle (for lateral-directional control), deg
$\Delta\delta_\beta$	Differential collective blade pitch angle (for lateral-directional control), deg
δ_c	Collective stick displacement, in.
δ_L	Lateral control stick displacement, in.
δ_P	Pedal displacement, in.
δ_s	Longitudinal control stick displacement, in.
δ_v	Vane deflection angle (for pitch control), deg
δ_β	Differential collective blade pitch angle (for pitch control), deg
η	Correction factor for side force of rear ducts in Eq. (7), $\eta = \eta_{i_D} + \eta_\alpha$
ζ	Damping ratio
θ	Instantaneous pitch attitude of aircraft with respect to horizon, rad
θ_e	Initial pitch attitude of aircraft with respect to horizon, rad
θ_F	Angle between horizontal reference line of fuselage and a line through center of gravity and axis of rotation of forward ducts, deg
θ_R	Angle between horizontal reference line of fuselage and a line through center of gravity and axis of rotation of aft ducts, deg
λ	Root of chracteristic equation
Λ	Parameter in Eq. (50)
π	Parameter in Eq. (50)
ρ	Local ambient air density, lb-sec^2/ft^4
ρ_0	Ambient air density at sea level, lb-sec^2/ft^4
σ	Ratio of local ambient air density to density at sea level, ρ/ρ_0
τ	Period of oscillation, $2\pi/\omega$, sec

τ_C First-order lag time constant in collective pitch control system, sec

τ_P First-order lag time constant in pitch control system, sec

τ_R First-order lag time constant in roll control system, sec

τ_Y First-order lag time constant in yaw control system, sec

ϕ Roll angle, rad

ω Damped frequency of oscillation, rad/sec

ω_n Undamped natural frequency of oscillation, rad/sec

Subscripts

i Denotes local conditions at a particular ducted propeller (i = 1 and 2 refers to left and right front ducts, respectively; i = 3 and 4 refers to left and right rear ducts, respectively)

p,q,r u,v,w etc. Denotes partial derivative of a parameter with respect to the subscript shown (e.g., roll rate damping $L_p = \partial L/\partial p$)

Superscripts

— Denotes Laplace transform of a variable

• Denotes the differential operator with respect to time, d/dt

VII. TABLES

TABLE I

SUMMARY OF LONGITUDINAL STABILITY DERIVATIVES FOR STEADY LEVEL FLIGHT CONDITIONS

	Stability Derivatives						
Velocity	X_u/m	Z_u/m	$M_u g/I_y$	X_w/m	Z_w/m	$M_w g/I_y$	M_q/I_y
Hover	-0.194	0	0.077	0	0	0	-0.185
20 ft/sec	-0.185	-0.144	0.062	0.276	-0.225	-0.159	-0.400
40	-0.170	-0.139	0.059	0.147	-0.253	-0.142	-0.441
67.5	-0.161	-0.130	0.055	0.080	-0.263	-0.073	-0.427
80	-0.158	-0.122	0.066	0.107	-0.278	-0.172	-0.485
100	-0.156	-0.159	0.059	0.055	-0.299	-0.160	-0.490
140	-0.156	-0.144	0.057	0.031	-0.329	-0.296	-0.591
180	-0.150	-0.122	0.074	0.015	-0.377	-0.156	-0.659
178 Kts; S.L.	-0.194	-0.271	0.086	-0.045	-0.616	-0.625	-1.467
250 Kts; S.L.	-0.229	0.008	0.037	-0.159	-0.664	-0.904	-1.783
178 Kts; 20K ft	-0.126	-0.207	0.068	-0.011	-0.345	-0.296	-0.590
250 Kts; 20K ft	-0.135	-0.002	0.027	-0.067	-0.393	-0.324	-1.179

Note: X_q/m and Z_q/m approximately zero

TABLE II

SUMMARY OF LATERAL-DIRECTIONAL STABILITY DERIVATIVES FOR STEADY LEVEL FLIGHT CONDITIONS

Velocity	Stability Derivatives*									Stability Derivatives**	
	L_v/I_x	N_v/I_z	Y_v/m	L_p/I_x	N_p/I_z	Y_p/m	L_r/I_x	N_r/I_z	Y_r/m	L_v/I_x	N_v/I_z
Hover	-0.0058	0.00067	-0.189	-0.284	0	0	0.1360	-0.293	0	-0.0045	0.00067
20 ft/sec	-0.0102	0.00173	-0.116	-0.333	0.0384	-0.377	0.0233	-0.198	0.299	-0.0094	0.00132
40	-0.0168	0.00385	-0.205	-0.518	0.0314	-0.294	0.0435	-0.347	0.368	-0.0153	0.00313
67.5	-0.0242	0.00518	-0.324	-0.587	0.0392	-0.212	0.0682	-0.500	0.588	-0.0219	0.00404
80	-0.0264	0.00388	-0.355	-0.640	0.0541	-0.207	0.0778	-0.588	0.856	-0.0238	0.00513
100	-0.0281	0.00269	-0.396	-0.741	0.0486	-0.322	0.0914	-0.770	1.049	-0.0252	0.00408
140	-0.0296	0.00040	-0.443	-0.815	0.0635	-0.732	0.1158	-0.869	1.472	-0.0264	0.00196
180	-0.0323	-0.00129	-0.488	-1.204	0.0392	-1.670	0.1376	-1.104	2.079	-0.0288	0.00042
178 Kts S.L.	-0.0315	-0.00320	-0.576	-1.639	0.0823	-0.677	0.4200	-1.200	3.084	-0.0274	-0.00118
178 Kts 20K ft	-0.0246	-0.00154	-0.379	-0.860	0.0776	-0.559	0.2466	-0.8114	1.347	-0.0219	-0.00021
250 Kts 20K ft	-0.0330	-0.00261	-0.520	-0.972	0.1176	-1.016	0.4888	-0.8230	0.766	-0.0292	-0.00079

* Nominal location of center of gravity

** Center of gravity moved forward 0.55 ft and upward 0.40 ft

TABLE III

SUMMARY OF TRANSITION FLIGHT PROFILES

Flight Profile	Thrust-to-Weight Ratio	Continuous Duct Tilt Rate, deg/sec	Maximum Normal Load Factor g's	Maximum Longitudinal Acceleration, g's
Accelerating Ascent	1.35	4	1.35	0.465
Accelerating Ascent	1.05	2	1.05	0.205
Constant Altitude Acceleration	Varied by constant altitude controller	2	1.00	0.285
Constant Altitude Deceleration	Varied by constant altitude controller	2	1.00	-0.185
Decelerating Descent	Varied by rate of descent controller	2	0.96, 1.06	-0.155

TABLE IV

SUMMARY OF EFFECTS OF INDIVIDUAL STABILITY DERIVATIVES ON THE LATERAL-DIRECTIONAL DYNAMICS IN THE TRANSITION SPEED RANGE

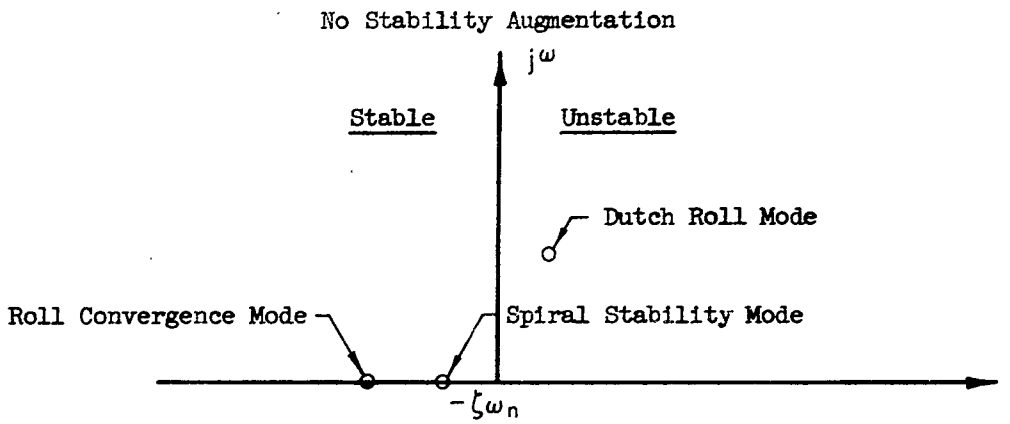

Stability Derivative	EFFECT ON ROOT LOCATIONS*		
	Roll Convergence	Spiral Stability	Dutch Roll
L_p/I_x	← Strong	→ Moderate	← Strong
L_r/I_x	Negligible	→ Very Slight	Negligible
L_v/I_x	← Moderate	← Very Slight	↗ Very Strong
N_p/I_z	→ Very Slight	← Very Slight	↑ Very Slight
N_r/I_z	→ Moderate	← Strong	↑ Small
N_v/I_z	→ Moderate	→ Very Slight	↖ Moderate
Y_v/m	← Small	Negligible	↙ Small

* Arrows indicate direction in which roots move for increasing values of the derivatives (150% of their nominal values).

TABLE V

SUMMARY OF PILOT TRAINING AND EXPERIENCE

Pilot A

Research Engineer, B.S. and M.S. in Aeronautical Engineering
Commercial Pilot Certificate
Total Flight Time - 350 hours
Total Instrument Time - 20 hours
Total Helicopter Time - 0 hours
Total Fixed-Wing Time - 350 hours
Total Tandem-Ducted VTOL Simulator Time - 80 hours

Pilot B

Engineering Test Pilot
Commercial Pilot Certificate; Airplane, Helicopter, Multi-Engine, and Instrument Ratings
Total Flight Time - 4340 hours
Total Instrument Time - 250 hours
Total Helicopter Time - 2275 hours
Total Fixed-Wing Time - 2065 hours
Total Tandem-Ducted VTOL Simulator Time - 3 hours

Pilot C

Engineering Test Pilot, B.S. in Civil Engineering
Commercial Pilot Certificate; Airplane, Helicopter, and Multi-Engine Ratings
Total Flight Time - 3500 hours
Total Instrument Time - 50 hours
Total Helicopter Time - 2500 hours
Total Fixed-Wing Time - 1000 hours
Total Tandem-Ducted VTOL Simulator Time - 2 hours

TABLE VI

COOPER PILOT OPINION RATING SYSTEM

	Adjective rating	Numerical rating		Primary mission accomplished	Can be landed
Normal operation	Satisfactory	1	Excellent, includes optimum	Yes	Yes
		2	Good, pleasant to fly	Yes	Yes
		3	Satisfactory, but with some mildly unpleasant characteristics	Yes	Yes
Emergency operation	Unsatisfactory	4	Acceptable, but with unpleasant characteristics	Yes	Yes
		5	Unacceptable for normal operation	Doubtful	Yes
		6	Acceptable for emergency condition only[1]	Doubtful	Yes
No operation	Unacceptable	7	Unacceptable even for emergency condition[1]	No	Doubtful
		8	Unacceptable - dangerous	No	No
		9	Unacceptable - uncontrollable	No	No
	Catastrophic	10	Motions possibly violent enough to prevent pilot escape	No	No

[1] Failure of a stability augmenter

TABLE VII

SUMMARY OF LONGITUDINAL STABILITY DERIVATIVES FOR
15,000-LB AIRCRAFT IN STEADY LEVEL FLIGHT

Stability Derivatives

Velocity	X_u/m	Z_u/m	$M_u g/I_y$	X_w/m	Z_w/m	$M_w g/I_y$	M_q/I_y
Hover	-0.202	0	0.118	0	0	0	-0.266
20 ft/sec	-0.192	-0.150	0.089	0.287	-0.234	-0.229	-0.575
40	-0.176	-0.145	0.086	0.153	-0.263	-0.204	-0.634
67.5	-0.167	-0.135	0.080	0.083	-0.273	-0.105	-0.614
80	-0.164	-0.127	0.096	0.111	-0.288	-0.248	-0.698
100	-0.162	-0.165	0.086	0.057	-0.310	-0.230	-0.706
140	-0.162	-0.150	0.083	0.032	-0.342	-0.426	-0.850
180	-0.156	-0.127	0.107	0.016	-0.391	-0.225	-0.949
178 Kts; S.L.	-0.202	-0.282	0.125	-0.047	-0.640	-0.900	-2.110
250 Kts; S.L.	-0.238	0.008	0.054	-0.165	-0.690	-1.300	-2.560
178 Kts; 20K ft	-0.131	-0.215	0.099	-0.011	-0.358	-0.426	-0.849
250 Kts; 20K ft	-0.140	-0.002	0.039	-0.070	-0.408	-0.466	-1.700

Note: X_q/m and Z_q/m approximately zero

TABLE VIII

SUMMARY OF LATERAL-DIRECTIONAL STABILITY DERIVATIVES FOR 15,000-LB AIRCRAFT IN STEADY LEVEL FLIGHT

Stability Derivatives

Velocity	L_v/I_x	N_v/I_z	Y_v/m	L_p/I_x	N_p/I_z	Y_p/m	L_r/I_x	N_r/I_z	Y_r/m
Hover	-0.0084	0.00096	-0.197	-0.400	0	0	0.1920	-0.421	0
20 ft/sec	-0.0144	0.00244	-0.121	-0.470	0.0541	-0.392	0.0328	-0.279	0.311
40	-0.0237	0.00542	-0.213	-0.730	0.0443	-0.306	0.0613	-0.489	0.354
67.5	-0.0342	0.00730	-0.336	-0.838	0.0552	-0.220	0.0961	-0.705	0.611
80	-0.0372	0.00547	-0.369	-0.902	0.0762	-0.215	0.1097	-0.828	0.890
100	-0.0396	0.00379	-0.412	1.043	0.0685	-0.335	0.1290	-1.087	1.091
140	-0.0417	0.00056	-0.460	1.150	0.0895	-0.761	0.1632	-1.226	1.530
180	-0.0456	-0.00182	-0.517	1.700	0.0552	-1.738	0.1940	-1.559	2.160
178 Kts S.L.	-0.0444	-0.00451	-0.598	-2.310	0.1160	-0.703	0.5920	-1.692	3.210
178 Kts 20K ft	-0.0347	-0.00217	-0.394	-1.185	0.1093	-0.581	0.3480	-1.142	1.402
250 Kts 20K ft	-0.0465	-0.00368	-0.540	-1.370	0.1660	-1.055	0.6880	-1.160	0.796

VIII. APPENDIXES

APPENDIX A

DESCRIPTION OF AERODYNAMIC, MASS, AND INERTIA CHARACTERISTICS OF THE AIRCRAFT

Details of the hypothetical 35,000-lb tandem tilting ducted propeller VTOL aircraft which was used as a basis for this study are shown in Figs. 2 and 62. This configuration was scaled up from a 1/7-scale wind tunnel model for which unpublished aerodynamic data were obtained from the NASA Langley Research Center. The data were modified and supplemented by the Research Laboratories using theoretical estimates and data from other sources.

Control moments were obtained from differential thrust of the ducted propellers and from flap-type vanes in the exits of the rear ducts. In hovering, differential vane deflection (left and right) provided yaw control and differential propeller pitch (fore and aft) provided roll control. In forward flight, roll and yaw control was provided by combinations of differential propeller blade pitch and differential vanes. In high speed conventional flight, rolling moment was derived primarily from differential vanes and yawing moment was derived primarily from differential collective pitch. At high flight speeds, pitching moment was derived entirely from the vanes. Constant-speed propellers were assumed; the propeller collective pitch provided control of altitude in hover and of power in forward flight.

The moments of inertia which were used for the full-scale 35,000-lb airplane are shown in Fig. 2. Although the roll moment of inertia I_x was relatively small, it was estimated that moving the rear ducts outboard a distance equal to one-half the diameter of the duct would increase I_x approximately 20%. The effect of changing the moment of inertia in roll on the lateral-directional dynamics of the aircraft is discussed in Section III.D.2.b.

1. Simulation of the Aerodynamic Characteristics of the Aircraft

The aerodynamic data for the configuration used in this study were obtained in model tests conducted by NASA in support of the evaluation by the Government of the Tri-Service VTOL Transport proposals. The data for this and other tandem ducted propeller configurations of the same aircraft have subsequently been published in Ref. 1. The 1/7-scale model was powered by four ducted propellers. Each duct contained a variable-speed electric motor which drove a fixed-pitch (blade angle

of 18 deg at 0.75 R) propeller. Lift, drag, and pitching moment of the model were measured at several duct incidence angles for power settings corresponding to unaccelerated, 1/4 g acceleration, and 1/4 g deceleration flight conditions. In addition, side force, rolling moment, and yawing moment were measured for unaccelerated level flight in partially converted configurations. Since aerodynamic data for ascending or descending transition flight conditions were not available, additional calculations were made by UAC to supplement the longitudinal and lateral-directional data to include the effects of angle attack.

a. Ducted Propellers

The ducted propellers were simulated on the analog computer in the form of nondimensional propeller force coefficients for each duct. For a given duct, the coefficients were based on the local advance ratio and inclination of the flow relative to the duct (obtained by adding the local induced velocities resulting from pitch, yaw, and roll rates to the free-stream velocity). In order to simulate the ducts over a wide range of inflow conditions, generalized empirical functions for the force coefficients K_L, K_D, and K_Y were formulated for a ducted propeller using as guides the data from a large number of tests (Refs. 2, 3, and 14). The general functions were then fitted to aerodynamic data for the NASA configuration without horizontal and vertical tails while making allowances for the effect of the fuselage. This method of simulation permitted the effects of aerodynamic interference to be included and also permitted the effects of linear and angular velocities of the aircraft on the aerodynamic forces and moments to be calculated directly by the analog computer.

An examination of data for ducted propellers having variable-pitch propellers showed that changing blade pitch angle at constant rotational speed had little effect on the normal force of the duct but resulted in a change in axial force which was approximately proportional to the pitch change. For the three-blade ducted propeller design of the NASA configuration the following expression was used:

$$\partial K_T / \partial \beta_C = 0.015 \text{ per deg} \tag{3}$$

The lift coefficient used in the simulation of one duct had the form

$$K_{L_i} = \left[0.347 + g_1 + \frac{\partial K_T}{\partial \beta_C} \left(\beta_C \pm \delta_\beta \pm \Delta\delta_\beta - 18.0 \right) \right] \sin \left(i_D + \alpha_i \right) \tag{4}$$

where g_1 is an empirical function of the local advance ratio as shown in Fig. 63, and $\partial K_T/\partial \beta_c$ is a constant given by Eq. (3). The subscript i ($i = 1$ and 2 for the left and right front ducts, respectively; $i = 3$ and 4 for the left and right rear ducts, respectively) denotes quantities applying only to the duct for which K_{L_i} is being calculated. The signs of δ_β and $\Delta\delta_\beta$ depend on the location of duct i on the aircraft. Figure 64 shows the variation of K_{L_i} with $i_D + \alpha_i$ for the case in which the blade angle of the propeller is equal to 18 deg. The figure also shows a portion of the wind tunnel data for the NASA configuration. The variation of K_{L_i} with the sine of $i_D + \alpha_i$ neglects a 2 or 3% loss in lift due to lip-stall which was apparent in the data at values of $i_D + \alpha_i$ near 90 deg, that is, when the axis of duct was nearly normal to the local flow direction. The full-scale effects of lip-stall could not be determined from the wind tunnel data because of the low test Reynolds numbers but would be expected to be smaller than those which were measured.

The drag coefficient used in the simulation of one duct had the form

$$K_{D_i} = g_2 + g_3 \left[0.570 + 0.00942\,(i_D + \alpha_i)\right] - \frac{\partial K_T}{\partial \beta_c}\left[\beta_c \pm \delta_\beta \pm \Delta\delta_\beta - 18.0\right] \cos\,(i_D + \alpha_i) \quad (5)$$

In Eq. (5), g_2 and g_3 are empirical functions of $i_D + \alpha_i$ and J_{0_i}, respectively, as shown in Fig. 65, and $\partial K_T/\partial \beta_c$ is a constant given by Eq. (3). Again, the functions and constants of Eq. (5) were determined by fitting the equation to the data.

The side force coefficient of each of the front ducts was determined to have the form

$$K_{Y_{1,2}} = -J_{0_{1,2}}^2 \left[0.0241 + 0.268\,(10)^{-3}\,(i_D + \alpha_{1,2}) + 0.334\,(10)^{-5}\,(i_D + \alpha_{1,2})^2\right]\beta_{1,2} \quad (6)$$

where $J_{0_{1,2}}$ is the local advance ratio of the duct and $\beta_{1,2}$ is the local yaw angle at the front ducts. The linear variation of $K_{Y_{1,2}}$ with local yaw angle at the duct is in good agreement with the wind tunnel data, which were available only for the range $-15 \leq \beta_{1,2} \leq +15$ deg. Figure 66 shows the variation of $K_{Y_{\beta_{1,2}}}$ with $i_D + \alpha_{1,2}$, as given by Eq. (6), and a portion of the wind tunnel data for the NASA configuration. Because of the effects of blockage by the fuselage and the interference of the slipstreams of the forward ducts on the rear ducts, to obtain the side force on the rear ducts it was necessary to multiply the side force of the forward ducts by an interference correction factor determined from the wind tunnel data. Hence, the side force coefficient for each of the rear ducts used in the simulation had the form

$$K_{Y_{3,4}} = -\eta J_{O_{3,4}}^2 \left[0.0241 + 0.286(10)^{-3}(i_D + \alpha_{3,4}) + 0.334(10)^{-5}(i_D + \alpha_{3,4})^2\right]\beta_{3,4} \quad (7)$$

As shown in Fig. 67, the empirical correction factor η was found to be the sum of a function η_{i_D} of the angle of incidence of the ducts and a function η_α of the angle of attack of the fuselage. For each test condition of the NASA model in which the tails were removed, the correction factor η was determined from the ratio of the side force on the front ducts to the side force on the rear ducts. The ratio of side forces was calculated from the total side force and yawing moment while assuming that the forces acted at the hub of the propeller. Since in reality the lateral center of pressure of the ducts did not remain at the hub of the propeller, the actual side force on each individual duct deviates slightly from the value given by Eqs. (6) and (7). However, the total side force and yawing moment of the aircraft agree with the data at the test conditions since the correction factor η was obtained by matching the side force given by Eqs. (6) and (7) to the wind tunnel side force and yawing moment data.

The moments produced by the ducts about all axes were calculated by the analog computer by summing the moments of the forces on the individual ducts with appropriate correction terms determined from the wind tunnel data to account for interference effects. For example, the pitching moment contribution of the right forward duct $(i = 2)$ about the center of gravity takes the form

$$M_2 = -Z_2\left[\ell_{1,2} + d_{SP}\cos i_D\right] + X_2\left[h_{1,2} - d_{SP}\sin i_D\right] + 0.25\,We_m \quad (8)$$

where Z_2 and X_2 are the forces on the duct in the body axes system. Then,

$$Z_2 = -\sigma\rho_0 n^2 D_P^4\left[K_{L_2}\cos\alpha_2 + K_{D_2}\sin\alpha_2\right] \quad (9)$$

and

$$X_2 = \sigma\rho_0 n^2 D_P^4\left[K_{L_2}\sin\alpha_2 - K_{D_2}\cos\alpha_2\right] \quad (10)$$

In Eq. (8) the forces X_2 and Z_2 were assumed to act at the hub (the intersection of the plane of the propeller and the axis of rotation of the propeller). The moment arm of each force about the center of gravity therefore is comprised of two parts: (1) the horizontal $\ell_{1,2}$ or vertical $h_{1,2}$ component of distance from

the center of gravity to the axis of rotation of the duct, and (2) the appropriate component of the distance along the propeller shaft between the axis of rotation of the duct and the hub of the propeller. The term e_m in Eq. (8) was a correction which was calculated from the wind tunnel data to take into account the moment about the hub (due to the fact that in reality the forces X_2 and Z_2 did not act at the hub). The wind tunnel data indicated that e_m could be approximated by a function of duct incidence angle i_D (Fig. 68). Figure 69 shows the variation pitching moment required to trim with velocity for the NASA wind tunnel model.

Similarly, the side force on the right forward duct is given by

$$Y_2 \approx \sigma \rho_0 n^2 D_P^4 \left[K_{Y_2} \cos \beta_2 \right] \tag{11}$$

where the side force coefficient K_{Y_2} is given by Eq. (6). The yawing moment contribution of the right front duct is

$$N_2 = Y_2 \left[\ell_{1,2} + d_{SP} \cos i_D \right] + \sigma \rho_0 n^2 D_P^4 \frac{\partial K_T}{\partial \beta_C} \frac{b}{2} \cos i_D \Delta \delta_\beta \tag{12}$$

where the moment arm $\ell_{1,2}$ is the same as that used for the pitching moment contribution.

Because of the large interference effects, the rolling moment of the ducted propellers could not be simulated by the technique used for the pitching and yawing moments in which the contribution of each duct was calculated separately. Equation (13) shows the form of the rolling moment contribution of the four ducted propellers as used in the simulation:

$$\begin{aligned} L_{DUCTS} = {} & \frac{\sigma \rho_0}{2} S b_{REF} C_{\ell\beta} \beta V^2 + 2 \sigma \rho_0 n^2 D_P^4 \frac{\partial K_T}{\partial \beta_C} b \sin i_D \Delta \delta_\beta \\ & - \sigma \rho_0 n^2 D_P^4 b \left[\frac{K_{L_{1,2}}}{\sin (i_D + \alpha_{1,2})} + \frac{K_{L_{3,4}}}{\sin (i_D + \alpha_{3,4})} \right] \left| \cos (i_D + \alpha) \right| \Delta \alpha_{2,4} \\ & - 17{,}030 \left[1 - 0.083 V \right] p \end{aligned} \tag{13}$$

The coefficient of rolling moment due to yaw angle $C_{\ell\beta}$ was taken directly from the data and was found to be satisfactorily represented by a function of duct incidence angle (Fig. 70). The third term of Eq. (13) accounts for the roll damping of the ducts due to the roll-induced angle of attack at the ducts. The term $\Delta \alpha_{2,4}$ is the change in angle of attack of the right ducts in radians due to the roll induced velocity and is approximated by

$$\Delta\alpha_{2,4} = \tan^{-1}\left[\frac{w + 0.5bp}{u}\right] - \tan^{-1}\frac{w}{u} \tag{14}$$

The last term of Eq. (13) accounts for the roll damping of the ducts due to changes in the local advance ratio resulting from roll-induced velocities at the ducts. This term is significant only for flight conditions near hover and was set equal to zero for $V \geq 12$ ft/sec.

Control moments were produced by systematically changing the blade angle of the propellers; differential changes of blade angle fore and aft produced pitching moments while differential changes left and right produced rolling and yawing moments. As a result of the previous assumption that changes in the propeller pitch angle alter only the axial force, the effectiveness of the controls may be written as:

$$\partial M/\partial\delta_\beta = -2\sigma\rho_0 n^2 D_P^4 \frac{\partial K_T}{\partial\beta_C}\left[d_F \sin(i_D + \theta_F) + d_R \sin(i_D + \theta_R)\right] \tag{15}$$

$$\partial L/\partial\Delta\delta_\beta = 2\sigma\rho_0 n^2 D_P^4 \frac{\partial K_T}{\partial\beta_C} b \sin i_D \tag{16}$$

$$\partial N/\partial\Delta\delta_\beta = 2\sigma\rho_0 n^2 D_P^4 \frac{\partial K_T}{\partial\beta_C} b \cos i_D \tag{17}$$

The distances d_F and d_R are the distances between the center of gravity of the aircraft and the axis of rotation of the front and rear ducts, respectively; θ_F and θ_R are the angles between the horizontal centerline of the fuselage and the lines joining the center of gravity and the axes of rotation of the front and rear ducts (both angles are positive); and b is the lateral distance between the centerlines of the ducts. The value of $\partial K_T/\partial\beta_C$ is given by Eq. (3). The direct dependence of the effectiveness of the differential collective pitch controls on altitude (σ is reduced to nearly 0.5 at 20,000 ft) and on the square of the rotational speed should be noted. Also, the origin of control coupling between roll and yaw at duct incidence angles other than 0 and 90 deg is indicated in Eqs. (16) and (17). The variation of control effectiveness of the ducted propellers with velocity in steady level flight is shown in Fig. 71.

b. Control Vanes

The vanes were flap-type control surfaces located in the exits of the rear ducts (Fig. 62). The effectiveness of the vanes was calculated using a normal force coefficient in conjunction with a reference area and the dynamic pressure at the exit of the duct. The coefficient of the force normal to the axis of the duct due to deflection of one vane was determined from the limited amount of wind tunnel data available to be 0.0475 per deg. The force was then calculated by multiplying this coefficient by the reference area of 18 ft^2 (the area of the vane not including the area of the centerbody which was intersected) and the exit dynamic pressure. Simple momentum theory results in the following expression which was used to calculate the exit dynamic pressure as a function of the inflow conditions and thrust coefficient of the ducted propeller, assuming that the slipstream was fully expanded to free-stream static pressure over the entire vane:

$$q_e = q_0 \left[\frac{\cos^2 i_D}{2} + \cos i_D \left(\frac{\cos^2 i_D}{4} + \frac{4K_T}{\pi J_0^2} \right)^{1/2} + \frac{4K_T}{\pi J_0^2} \right] \qquad (18)$$

Differential operation of the left and right vanes $\Delta\delta_v$ provided roll and yaw control in transition flight, while at low duct incidence angles deflection of the vanes in the same direction δ_v provided pitch control of the aircraft. Each vane was simulated separately on the analog computer so that all control moments resulting from pilot inputs could be calculated based on the instantaneous flight condition of the aircraft. The variation of control effectiveness of the vanes with velocity for steady level flight is shown in Fig. 72. As shown in Fig. 72, the control derivative $L_{\Delta\delta_v}/I_x$ was positive while $N_{\Delta\delta_v}/I_z$ was negative, but from Fig. 71 both $L_{\Delta\delta\beta}/I_x$ and $N_{\Delta\delta\beta}/I_z$ of the ducted propellers were positive. Because of this fact, differential deflection of the vanes and propeller pitch could be phased or mixed to alleviate control coupling in roll and yaw during transition flight.

c. Fuselage, Horizontal Tail, and Vertical Tail

The aerodynamic simulation of the fuselage was based on data obtained in drag clean-up tests conducted by NASA. Figure 73 shows the lift and drag coefficients of the fuselage, for the angle-of-attack range $-12 \leq \alpha \leq 20$ deg, that were measured with the ducts and tail assembly removed. At an angle of attack of zero deg the equivalent drag area of the full-scale fuselage was approximately 10.7 sq ft. The simulation also included estimated values of pitching moment, side force, and yawing moment coefficient for the fuselage.

The horizontal tail panels, which had a total area of 126 sq ft, were mounted outboard of the rear ducts (Fig. 2) and remained fixed relative to the fuselage during rotation of the ducts. For this aircraft configuration, interference caused by impingement of the slipstream of the forward duct on the tail was minimized since the tail panels were located at a spanwise station outboard of the forward ducts. The lift, drag, and pitching moment coefficients obtained from the wind tunnel data were programmed on the computer as a function of the local angle of attack at each of the two tail panels. The initial lift-curve slope of the tail was approximately 0.02 per deg based on the reference area of the airplane (305 sq ft). Stall of the tail occurred at an angle of attack of approximately 25 deg. The forces on the tail were calculated by the computer for the local angle of attack at each tail panel; therefore, the contribution of the horizontal tail to rolling moment due to roll rate and yaw rate was

$$L_{TAIL} = -0.5\,\sigma\rho_0 S\, C_{L_{\alpha_{TAIL}}} \bar{y}^2 V_{et}\, p + \sigma\rho_0 S\, C_{L_{TAIL}} \bar{y}_t^2 V_{et}\, r \qquad (19)$$

where $\bar{y}_t$ is the length of the roll moment arm of the horizontal tail ($\bar{y}_t$ = 18.5 ft). Initially the tail was equipped with full-span, 40%-chord elevators. However, a completely fixed tail was used for most of the simulator program because the elevators were found to be relatively ineffective for pitch control, even at cruise flight conditions, as compared with the vanes.

The vertical tail of the full-scale aircraft had an area of 97 sq ft. Comparison of the wind tunnel data for the model with and without the vertical tail showed large interference effects apparently due to the slipstream from the ducted propellers. As a result, the slope of the side force coefficient $C_{Y_{\beta_{FIN}}}$ of the vertical tail was programmed as a function of duct incidence angle on the computer as shown in Fig. 74. The resulting form of the side force acting on the vertical tail, which includes the effects of roll rate induced velocities, is given by

$$Y_{FIN} = \frac{\sigma\rho_0}{2} S C_{Y_{\beta_{FIN}}} \left[V_{et}^2 \beta_{et} + \bar{Z}_{FIN} V_{et}\, p \right] \qquad (20)$$

where $\bar{Z}_{FIN}$ is the vertical component of distance from the center of gravity to the center of pressure of the vertical tail ($\bar{Z}_{FIN}$ = 7.63 ft). The rolling and yawing moment contributions of the vertical tail were then obtained by multiplying Y_{FIN} by the appropriate moment arms.

2. Discussion of Analog Computer Simulation

In the simulation of the tandem tilting ducted propeller aircraft the complete nonlinear equations of motion were solved on the analog computer along with the aerodynamic and propulsion calculations. Assuming mirror symmetry of the aircraft with respect to the $X-Z$ plane, the equations of motion in the body axis system reduce to Eqs. (21) to (26).

$$\dot{u} + qw - rv + g\sin\theta = \sum X/m \tag{21}$$

$$\dot{v} + ru - pw - g\sin\phi\cos\theta = \sum Y/m \tag{22}$$

$$\dot{w} + pv - qu - g\cos\phi\cos\theta = \sum Z/m \tag{23}$$

$$\dot{q} + (p^2 - r^2)\frac{I_{xz}}{I_y} + pr\left[\frac{I_x - I_z}{I_y}\right] = \sum M/I_y \tag{24}$$

$$\dot{p} - (\dot{r} + pq)\frac{I_{xz}}{I_x} + rq\left[\frac{I_z - I_y}{I_x}\right] = \sum L/I_x \tag{25}$$

$$\dot{r} + (qr - \dot{p})\frac{I_{xz}}{I_z} + qp\left[\frac{I_y - I_x}{I_z}\right] = \sum N/I_z \tag{26}$$

The forces X, Y, and Z are the total aerodynamic and propulsive forces on the aircraft in the body axis system. The moments L, M, and N are the total moments

about the center of gravity of the aircraft, also in the body axis system.

The representative transition flight profiles along which detailed studies of the dynamics of the aircraft were made were calculated using the longitudinal three-degree-of-freedom unpiloted simulation. Constant duct tilt rates and high-gain control circuits were used to maintain the attitude and flight path of the aircraft in order to obtain flight profile repeatability. At selected points along each profile (usually in increments of 20 ft/sec), all of the flight variables (velocity components, control positions, etc.) were recorded by setting the computer in the "hold" mode of operation. Subsequently the flight variables at each point were entered in the computer while in the "initial condition" mode of operation. The aerodynamic derivatives were then calculated by varying, one at a time, each of the linear and angular velocity components over a small range about its nominal value while recording the variation of all the force and moment components. For example, the speed stability derivative M_u was calculated by varying the longitudinal component of velocity u by plus and minus 10 ft/sec about the nominal value u_0 while simultaneously plotting pitching moment M versus u. The value of the derivative was then obtained by measuring the slope of the curve. The effectiveness of the controls (Figs. 71 and 72) were obtained at each point in a similar manner. Results showing the variation of longitudinal and lateral-directional stability derivatives with velocity during steady level flight for the nominal location of the center of gravity are shown in Tables I and II. The values of the derivatives L_v/I_x and N_v/I_z with the center of gravity moved forward 0.55 ft and up 0.40 ft are also shown in Table II.

APPENDIX B

THEORETICAL ANALYSIS OF LONGITUDINAL DYNAMICS

A discussion of the principal methods used in the theoretical analysis of the longitudinal dynamics of the aircraft is presented in this Appendix. The complete longitudinal three-degree-of-freedom characteristic equation is derived and the interpretation of roots by means of a root-locus diagram is described. Changes in the longitudinal characteristic equation to account for the effects of lags in the longitudinal stability augmentation system are also discussed.

1. Longitudinal Characteristic Equation

The generalized equations which describe the perturbed motion of an aircraft or helicopter about its initial flight path may be written in the following form:

$$X_u u + X_w w + X_q \dot{\theta} - \left[mg \cos(\theta_e + \alpha_e) \right] \theta - m\dot{u} = m\dot{u}_o \tag{27}$$

$$Z_u u + Z_w w + Z_q \dot{\theta} - \left[mg \sin(\theta_e + \alpha_e) \right] \theta - m(w - V_e \dot{\theta}) = m\dot{w}_o \tag{28}$$

$$M_u u + M_w w + M_q \dot{\theta} + M_\theta \theta - I_y \ddot{\theta} = 0 \tag{29}$$

Following conventional nomenclature (see, for example, Ref. 15), X, Z, and M are the forces and pitching moment in the x, y, z stability axis system; u and w are the velocity perturbations in the x and z directions, respectively, and θ is the angular perturbation about the y axis. The initial attitude of the aircraft and the magnitude and direction of the initial flight path vector are described by θ_e, α_e, and V_e as shown in Fig. 75 (note that α_e is positive in a climb).

Equations (27) through (29) differ from the conventional small-perturbation equations of motion in that they include the terms $m\dot{u}_o$ and $m\dot{w}_o$ which account

for arbitrary initial acceleration conditions along the x and z axes. Under the hypothetical condition that the coefficients of the equations remain constant (i.e., that the stability derivatives of the aircraft do not vary during the ensuing motion), and assuming that the initial accelerations are small so that the perturbations in u, w, and θ also remain small, these equations would accurately describe the motion of the aircraft even for nonequilibrium initial flight conditions. As mentioned in the following paragraphs, these and several other assumptions implicit in the small perturbation equations of motion are not completely satisfied for some flight conditions encountered by VTOL aircraft, particularly during rapid transitions. At these conditions the characteristic equation derived from the equations of motion is useful as an indication of the quasi-steady state of the stability of the aircraft, but analog computer techniques must be used if accurate dynamic response information is required.

From a purely mathematical standpoint, introduction of arbitrary initial acceleration conditions does not affect the derivation of the characteristic equation. The terms $m\dot{u}_0$ and mw_0 contribute only a constant "particular solution" to the equations, while the "homogeneous solution," which is the portion of the total solution which contains the independent variable time, is unaffected. The "homogeneous solution" of the equations of motion consists of terms of the form $e^{\lambda t}$; upon stubstituting and dividing the force equations by the mass of the aircraft m and the moment equation by the moment of inertia I_y, the following set of simultaneous algebraic equations are obtained:

$$\left(\frac{X_u}{m} - \lambda\right) u + \frac{X_w}{m} w + \left(\frac{X_q}{m}\lambda - g\cos(\theta_e + \alpha_e)\right)\theta = 0 \tag{30}$$

$$\frac{Z_u}{m} u + \left(\frac{Z_w}{m} - \lambda\right) w + \left(\left[\frac{Z_q}{m} + V_e\right]\lambda - g\sin(\theta_e + \alpha_e)\right)\theta = 0 \tag{31}$$

$$\frac{1}{g}\frac{M_u g}{I_y} u + \frac{1}{g}\frac{M_w g}{I_y} w + \left(\frac{M_\theta}{I_y} + \frac{M_q}{I_y}\lambda - \lambda^2\right)\theta = 0 \tag{32}$$

In order for a solution to exist, the determinant of the coefficients must be equal to zero:

$$\begin{vmatrix} \left(\frac{X_u}{m} - \lambda\right) & \frac{X_w}{m} & \left(\frac{X_q}{m}\lambda - g\cos(\theta_e+\alpha_e)\right) \\ \frac{Z_u}{m} & \left(\frac{Z_w}{m} - \lambda\right) & \left(\left[\frac{Z_q}{m} + V_e\right]\lambda - g\sin(\theta_e+\alpha_e)\right) \\ \frac{1}{g}\frac{M_u g}{I_y} & \frac{1}{g}\frac{M_w g}{I_y} & \left(\frac{M_\theta}{I_y} + \frac{M_q}{I_y}\lambda - \lambda^2\right) \end{vmatrix} = 0 \tag{33}$$

Expansion of the determinant then yields the complete three-degree-of-freedom longitudinal characteristic equation:

$$\begin{aligned} 0 = \lambda^4 &+ \left[-\frac{X_u}{m} - \frac{Z_w}{m} - \frac{M_q}{I_y}\right]\lambda^3 \\ &+ \left[-\frac{M_w g}{I_y}\left(\frac{Z_q}{m} + V_e\right)\frac{1}{g} + \frac{Z_w}{m}\frac{M_q}{I_y} + \frac{X_u}{m}\frac{M_q}{I_y} + \frac{X_u}{m}\frac{Z_w}{m}\right. \\ &\left. - \frac{1}{g}\frac{X_q}{m}\frac{M_u g}{I_y} - \frac{X_w}{m}\frac{Z_u}{m} - \frac{M_\theta}{I_y}\right]\lambda^2 \\ &+ \left[\left(\frac{X_u}{m}\frac{M_w g}{I_y} - \frac{X_w}{m}\frac{M_u g}{I_y}\right)\left(\frac{Z_q}{m} + V_e\right)\frac{1}{g} + \frac{1}{g}\frac{X_q}{m}\frac{M_u g}{I_y}\frac{Z_w}{m} - \frac{X_u}{m}\frac{M_q}{I_y}\frac{Z_w}{m}\right. \\ &+ \frac{M_w g}{I_y}\sin(\theta_e+\alpha_e) + \frac{X_w}{m}\frac{Z_u}{m}\frac{M_q}{I_y} - \frac{1}{g}\frac{X_q}{m}\frac{Z_u}{m}\frac{M_w g}{I_y} \\ &\left. + \frac{M_u g}{I_y}\cos(\theta_e+\alpha_e) + \frac{X_u}{m}\frac{M_\theta}{I_y} + \frac{Z_w}{m}\frac{M_\theta}{I_y}\right]\lambda \\ &+ \left[-\sin(\theta_e+\alpha_e)\left(\frac{X_u}{m}\frac{M_w g}{I_y} - \frac{X_w}{m}\frac{M_u g}{I_y}\right) - \cos(\theta_e+\alpha_e)\left[\frac{M_u g}{I_y}\frac{Z_w}{m} - \frac{Z_u}{m}\frac{M_w g}{I_y}\right]\right. \\ &\left. + \frac{X_w}{m}\frac{Z_u}{m}\frac{M_\theta}{I_y} - \frac{X_u}{m}\frac{M_\theta}{I_y}\frac{Z_w}{m}\right] \end{aligned} \tag{34}$$

As mentioned previously, the stability derivatives in Eq. (34) are in the stability-axis system. In the present study an IBM 7090 digital computer program was written which would accept the initial conditions and stability derivatives in the body-axis

system, convert to the stability-axis system derivatives, calculate the coefficients of the characteristic equation, and solve for the roots using a root-extraction program which had previously been prepared at the UAC Research Laboratories.

At this point it would be worthwhile to mention the assumptions which are implicit in Eq. (34) and to re-emphasize the conditions under which it is valid.

1. It is assumed that the perturbations in u, w, and θ are small so that the rigorous equations of motion may be linearized.

2. It is assumed that the stability derivatives are independent of time. This is equivalent to assuming that the stability derivatives are not functions of the dependent variables u, w, and θ, and that the geometry of the aircraft remains unchanged for the length of time during which the perturbations are of interest (i.e., constant duct incidence angle in the present case).

3. It is assumed that coupling between the longitudinal and lateral-directional motions is negligible.

4. When the flight conditions are such that the above three assumptions are valid, then the characteristic equation accurately describes the motion of the aircraft. Thus for the present application to a VTOL aircraft, the roots of Eq. (34) accurately describe the dynamic characteristics at equilibrium flight conditions, while at nonequilibrium flight conditions such as in transitions the roots serve only as indicators of the quasi-steady state of the stability of the aircraft. Nevertheless, this information is useful since it indicates approximate divergence rates and periods of oscillation.

The transfer functions for pitching response to a longitudinal control stick input and for altitude response to a collective pitch stick input all have the characteristic equation as their denominator (see Appendix D).

2. Longitudinal Root-Locus Diagrams

A convenient technique used by control systems analysts in determining the closed-loop dynamic response characteristics of a system is the root-locus diagram. As indicated in Refs. 16 and 17, root-locus diagrams may also be used to analyze the effect of varying the individual stability derivatives, mass, and moment of inertia on the stability characteristics of the aircraft. In the present investigation the root-locus technique was used for these purposes and in addition was used to analyze the stability changes over continuous flight profiles, to determine the effect of varying the gains and lags in the stability augmentation system on

the stick-fixed dynamics of the aircraft, and to a lesser extent to calculate the closed-loop responses of the aircraft to control inputs (the analog computer program was used as the primary method for assuring that the closed-loop control responses were satisfactory).

The roots of the characteristic equation are a direct indication of the rate of convergence or divergence of the motion of the aircraft following a disturbance, and if the motion is oscillatory, of the frequency and period of the oscillation. The roots may be real, imaginary, or complex, and may have positive or negative real parts. Imaginary and complex roots always occur in conjugate pairs. Since the characteristic equation was derived assuming solutions of the form $e^{\lambda t}$, the presence of a negative real root indicates that the perturbation subsides as time increases while a positive real root indicates that the perturbation amplifies. Similarly, a pair of conjugate complex roots indicates an oscillation which either subsides or amplifies, depending on whether their real part is negative or positive, respectively.

For a real positive root, the time to double amplitude in seconds is given by

$$T_2 = \frac{.693}{\lambda} \tag{35}$$

and for a real negative root the time to halve amplitude in seconds is given by

$$T_{1/2} = \frac{-.693}{\lambda} \tag{36}$$

The conjugate imaginary and conjugate complex roots may be written in the following form:

$$\lambda = -\zeta\omega_n \pm j\omega \tag{37}$$

In Eq. (37) ζ is the damping ratio, ω_n is the undamped natural frequency in rad/sec, and ω is the damped frequency in rad/sec. The period of the motion contributed by this root is $\tau = 2\pi/\omega$ in seconds. If the real part $-\zeta\omega_n$ is positive the oscillation is unstable and will double amplitude in a time

$$T_2 = \frac{.693}{-\zeta\omega_n} \tag{38}$$

while if the real part $-\zeta\omega_n$ is negative the oscillation is stable and will damp to half amplitude in a time

$$T_{1/2} = \frac{-.693}{-\zeta\omega_n} \tag{39}$$

All of the roots calculated for a given flight condition may be plotted on a root-locus diagram in which the ordinate is an imaginary axis and the abscissa is a real axis. Figure 76 is an example of a root-locus diagram showing four roots (a complex conjugate pair, and positive and negative real roots). Only the upper half of the diagram is shown, as is the usual case, since the lower half is merely a mirror image. Note that the stable side is to the left of the vertical axis while the unstable side is to the right. Also note the vertical lines of constant time to halve and double amplitude, the sloping lines of constant damping ratio, and the semicircles of constant undamped natural frequency.

Since the longitudinal characteristic equation for the tandem tilting ducted propeller VTOL is a quartic, there are always four roots. Figure 77 illustrates the manner in which the longitudinal root locations vary for steady level flight over a wide range of speeds. Note that at the high cruise speed the dynamics consist of a moderately damped, high frequency oscillation, and a well damped, low frequency (long period) oscillation, corresponding to the usual short-period and phugoid modes of fixed-wing aircraft, respectively. The phugoid mode consists of an oscillation in speed and pitch attitude (with respect to the horizon) at essentially constant angle of attack. The classical short-period mode consists of an oscillation in angle of attack at constant speed; however, since angle of attack is related to the velocity components by $\tan\alpha = \frac{w}{u}$, it is convenient to think of the short-period mode in terms of oscillations of u and w. As speed is decreased from cruise, the phugoid mode increases in frequency and becomes unstable while the short-period mode decreases in frequency until at zero damped frequency the roots split, one going to the origin and one going in the direction of the negative axis. At hover, the root which is on the negative axis is a measure of the time required for a perturbation in u to subside, while the root at the origin indicates that since the height damping is negligible a perturbation in w will neither amplify nor subside. In this report the two sets of roots are referred to as the short-period mode and the phugoid mode according to their root locations at high speeds. Thus the two aperiodic roots at hover are referred to as the short-period mode even though at low speeds the period of the phugoid mode is shorter.

3. Effects of Lags in Stability Augmentation System

The effects on the three-degree-of-freedom stick-fixed dynamics of lags in the stability augmentation system were also studied using the root-locus technique. A first-order lag was assumed as an approximation to the total transfer function of the control system hardware. For purposes of calculating the stick-fixed dynamics the lag may be assumed to be in either the forward loop or the feedback loop. The control system model shown in Fig. 19 was used.

If the longitudinal characteristic equation (Eq. (34)) without stability augmentation and without lag is calculated to be

$$A_4\lambda^4 + A_3\lambda^3 + A_2\lambda^2 + A_1\lambda + A_0 = 0 \tag{40}$$

then the characteristic equation with a stability augmentation system having a first-order lag τ_p was derived to be

$$A_5'\lambda^5 + A_4'\lambda^4 + A_3'\lambda^3 + A_2'\lambda^2 + A_1'\lambda + A_0' = 0 \tag{41}$$

Thus the order of the characteristic equation is increased from fourth-order to fifth-order. The coefficients of the new characteristic equation may be easily calculated from the coefficients of Eq. (40) using the following relationships:

$$\begin{aligned}
A_5' &= \tau_p A_4 \\
A_4' &= A_4 + \tau_p A_3 \\
A_3' &= A_3 + \tau_p A_2 - \frac{M_{\delta\beta}}{I_y} K_{\delta\beta} K_p \\
A_2' &= A_2 + \tau_p A_1 - \frac{M_{\delta\beta}}{I_y} \left(K_\theta - K_p C_1\right) K_{\delta\beta} \\
A_1' &= A_1 + \tau_p A_0 - \frac{M_{\delta\beta}}{I_y} \left(K_p C_2 - K_\theta C_1\right) K_{\delta\beta} \\
A_0' &= A_0 - \frac{M_{\delta\beta}}{I_y} K_{\delta\beta} K_\theta C_2 \\
C_1 &= \frac{Z_w}{m} + \frac{X_u}{m} \\
C_2 &= \frac{X_u}{m}\frac{Z_w}{m} - \frac{X_w}{m}\frac{Z_u}{m}
\end{aligned} \tag{42}$$

In Eq. (42), $M_{\delta\beta}/I_y$ is the pitching moment effectiveness of the differential collective pitch in rad/sec^2-deg, $K_{\delta\beta}$ is the longitudinal stick gain in deg/in., K_p is the pitch rate stabilization gain in in.-sec/rad, K_θ is the attitude stabilization gain in in./rad, and τ_p is the first-order lag time constant in sec.

APPENDIX C

THEORETICAL ANALYSIS OF LATERAL-DIRECTIONAL DYNAMICS

This Appendix contains a discussion of the methods used in the theoretical analysis of the lateral-directional dynamics of the aircraft. The complete lateral-directional three-degree-of-freedom characteristic equation is derived and the lateral-directional root-locus diagram is discussed. Changes in the lateral-directional characteristic equation to account for the effects of lags in the lateral-directional stability augmentation system are also discussed. The effects of the flight profiles on the lateral-directional control phasing required to eliminate control coupling are shown, and the effects of incorrect phasing on the dynamics of the aircraft with stability augmentation are discussed.

1. Lateral-Directional Characteristic Equation

The characteristic equation for the lateral-directional motions of the aircraft was derived in a manner analogous to that used in deriving the longitudinal characteristic equation (see Appendix B). Using the axis system shown in Fig. 78, the complete three-degree-of-freedom equations of motion may be written as

$$\begin{aligned} Y_v v + Y_p p + Y_r r - m\dot{v} - mrV_e \cos\alpha_e - mpV_e \sin\alpha_e + mg\phi &= 0 \\ L_v v + L_p p + L_r r - I_x \dot{p} - I_{xz} \dot{r} &= 0 \\ N_v v + N_p p + N_r r - I_z \dot{r} + I_{xz} \dot{p} &= 0 \end{aligned} \tag{43}$$

The underlying assumptions inherent in Eq. (43) are identical with those required for the longitudinal small-perturbation equations of motion with the exception that the initial acceleration along the y-axis is zero. In addition, it is assumed that the angle of attack α_e is small and that the attitude of the aircraft with respect to the horizon θ_e is zero. Note in Fig. 78 that according to the sign convention used herein α_e is positive in a climb. The stability derivatives in Eq. (43) are in the body-axis system.

As in the derivation of the longitudinal characteristic equation (see Eqs. (30) through (33)) substitution of solutions of the form $e^{\lambda t}$ results in a set of simultaneous algebraic equations. In order for a solution to exist, the

determinant of the coefficients of these equations must be equal to zero. Therefore, after dividing through by the mass m and the moments of inertia in roll I_x and yaw I_z, the following equation is obtained:

$$\begin{vmatrix} \left(\frac{Y_v}{m} - \lambda\right) & \left(\frac{Y_p}{m}\lambda - V_e \sin\alpha_e \lambda + g\right) & \left(\frac{Y_r}{m} - V_e \cos\alpha_e\right) \\ \frac{L_v}{I_x} & \left(\frac{L_p}{I_x}\lambda - \lambda^2 + \frac{L_\phi}{I_x}\right) & \left(\frac{L_r}{I_x} + \frac{I_{xz}}{I_x}\lambda\right) \\ \frac{N_v}{I_z} & \left(\frac{N_p}{I_z}\lambda + \frac{I_{xz}}{I_z}\lambda^2\right) & \left(\frac{N_r}{I_r} - \lambda\right) \end{vmatrix} = 0 \qquad (44)$$

Expansion of this determinant then results in the complete three-degree-of-freedom lateral-directional characteristic equation:

$$\begin{aligned} 0 = {} & \left[1 - \frac{I_{xz}^2}{I_x I_z}\right]\lambda^4 + \left[-\frac{Y_v}{m} + \frac{Y_v}{m}\frac{I_{xz}^2}{I_x I_z} - \frac{N_r}{I_z} - \frac{L_p}{I_x} - \frac{N_p}{I_z}\frac{I_{xz}}{I_x} - \frac{L_r}{I_x}\frac{I_{xz}}{I_z}\right]\lambda^3 \\ & + \left[\frac{Y_v}{m}\frac{N_r}{I_z} + \frac{Y_v}{m}\frac{L_p}{I_x} + \frac{Y_v}{m}\frac{N_p}{I_z}\frac{I_{zx}}{I_x} + \frac{Y_v}{m}\frac{L_r}{I_x}\frac{I_{xz}}{I_z} + \frac{L_p}{I_x}\frac{N_r}{I_z} - \frac{L_\phi}{I_x} - \frac{N_p}{I_z}\frac{L_r}{I_x}\right. \\ & \quad - \left(\frac{Y_p}{m} - V_e \sin\alpha_e\right)\frac{L_v}{I_x} - \left(\frac{Y_p}{m} - V_e \sin\alpha_e\right)\frac{N_v}{I_z}\frac{I_{xz}}{I_x} - \left(\frac{Y_r}{m} - V_e \cos\alpha_e\right)\frac{L_v}{I_x}\frac{I_{xz}}{I_z} \\ & \quad \left. - \left(\frac{Y_r}{m} - V_e \cos\alpha_e\right)\frac{N_v}{I_z}\right]\lambda^2 \qquad (45) \\ & + \left[-\frac{Y_v}{m}\frac{L_p}{I_x}\frac{N_r}{I_z} + \frac{Y_v}{m}\frac{L_\phi}{I_x} + \frac{Y_v}{m}\frac{N_p}{I_z}\frac{L_r}{I_x} + \frac{L_\phi}{I_x}\frac{N_r}{I_z} - \left(\frac{Y_p}{m} - V_e \sin\alpha_e\right)\frac{N_v}{I_z}\frac{L_r}{I_x} - g\frac{L_v}{I_x}\right. \\ & \quad - g\frac{N_v}{I_z}\frac{I_{xz}}{I_x} + \left(\frac{Y_p}{m} - V_e \sin\alpha_e\right)\frac{L_v}{I_x}\frac{N_r}{I_z} - \left(\frac{Y_r}{m} - V_e \cos\alpha_e\right)\frac{L_v}{I_x}\frac{N_p}{I_z} \\ & \quad \left. + \left(\frac{Y_r}{m} - V_e \cos\alpha_e\right)\frac{N_v}{I_z}\frac{L_p}{I_x}\right]\lambda \\ & + \left[-\frac{Y_v}{m}\frac{L_\phi}{I_x}\frac{N_r}{I_z} + \left(\frac{Y_r}{m} - V_e \cos\alpha_e\right)\frac{N_v}{I_z}\frac{L_\phi}{I_x} - g\frac{N_v}{I_z}\frac{L_r}{I_x} + g\frac{L_v}{I_z}\frac{N_r}{I_z}\right] \end{aligned}$$

An IBM 7090 digital computer program was prepared which would accept the initial conditions and stability derivatives in the body-axis system, calculate the coefficients of the lateral-directional characteristic equation, and solve for the roots using a root-extraction program which had previously been prepared at the UAC Research Laboratories.

It should be mentioned that the stability derivative L_ϕ was included in Eq. (45) but was retained in only a limited number of calculations in which the effect of roll attitude stabilization was investigated. For all other calculations L_ϕ was set equal to zero. The lateral-directional transfer functions presented in Appendix D were derived assuming L_ϕ equal to zero.

2. Lateral-Directional Root-Locus Diagrams

The real and imaginary parts of the roots of the lateral-directional characteristic equation have the same significance as was previously discussed for the roots of the longitudinal characteristic equation (see Section VIII. B. 2. of Appendix B). The variations of the stick-fixed dynamics during a flight profile, and the effects of stability augmentation, of changes in the stability derivatives of the aircraft, and of lags in the stability augmentation system, may also be analyzed conveniently by means of root-locus diagrams.

A sketch of the root-locus diagram for the tandem tilting ducted propeller aircraft which was used as a basis for the present study is shown in Fig. 79. It should be emphasized that the root locations shown in Fig. 79 do not represent satisfactory dynamics for the aircraft without stability augmentation. The solution of the lateral-directional characteristic equation consists of two real negative roots and a complex conjugate pair. The larger of the two real roots is the roll convergence mode and is a measure of the roll rate response of the aircraft following an input to the lateral control stick. An increase in roll rate damping will cause this root to move to the left. Therefore, if the lateral control power is held constant while the roll convergence root moves to the left, the steady state roll rate for a given lateral stick input will decrease and the time required to reach essentially steady state conditions will be decreased.

The smaller of the two real roots represents the spiral stability mode. When this root is positive the aircraft is spirally unstable in that if the aircraft is suddenly banked from a level flight condition the bank angle will tend to increase and a continuously tightening spiral turn will develop in the direction of the bank. A small amount of spiral instability is not necessarily undesirable since it increases the initial response of the aircraft in turns. However, for satisfactory handling qualities, the spiral stability root should be close to the origin. For the tandem tilting ducted propeller aircraft, the spiral stability increased during transitions from hover (Fig. 79) since the strong dihedral effect overpowered the decreasing directional static stability.

The complex conjugate roots represent the familiar Dutch roll mode. The Dutch roll mode was found to be unstable at all flight conditions for the basic aircraft without stability augmentation. As shown in Fig. 79, the frequency of the Dutch roll motion increased with increasing speed until near the end of transition. Over this speed range, time to double amplitude decreased slightly and then increased to a maximum of about 15 sec at the end of transition. As the speed increased with further small changes of duct incidence angle, both frequency and time to double amplitude decreased. Increasing the altitude for steady level flight at a constant speed had little effect on frequency but sharply decreased the time to double amplitude.

The reciprocal of the number of cycles to damp to half amplitude $1/C_{1/2}$ is a parameter which corresponds to the damping ratio ζ in the pitch plane. Lines of constant $1/C_{1/2}$ radiate from the origin of the root-locus diagram as shown in Fig. 79. The value of $1/C_{1/2}$ may be calculated from the real and imaginary parts of the Dutch roll roots using the following relationship:

$$\frac{1}{C_{1/2}} = \frac{2\pi/\omega}{T_{1/2}} = \frac{-9.06\,(-\zeta\omega_n)}{\omega} \qquad (46)$$

It is desirable to have the Dutch roll mode as heavily damped as possible. When the damping is light, the value of $1/C_{1/2}$ as a function of the ratio of roll angle to effective sideslip velocity $(1/\sqrt{\sigma})|\phi/v|$ is sometimes used as a criterion for acceptability (Ref. 18). The equation for calculating this roll parameter is presented in Section VIII. D. 4. of Appendix D. In the present study, calculations of $1/C_{1/2}$ vs $(1/\sqrt{\sigma})|\phi/v|$ were made for steady level flight conditions but the flight simulator was used as the primary means of judging the acceptability of the Dutch roll damping at all flight conditions.

3. Effects of Incorrect Phasing Gains on Lateral-Directional Dynamics

The effects of incorrect phasing gains of the lateral-directional controls were also studied systematically at one flight condition. The general lateral-directional control system model shown in Fig. 30 was used as a basis for studying the effects of stability augmentation, control lags and incorrect compensatory phasing on the dynamics and for deriving the lateral-directional transfer functions. In Fig. 30, K_R and K_Y are the gains in the roll rate and yaw rate loops of the stability augmentation system, respectively, in in.-sec/rad. The lateral control stick gain is $K_{\Delta\delta\beta}$ in degrees of differential collective pitch per inch of stick deflection, and $K_{\Delta\delta_V}$ is the pedal gain in degrees of differential vanes per inch of pedal deflection. The compensatory gains are G_{VL} (degrees of differential vanes per degree differential collective pitch commanded by the lateral control stick) and $G_{\beta P}$ (degrees of differential collective pitch per degree of differential vanes commanded by the pedals).

The stability derivatives in the characteristic equation (Eq. (45)) must be modified according to the gains in the stability augmentation system and the phasing gains:

$$\frac{L_p}{I_x} = \left(\frac{L_p}{I_x}\right)_{\substack{\text{BASIC}\\\text{AIRCRAFT}}} + K_{\Delta\delta_\beta} K_R \left[\frac{L_{\Delta\delta_\beta}}{I_x} + f_1 G_{VL} \frac{L_{\Delta\delta_V}}{I_x}\right]$$

$$\frac{N_r}{I_z} = \left(\frac{N_r}{I_z}\right)_{\substack{\text{BASIC}\\\text{AIRCRAFT}}} + K_{\Delta\delta_V} K_Y \left[\frac{N_{\Delta\delta_V}}{I_z} + f_2 G_{\beta P} \frac{N_{\Delta\delta_\beta}}{I_z}\right] \qquad (47)$$

$$\frac{L_r}{I_x} = \left(\frac{L_r}{I_x}\right)_{\substack{\text{BASIC}\\\text{AIRCRAFT}}} + K_{\Delta\delta_V} K_Y \left[\frac{L_{\Delta\delta_V}}{I_x} + f_2 G_{\beta P} \frac{L_{\Delta\delta_\beta}}{I_x}\right]$$

$$\frac{N_p}{I_z} = \left(\frac{N_p}{I_z}\right)_{\substack{\text{BASIC}\\\text{AIRCRAFT}}} + K_{\Delta\delta_\beta} K_R \left[\frac{N_{\Delta\delta_\beta}}{I_z} + f_1 G_{VL} \frac{N_{\Delta\delta_V}}{I_z}\right]$$

In Eq. (47), f_1 and f_2 represent the fractions of the correct phasing gains G_{VL} and $G_{\beta P}$.

The effects of f_1 and f_2 from 0.7 to 1.3 independently and simultaneously were calculated for steady level flight with stability augmentation system gains of 50% of those finally chosen as satisfactory in the flight simulator program. These gains resulted in a level of artificial roll rate stabilization of $L_P/I_X = -.87$ and a level of artificial yaw rate stabilization of $N_r/I_Z = -.17$ for f_1 and f_2 equal to 1.0. Because of the low gain K_Y, the effect of f_2 (in the yaw rate loop) on the Dutch roll and roll convergence roots was found to be negligible and its effect on the spiral stability root was very small (increasingly stable as f_2 increased from 0.7 to 1.3). The effect of f_1 on the dynamics was larger, due in part to the higher roll rate stabilization gain K_R. Figure 80 shows the combined effect of simultaneously varying both f_1 and f_2 from 0.7 to 1.3 (i.e., 70% of the correct phasing to 130% of the correct phasing). As f_1 and f_2 were increased, the frequency of the Dutch roll oscillation decreased by about 5%; the effects on the roll convergence and spiral stability roots also were small. These results, although not fully conclusive, seem to indicate that at flight conditions where high gains are required with the result that the weaker of the two controls (usually the differential vanes) becomes saturated under normal operating conditions, it may be acceptable to decrease the phasing gain of the weaker control. This would result in higher roll and yaw rates required for saturation of the system.

4. Effect of Lags in Stability Augmentation System

The effects on the stick-fixed dynamics of lags in the roll and yaw lateral-directional stability augmentation system were also studied. As was done for the longitudinal stability augmentation system, the appropriate modifications were made in the characteristic equation and the effects of first-order lags on the root locations were calculated. Unfortunately, the resulting characteristic equation is considerably more complex than the modified longitudinal characteristic equation.

For the purpose of analysis the model control and stability augmentation system shown in Fig. 30 was used. In Fig. 30, τ_Y and τ_R are the first-order time lags in the yaw and roll control systems. Note that in calculating the stick-fixed dynamics the lags may be in either the forward loop (as shown) or the feedback loop. The compensatory phasing gains G_{VL} and $G_{\beta P}$ were assumed to be exact. The transfer functions of the basic aircraft are presented in Appendix D, and other symbols appearing in Fig. 30 were discussed in the preceding section of this Appendix.

The lateral-directional characteristic equation without stability augmentation and without lags (i.e., with K_R, K_Y, τ_R and τ_Y all equal to zero) is given by

$$B_4\lambda^4 + B_3\lambda^3 + B_2\lambda^2 + B_1\lambda + B_0 = 0 \tag{48}$$

where the coefficients B_0 through B_4 are calculated using Eq. (45), and the corresponding characteristic equation with stability augmentation and with the two first-order lags is of sixth-order:

$$B_6'\lambda^6 + B_5'\lambda^5 + B_4'\lambda^4 + B_3'\lambda^3 + B_2'\lambda^2 + B_1'\lambda + B_0' = 0 \tag{49}$$

The coefficients of Eq. (49) may be calculated from the following expressions:

$$B_6' = B_4(\tau_Y \tau_R)$$

$$B_5' = B_4(\tau_Y + \tau_R) + B_3(\tau_Y \tau_R)$$

$$B_4' = B_4 + B_3(\tau_Y + \tau_R) + B_2(\tau_Y \tau_R) + \pi K_R \tau_Y + \Lambda K_Y \tau_R$$

$$B_3' = B_3 + B_2(\tau_Y + \tau_R) + B_1(\tau_Y \tau_R) + \pi K_R + \Lambda K_Y - \pi K_R \tau_Y \left(\frac{Y_v}{m} + \frac{N_r}{I_z}\right) - \Lambda K_Y \tau_R \left(\frac{Y_v}{m} + \frac{L_p}{I_x}\right)$$

$$\begin{aligned} B_2' = {} & B_2 + B_1(\tau_Y + \tau_R) + B_0(\tau_Y \tau_R) + \pi K_R \Lambda K_Y - \pi K_R \left(\frac{Y_v}{m} + \frac{N_r}{I_z}\right) \\ & - \pi K_R \tau_Y \left(\frac{Y_v}{m} \frac{N_r}{I_z} - \frac{N_v}{I_z}\left[\frac{Y_r}{m} - V_e \cos \alpha_e\right]\right) - \Lambda K_Y \left(\frac{Y_v}{m} + \frac{L_p}{I_x}\right) \\ & + \Lambda K_Y \tau_R \left(\frac{Y_v}{m} \frac{L_p}{I_x} - \frac{L_v}{I_x}\left[\frac{Y_p}{m} - V_e \sin \alpha_e\right]\right) \end{aligned} \qquad (50)$$

$$\begin{aligned} B_1' = {} & B_1 + B_0(\tau_Y + \tau_R) - \pi K_R \Lambda K_Y \frac{Y_v}{m} + \pi K_R \left(\frac{Y_v}{m} \frac{N_r}{I_z} - \frac{N_v}{I_z}\left[\frac{Y_r}{m} - V_e \cos \alpha_e\right]\right) \\ & + \Lambda K_Y \left(\frac{Y_v}{m} \frac{L_p}{I_x} - \frac{L_v}{I_x}\left[\frac{Y_p}{m} - V_e \sin \alpha_e\right]\right) - \Lambda K_Y \tau_R g \frac{L_v}{I_x} \end{aligned}$$

$$B_0' = B_0 - \Lambda K_Y g \frac{L_v}{I_x}$$

$$\pi = K_{\Delta\delta\beta}\left[\frac{L_{\Delta\delta\beta}}{I_x} + G_{VL}\frac{L_{\Delta\delta_v}}{I_x}\right]$$

$$\Lambda = K_{\Delta\delta_v}\left[\frac{N_{\Delta\delta_v}}{I_z} + G_{\beta P}\frac{N_{\Delta\delta\beta}}{I_z}\right]$$

5. Lateral-Directional Control Phasing

The phasing gain programs for alleviating roll-yaw control coupling were determined from plots of the exact phasing gains required to eliminate coupling on transition flight profiles and at cruise conditions. The exact phasing gains were calculated from the rolling moment and yawing moment effectiveness of differential collective pitch and differential vanes. The yawing moment per inch of lateral control stick is given by

$$\frac{N_{\delta_L}}{I_z} = K_{\Delta\delta\beta}\left[\frac{N_{\Delta\delta\beta}}{I_z} + G_{VL}\frac{N_{\Delta\delta_V}}{I_z}\right] \tag{51}$$

where $K_{\Delta\delta\beta}$ is the lateral control stick gain (degrees of differential collective pitch per inch of stick displacement), G_{VL} is the phasing gain (degrees of differential vanes per degree of differential collective pitch), and $N_{\Delta\delta\beta}/I_z$ and $N_{\Delta\delta_V}/I_z$ are the yawing moments per degree of differential collective pitch and per degree of differential vane deflection, respectively. For exact phasing (i.e., elimination of the yawing moment due to a lateral control stick input), Eq. (51) must equal zero. This results in the following expression for the phasing gain G_{VL} :

$$G_{VL} = -\frac{N_{\Delta\delta\beta}/I_z}{N_{\Delta\delta_V}/I_z} \tag{52}$$

A similar analysis yields the following expression for the phasing gain $G_{\beta P}$ (degrees of differential collective pitch per degree of differential vane deflection):

$$G_{\beta P} = -\frac{L_{\Delta\delta_V}/I_x}{L_{\Delta\delta\beta}/I_x} \tag{53}$$

Figure 53 shows the exact values of G_{VL} required to eliminate coupling at all flight conditions which were studied and also shows the final gain phasing program which was selected during the flight simulator program. The phasing required during transitions (all at sea level) is affected only a small amount by the particular transition flight profile, with the exception of the rapid decelerating descent at reduced propeller rotational speed. At high speeds, however, the effect of altitude on the values of the phasing gains which are required is appreciable. This is caused by a difference in the effects of decreasing ambient density ρ on the change in propeller thrust per degree of change in blade angle and on the forces acting on the vanes per degree of deflection angle. The change in thrust per degree of change in blade angle decreases in direct proportion to ρ. The forces acting on the vanes per degree of deflection

are directly proportional to the exit dynamic pressure which is dependent upon the free-stream dynamic pressure q_0, the propeller thrust coefficient K_T, and the advance ratio J_0:

$$q_e = q_0\left[\frac{\cos^2 i_D}{2} + \cos i_D\left(\frac{\cos^2 i_D}{4} + \frac{4K_T}{\pi J_0^2}\right)^{1/2} + \frac{4K_T}{\pi J_0^2}\right] \tag{54}$$

Analysis of Eq. (54) reveals that for constant advance ratio and constant duct incidence angle, the change in thrust coefficient required for steady level flight at increasing altitude causes the exit dynamic pressure to decrease slightly less rapidly than $\sqrt{\rho}$. Thus the differential vane effectiveness decreases less rapidly with increasing altitude than does the differential collective pitch effectiveness.

The final gain program for G_{VL} which was selected is also shown in Fig. 53. This program provides exact phasing at the high-speed, high-altitude flight conditions and results in some coupling at the high-speed, low-altitude flight conditions. As discussed in Section III. F. 3., the resulting coupling was found to be quite noticeable in the flight simulator program but did not seem to be objectionable.

Figure 54 shows the exact values of $G_{\beta P}$ required to eliminate rolling moment due to pedal deflection and also shows the final gain phasing program. As was the case for the gain G_{VL} the phasing required varied little between transition flight profiles but was affected appreciably by altitude at the high-speed flight conditions. The gain program which was selected provides exact phasing at the 250-knot cruise design points at both sea level and 20,000 ft and provides nearly exact phasing at 178 knots at 20,000 ft.

APPENDIX D

SUMMARY OF TRANSFER FUNCTIONS

The transfer functions which describe the responses of the aircraft to pilot inputs to the longitudinal, lateral, directional, and collective (altitude) controls are presented in this Appendix. These transfer functions may be used to calculate the transient response of other VTOL aircraft which satisfy the conditions assumed in the derivations of the longitudinal and lateral-directional characteristic equations (see Appendixes B and C). Application to rotary-wing aircraft would require the additional assumptions that the rotor reacts instantaneously to changes in u, w, and θ and that the rotational speed of the rotor remains constant. Additional restrictions on the application of these transfer functions to other types of VTOL aircraft are mentioned in the following paragraphs.

In the present study the transfer functions were used only for calculating the transient response to control inputs for the hovering flight condition. As previously discussed, the flight simulator program was used to assure that the closed loop response was acceptable over the entire range of flight conditions.

1. Response to Longitudinal and Collective Stick Inputs

The response of the basic aircraft without stability augmentation to a longitudinal control stick input is given by the following transfer functions:

$$\frac{\bar{\theta}}{\bar{\delta}_s} = \frac{-K_{\delta\beta}\frac{M_{\delta\beta}}{I_y}\left[S^2 - \left(\frac{X_u}{m} + \frac{Z_w}{m}\right)S + \left(\frac{X_u}{m}\frac{Z_w}{m} - \frac{X_w}{m}\frac{Z_u}{m}\right)\right]}{\text{LONGITUDINAL CHARACTERISTIC EQUATION}}$$

$$\frac{\bar{u}}{\bar{\delta}_s} = \frac{-K_{\delta\beta}\frac{M_{\delta\beta}}{I_y}\left[\frac{X_q}{m}S^2 + \left(\frac{X_w}{m}V_e + \frac{Z_q}{m}\frac{X_w}{m} - \frac{X_q}{m}\frac{Z_w}{m} - g\right)S + g\frac{Z_w}{m}\right]}{\text{LONGITUDINAL CHARACTERISTIC EQUATION}} \qquad (55)$$

$$\frac{\bar{w}}{\bar{\delta}_s} = \frac{-K_{\delta\beta}\frac{M_{\delta\beta}}{I_y}\left[\left(\frac{Z_q}{m} + V_e\right)S^2 - \left(\frac{X_u}{m}V_e - \frac{X_u}{m}\frac{Z_q}{m}\right)S + \frac{1}{g}\frac{X_w}{m}\frac{M_u g}{I_y}\right]}{\text{LONGITUDINAL CHARACTERISTIC EQUATION}}$$

In Eq. (55) the barred symbols indicate the Laplace transforms of pitch attitude change θ in radians, longitudinal control stick input δ_s in inches, and changes in velocity u and w in ft/sec from the initial equilibrium flight conditions. The aircraft is assumed to be a trimmed equilibrium flight condition at a velocity V_e, pitch attitude with respect to the horizon θ_e, and angle of attack α_e (see Fig. 75). The initial conditions are that the values of θ, u, and w, and of the derivatives of these variables are zero. All stability derivatives are in the stability-axes system. The term K_{δ_β} is the control stick gain in degrees of differential collective pitch per inch of stick displacement, and M_{δ_β}/I_y is the pitching moment effectiveness of differential collective pitch of the fore and aft ducted propellers in rad/sec^2-deg. The denominator in Eq. (55) is the longitudinal characteristic equation (Eq. (34)) with the Laplace operator s substituted for λ.

Application of Eq. (55) is restricted primarily to tandem VTOL aircraft since the transfer functions were derived assuming that differential collective pitch results in a pure pitching moment (i.e., no X or Z forces associated with the applied control moment).

The response of the aircraft to a collective pitch stick input δ_c at hover is given by the following set of transfer functions:

$$\frac{\bar{w}}{\bar{\delta}_c} = \frac{-K_c \frac{Z_\beta}{m}\left[S^3 + \left(-\frac{M_q}{I_y} - \frac{X_u}{m}\right)S^2 + \left(\frac{X_u}{m}\frac{M_q}{I_y} - \frac{1}{g}\frac{X_q}{m}\frac{M_u g}{I_y} - \frac{M_\theta}{I_y}\right)S + \left(\frac{X_u}{m}\frac{M_\theta}{I_y} + \frac{M_u g}{I_y}\right)\right]}{\text{LONGITUDINAL CHARACTERISTIC EQUATION}}$$

$$\frac{\bar{u}}{\bar{\delta}_c} = \frac{-K_c \frac{Z_\beta}{m}\left[\frac{X_w}{m}S^2 + \left(-\frac{X_w}{m}\frac{M_q}{I_y} + \frac{1}{g}\frac{X_q}{m}\frac{M_w g}{I_y}\right)S + \left(-\frac{M_w g}{I_y} - \frac{X_w}{m}\frac{M_\theta}{I_y}\right)\right]}{\text{LONGITUDINAL CHARACTERISTIC EQUATION}} \qquad (56)$$

$$\frac{\bar{\theta}}{\bar{\delta}_c} = \frac{-K_c \frac{Z_\beta}{m}\left[\frac{1}{g}\frac{M_w g}{I_y}S + \frac{X_w}{m}\frac{M_u g}{I_y} - \frac{1}{g}\frac{X_u}{m}\frac{M_w g}{I_y}\right]}{\text{LONGITUDINAL CHARACTERISTIC EQUATION}}$$

The transfer functions in Eq. (56) were derived for the case where a collective pitch change does not result in a pitching moment (i.e., for the hovering case when the center of gravity is located midway between the forward and aft ducted propellers). The term K_c is the collective pitch stick gain in deg/in., and Z_β/m is the normal force effectiveness of collective pitch changes.

For the tandem tilting ducted propeller configuration at hover and low speeds the aerodynamic coupling of vertical speed w with the other two variables u and θ

was weak; therefore the transfer function for w with the stability derivative X_q set equal to zero will give an adequate description of the motion of the aircraft following a change in the position of the collective pitch stick. Similarly, the derivatives X_q and Z_q were negligible and the transfer functions for the response to longitudinal control stick inputs (Eq. (55)) could be simplified considerably by assuming these derivatives to be equal to zero.

Equations (55) and (56) may also be used as transfer functions for the response of the aircraft with pitch rate stabilization and attitude stabilization by making appropriate changes in M_q/I_y and M_θ/I_y. Using the control system model shown in Fig. 19 without a lag ($\tau_p = 0$), the values of these derivatives become

$$\frac{M_q}{I_y} = \left(\frac{M_q}{I_y}\right)_{\substack{\text{BASIC}\\ \text{AIRCRAFT}}} + K_p K_{\delta\beta} \frac{M_{\delta\beta}}{I_y} \tag{57}$$

and

$$\frac{M_\theta}{I_y} = K_\theta K_{\delta\beta} \frac{M_{\delta\beta}}{I_y} \tag{58}$$

Equation (57) expresses the equivalent total pitch rate damping (the sum of the aerodynamic damping of the basic aircraft and the damping due to pitch rate stabilization). Equation (58) includes only the attitude stabilization term since the natural attitude stability of the aircraft is zero (attitude stability is not to be confused with static stability with respect to angle of attack which is represented by the stability parameter $M_w g/I_y$). When equivalent values of M_q/I_y and M_θ/I_y are calculated from Eqs. (57) and (58) and are substituted into both the denominators and the numerators of Eqs. (55) and (56), then these transfer functions are also valid for computing the transient response of the aircraft with stability augmentation. Although substitution and recalculation of the coefficients of the characteristic equation would be tedious if done by hand, it was readily accomplished using the IBM 7090 digital computer program which was prepared during the present study.

2. Response to Lateral Stick and Pedal Inputs

The transfer functions which describe the roll, yaw, and sideslip responses of the aircraft to pilot inputs to the lateral control stick and the pedals were derived in a manner similar to that used in the pitch plane.

For the basic aircraft without stability augmentation about the roll and yaw axes, and assuming that the compensatory phasing of differential collective pitch and vane deflection is exact (e.g., a lateral stick displacement will result in a

pure rolling moment and no yawing moment), the complete transfer functions for roll angle, yaw rate, and sideslip velocity due to a lateral stick input are:

$$\frac{\bar{\phi}}{\bar{\delta}_L} = \frac{K_{\Delta\delta_\beta}\left(\frac{L_{\Delta\delta_\beta}}{I_x} + G_{VL}\frac{L_{\Delta\delta_V}}{I_x}\right)\left[S^2 - \left(\frac{N_r}{I_z} + \frac{Y_v}{m}\right)S + \left(\frac{N_r}{I_z}\frac{Y_v}{m} - \frac{N_v}{I_z}\frac{Y_r}{m} + V_e\cos\alpha_e\frac{N_v}{I_z}\right)\right]}{\text{LATERAL - DIRECTIONAL CHARACTERISTIC EQUATION}}$$

$$\frac{\bar{r}}{\bar{\delta}_L} = \frac{K_{\Delta\delta_\beta}\left(\frac{L_{\Delta\delta_\beta}}{I_x} + G_{VL}\frac{L_{\Delta\delta_V}}{I_x}\right)\frac{I_{xz}}{I_z}\left[S^3 + \left(\frac{N_p}{I_z}\frac{I_z}{I_{xz}} - \frac{Y_v}{m}\right)S^2 - \frac{I_z}{I_{xz}}\left(\frac{Y_v}{m}\frac{N_p}{I_z} + \frac{Y_p}{m}\frac{N_v}{I_z} - V_e\sin\alpha_e\frac{N_v}{I_z}\right)S - g\frac{I_z}{I_{xz}}\frac{N_v}{I_z}\right]}{\text{LATERAL - DIRECTIONAL CHARACTERISTIC EQUATION}} \quad (59)$$

$$\frac{\bar{v}}{\bar{\delta}_L} = \frac{K_{\Delta\delta_\beta}\left(\frac{L_{\Delta\delta_\beta}}{I_x} + G_{VL}\frac{L_{\Delta\delta_V}}{I_x}\right)\left[\left(\frac{Y_p}{m} - V_e\sin\alpha_e + \frac{Y_r}{m}\frac{I_{xz}}{I_z} - V_e\cos\alpha_e\frac{I_{xz}}{I_z}\right)S^2 + \left(\frac{Y_r}{m}\frac{N_p}{I_z} - V_e\cos\alpha_e\frac{N_p}{I_z} - \frac{Y_p}{m}\frac{N_r}{I_z} + V_e\sin\alpha_e\frac{N_r}{I_z} + g\right)S - g\frac{N_r}{I_z}\right]}{\text{LATERAL - DIRECTIONAL CHARACTERISTIC EQUATION}}$$

The corresponding transfer functions for response to a pedal input are:

$$\frac{\bar{\phi}}{\bar{\delta}_P} = \frac{K_{\Delta\delta_V}\left(\frac{N_{\Delta\delta_V}}{I_z} + G_{\beta P}\frac{N_{\Delta\delta_\beta}}{I_z}\right)\left[-\frac{I_{xz}}{I_x}S^2 + \left(-\frac{L_r}{I_x} + \frac{Y_v}{m}\frac{I_{xz}}{I_x}\right)S + \left(\frac{Y_v}{m}\frac{L_r}{I_x} + \frac{L_v}{I_x}\frac{Y_r}{m} - V_e\cos\alpha_e\frac{L_v}{I_x}\right)\right]}{\text{LATERAL - DIRECTIONAL CHARACTERISTIC EQUATION}}$$

$$\frac{\bar{r}}{\bar{\delta}_P} = \frac{K_{\Delta\delta_V}\left(\frac{N_{\Delta\delta_V}}{I_z} + G_{\beta P}\frac{N_{\Delta\delta_\beta}}{I_z}\right)\left[S^3 - \left(\frac{Y_v}{m} + \frac{L_p}{I_x}\right)S^2 + \left(\frac{Y_v}{m}\frac{L_p}{I_x} - \frac{L_\phi}{I_x} - \frac{L_v}{I_x}\frac{Y_p}{m} + V_e\sin\alpha_e\frac{L_v}{I_x}\right)S + \left(\frac{Y_v}{m}\frac{L_\phi}{I_x} - g\frac{L_v}{I_x}\right)\right]}{\text{LATERAL - DIRECTIONAL CHARACTERISTIC EQUATION}} \quad (60)$$

$$\frac{\bar{v}}{\bar{\delta}_P} = \frac{K_{\Delta\delta_V}\left(\frac{N_{\Delta\delta_V}}{I_z} + G_{\beta P}\frac{N_{\Delta\delta_\beta}}{I_z}\right)\left[\left(\frac{Y_p}{m}\frac{I_{xz}}{I_x} - V_e\sin\alpha_e\frac{I_{xz}}{I_x} + \frac{Y_r}{m} - V_e\cos\alpha_e\right)S^2 + \left(\frac{L_r}{I_x}\frac{Y_p}{m} - V_e\sin\alpha_e\frac{L_r}{I_x} + g\frac{I_{xz}}{I_x} - \frac{Y_r}{m}\frac{L_p}{I_x} + V_e\cos\alpha_e\frac{L_p}{I_x}\right)S + \left(\frac{L_r}{I_x}g - \frac{Y_r}{m}\frac{L_\phi}{I_x} + V_e\cos\alpha_e\frac{L_\phi}{I_x}\right)\right]}{\text{LATERAL - DIRECTIONAL CHARACTERISTIC EQUATION}}$$

Equations (59) and (60) were derived using the control and stability augmentation system model shown in Fig. 30 with the lag time constants τ_Y and τ_R equal to zero. The barred symbols indicate the Laplace transforms of roll angle ϕ in radians, yaw rate r in rad/sec, sideslip velocity v in ft/sec, lateral control stick displacement δ_L in inches, and pedal displacement δ_P in inches. For these transfer functions the aircraft is assumed to be in a trimmed equilibrium flight condition at a velocity V_e, an angle of attack α_e, and at a pitch attitude with respect to the horizon θ_e equal to zero (see Fig. 78). The initial conditions on ϕ, r and v are also zero. It is also assumed that application of differential collective pitch and differential vanes does not cause a change in the net side force. In Eqs. (59) and (60), $K_{\Delta\delta_\beta}$ and $K_{\Delta\delta_V}$ are the gains of the lateral control stick and pedals in degrees of differential collective pitch per inch of stick displacement and in degrees of differential vanes per inch of pedal displacement, respectively. The gains G_{VL} and $G_{\beta P}$ are the phasing gains in degrees of differential vanes per degree of differential collective pitch called for, and in degrees of differential collective pitch per degree of differential vanes called for, respectively. The gains K_R and K_Y are the roll rate and yaw rate stabilization gains in in./rad-sec. The stability derivatives $L_{\Delta\delta_\beta}/I_x$, $L_{\Delta\delta_V}/I_x$, $N_{\Delta\delta_\beta}/I_z$, and $N_{\Delta\delta_V}/I_z$ express the rolling moment and yawing moment effectiveness of differential collective pitch and differential vanes in rad/sec^2.

Equations (59) and (60) may also be used to represent the transient response of the aircraft with rate stability augmentation (i.e., L_ϕ equal to zero) when appropriate changes are made in the damping derivatives, as was previously described for the pitch transfer functions. The adjusted values of these derivatives are given by

$$\frac{L_p}{I_x} = \left(\frac{L_p}{I_x}\right)_{\substack{\text{BASIC}\\ \text{AIRCRAFT}}} + K_R K_{\Delta\delta_\beta}\left[\frac{L_{\Delta\delta_\beta}}{I_x} + G_{VL}\frac{L_{\Delta\delta_V}}{I_x}\right] \tag{61}$$

and

$$\frac{N_r}{I_z} = \left(\frac{N_r}{I_z}\right)_{\substack{\text{BASIC}\\ \text{AIRCRAFT}}} + K_Y K_{\Delta\delta_V}\left[\frac{N_{\Delta\delta_V}}{I_z} + G_{\beta P}\frac{N_{\Delta\delta_\beta}}{I_z}\right] \tag{62}$$

The values of the derivatives given by Eqs. (61) and (62) must be substituted into both the denominator (the lateral-directional characteristic equation) and the numerator.

In order to calculate the stick-fixed dynamics in the general case in which the phasing gains G_{VL} and $G_{\beta P}$ are not exact, additional modifications were made in the stability derivatives. When the phasing is not exact, coupling will result in

both the control and the stability augmentation systems. Coupling in the stability augmentation system results in artificially induced yawing moments due to roll rate and rolling moments due to yaw rate, thereby necessitating modifications to the stability derivatives N_p and L_r :

$$\frac{N_p}{I_z} = \left(\frac{N_p}{I_z}\right)_{\substack{\text{BASIC}\\ \text{AIRCRAFT}}} + K_R K_{\Delta\delta_\beta}\left[\frac{N_{\Delta\delta_\beta}}{I_z} + G_{VL}\frac{N_{\Delta\delta_V}}{I_z}\right] \tag{63}$$

and

$$\frac{L_r}{I_x} = \left(\frac{L_r}{I_x}\right)_{\substack{\text{BASIC}\\ \text{AIRCRAFT}}} + K_Y K_{\Delta\delta_V}\left[\frac{L_{\Delta\delta_V}}{I_x} + G_{\beta P}\frac{L_{\Delta\delta_\beta}}{I_x}\right] \tag{64}$$

Therefore, to calculate the stick-fixed dynamics, the modifications given by Eqs. (63) and (64) were incorporated into the characteristic equation analysis.

The complete lateral-directional transfer functions for the aircraft with cross-coupling of the controls were not derived in the present study. The determinants for the numerators of the complete transfer functions were set up, but only the highest-order terms (either s^2 or s^3) were evaluated for use with the Laplace initial value theorem, as described in the next section of this Appendix.

3. Laplace Initial and Final Value Theorems

The Laplace initial and final value theorems may be applied to the foregoing transfer functions when the closed-loop system is stable (i.e., when the roots of the characteristic equation are in the left half-plane of the root-locus diagrams). If $F(s)$ is the transfer function of output to input, then the initial value theorem is

$$\lim_{t\to 0} F(t) = \lim_{s\to\infty} sF(s) \tag{65}$$

and the final value theorem is

$$\lim_{t\to\infty} F(t) = \lim_{s\to 0} sF(s) \tag{66}$$

In the present study, the Laplace initial value theorem was applied to the lateral-directional transfer functions to obtain expressions for the initial rolling

and yawing accelerations following step control inputs in the presence of control coupling. First, the coefficients of highest-order terms in the numerators of the transfer functions for coupled control inputs were derived. Then the coefficients of the highest-order terms in the numerators of the corresponding rolling and yawing acceleration transfer functions were obtained by multiplying these coefficients by the Laplace operator s or s^2, since $\ddot{\bar{\phi}} = s^2\bar{\phi}$ and $\dot{\bar{r}} = s\bar{r}$. The initial rolling and yawing accelerations following a step input to the lateral control stick, in rad/sec^2-in., were then derived using the Laplace initial value theorem:

$$\frac{\ddot{\phi}_0}{\delta_L} = \lim_{s\to\infty} \frac{s\ddot{\bar{\phi}}}{s} = \lim_{s\to\infty} s^2\bar{\phi}$$

$$= \frac{K_{\Delta\delta_\beta}\left[\left(\frac{L_{\Delta\delta_\beta}}{I_x} + G_{VL}\frac{L_{\Delta\delta_V}}{I_x}\right) + \frac{I_{xz}}{I_x}\left(\frac{N_{\Delta\delta_\beta}}{I_z} + G_{VL}\frac{N_{\Delta\delta_V}}{I_z}\right)\right]}{1 - \frac{I_{xz}^2}{I_x I_z}} \qquad (67)$$

$$\frac{\dot{r}_0}{\delta_L} = \lim_{s\to\infty} \frac{s\dot{\bar{r}}}{s} = \lim_{s\to\infty} s\bar{r}$$

$$= \frac{K_{\Delta\delta_\beta}\left[\left(\frac{N_{\Delta\delta_\beta}}{I_z} + G_{VL}\frac{N_{\Delta\delta_V}}{I_z}\right) + \frac{I_{xz}}{I_z}\left(\frac{L_{\Delta\delta_\beta}}{I_x} + G_{VL}\frac{L_{\Delta\delta_V}}{I_x}\right)\right]}{1 - \frac{I_{xz}^2}{I_x I_z}}$$

In a similar manner, the initial yawing and rolling accelerations following a step input to the pedals, in rad/sec^2-in., were derived:

$$\frac{\dot{r}_0}{\delta_P} = \frac{K_{\Delta\delta_V}\left[\left(\frac{N_{\Delta\delta_V}}{I_z} + G_{\beta P}\frac{N_{\Delta\delta_\beta}}{I_z}\right) + \frac{I_{xz}}{I_z}\left(\frac{L_{\Delta\delta_V}}{I_x} + G_{\beta P}\frac{L_{\Delta\delta_\beta}}{I_x}\right)\right]}{1 - \frac{I_{xz}^2}{I_x I_z}}$$

$$\frac{\ddot{\phi}_0}{\delta_P} = \frac{K_{\Delta\delta_V}\left[\left(\frac{L_{\Delta\delta_V}}{I_x} + G_{\beta P}\frac{L_{\Delta\delta_\beta}}{I_x}\right) + \frac{I_{xz}}{I_x}\left(\frac{N_{\Delta\delta_V}}{I_z} + G_{\beta P}\frac{N_{\Delta\delta_\beta}}{I_z}\right)\right]}{1 - \frac{I_{xz}^2}{I_x I_z}} \qquad (68)$$

The Laplace final value theorem was applied to study the effect of attitude stabilization and pitching moment due to collective pitch change on the steady-state rate of climb following a step input in collective pitch. In this case, the steady-state rate of climb (positive downward) in ft/sec-in. is given by

$$\frac{w_\infty}{\delta_c} = \frac{K_c\left[\frac{Z_u}{m}\left(g\frac{M_\beta}{I_y} + \frac{X_\beta}{m}\frac{M_\theta}{I_y}\right) - \frac{Z_\beta}{m}\left(\frac{M_u g}{I_y} + \frac{X_u}{m}\frac{M_\theta}{I_y}\right)\right]}{-\left(\frac{M_u g}{I_y}\frac{Z_w}{m} - \frac{Z_u}{m}\frac{M_w g}{I_y}\right)+\left(\frac{X_w}{m}\frac{Z_u}{m}\frac{M_\theta}{I_y} - \frac{X_u}{m}\frac{M_\theta}{I_y}\frac{Z_w}{m}\right)} \tag{69}$$

Equation (69) is valid for steady level flight at low speeds. The parameters X_β/m, Z_β/m, and M_β/I_y represent the forces and moment changes due to a change in collective pitch.

4. Roll-to-Sideslip Ratio

A parameter which is sometimes used as a criterion in analyses of the Dutch roll mode (Ref. 18) is the effective roll-to-sideslip ratio $(1/\sqrt{\sigma})|\phi/v|$. Using the notation of this report, the ratio $(1/\sqrt{\sigma})|\phi/v|$ was derived from the lateral-directional small perturbation equations of motion (Eq. (43)). If λ is one of the complex conjugate Dutch roll roots then

$$\frac{\phi}{v} = \frac{\left(\frac{L_v}{I_x}\frac{N_r}{I_z} - \frac{N_v}{I_z}\frac{L_r}{I_x}\right) - \left(\frac{L_v}{I_x} + \frac{I_{xz}}{I_x}\frac{N_v}{I_z}\right)\lambda}{\left(\frac{I_{xz}^2}{I_x I_z} - 1\right)\lambda^3 + \left(\frac{I_{zx}}{I_x}\frac{N_p}{I_z} + \frac{I_{xz}}{I_z}\frac{L_r}{I_x} + \frac{L_p}{I_x} + \frac{N_r}{I_z}\right)\lambda^2 + \left(\frac{L_r}{I_x}\frac{N_p}{I_z} - \frac{N_r}{I_z}\frac{L_p}{I_x}\right)\lambda} \tag{70}$$

Equation (70) results in a complex number which is a vector in the λ-plane. The magnitude of the vector may be easily calculated, and the effective roll-to-sideslip ratio in deg-sec/ft is then

$$\frac{57.3}{\sqrt{\sigma}}\left|\frac{\phi}{v}\right| \tag{71}$$

APPENDIX E

DESCRIPTION OF FINAL GAIN PROGRAMS

The gain programs which were finally selected during the flight simulator program are described in this Appendix. Although these gain programs would be expected to be of similar form for different tandem ducted propeller aircraft designs, the levels of the gains would be dependent upon such factors as the performance characteristics of the propellers, the propeller rotational speed, the ratio of duct exit area to propeller disc area, and the areas and locations of the vanes for each individual design. For these reasons, the gain programs presented herein are exactly as used on the analog computer, and are to be considered only as guides in extrapolating the results to other designs (see for example Appendix H).

1. Longitudinal Mode

The block diagram of the longitudinal control and stability augmentation system is shown in Fig. 32. This diagram includes the longitudinal pitch attitude control, the collective pitch control, the duct incidence angle control, and the pitch rate stabilization loop. In Fig. 32, K_{δ_β} and K_{δ_v} represent the gains through which inputs to the longitudinal control stick were converted to differential changes in propeller collective pitch for the fore and aft propellers, and to deflections of the vanes located in the aft ducts, respectively. The final programs for K_{δ_β} and K_{δ_v} are shown in Fig. 25. The differential collective pitch gain K_{δ_β} was held constant as duct incidence angle decreased to 40 deg and was then phased out linearly with decreasing duct incidence angle to 15 deg. The vane deflection gain K_{δ_v} was phased in linearly with decreasing duct angle below 40 deg and was constant at duct incidence angles below 25 deg. These programs for K_{δ_β} and K_{δ_v} resulted in the variation of longitudinal control stick sensitivity and maximum longitudinal control power with duct incidence angle for steady level flight which are shown in Figs. 36 and 38, respectively. At duct incidence angles below approximately 32 deg, the maximum longitudinal control powers shown in Fig. 38 are for a vane deflection limit of $\pm$30 deg. The flight simulator program indicated that control deflections of this magnitude were required for longitudinal trim with sufficient control margin for maneuvering. Since vane deflections are also required for yaw and roll control, vanes would also have to be provided in the front ducts so that sufficient deflection angles would be available for control and stability augmentation about all three axes. This deficiency in the design of the aircraft which was used as a basis for this study was recognized, and the analog simulation effectively included vanes in the front and rear ducts (see discussion in Section III.F.1.).

Pitch rate stabilization was added directly to the displacement signal which went to the differential collective pitch linkage. In the aircraft the pitch rate

stabilization signal would operate a servo-driven extensible link in the pushrods. The gain K_P was held constant at 7.50-in.-sec/rad which resulted in a value of pitch rate stability augmentation of approximately $(M_q/I_y)_{SAS} = -2.0$ per sec at hover. Since the signal was fed only to differential collective pitch, the pitch rate stabilization was phased out according to the gain $K_{\delta\beta}$ (Fig. 25). The resulting variation of pitch rate damping with duct incidence for steady level flight is shown in Fig. 37.

The collective pitch stick controlled the blade angles of all four propellers simultaneously. It was assumed that the propellers were equipped with governors which would adjust fuel flow rate rather than blade pitch to maintain constant propeller rotational speed. The effects of first-order lags in thrust change following a collective stick displacement were studied in the flight simulator program; however, consideration of the governor, fuel control, and possible lead compensation which would be required was beyond the scope of this project. A value of collective gain K_C of 1.5 deg/in., which resulted in a normal acceleration gradient of 0.093 g/in. of collective stick displacement at hover, was found to be satisfactory for precision hovering. With 7.5-in. total travel, the collective control stick could change blade angle by a maximum of 11.2 deg. This range of blade angles was adequate for hover and transitions. In order to obtain cruise power, it was necessary to use a thumb-actuated beeper switch on the collective pitch stick for changing blade angle at a rate K_{CB} of 0.5 deg/sec (Fig. 32).

The duct incidence angle was varied by means of another thumb-actuated beeper switch located on the longitudinal control stick. Experience with the flight simulator indicated that a duct tilt rate of about 7 or 8 deg/sec was satisfactory during transitions. The pilots would tilt the ducts intermittently at an average rate of 4 or 5 deg/sec during take-off transitions. The high duct tilt rates desired for transitions were unsatisfactory at high speeds in that they produced large fluctuations in normal acceleration; values closer to 1.0 deg/sec were found to be desirable. The gain K_{i_D} was programmed linearly with duct incidence angle according to $K_{i_D} = 0.08\, i_D$ (i_D in deg). This resulted in duct tilt rates of 7.2 deg/sec at hover and 1.3 deg/sec at cruise (250 knots at 20,000 ft).

2. Lateral and Directional Models

A block diagram of the lateral-directional control and stability augmentation system is shown in Fig. 34. Included in this diagram are the lateral control stick, the pedals, and the roll rate and yaw rate stabilization loops. The gains $K_{\Delta\delta\beta}$ and G_{VL} determine the lateral control stick sensitivity and control power. A lateral control stick input produced a differential collective pitch angle proportional to $K_{\Delta\delta\beta}$ (deg/in.) and also a differential vane angle proportional to the product of $K_{\Delta\delta\beta}$ and G_{VL}. The phasing gain G_{VL} was required to

alleviate the unwanted yawing moment which accompanied the rolling moment and has the units deg/deg. Both $K_{\Delta\delta_\beta}$ and G_{VL} were programmed as functions of duct incidence angle as shown in Figs. 81 and 82.

The value of $K_{\Delta\delta_\beta}$ (Fig. 81) was held constant at a level which was found acceptable at hover for duct incidence angles greater than about 72 deg; at this duct incidence angle the differential vane angle which accompanied full lateral control stick deflection reached its limit of 30 deg for the final gain level. From a duct incidence angle of 72 deg to approximately 30 deg, $K_{\Delta\delta_\beta}$ was decreased at a rate which resulted in attaining the maximum differential vane angle limit of 30 deg for full lateral control stick (a higher gain would have caused control coupling since insufficient differential vane angle would have been available). The increase in $K_{\Delta\delta_\beta}$ below a duct incidence angle of 30 deg was indirectly related to the stick-fixed lateral-directional dynamics of the aircraft; the increasingly unstable Dutch roll mode had to be damped by a large amount of roll rate stabilization, which in turn required an increase in lateral control stick sensitivity for maneuvering. Some control coupling was unavoidably present at full lateral control stick displacement.

The program for the phasing gain G_{VL}, shown in Fig. 82, was determined from plots of the exact values of phasing required for the transition flight profiles and for the high-speed cruise conditions (see Section VIII. C. 5. of Appendix C). The gain G_{VL} was exact for the design conditions of 250 and 178 knots at 20,000 ft; the gain was low for the same speeds at sea level, with resultant control coupling. The variations of lateral control stick sensitivity and maximum lateral control power with duct incidence angle for these gain programs in steady level flight are shown in Figs. 43 and 45, respectively.

The program for the roll rate stabilization gain K_R (in.-sec/rad) is shown in Fig. 83, and the resulting variation of roll rate damping with duct incidence angle in steady level flight is shown in Fig. 44. The value of K_R at hover was determined in the flight simulator program. Starting at a duct incidence angle of about 79 deg, K_R was decreased rapidly in order to avoid large deflections of the vanes during maneuvers where roll rate stabilization was not as critical as at hover. At duct incidence angles of about 40 deg the roll rate damping L_p/I_x had to be increased to compensate for the increasingly unstable Dutch roll mode. Therefore, the gain K_R was held constant but the lateral control stick gain $K_{\Delta\delta_\beta}$ was increased rapidly (Fig. 81), causing both the lateral control stick sensitivity and the roll rate stabilization to increase.

As shown in Fig. 34, the gains $K_{\Delta\delta_V}$ and $G_{\beta P}$ determined the pedal sensitivity and control power. A pedal displacement resulted in a differential vane angle proportional to $K_{\Delta\delta_V}$ (deg/in.) and also a differential collective pitch angle proportional to $K_{\Delta\delta_V}G_{\beta P}$ ($G_{\beta P}$ in deg/deg). The gains $K_{\Delta\delta_V}$ and $G_{\beta P}$ were also programmed as functions of duct incidence angle as shown in Figs. 84 and 85.

As noted in the discussion of results of the flight simulator program, the handling qualities of the aircraft were not affected appreciably by changes in the yaw gain programs at low speeds. The program for the rudder pedal gain $K_{\Delta\delta_V}$ which was found acceptable, although not fully satisfactory because of insufficient control power of the two vanes at hover and low speeds, is shown in Fig. 84. The gain had to be decreased to the levels shown below duct incidence angles of approximately 30 deg because of increased pedal sensitivity attributable to the fact that powerful yawing moments were obtained from differential collective pitch at these low duct incidence angles.

The program for the phasing gain $G_{\beta P}$ is shown in Fig. 85. As was the case with the phasing gain G_{VL}, this gain program was determined from an analysis of the exact phasing required to eliminate unwanted rolling moments for all transition flight profiles and for the cruise conditions (see Section VIII. C. 5. of Appendix C). At low duct incidence angles the program was exact for cruise at 250 and 178 knots at 20,000 ft, and for cruise at 250 knots at sea level. The variations in steady level flight of pedal sensitivity and maximum yaw control power with duct incidence angle which resulted from the programs for $K_{\Delta\delta_V}$ and $G_{\beta P}$ are shown in Figs. 46 and 48, respectively.

It was found that satisfactory handling qualities resulted with the yaw rate stabilization gain K_Y held constant at $K_Y = -3.0$ in. sec/rad. Again, the differential vane effectiveness was marginal with the result that yaw rate damping made only a small contribution to handling qualities. It was therefore difficult to observe the effects of changes in the K_R gain program on the handling qualities except near hover. The variation in steady level flight of yaw rate damping with duct incidence angle is shown in Fig. 47.

APPENDIX F

DESCRIPTION OF SIKORSKY V/STOL AIRCRAFT SIMULATOR AND CONTACT ANALOG DISPLAY

The Sikorsky V/STOL aircraft simulator facility, consisting of a full-scale, fixed-based Sikorsky S-61 cockpit with a contact analog display, has been used for studying the performance and handling qualities of a wide range of helicopter and V/STOL aircraft configurations. This facility, which includes three Beckman-Berkeley EASE Model 1133 analog computers and other auxiliary equipment, is operated by the Analog Computation Group at the UAC Research Laboratories.

A photograph showing the interior of the cockpit and contact analog display is shown in Fig. 86. In addition to the standard helicopter-type controls, the S-61 cockpit is modified with special controls and instruments useful for simulation of V/STOL configurations. A wide range of artificial lateral and longitudinal stick-force gradients and pedal-force gradients can be produced by a hydraulically driven system. Aircraft flight instruments (Fig. 87) are displayed separately to the pilot and co-pilot, while control position, aircraft configuration, and engine performance instruments (Fig. 88) are displayed on a central panel.

In this study of the tandem tilting ducted propeller aircraft, no artificial force gradients were added to the inherent friction of the stick and pedals. Displacements of the longitudinal and lateral control sticks and pedals were transmitted through appropriate phasing to the analog computer to obtain simulated roll, pitch, and yaw control commands. The collective pitch angle of the simulated propeller blades was controlled by the collective stick; hence, in hover the collective stick served as the altitude control and in forward flight as a power control. Because of the large difference in collective pitch angles required for hover and high speed flight, a beeper switch on the collective stick was used to change the range of blade angles commanded by the full control displacement. This permitted the pilot to select any desired trim position of the collective stick at all velocities. The ducts were rotated by means of a beeper switch on the end of the longitudinal control stick.

The travels of the controls which were used in the present study were as follows:

δ_S	(longitudinal control stick):	$\pm$6.63 in.
δ_L	(lateral control stick):	$\pm$6.50 in.
δ_P	(pedals):	$\pm$3.19 in.
δ_C	(collective stick):	7.50 in.

The instruments used in the simulation of the tandem tilting ducted propeller VTOL are labeled in Figs. 87 and 88. Pilot experience indicated that an Instantaneous Vertical Speed Indicator (IVSI) was desirable. Since the rate of climb instrument had an inherent lag, the lateral airspeed indicator was calibrated to serve as an IVSI.

The Norden Contact Analog system provides the pilot with an inside-out type of visual display of the complete aircraft motion relative to the earth. The display includes four basic elements: earth elements, pathway, earth position markers, and screen position markers (Fig. 86). The television screen displaying these elements represents a "window" permitting viewing angles of about 15 deg vertically and horizontally.

The earth elements include the ground grid, horizon line, and clouded sky. The ground grid size and pattern vary to indicate altitude as shown in Figs. 89a and 89b. The sweep of the ground grid, which is a function of aircraft speed and altitude, indicates the translational motions of the aircraft. Pathway elements (Fig. 86), which are referenced to the earth axes, include a white roadway, black roadway centerline, and lateral tarstrips. Motion relative to the pathline is exhibited by sweep of the tarstrips. The pathway may serve either as a commandable pathway or as a display of the aircraft flight path. Two earth position markers (not shown), about the size of one grid square, are fixed on the plane of the earth and therefore may be used to mark landing and take-off points. Two screen position markers (a white cross and a white square in Fig. 90) can be adapted to display special information since they are independent of ground plane and path data.

Display elements used in the simulation of the tandem tilting ducted propeller VTOL aircraft are shown in Fig. 90. The white cross was fixed in the center of the screen so that it indicated the position of the nose of the aircraft relative to the earth. The triangular tip of the pathway, shown in this flight condition to be to the left of the cross, was fixed at north in order to aid the pilot in distinguishing between yaw rate and lateral translation in hover and low-speed flight. The white square served as a sensitive altitude indicator in hover. Descent of the aircraft to an altitude of 18 ft was marked by the appearance of the square at the bottom of the screen; further descent to touch-down was indicated by the square moving to the top of the screen.

APPENDIX G

ESTIMATES OF RELATIVE COST, WEIGHT, AND RELIABILITY OF ALTERNATE STABILITY AUGMENTATION SYSTEMS*

The results of the theoretical analyses and flight simulator program indicated that a relatively simple programmed-gain control and stability augmentation system would provide satisfactory handling qualities for a tandem tilting ducted propeller aircraft. It was found that rate stabilization about all three axes would be required. Pitch rate and yaw rate stabilization were added directly to the longitudinal control stick and pedal inputs and were therefore programmed with duct incidence angle through the same phasing and gains as were the controls. Roll rate stabilization was added to the lateral control stick input but was also modulated with duct incidence angle to provide adequate Dutch roll damping at all flight conditions. Additionally, it was found that for the configuration studied, a safe landing following a full failure of the stability augmentation system would be doubtful, particularly if the failure were to occur during take-off or landing.

A brief study of alternate methods of implementing the stability augmentation system was conducted. Estimates were made of the relative weight, cost, and reliability of the basic programmed-gain system, of a programmed-gain system in which the pilot could manually adjust the level of roll rate damping, and of a rate-command adaptive control system. Both duplicated systems, in which the pilot would manually test and reset the operative channel, and triplicated systems, in which the one failed channel would automatically be disengaged, were considered.

1. Description of Duplicated Systems

a. Programmed-Gain Duplicated SAS

Block diagrams of the basic programmed-gain duplicated stability augmentation system are shown in Figs. 91 and 92. Each channel of the system would consist of a dual electronics section terminating in a single limited authority, extensible link actuator. An automatic failure warning circuit would be provided to indicate that a failure had occurred and that the system had disengaged. The pilot would manually determine which channel was operative by means of a test input circuit providing a visual signal, and would re-engage the operative channel. Upon re-engagement of the system, the aircraft would have one-half the normal stability augmentation gain with both channels operative.

---

* The preliminary design study reported in this Appendix was conducted by Vincent F. Lombardi, Electronics Department, Hamilton Standard Division of United Aircraft Corporation, Broad Brook, Connecticut.

Rate gyros would be used as the basic motion sensors in the system. The gyro outputs would be passed through pre-amplifiers having provisions for flight test gain adjustments. All amplifiers would be of the A.C. push-pull, transistorized type, and the sensor pickoffs would be of the A.C. inductive type. The servo-amplifiers would provide the control power required to drive the servo-motors and actuators. Feedback transducers would be used between the actuator output and servo-amplifier input to provide a nearly proportional closed-loop system.

Electro-mechanical actuators in the form of extensible links would be used. Final choice of the actuators would depend primarily on the frequencies of the predominant modes of oscillation, on the force levels required, and upon the cost, weight, and response requirements. Dual power supplies would be used.

In view of the large authority required by the stability augmentation system, means would be provided for automatic recentering of the extensible link following a failure. As shown in Fig. 91, a clutch would be operated by the output of the failure warning circuit, and a spring would provide recentering. Although not shown in Fig. 91, the clutch would include a hold circuit which would keep the actuator disengaged until the pilot had tested and re-energized the system.

The components of the pitch and yaw channels would be identical. The roll channel would differ only in that the roll rate feedback signal would be modulated as a function of duct incidence angle by means of dual shaped potentiometers and servo-multipliers (Fig. 92).

b. Programmed-Gain Duplicated SAS with Pilot Adjust

The pitch and yaw channels of this system would be identical to those described in the preceding section for the programmed-gain system. The roll channel would also include the same elements as before, with the exception that the shaped potentiometers and servo-multipliers would be replaced by a selector switch in the cockpit which would operate dual potentiometers. The pilot would manually adjust roll rate stabilization to the levels which he desired at each flight condition.

c. Rate-Command Duplicated Adaptive Control System

Estimates of the relative cost, weight, and reliability for an adaptive control system were also made, even though the flight simulator program indicated that the improvements in handling qualities which might be realized with such a system would be expected to be small and inconsequential. A rate command adaptive control system was considered in which the pilot control inputs would be transmitted to a model which would generate the desired transient-pitch rate response; the

adaptive system would then force the aircraft to follow the output of the model as closely as possible. A functional block diagram of the pitch channel of such a system, which is similar in operating principles to the system developed by Minneapolis-Honeywell for the X-15 research airplane, is shown in Fig. 93. Similar channels would be provided for roll and yaw.

Pilot inputs from the longitudinal control stick would be passed through a pitch rate model. An error signal would be generated proportional to the difference between the model response and the aircraft response. The error signal would then be passed through a variable gain amplifier and a servo-amplifier to a servo-motor/actuator. The output of the actuator would command changes in differential collective pitch, thereby causing the aircraft to follow the response of the model. In operation it would be necessary to maintain the loop gain as high as possible to maintain a large bandwidth for the system. Accordingly, the system would automatically maintain its gain at a level for which a controlled limit cycle oscillation would occur.

The adaptive control system illustrated in Fig. 93 is a duplicated system. Consequently, if an open-circuit type of failure occurred in one channel, the remaining channel would automatically continue operating at full gain. If a hard-over failure occurred, however. there would be no logic circuitry which would automatically disengage the malfunctioning channel while keeping the operative channel connected. Therefore the flight safety of the adaptive control system as described is comparable to that of the duplicated programmed-gain systems previously described.

The principal changes in components required to transform the programmed-gain system shown in Figs. 91 and 92 into a rate-command adaptive control system are as follows: (1) the dual shaped potentiometers and servo-multipliers for the roll rate stabilization loop would be eliminated, (2) two rate response models would be added for each of the pitch, yaw and roll loops (a total of six electro-mechanical transducers) and (3) dual gain changing circuitry would be added including bandpass filters, rectifier filters. integrators and comparators. The comparator block would contain logic circuitry consisting of several difference amplifiers and gates or switching relays.

2. Description of Triplicated Systems

The duplicated stability augmentation system would provide an automatic failure warning system but the pilot would have to test each channel manually and re-engage the channel which was still operative. A triplicated system would include the necessary circuitry to sense a failure automatically and to isolate and disengage the channel in which the failure had occurred. Such a system would provide

additional insurance against a complete loss of stability augmentation during critical maneuvers near the ground.

Details of the additional circuitry required are similar for the programmed-gain, programmed-gain with pilot adjust, and adaptive control systems. A preliminary block diagram of the triplicated pitch channel of the programmed-gain stability augmentation system is shown in Fig. 94. A total of three model/monitoring channels would be required (one each for pitch, yaw, and roll). A separate power supply would be provided for each model/monitoring channel so that operation of this third channel would be completely independent of the two stability augmentation channels.

The basic assumption in the design of the triplicated system is that a malfunction would occur in the model/monitoring channel or in either of the two stability augmentation channels, but never in two of the three channels simultaneously. The model/monitoring channel would consist of a rate gyro and a passive network which would simulate the normal operating characteristics of dual stability augmentation channels. A comparison of the outputs of all three channels would provide an indication of a failure in any one channel, and by means of logic circuitry, the failed channel would be disengaged.

The primary additions which would be required to achieve triplication of the pitch, yaw, and roll channels are as follows (see Fig. 94): three rate gyros, three power supplies, three model networks, three difference circuits, three threshold adjustment circuits, six switching circuits, six inverters, six "and" circuits, six "or" circuits, and one shaped potentiometer and one servo-multiplier (for the roll channel of the programmed-gain system without pilot adjust).

3. Comparison of Relative Weight, Cost and Reliability of Alternate Systems

Preliminary estimates of the weight, cost and reliability were made for each of the alternate types of control systems described in the previous section. The estimates were based on the use of standard components; component weights, costs, and failure rates were based on data obtained during previous studies conducted at the Hamilton Standard Electronics Department. The results, which are presented in terms of weight, cost, and reliability relative to the basic programmed-gain duplicated stability augmentation system, are discussed in the following paragraphs.

a. Relative Weights

A comparison of the relative weights of the alternate types of stability augmentation systems is shown in Fig. 60. The weights of the linkages and mechanisms which would change the phasing of differential collective pitch vanes, and differential vanes were not included in this analysis since these components are

considered to be parts of the control system, rather than the stability augmentation system.

The reductions in weight from programmed-gain to programmed-gain with pilot adjust are small for both the duplicated and triplicated systems, and reflect only the substitution of a manual selector switch in the cockpit and dual adjustable potentiometers for dual shaped potentiometers and servomultipliers in the roll stabilization channel. The principal result to be noted in Fig. 60 is that a triplicated programmed-gain or adaptive control system would weigh approximately 37% more than the corresponding duplicated system. Also, a duplicated rate-command adaptive control system was estimated to weigh 60% more than the basic duplicated programmed-gain system. The triplicated adaptive control system would weigh about 119% more than the basic duplicated programmed-gain system.

b. Relative Costs

The relative costs of the alternate types of stability augmentation systems are compared in Fig. 61. These costs are based on low quantities (one or two aircraft), and include manufacturing labor but not engineering labor.

The costs of the programmed-gain and programmed-gain with pilot adjust systems were, as would be expected, approximately the same. The cost of a triplicated programmed-gain or adaptive control system would be approximately 48% greater than that of the corresponding duplicated system. A duplicated adaptive control system of the type described would cost 30% more than the basic duplicated programmed-gain system, a triplicated adaptive control system would cost about 92% more than the basic duplicated programmed-gain system. It should be noted that the duplicated adaptive control system, although costing less than the triplicated programmed-gain system would not provide the same level of flight safety during take-off and landings.

c. Relative Reliabilities

The preliminary reliability analysis which was conducted was not sufficiently detailed to draw conclusions regarding the relative reliabilities of the alternate systems. The reliabilities which were calculated were found to be primarily dependent on the single electro-mechanical link actuators (extensible links) which were operated by the dual-channel electronic sections (see Fig. 91). These actuators were in series with the dual electronics sections, and were common to all of the alternate systems which were studied. It would probably be worthwhile, in a more detailed design study, to consider dual extensible links, and to reconsider the duplication of several components in the electronic circuits. Such changes would not be expected to alter appreciably the conclusions regarding relative weights and costs discussed in the preceding sections.

APPENDIX H

EXTRAPOLATION OF RESULTS TO 15,000-LB RESEARCH AIRCRAFT

An analytical study was conducted to determine how the results of this investigation might be applied to the 15,000-lb tandem tilting ducted propeller Tri-Service Research Aircraft presently being considered by the Navy. Aerodynamic mass and inertia characteristics of the 35,000-lb transport (Appendix A) were scaled down to represent the lighter aircraft. Calculations of the roots of the longitudinal and lateral-directional characteristic equations were made for steady level flight, and the control sensitivities and damping which might be required were estimated. The results of these calculations and estimates were compared with a limited amount of advance data for the Tri-Service Research Aircraft which were made available by the Bell Aerosystems Company.

1. Scaling of Aerodynamic, Mass and Inertia Characteristics

The hypothetical 15,000-lb aircraft used as a basis for this study was a scaled-down version of the 35,000-lb tandem tilting ducted propeller transport shown in Fig. 2. Aerodynamic, mass, and inertia characteristics were scaled such that the mass, length of the fuselage, and the diameter of the ducts corresponded to those of the proposed Tri-Service VTOL Research Aircraft (Ref. 19). Based on the reduced fuselage length of 34.4 ft, all dimensions of the 15,000-lb aircraft except the dimensions of the ducts corresponded to those shown in Fig. 2 multiplied by a factor of 0.69. The dimensions of the ducts and control vanes were obtained by multiplying the dimensions shown in Fig. 62 by a factor of 0.80. The following moments of inertia were used for the 15,000-lb aircraft:

$$\text{roll} \quad I_x = 13{,}000 \text{ slug-ft}^2$$

$$\text{pitch} \quad I_y = 32{,}000 \text{ slug-ft}^2$$

$$\text{yaw} \quad I_z = 37{,}000 \text{ slug-ft}^2$$

$$I_{xz} = 2{,}600 \text{ slug-ft}^2$$

With the exception of the roll moment of inertia, these values were in close agreement with the moments of inertia of the Tri-Service Aircraft as presented in Ref. 19. The roll moment of inertia of the Tri-Service Aircraft will be approximately 30% higher because the aft ducts will be located further outboard from the fuselage.

The aerodynamic derivatives used in evaluating the 15,000-lb aircraft were obtained by scaling the derivatives of the 35,000-lb aircraft. Neglecting Reynolds number effects, the forces on the horizontal and vertical tails and the fuselage at a given velocity vary as the change in area, that is, as the square of the scale factor of the airframe. At a given velocity the forces on the ducted propellers vary as the fourth power of the diameter and the square of the rotational speed of the ducted propellers when the duct incidence angle and advance ratio of the propeller are held constant. At a given velocity the advance ratio remains unchanged for a duct of decreased diameter if the rotational speed of the propeller is increased as the inverse of the duct scale factor so that the linear velocity of the propeller tip remains unchanged.

The aerodynamic derivatives which were obtained in this manner are tabulated in Tables VII and VIII for steady level flight conditions. The derivatives are influenced principally by the forces and moments on the ducted propellers. Compared with the derivatives in Tables I and II for the 35,000-lb aircraft, the force derivatives for the 15,000-lb aircraft were not changed appreciably while the moment derivatives were increased by a factor of about 1.4.

2. Calculated Longitudinal and Lateral-Directional Dynamics

The roots of the longitudinal characteristic equation were calculated for steady level flight without stability augmentation and are shown in Fig. 95. The dynamic characteristics for the scaled-down aircraft were similar to those shown in Fig. 13 for the 35,000-lb transport. The short-period mode was aperiodic at hover but became oscillatory between hover and a speed of 20 ft/sec. At cruise the short-period root did not fall within either of the two acceptability boundaries. The phugoid mode was unstable up to a speed of about 25 ft/sec. At hover the period of the phugoid was 15.2 sec and the time to double amplitude was 7.3 sec. This instability, while not meeting the criteria of MIL-H-8501A for IFR flight, nevertheless would be acceptable for contact flight. Calculations of the effect of pitch rate stabilization on the root locations indicated that an amount of stabilization corresponding to $(M_q/I_y)_{SAS} = -0.7$ per sec would result in at least neutrally stable dynamics of the phugoid mode at all steady level flight conditions.

The lateral-directional root locations for steady level flight without stability augmentation are shown in Fig. 96. As was the case for the 35,000-lb transport (Fig. 26), the Dutch roll instability was the predominant feature of the lateral-directional dynamics. The Dutch roll instability was more severe for the lighter aircraft, particularly at the higher speeds. Scaling of the aerodynamic characteristics resulted in increases of 40% in the derivatives L_v/I_x and N_v/I_z; both of these increases were destabilizing at high speeds (the aircraft was directionally unstable above about 140 ft/sec; see Table VIII). The damping derivatives L_p/I_x and N_r/I_z also were increased by 40%, but since these derivatives were small,

their stabilizing effects on the Dutch roll root were overpowered by the destabilizing effects of L_v/I_x and N_v/I_z. At the cruise flight condition of 250 knots at 20,000 ft the resulting Dutch roll oscillation had a period of 20.4 sec and a time to double amplitude of 1.2 sec. Such a large instability as was calculated for the basic scaled-down aircraft without stability augmentation would be unacceptable and would require design changes. The most important objectives of the changes would be to attain positive directional stability at high speeds and to decrease the dihedral effect; these might be accomplished by rearranging the aircraft to move the center of gravity forward and upward relative to the ducts, or alternatively by mounting both fore and aft ducts further aft and lower on the fuselage relative to the center of gravity. The addition of a ventral fin would also help.

Calculations were made to determine the effects of roll rate and yaw rate stabilization on the Dutch roll root locations. The results for roll rate stabilization, which was more effective than yaw rate stabilization, are shown in Fig. 97 for hover, steady level flight at 40 knots, and the cruise condition of 250 knots at 20,000 ft. A roll rate stabilization gain which increased the damping by about $(L_p/I_x)_{SAS} = -0.6$ per sec at hover resulted in at least neutrally stable roots at sea level at all steady level flight speeds up to 180 ft/sec. At the extremely unstable cruise condition, increasing the roll rate stabilization to an extreme value of $(L_p/I_x)_{SAS} = -20.0$ per sec caused the roots to become aperiodic but would not result in stability with further increases.

3. Estimates of Control Sensitivity and Damping Required

The dynamic characteristics of the scaled-down 15,000-lb aircraft and the 35,000-lb transport were found to be similar for steady level flight at speeds from hover to about 180 ft/sec. Since the installed power of the lighter aircraft would also be scaled down, the transition flight profiles and therefore the variation of the dynamics along the transition flight profiles would also be expected to be similar. The levels of control sensitivity and damping at hover which were found to be satisfactory in the simulation of the 35,000-lb transport would therefore provide an indication of the control sensitivity and damping required for the scaled-down aircraft. These approximate levels at hover may be summarized as follows (rate dampings shown are the sum of aerodynamic damping and stability augmentation):

Longitudinal Control Stick Sensitivity	$M_{\delta_s}/I_y = 0.25$ to 0.30 rad/sec^2-in.
Lateral Control Stick Sensitivity	$L_{\delta_L}/I_x = 0.40$ rad/sec^2-in.
Pedal Sensitivity	$N_{\delta_P}/I_z = 0.10$ to 0.15 rad/sec^2-in.
Collective Stick Sensitivity	$Z_{\delta_C}/W = 0.10$ g/in.
Pitch Rate Damping	$M_q/I_y = -2.0$ to -2.5 per sec
Roll Rate Damping	$L_p/I_x = -4.0$ per sec
Yaw Rate Damping	$N_r/I_z = -0.5$ to -1.0 per sec

In addition, it is probable that for the scaled-down aircraft at hover a maximum longitudinal control power of $M_{MAX}/I_{y_2} = 2.0$ rad/sec^2, a maximum lateral control power of $L_{MAX}/I_x = 2.0$ to 2.5 rad/sec^2, and a maximum yaw control power of $N_{MAX}/I_z = 0.5$ to 1.0 rad/sec^2 would be adequate for control through transitions if the aircraft were to be used as a light utility transport. The linear duct tilt rate program (duct tilt rate directly proportional to duct incidence angle) with rates of about 7 or 8 deg/sec at hover would also be satisfactory for the lighter aircraft.

The speed stability derivative $M_u g/I_y$ has a strong influence on the pitch rate damping and longitudinal control stick sensitivity required for satisfactory handling qualities. This derivative is dependent to a large extent on the geometry of the ducted propellers and on the aerodynamic interference between fore and aft ducts. Because the geometries of the scaled-down aircraft and the Tri-Service Aircraft are not identical it is probable that the Tri-Service Aircraft will have a different value of this derivative than that calculated for the scaled-down 15,000-lb aircraft. The advance data of Ref. 19 indicate that the speed stability derivative may be higher than that calculated for the scaled-down aircraft. On the basis of the results of the flight simulator study of the effect of changes in the speed stability derivative on handling qualities, it would be expected that for values of $M_u g/I_y$ increasing from 0.12 to about 0.4, the estimated level of pitch rate damping required for hover would increase to perhaps $M_q/I_y = -2.5$ to -3.0 per sec while the longitudinal control stick sensitivity would increase to perhaps $M_{\delta_s}/I_y = 0.35$ to 0.40 rad/sec^2-in. With further increases in $M_u g/I_y$ the time to double amplitude would be decreased below 3.0 sec, and both the damping and the control sensitivity required for satisfactory handling qualities would increase more rapidly.

4. Application of Programmed-Gain Control and Stability Augmentation System to 15,000-Lb Aircraft

Assuming that changes in the design of the aircraft would result in an alleviation of the extreme Dutch roll instability at the high-speed cruise condition, a programmed-gain control and stability augmentation system of the type selected for the 35,000-lb transport would also be suitable for the lighter aircraft. It is probable that by proper design the Dutch roll mode of the basic aircraft would be at least lightly damped, in which case it might be possible to simplify the stability augmentation system even further by eliminating the program for roll rate stabilization gain K_R. In any case, it is certain that a more sophisticated system such as an adaptive control system would not be required. The requirement for a triplicated stability augmentation system, rather than a duplicated system with pilot reset, will have to be evaluated on the basis of the locations of the Dutch roll roots of the final aircraft design.

LIST OF FIGURES

Fig. No.

Fig. No.

Fig. No.

Fig. No.

Fig. No.

FIG. 1

SKETCH OF TANDEM TILTING DUCTED PROPELLER AIRCRAFT IN HOVER AND FORWARD FLIGHT

HOVER

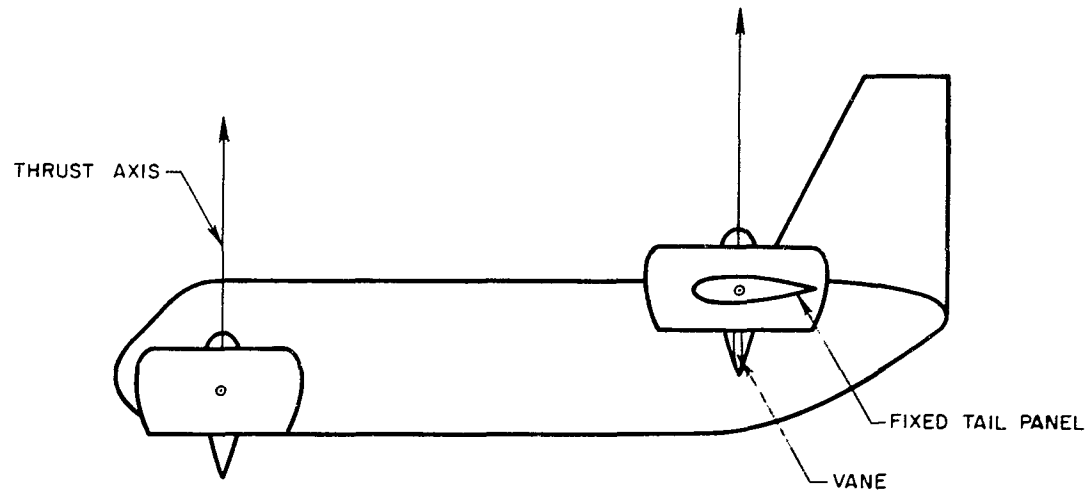

FORWARD FLIGHT

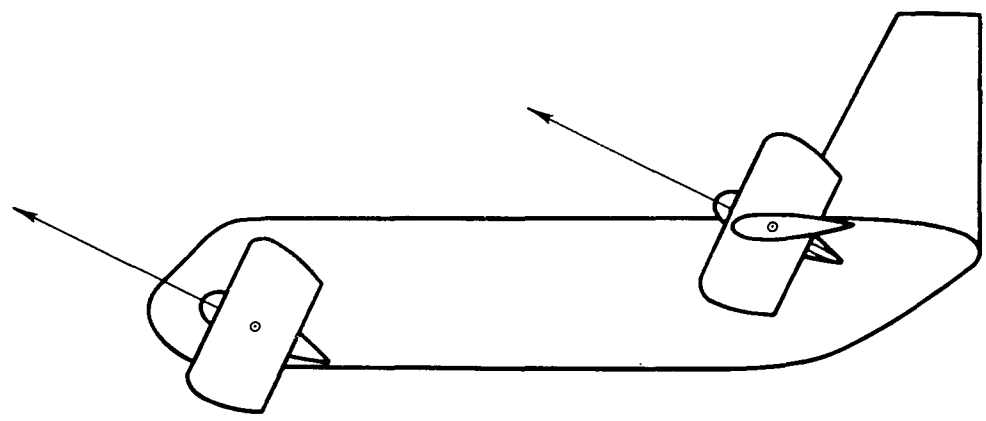

FIG. 2

GENERAL ARRANGEMENT

TANDEM TILTING DUCTED PROPELLER AIRCRAFT

NOTE: 1. SEE SEPARATE FIGURE FOR DETAILS OF DUCTED PROPELLERS AND CONTROL VANES

2. ALL DIMENSIONS IN FEET

3. WEIGHT AND INERTIAS
   W = 35,000 LB
   I_x = 60,000 SLUG FT^2
   I_y = 150,000 SLUG FT^2
   I_z = 170,000 SLUG FT^2
   I_{xy} = 12,000 SLUG FT^2

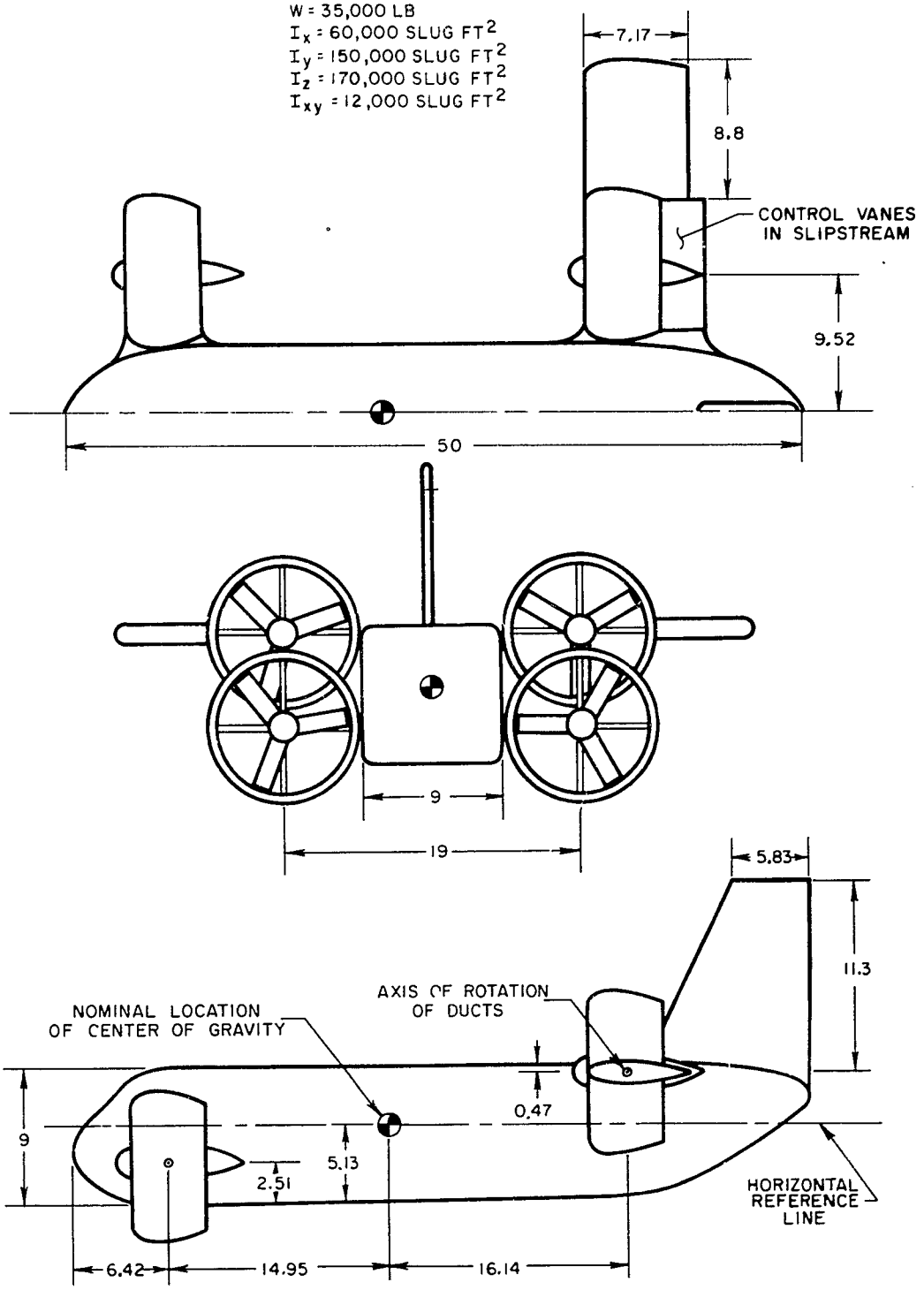

HIGH-GAIN CONTROL CIRCUITS FOR CALCULATING TRANSITION FLIGHT PROFILES

(a.) CONSTANT ATTITUDE CONTROLLER

K_1 = 200 DEG/RAD

K_2 = 100 DEG-SEC/RAD

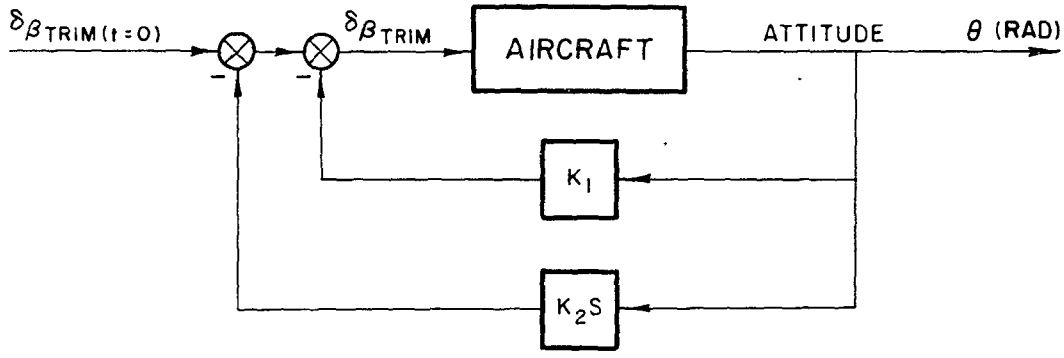

(b.) CONSTANT ALTITUDE CONTROLLER

K_3 = 0.4 DEG/FT

K_4 = 8.0 DEG-SEC/FT

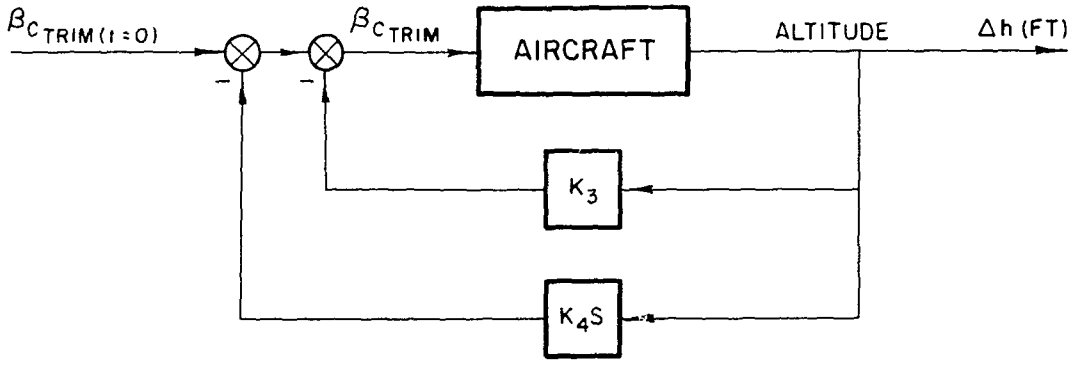

FIG. 4

HIGH-GAIN ALTITUDE CONTROL CIRCUIT FOR CALCULATING DECELERATING DESCENT FLIGHT PROFILE

K_3 = 0.4 DEG/FT

K_4 = 8.0 DEG-SEC/FT

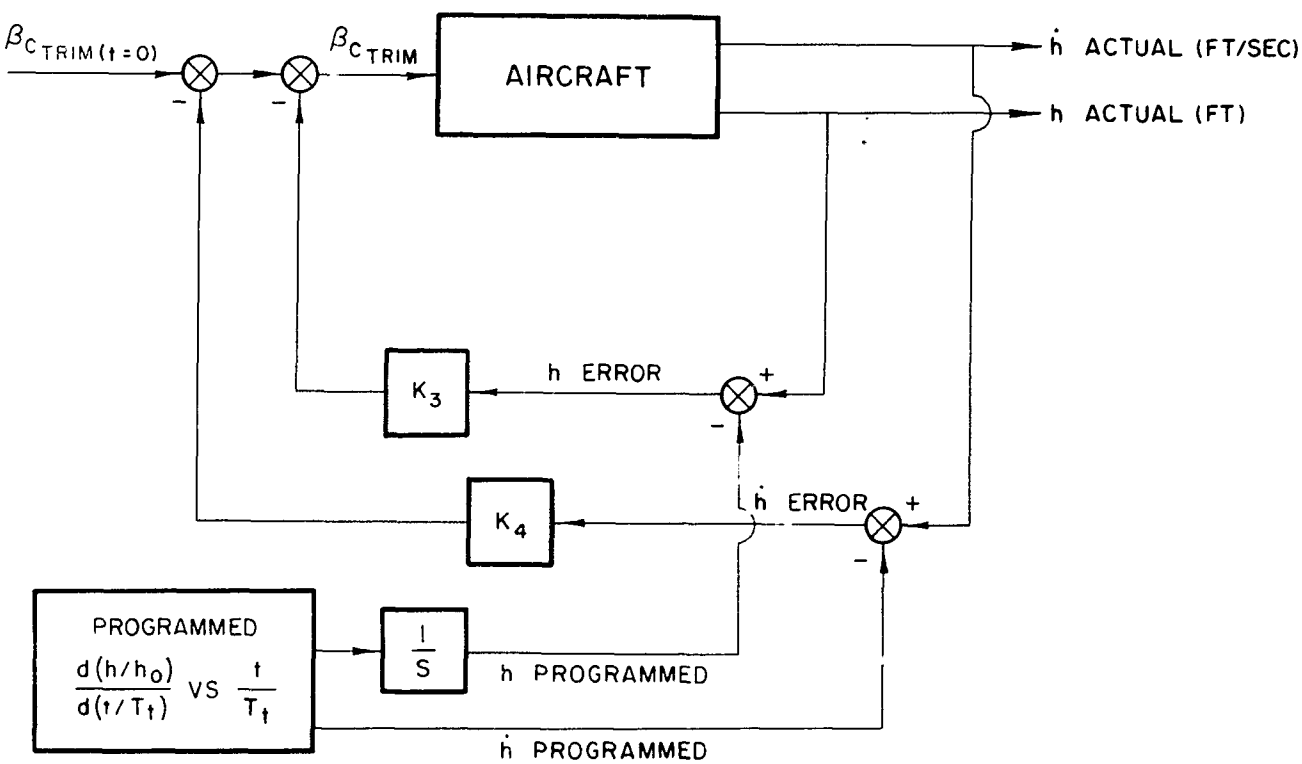

R-1624-5

FIG. 5

VARIATION OF FLIGHT VARIABLES WITH VELOCITY FOR STEADY LEVEL FLIGHT

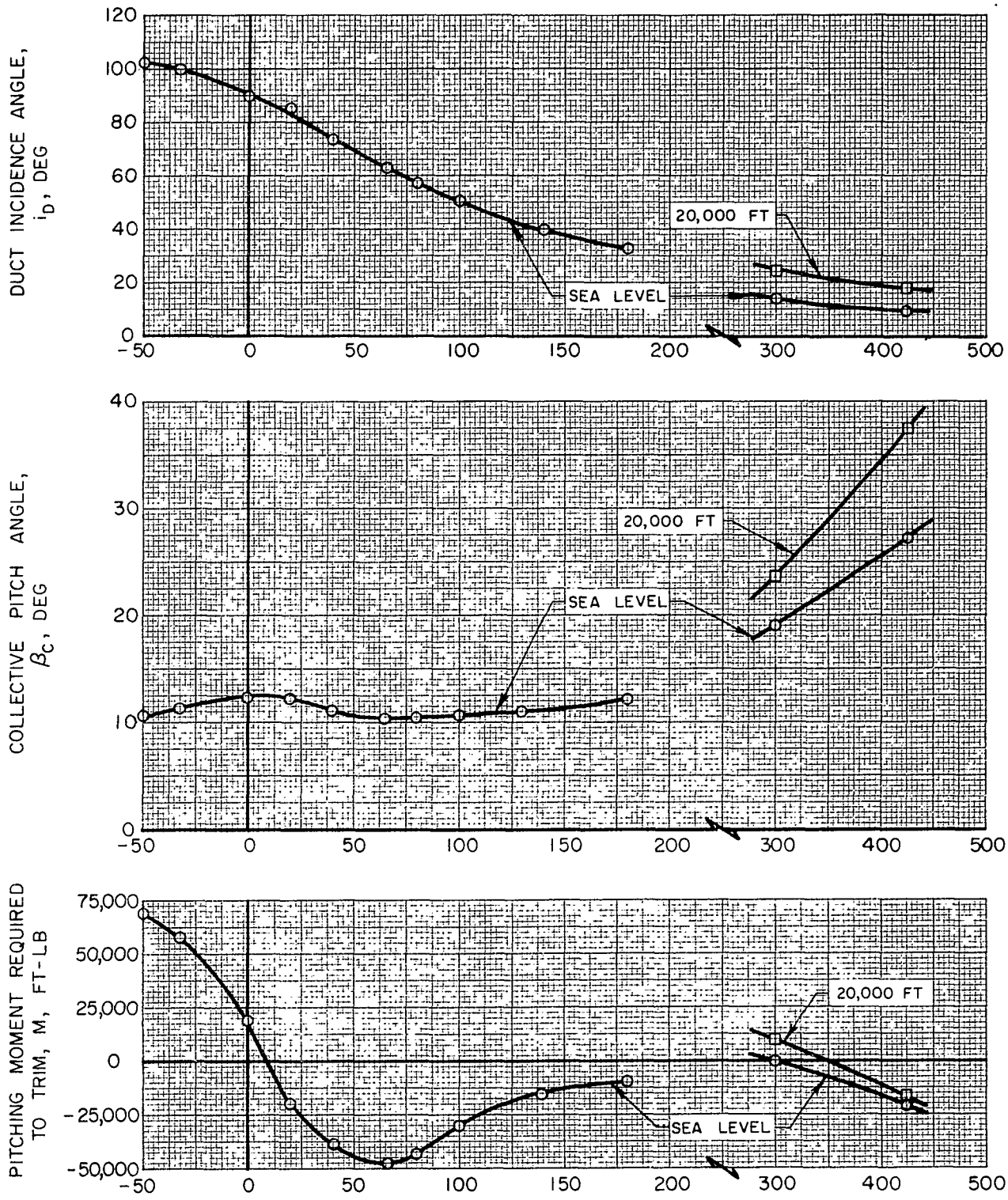

FLIGHT PATHS OF ACCELERATING ASCENT FLIGHT PROFILES

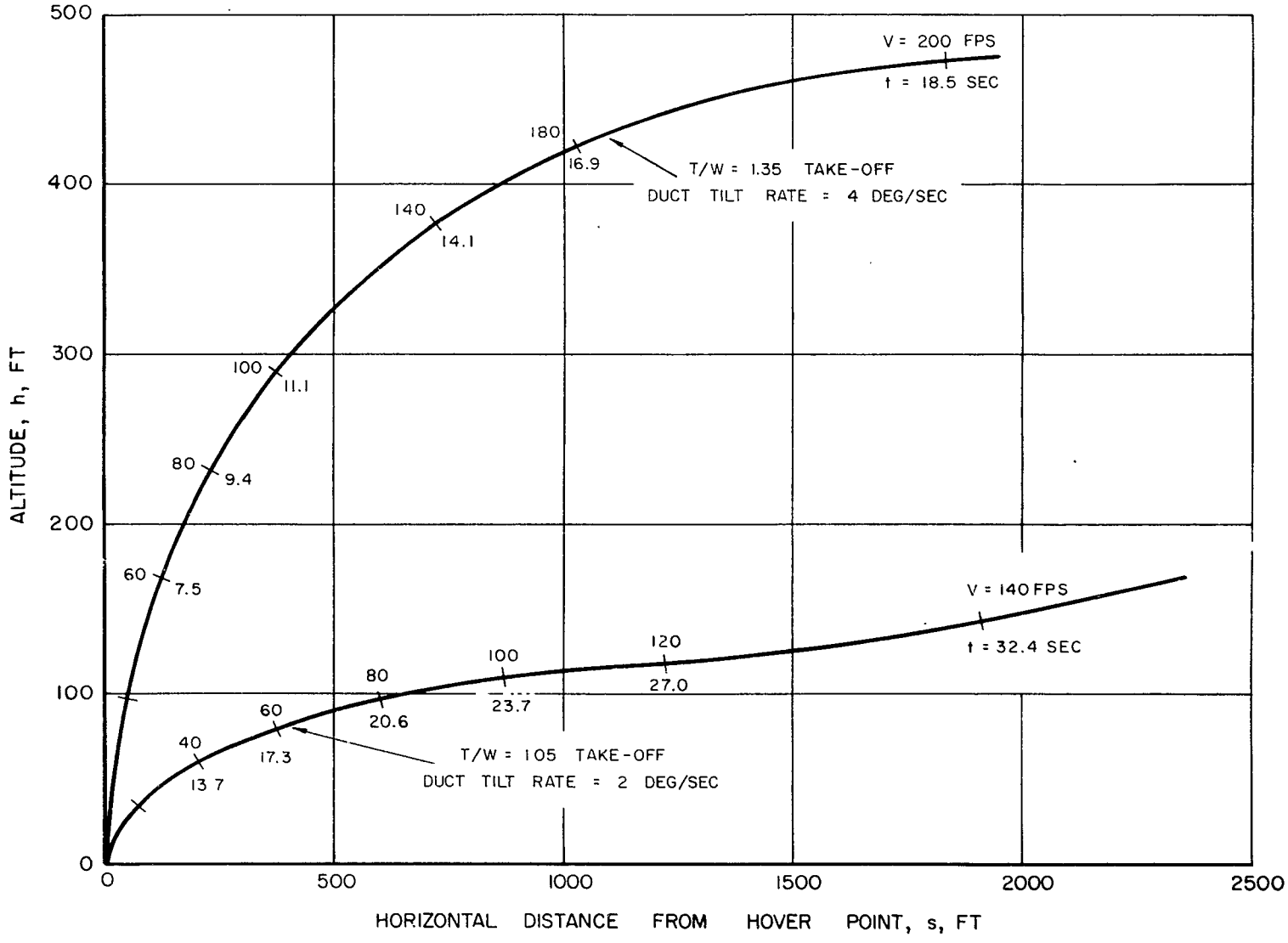

FIG. 6

FIG. 7

VARIATION OF FLIGHT VARIABLES WITH VELOCITY FOR ACCELERATING ASCENT FLIGHT PROFILES

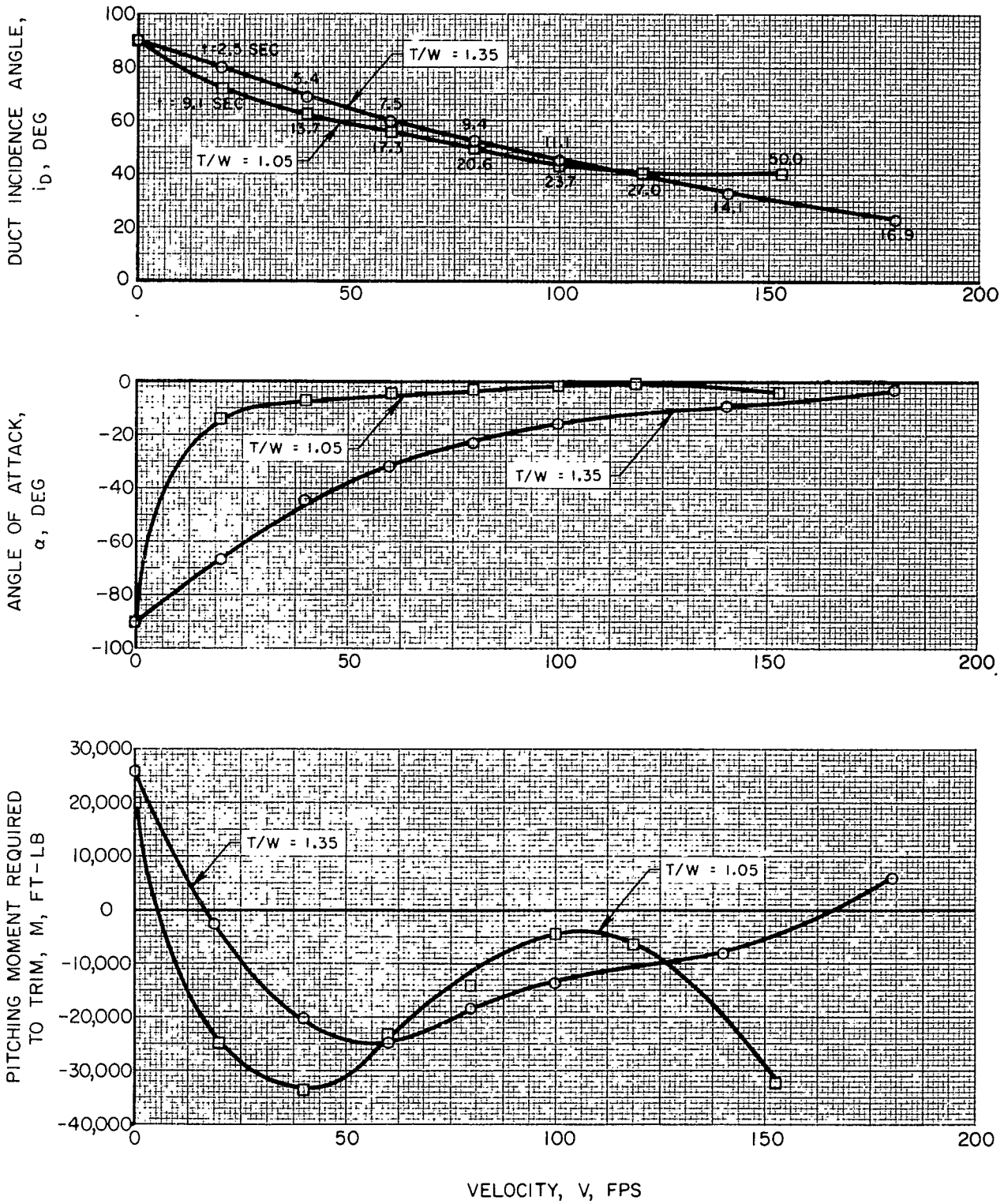

FIG. 8

EFFECT OF THRUST-TO-WEIGHT RATIO AND DUCT TILT RATE ON TAKE-OFF FLIGHT PROFILE

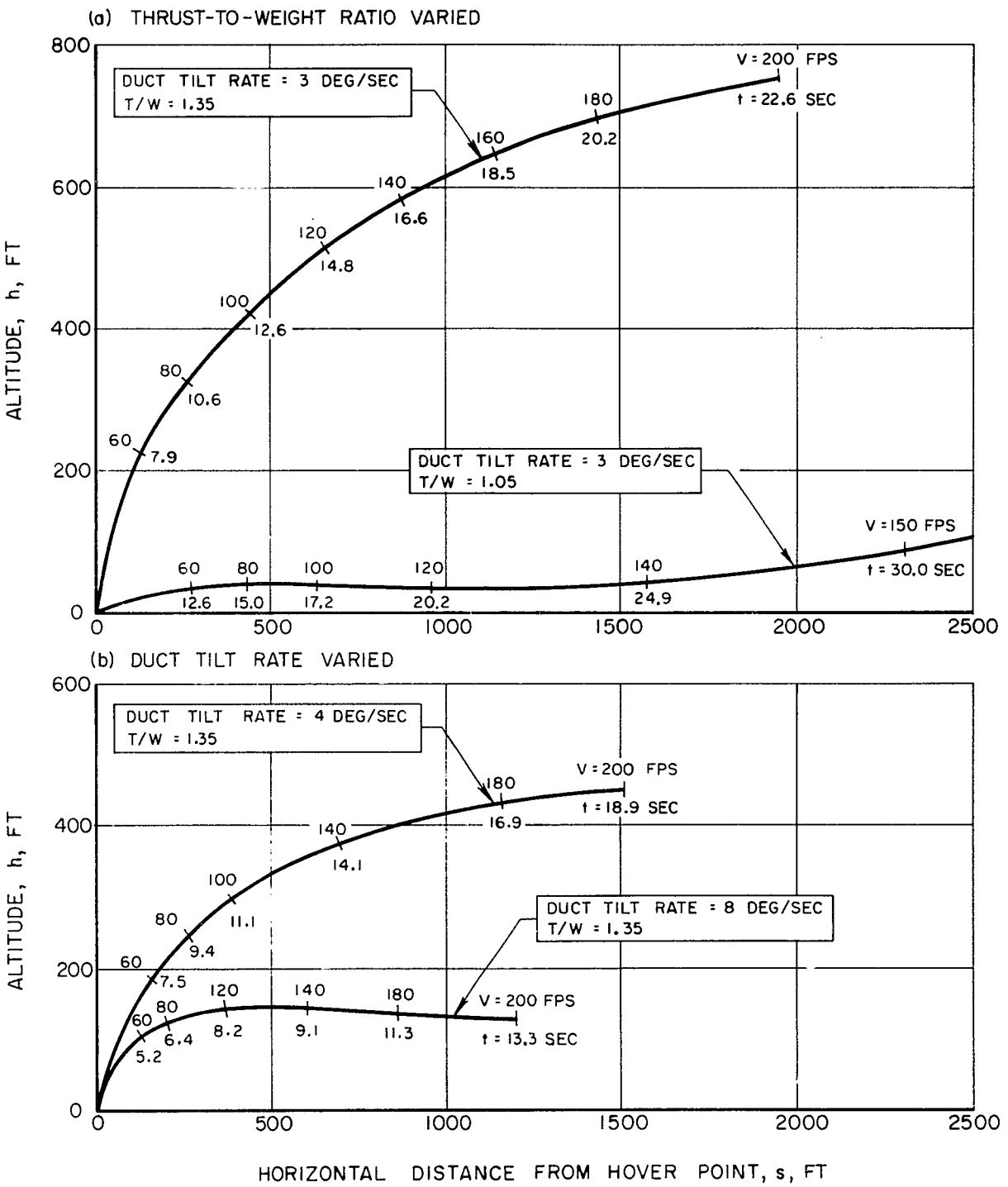

FIG. 9

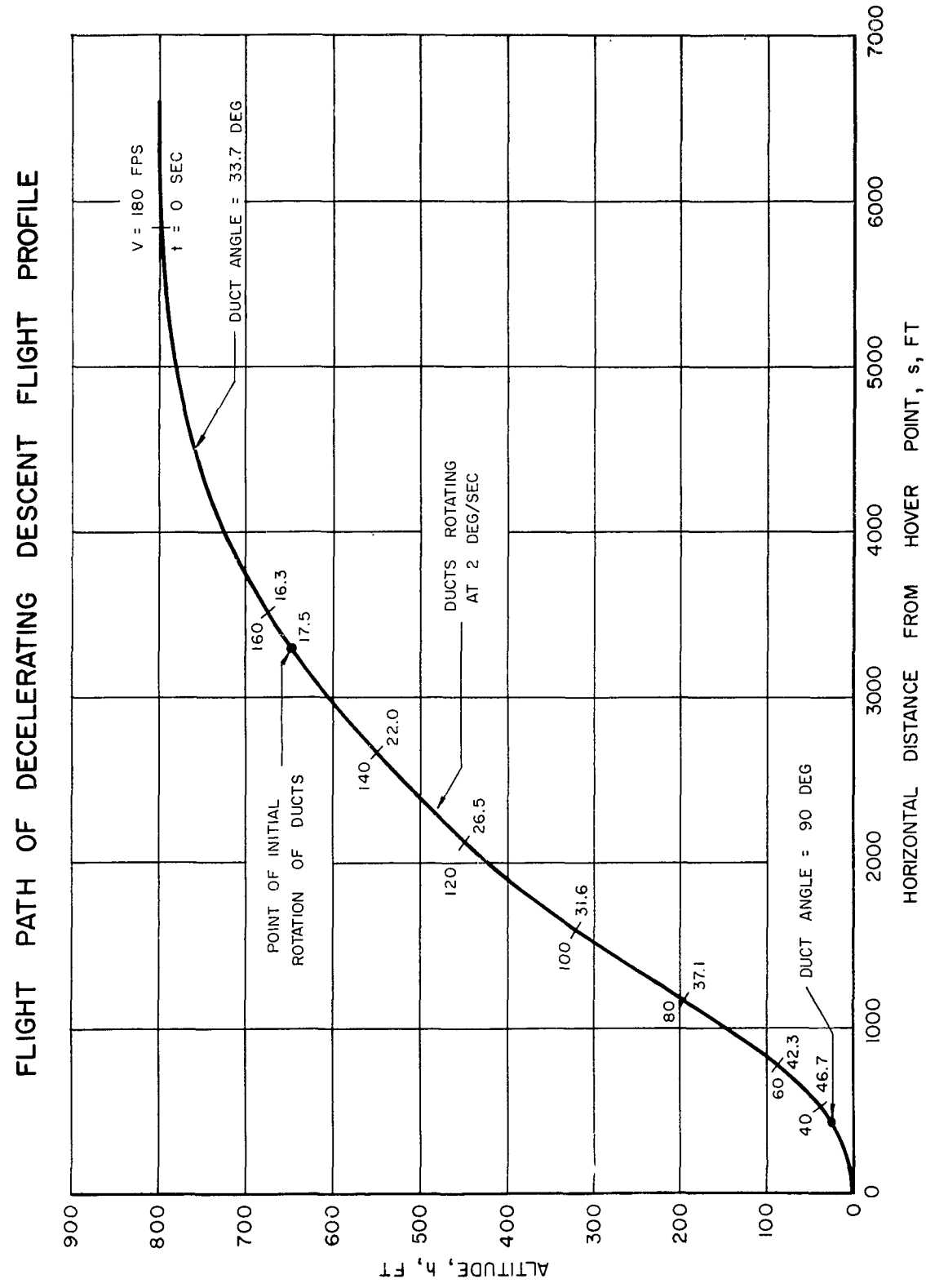
FLIGHT PATH OF DECELERATING DESCENT FLIGHT PROFILE
V = 180 FPS
t = 0 SEC
DUCT ANGLE = 33.7 DEG
POINT OF INITIAL ROTATION OF DUCTS
DUCTS ROTATING AT 2 DEG/SEC
DUCT ANGLE = 90 DEG
160
16.3
17.5
140
22.0
120
26.5
100
31.6
80
37.1
60
42.3
40
46.7
ALTITUDE, h, FT
HORIZONTAL DISTANCE FROM HOVER POINT, s, FT
0
100
200
300
400
500
600
700
800
900
1000
2000
3000
4000
5000
6000
7000

FIG. 10

VARIATION OF FLIGHT VARIABLES WITH VELOCITY FOR DECELERATING DESCENT FLIGHT PROFILE

DUCT TILT RATE = 2 DEG/SEC
SEA LEVEL

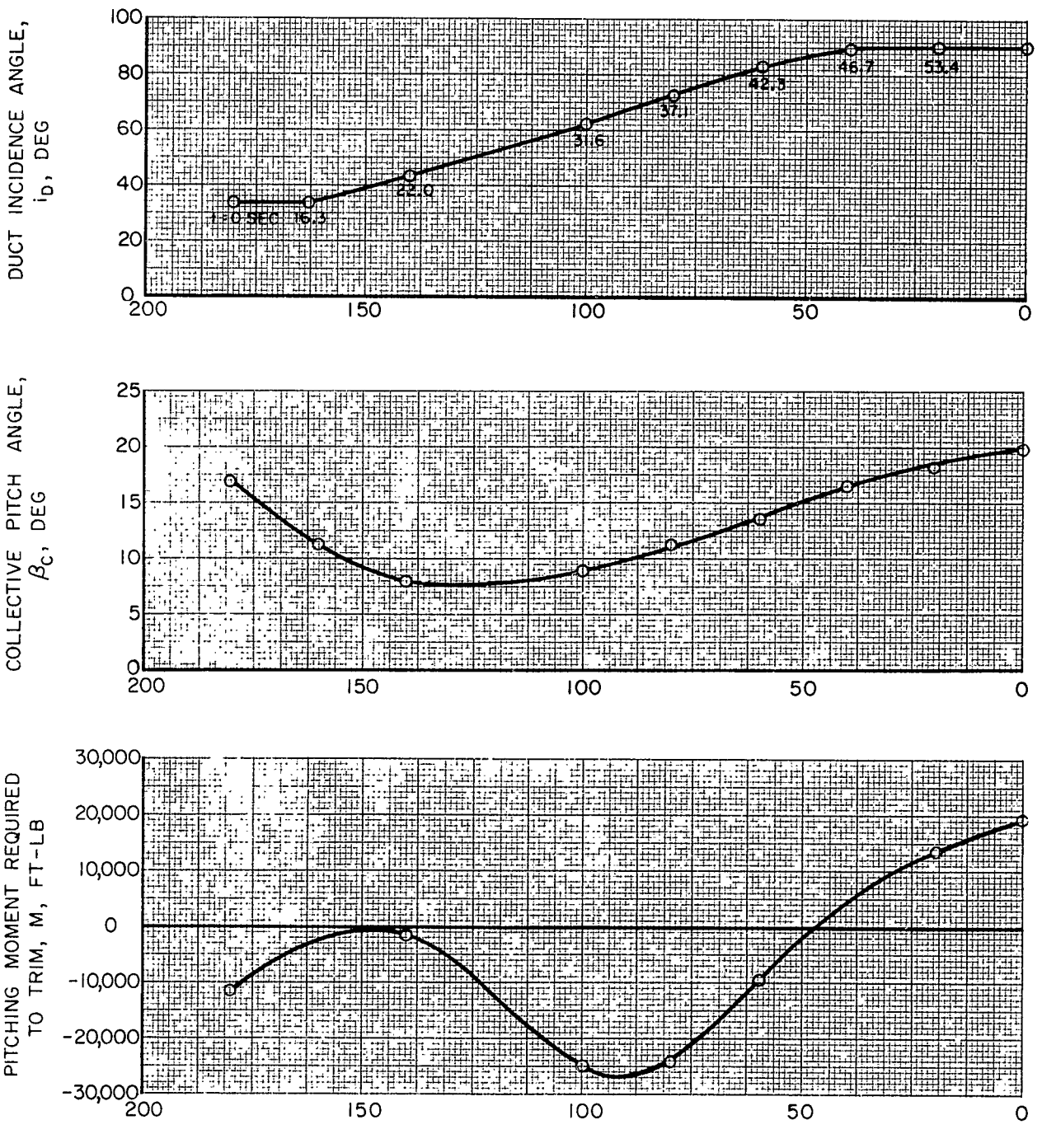

FIG. 11

VARIATION OF FLIGHT VARIABLES WITH VELOCITY FOR CONSTANT ALTITUDE ACCELERATION FLIGHT PROFILE

DUCT TILT RATE = 2 DEG/SEC

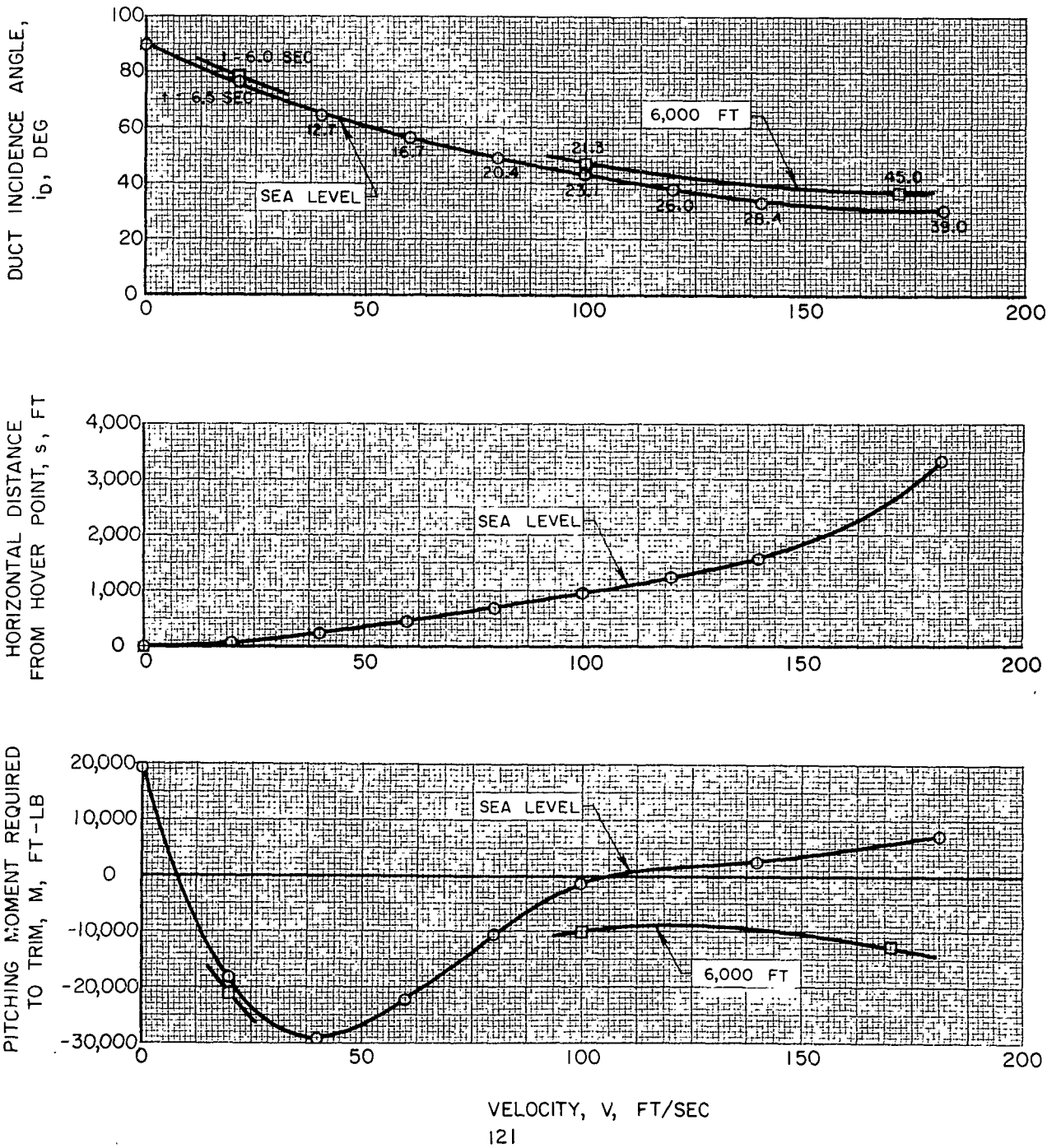

FIG. 12

VARIATION OF FLIGHT VARIABLES WITH VELOCITY FOR CONSTANT ALTITUDE DECELERATION FLIGHT PROFILE

DUCT TILT RATE = 2 DEG/SEC

SEA LEVEL

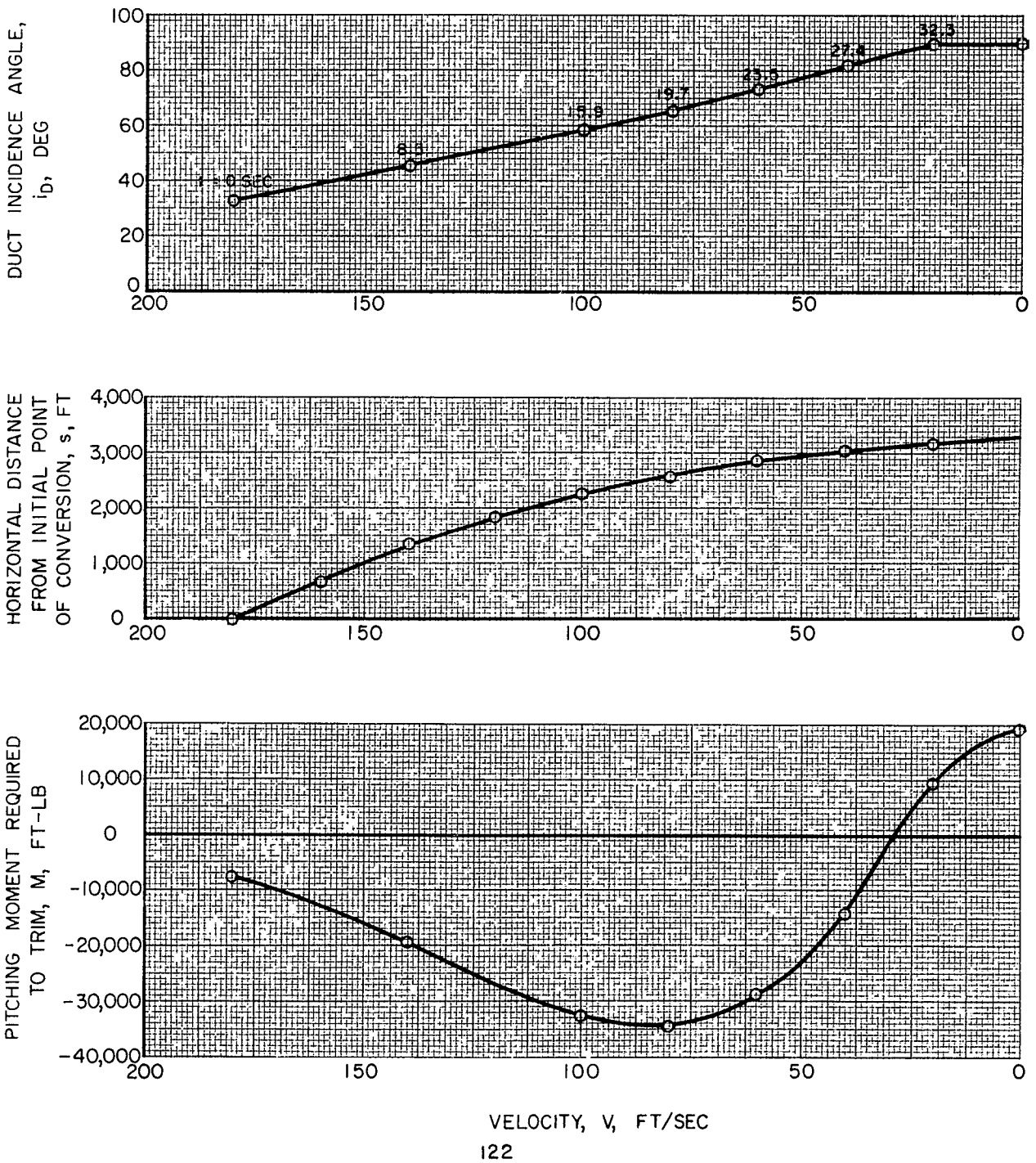

SUMMARY OF LONGITUDINAL ROOT LOCATIONS FOR S
FLIGHT AT SPEEDS FROM -30 KTS TO +25
NO STABILITY AUGMENTATION

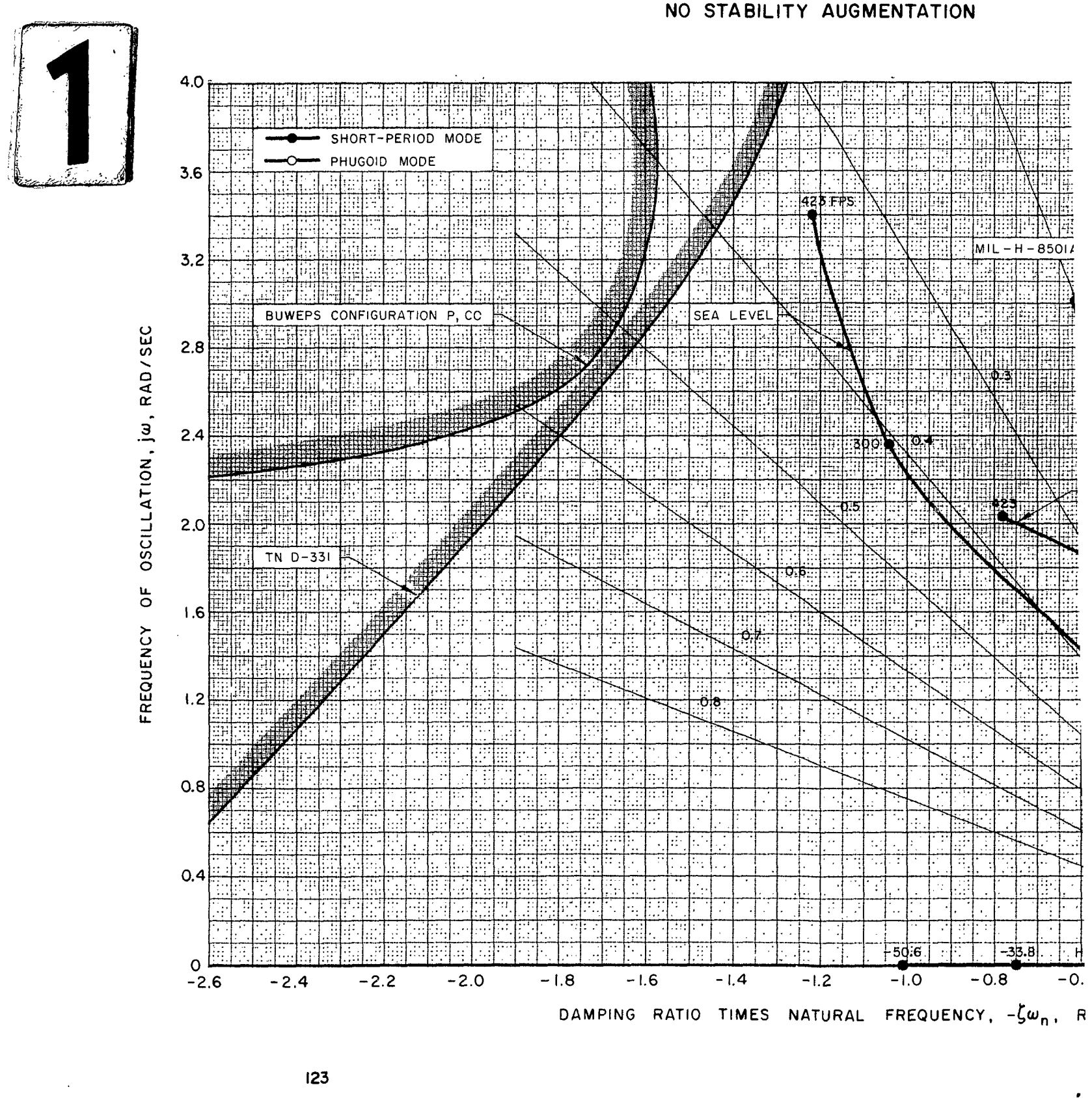

)INAL ROOT LOCATIONS FOR STEADY LEVEL
EEDS FROM -30 KTS TO +250 KTS
STABILITY AUGMENTATION

FIG. 13

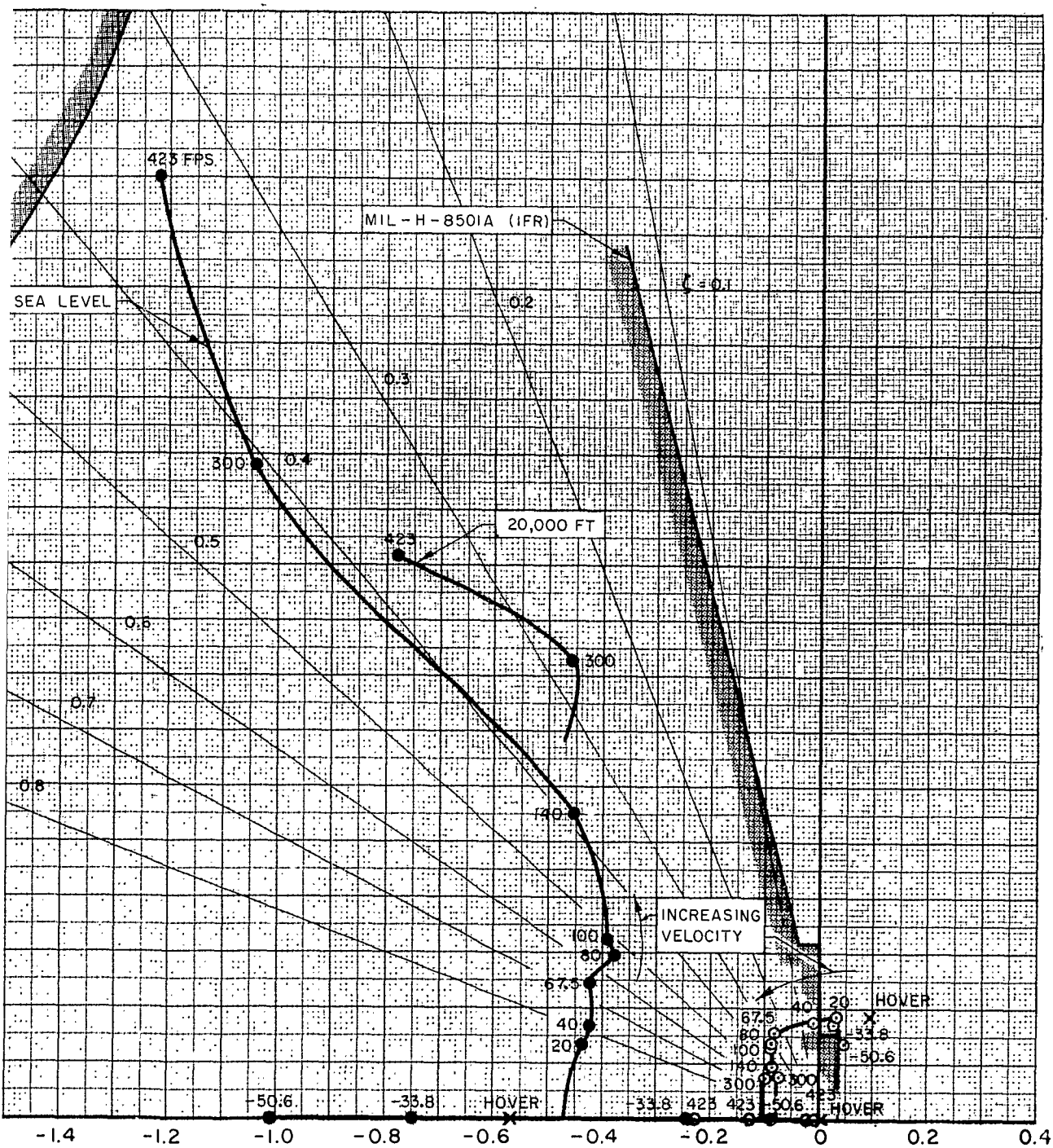

2

O TIMES NATURAL FREQUENCY, $-\zeta\omega_n$, RAD/SEC

FIG. 14

EFFECT OF INCREASING STABILITY AUGMENTATION ON LOCATION OF PHUGOID ROOTS IN HOVER

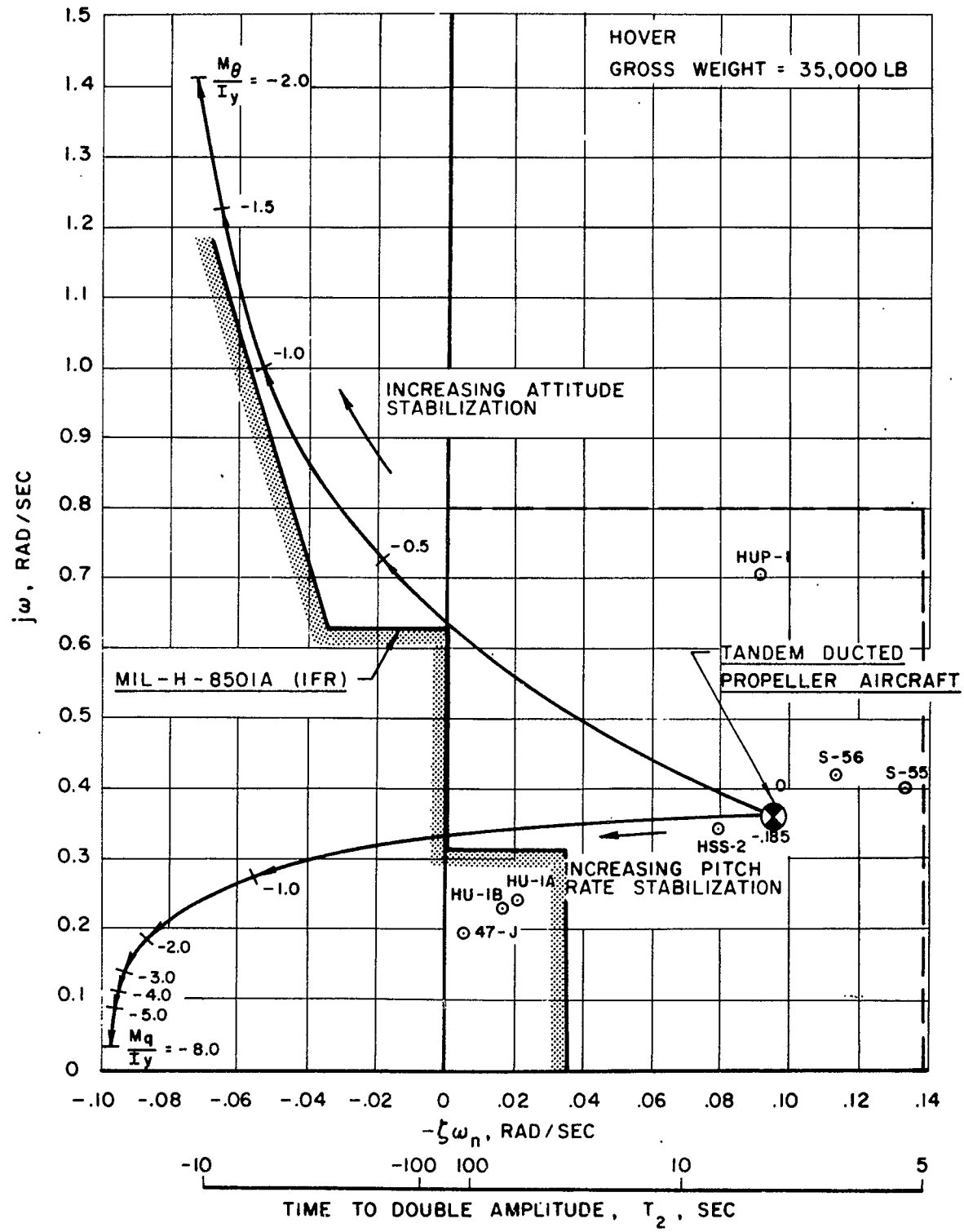

R-1624-5

SUMMARY OF LONGITUDINAL ROOT LOCATIONS FOR REPRESE

NO STABILITY AUGMENTATION

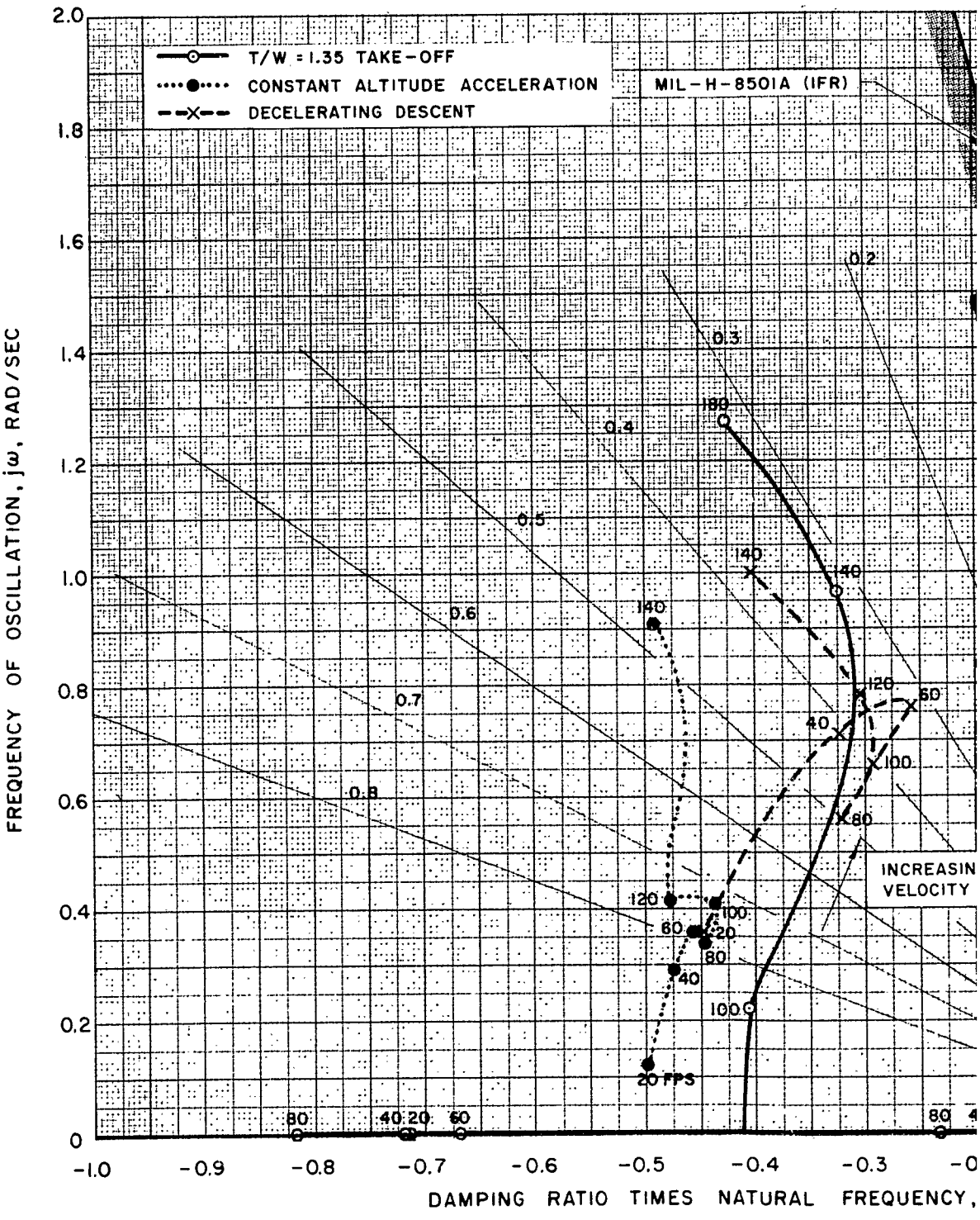

1

FIG. 15

LOCATIONS FOR REPRESENTATIVE TRANSITION MANEUVERS

NO STABILITY AUGMENTATION

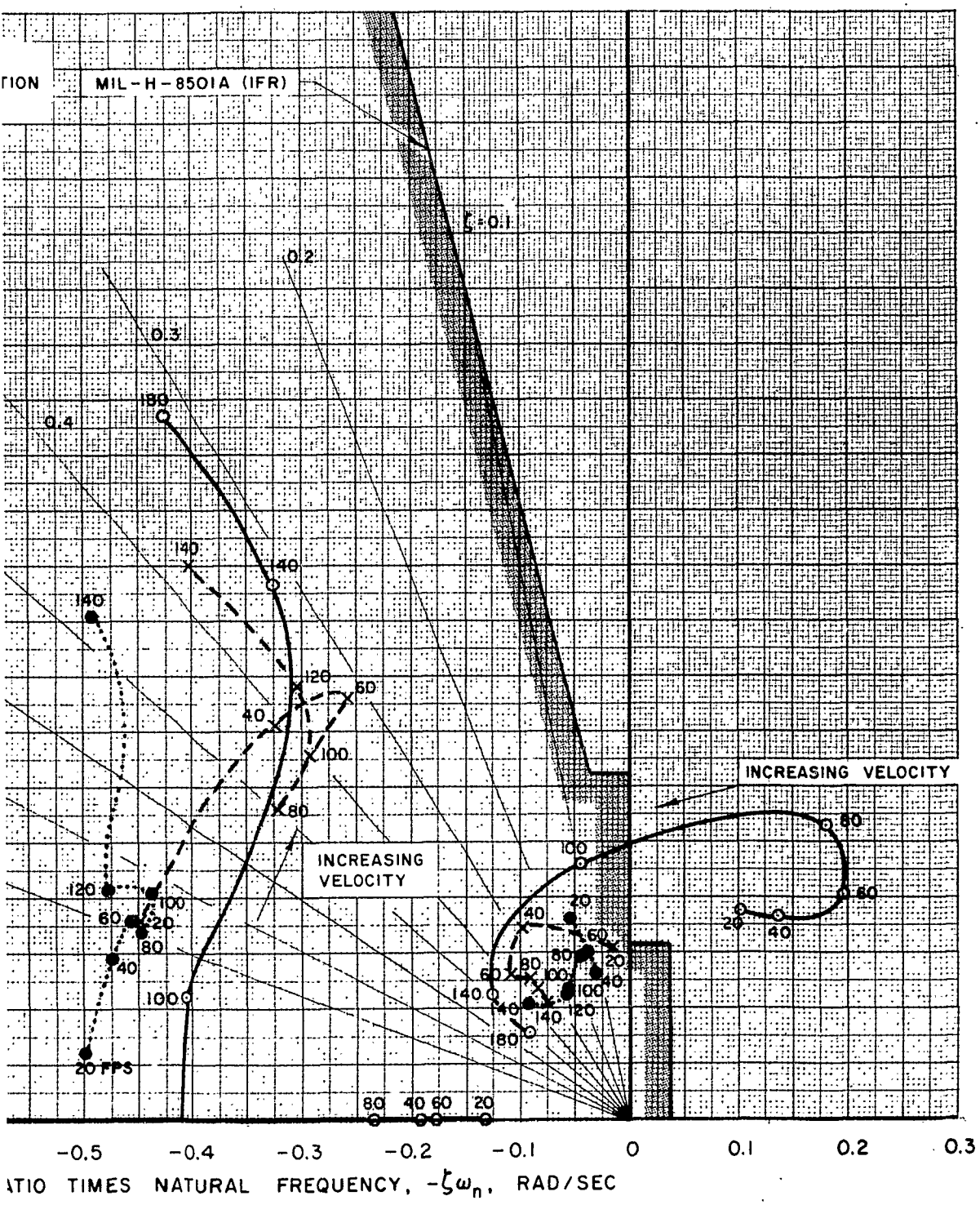

2

EFFECT OF DOUBLING AND HALVING STABILITY DERIVATIVES ON LOCATION OF PHUGOID ROOTS IN HOVER

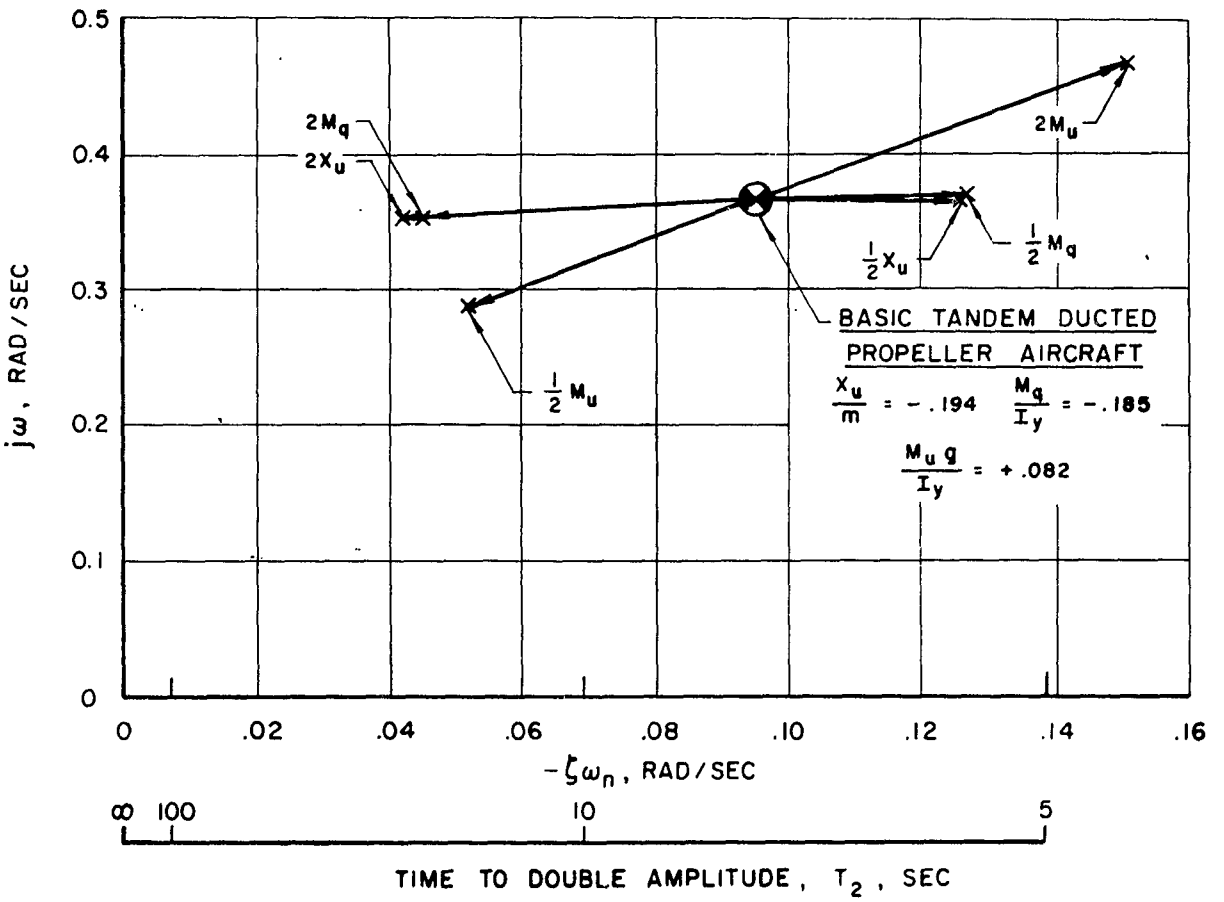

EFFECT OF INDIVIDUAL STABILITY DERIVATIVES OI

NO STABILITY AUGMENTATION

V=80 FT/SEC ON T/W = 1.35 FLIGHT PR

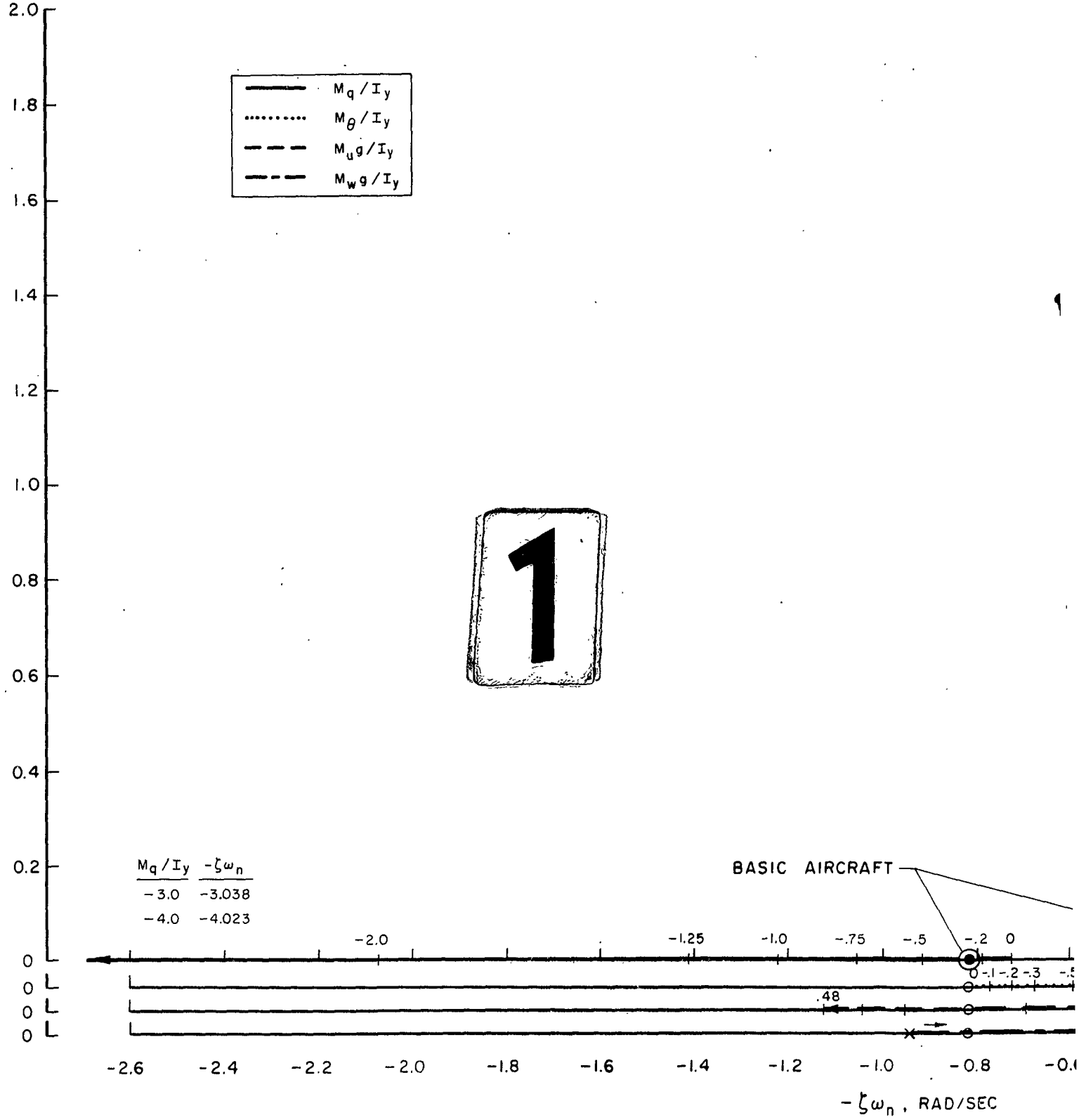

BILITY DERIVATIVES ON LONGITUDINAL DYNAMICS

FIG. 17

O STABILITY AUGMENTATION

T/SEC ON T/W = 1.35 FLIGHT PROFILE

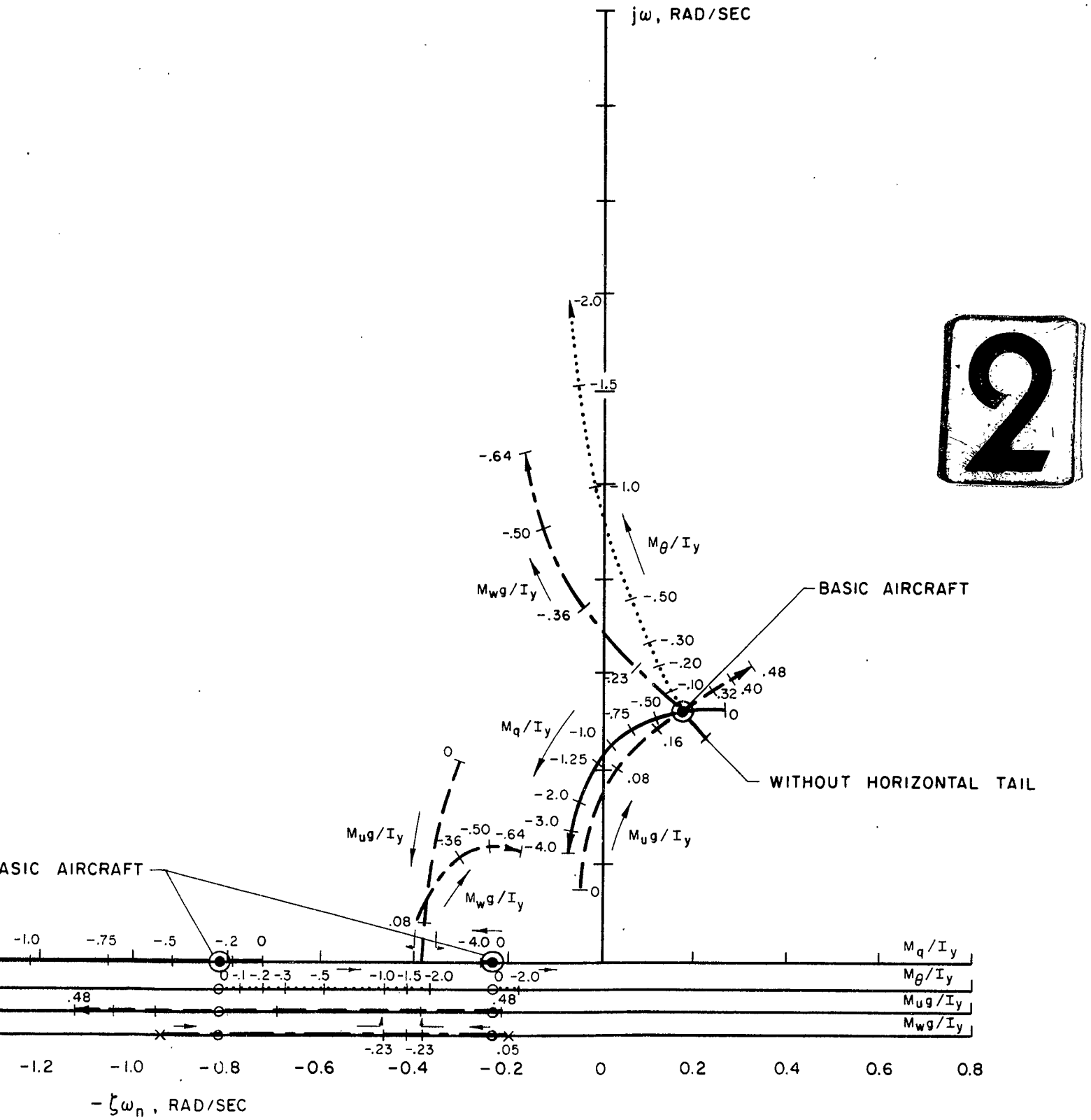

AVERAGE ANGLE OF ATTACK OF HORIZONTAL TAIL FOR MOST CRITICAL TRANSITION FLIGHT PROFILES

(a.) FIXED TAIL

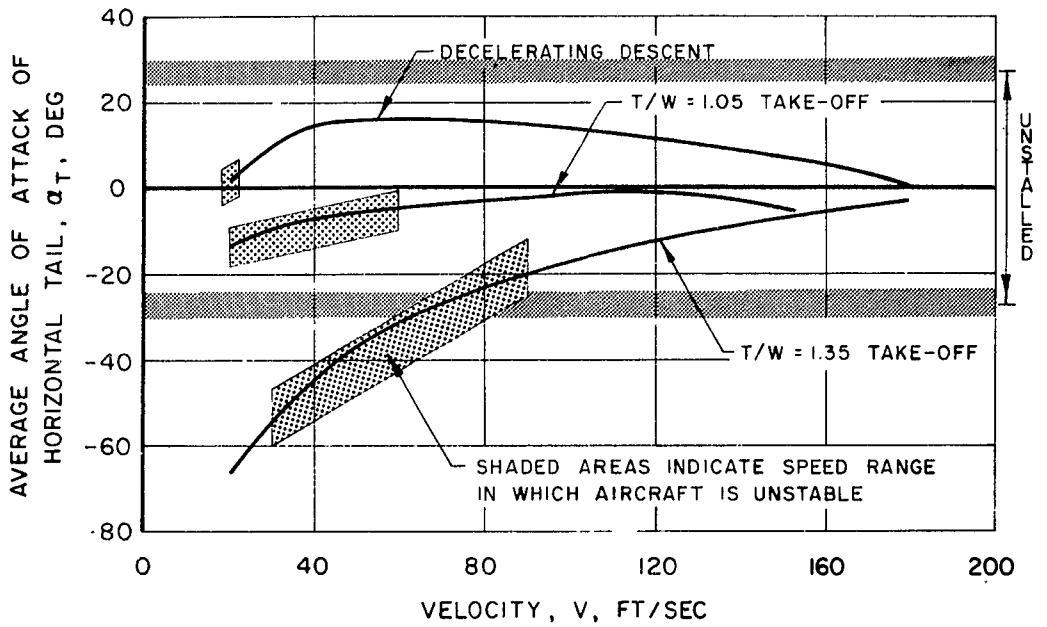

(b.) ROTATING TAIL

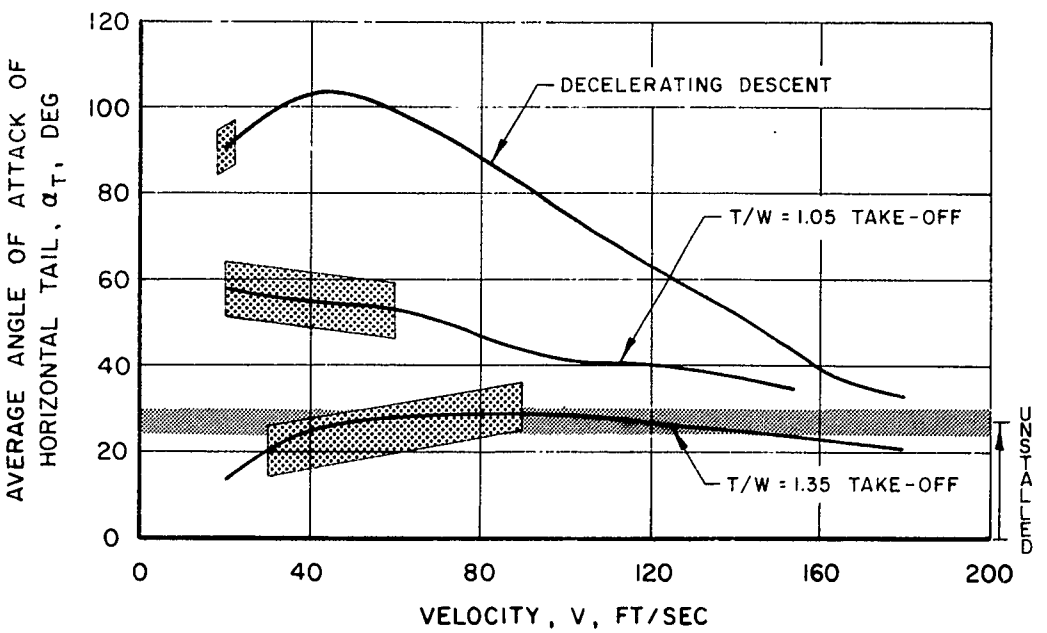

MODEL OF CONTROL AND STABILITY AUGMENTATION SYSTEM WITH FIRST ORDER LAG

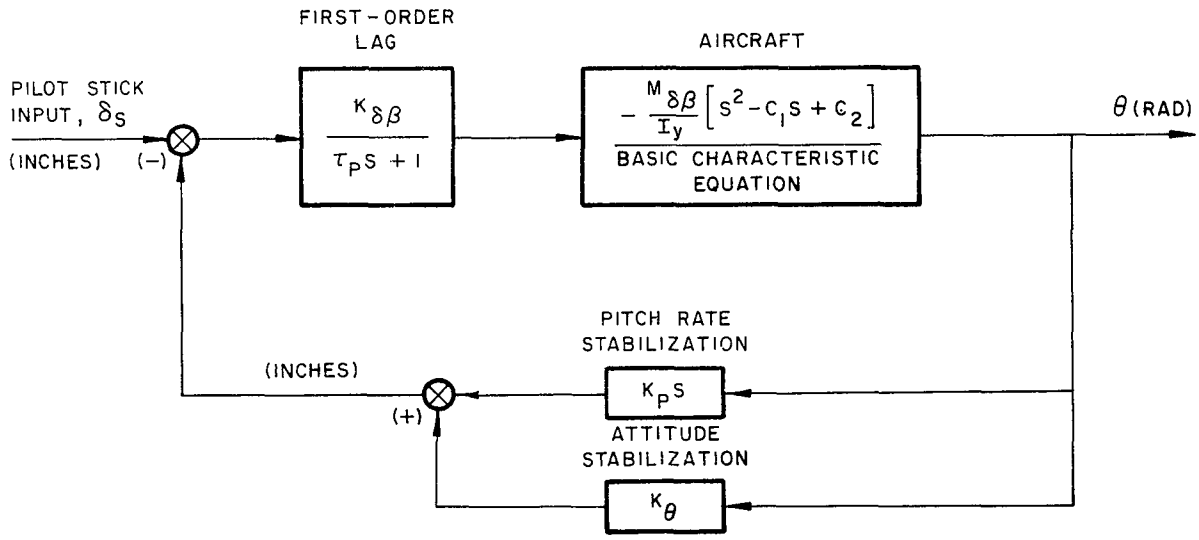

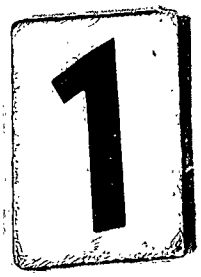

EFFECT OF LAGS IN STABILITY AUGMENTATION SYSTEM

STEADY LEVEL FLIGHT AT 40 KTS

NO LAG

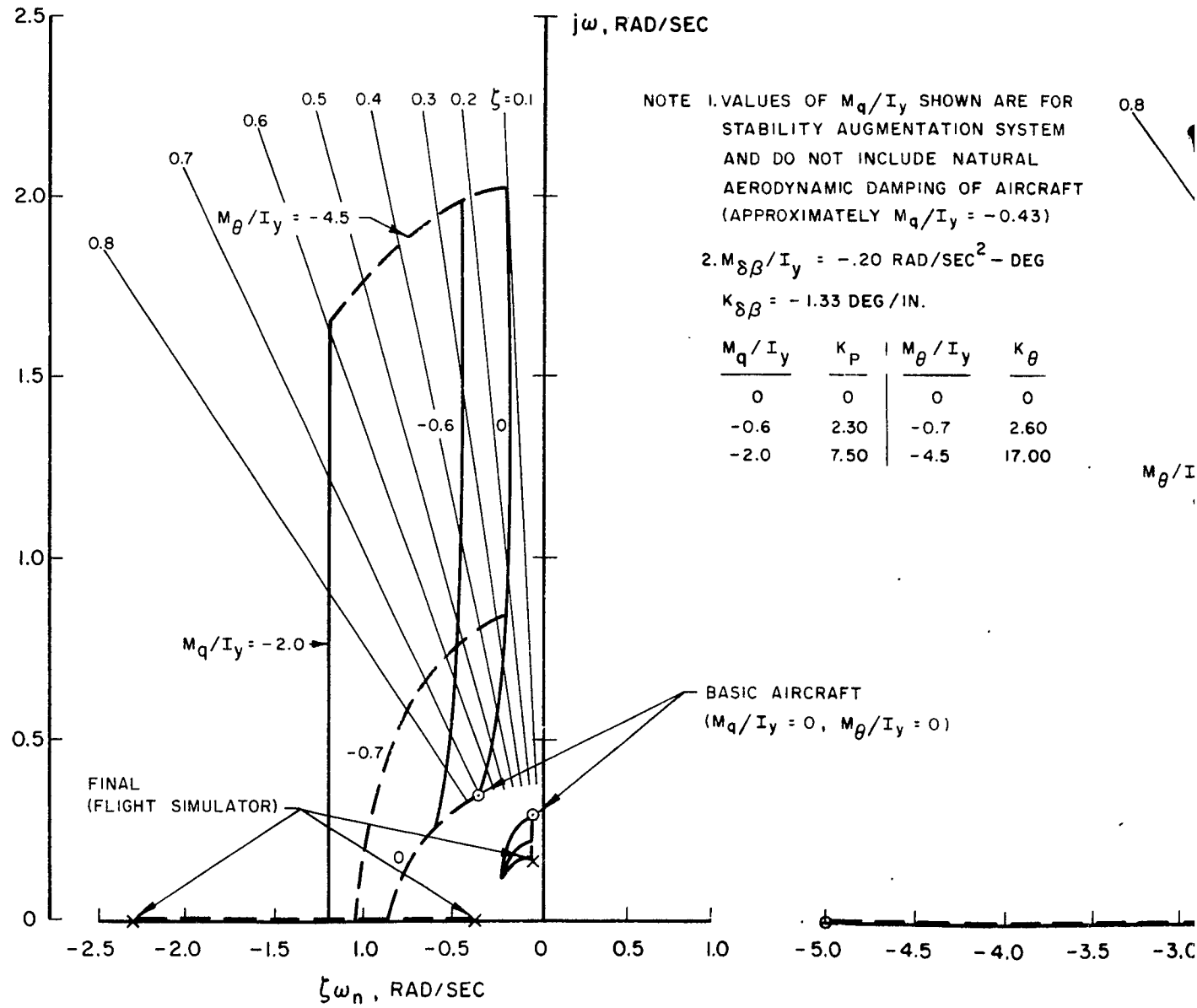

NOTE 1. VALUES OF M_q/I_y SHOWN ARE FOR STABILITY AUGMENTATION SYSTEM AND DO NOT INCLUDE NATURAL AERODYNAMIC DAMPING OF AIRCRAFT (APPROXIMATELY M_q/I_y = -0.43)

2. $M_{\delta\beta}/I_y$ = -.20 RAD/SEC^2 - DEG

$K_{\delta\beta}$ = - 1.33 DEG/IN.

M_q/I_y	K_P	M_θ/I_y	K_θ
0	0	0	0
-0.6	2.30	-0.7	2.60
-2.0	7.50	-4.5	17.00

0.8

M_θ/I

FIG. 20

GMENTATION SYSTEM ON LONGITUDINAL DYNAMICS

EVEL FLIGHT AT 40 KTS

LAG TIME CONSTANT $\tau_p = 0.2$ SEC

M_q/I_y SHOWN ARE FOR
AUGMENTATION SYSTEM
IT INCLUDE NATURAL
MIC DAMPING OF AIRCRAFT
ATELY $M_q/I_y = -0.43$)

$-.20$ RAD/SEC^2 – DEG

3 DEG/IN.

K_p	M_θ/I_y	K_θ
0	0	0
2.30	-0.7	2.60
7.50	-4.5	17.00

RAFT
, $M_\theta/I_y = 0$)

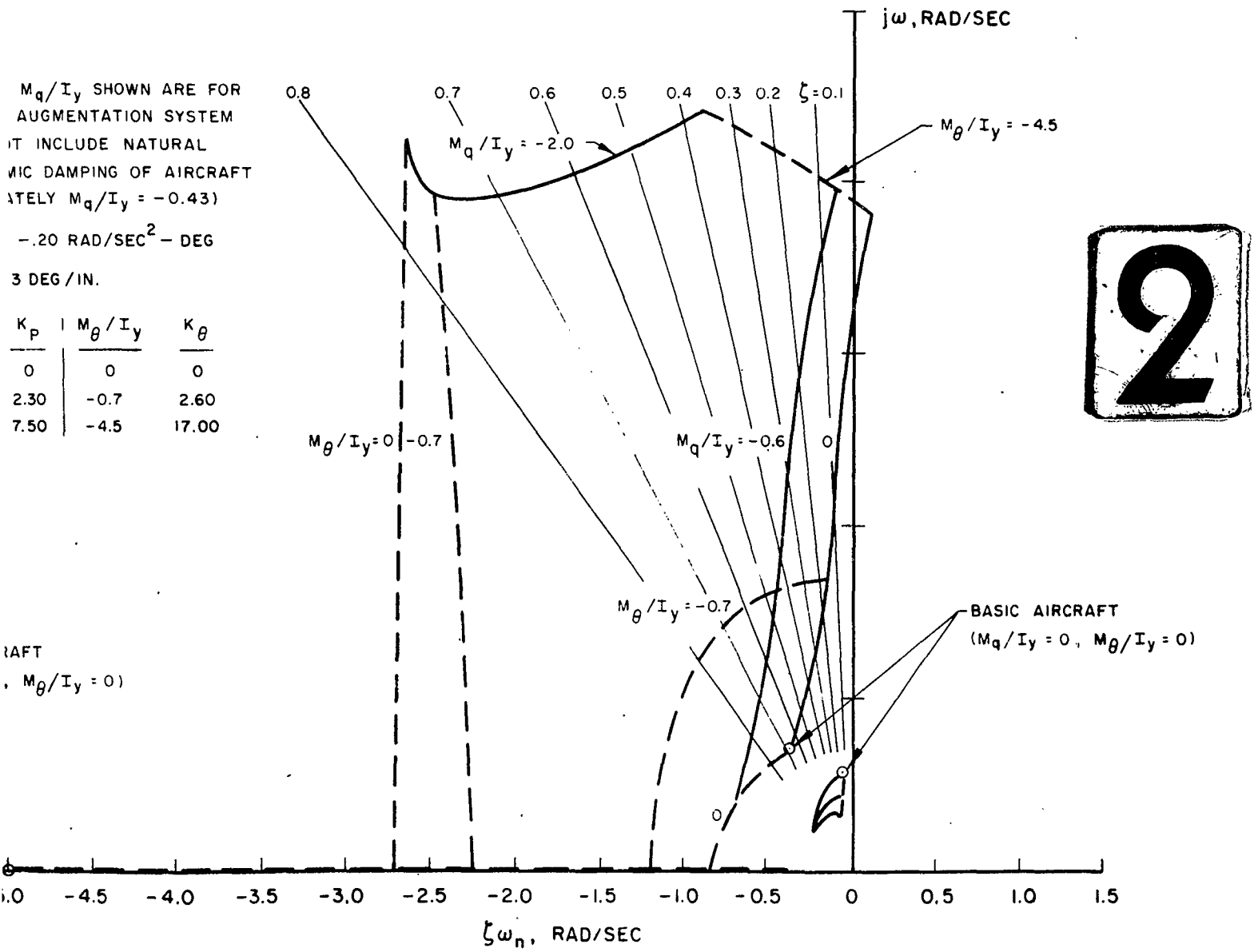

2

FIG. 21

TYPICAL CRITERIA FOR LONGITUDINAL HANDLING QUALITIES IN HOVER

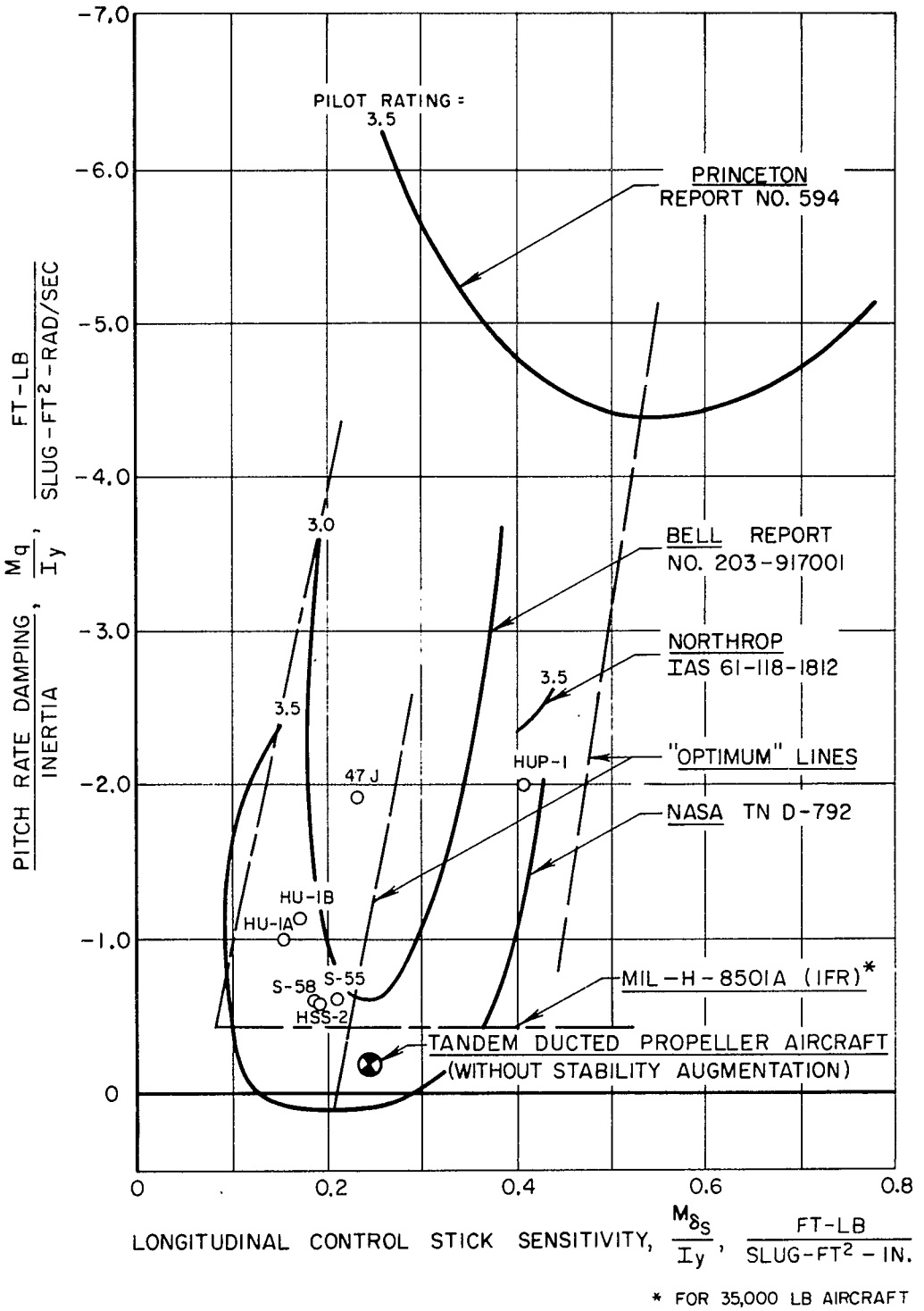

* FOR 35,000 LB AIRCRAFT

FIG. 22

VARIATION OF DAMPING AND CONTROL SENSITIVITY WITH VELOCITY DURING TRANSITIONS

NO STABILITY AUGMENTATION
FINAL K_{δ_β} PROGRAM

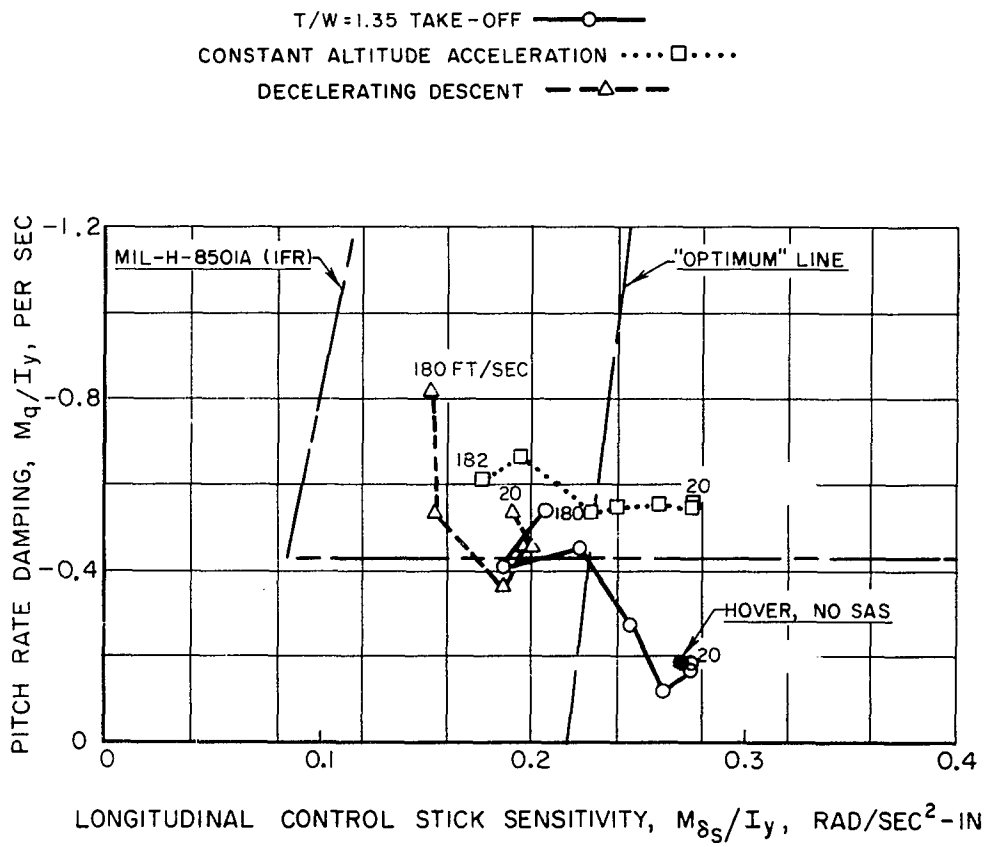

FIG. 23

VARIATION OF DAMPING AND CONTROL SENSITIVITY WITH VELOCITY DURING TRANSITIONS

FINAL STABILITY AUGMENTATION
FINAL K_{δ_β} PROGRAM

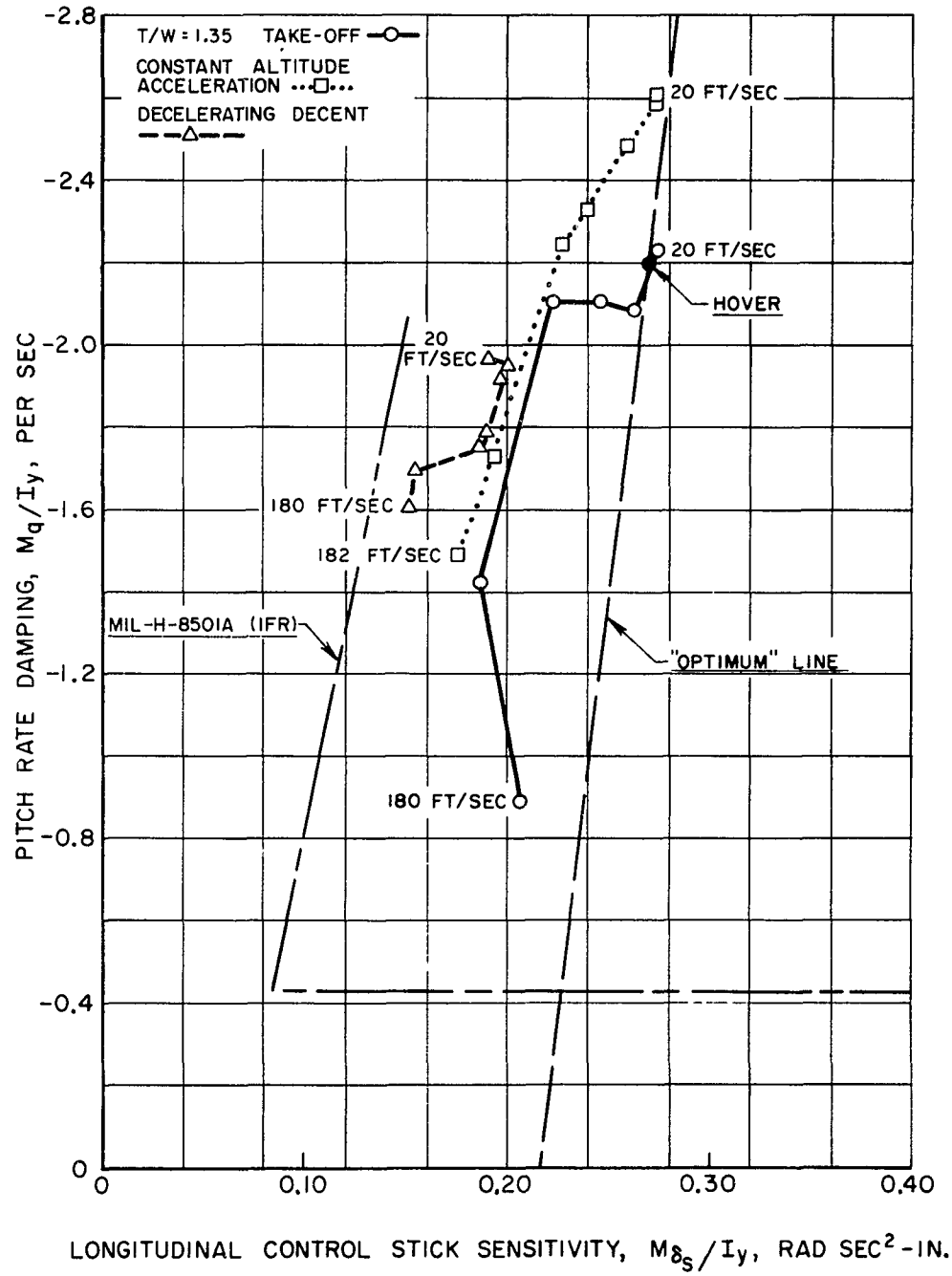

FIG. 24

VARIATION OF DAMPING AND CONTROL SENSITIVITY WITH VELOCITY DURING TRANSITIONS

FINAL STABILITY AUGMENTATION $1/n^2$, $SIN\, i_D$ PROGRAM FOR K_{δ_β}

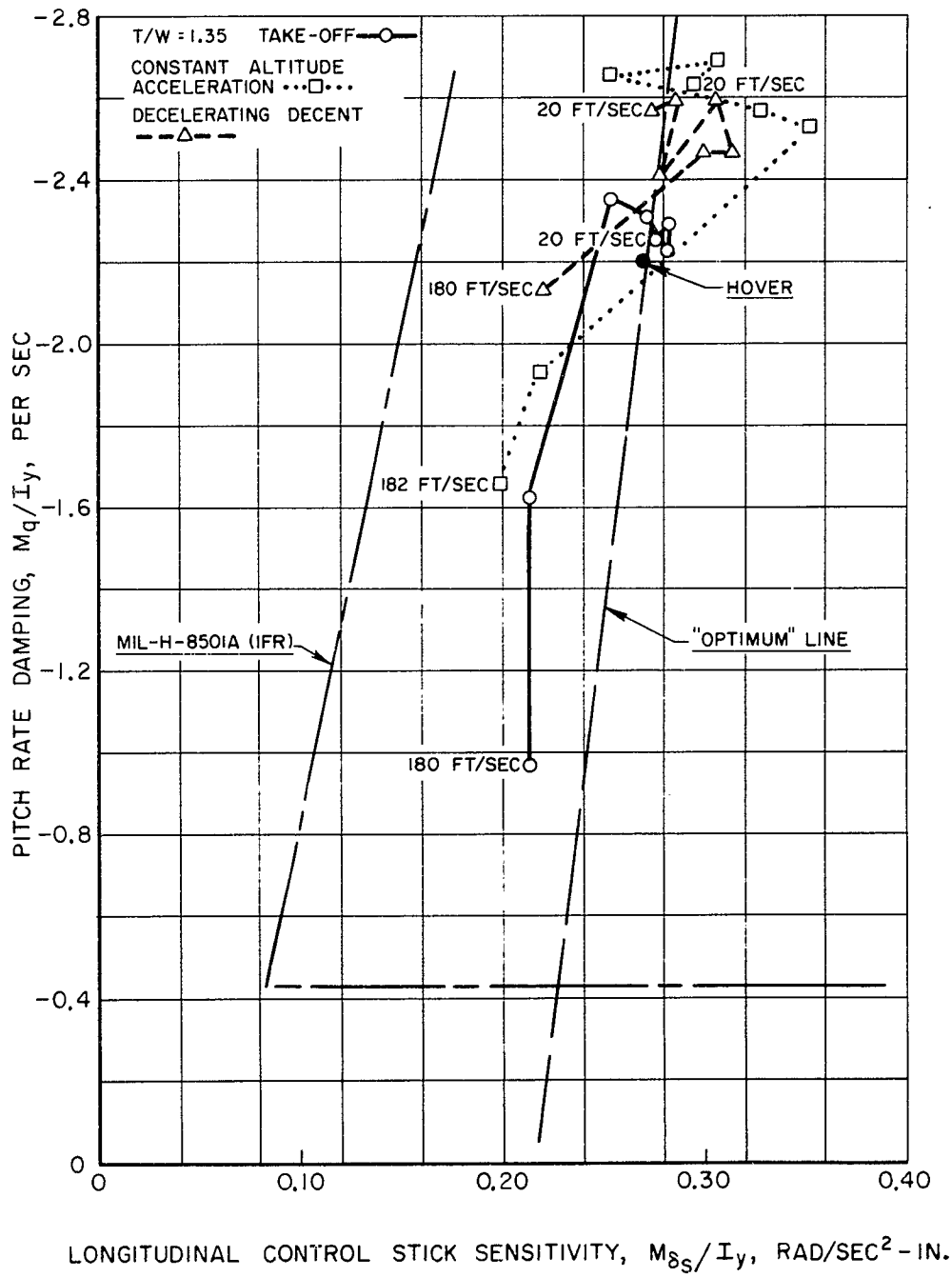

GAIN PROGRAMS FOR LONGITUDINAL CONTROL STICK

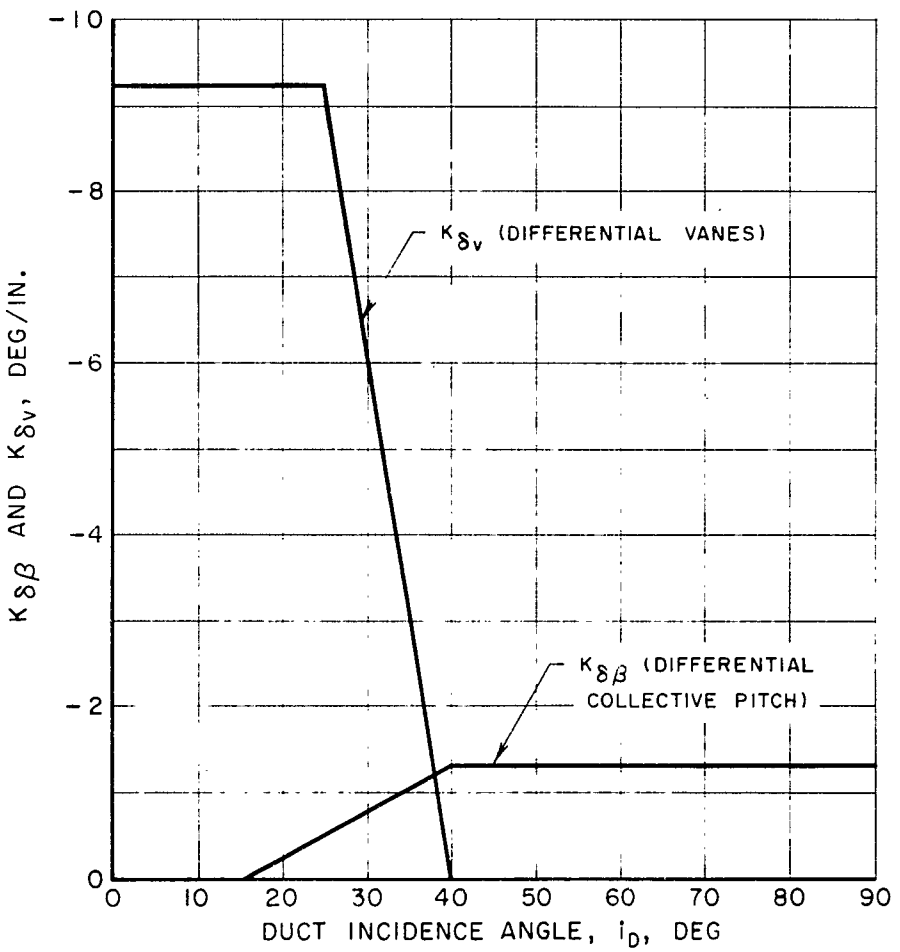

R-1624-5

SUMMARY OF LATERAL-DIRECTIONAL ROOT
STEADY LEVEL FLIGHT AT SPEEDS FROM HI
NO STABILITY AUGMENTATION

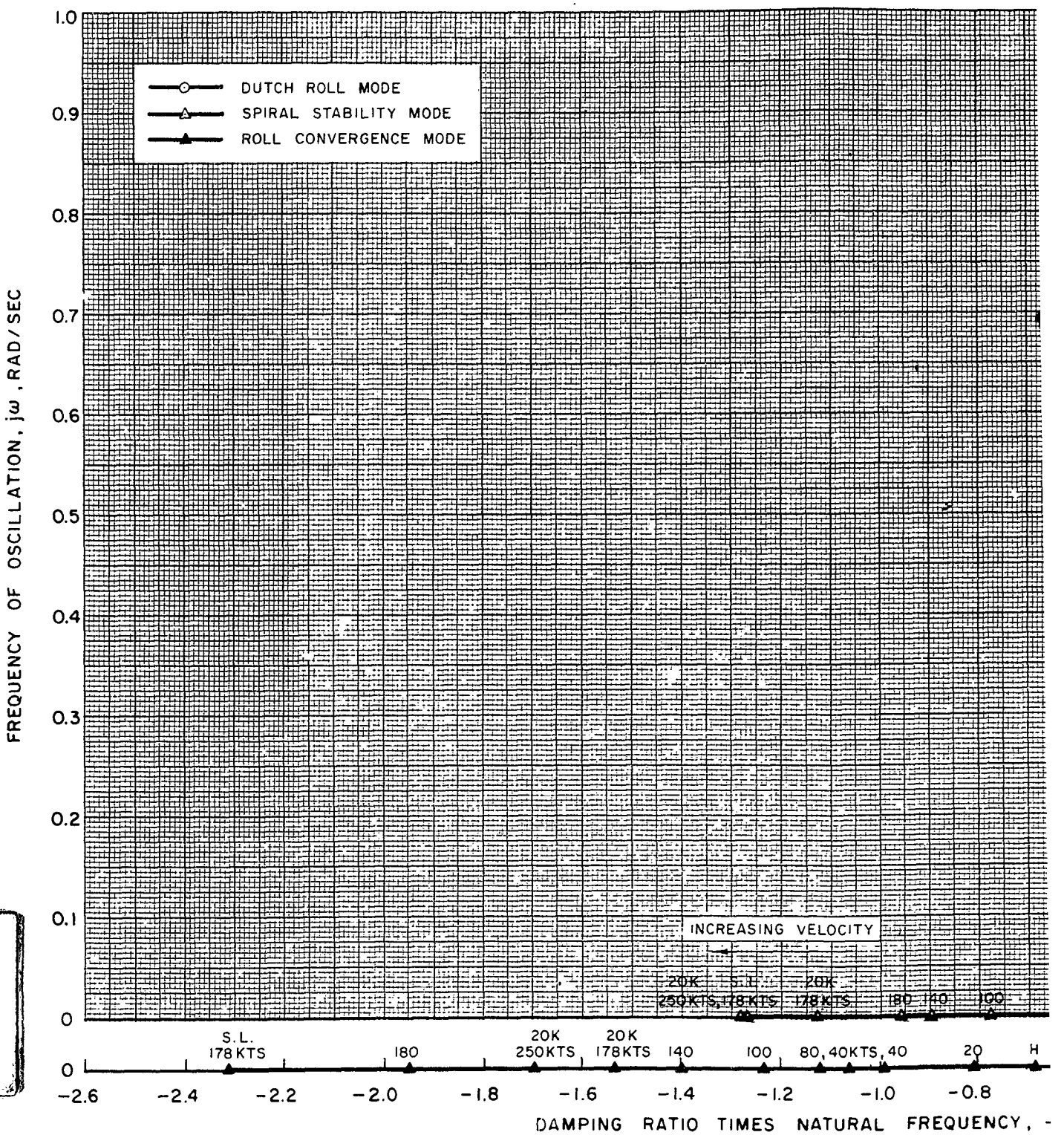

1

ERAL-DIRECTIONAL ROOT LOCATIONS FOR
HT AT SPEEDS FROM HOVER TO 250 KTS
O STABILITY AUGMENTATION

FIG. 26

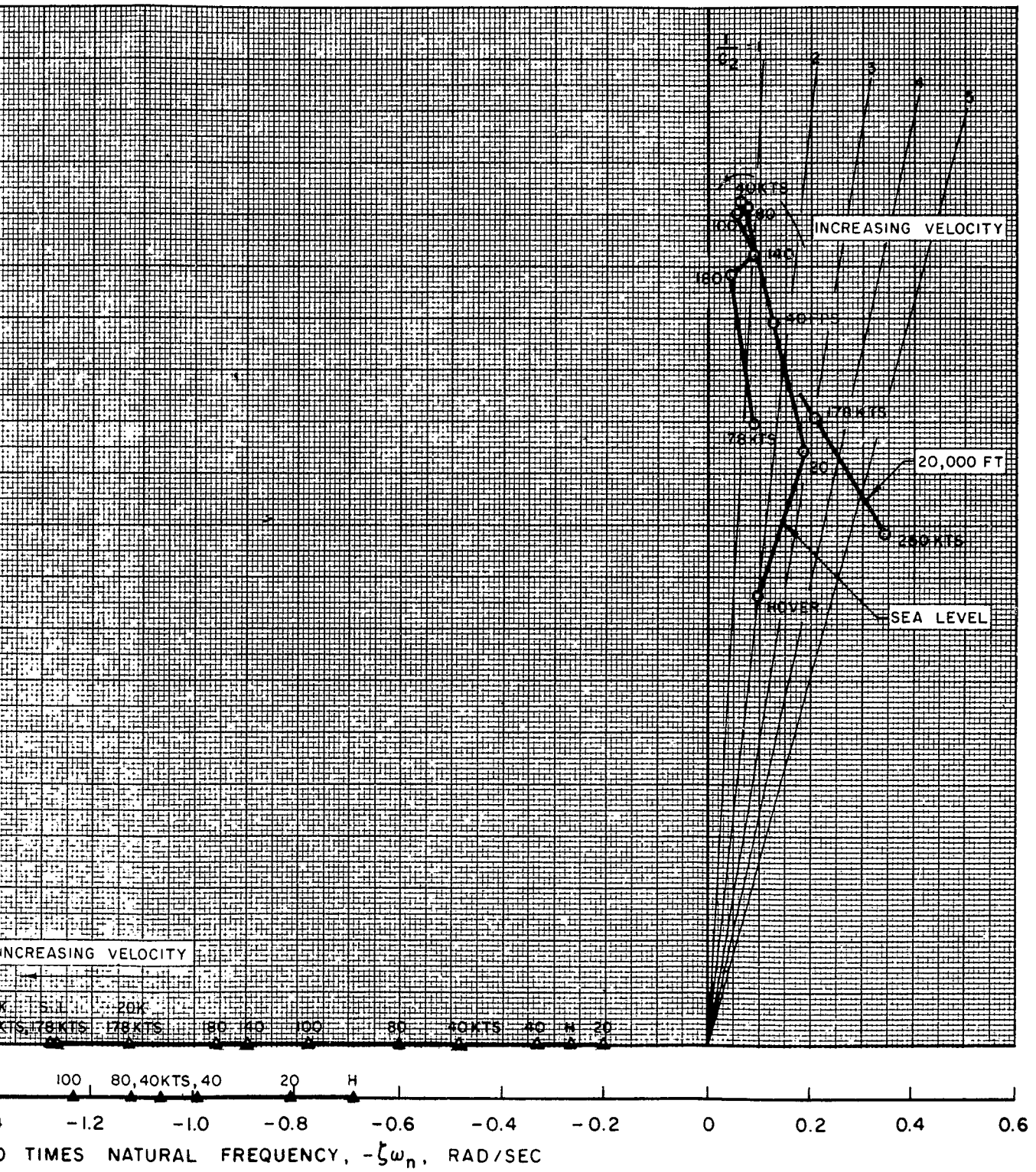

SUMMARY OF LATERAL-DIRECTIONAL ROOT LOCATIONS FOR NO STABILITY AUGMENTA

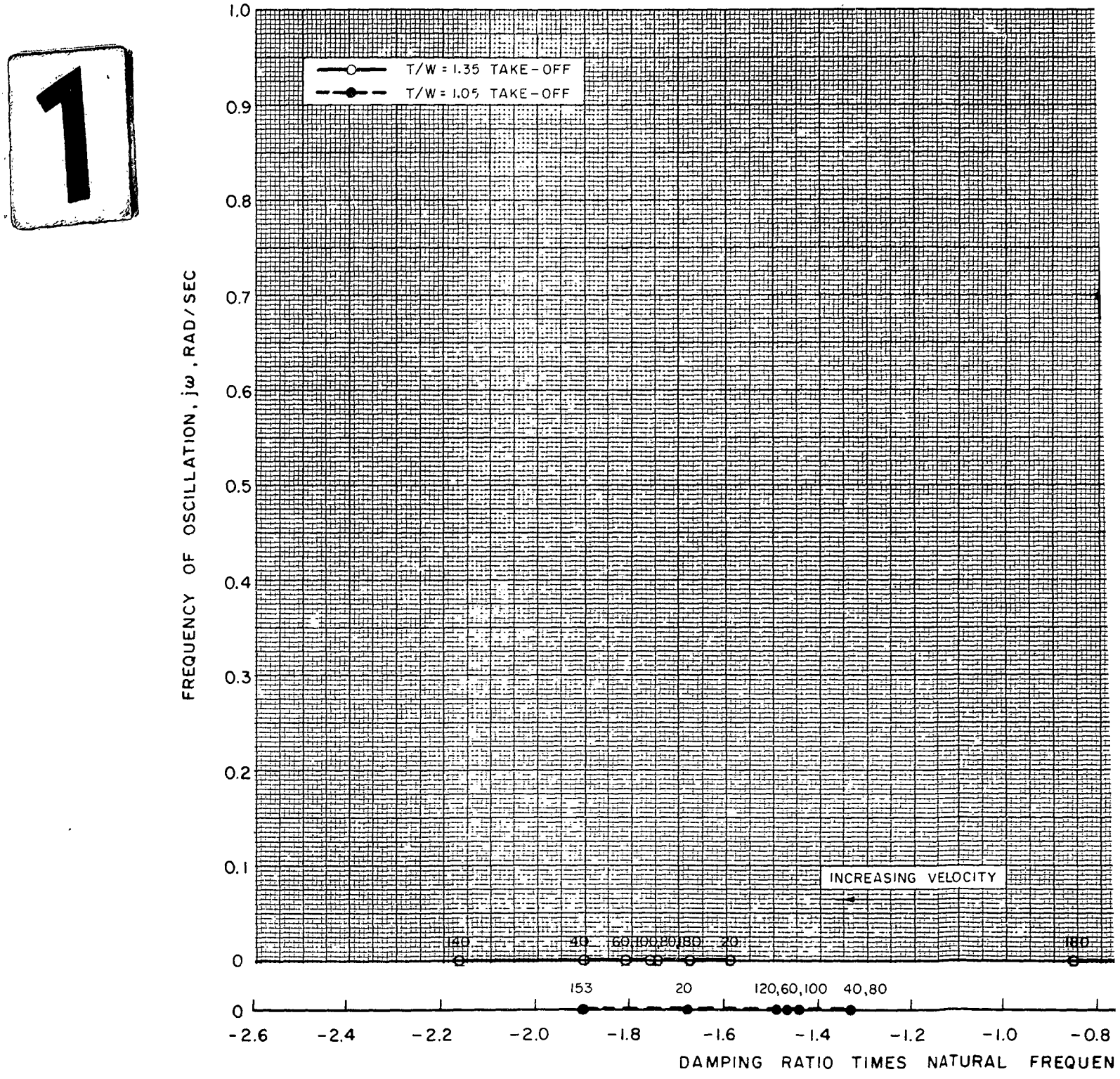

FIG. 27

)OT LOCATIONS FOR REPRESENTATIVE TRANSITION MANEUVERS
O STABILITY AUGMENTATION

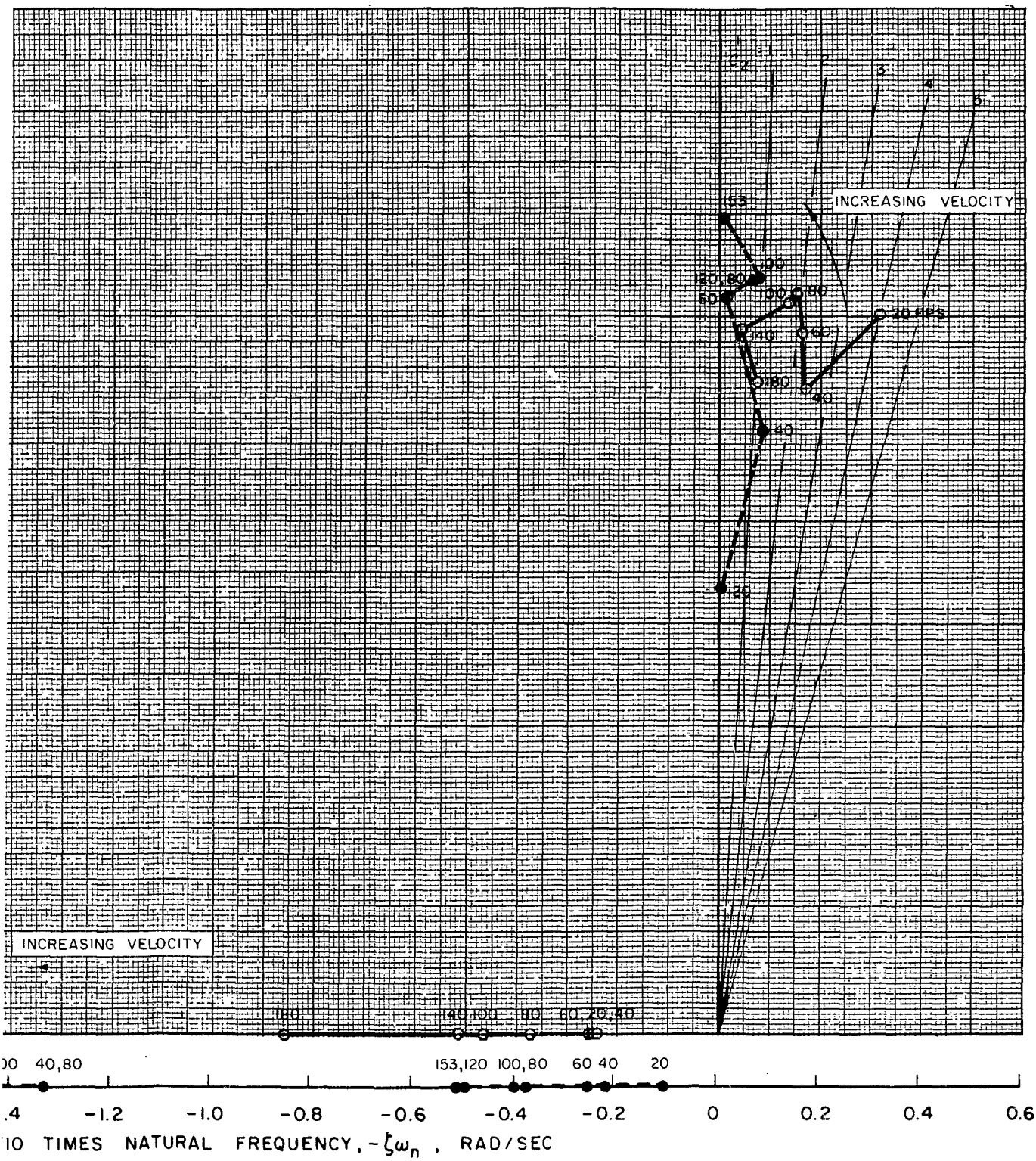

2

FIG. 28

EFFECTS OF IMPORTANT STABILITY DERIVATIVES ON LATERAL-DIRECTIONAL DYNAMICS IN STEADY LEVEL FLIGHT AT 40 KTS

NO STABILITY AUGMENTATION
NOMINAL CENTER OF GRAVITY LOCATION

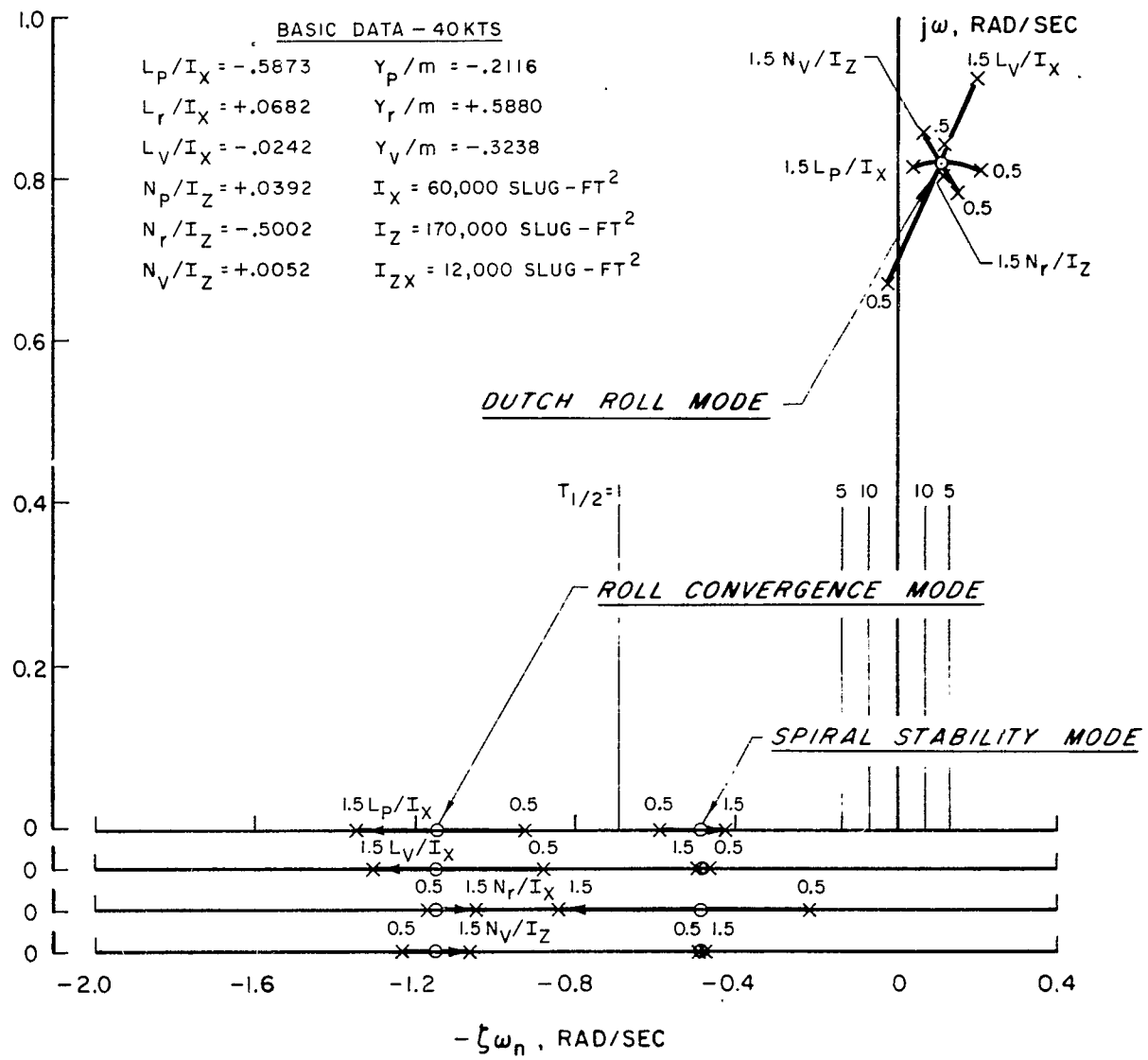

FIG. 29

EFFECTS OF MASS AND MOMENTS OF INERTIA ON LATERAL-DIRECTIONAL DYNAMICS IN STEADY LEVEL FLIGHT AT 40 KTS

NO STABILITY AUGMENTATION
NOMINAL CENTER OF GRAVITY LOCATION

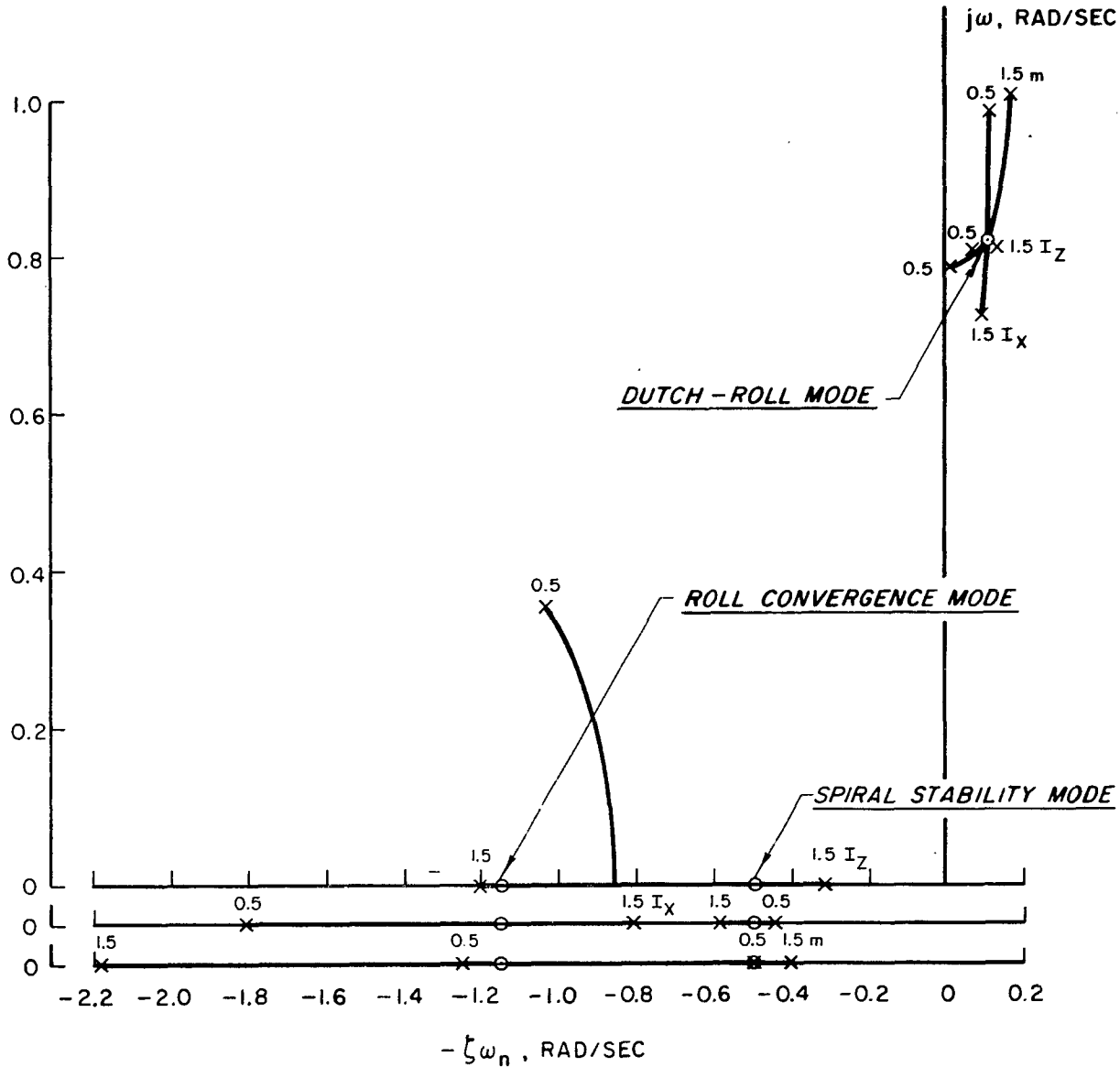

FIG. 30

MODEL OF LATERAL-DIRECTIONAL CONTROL AND STABILITY AUGMENTATION SYSTEM

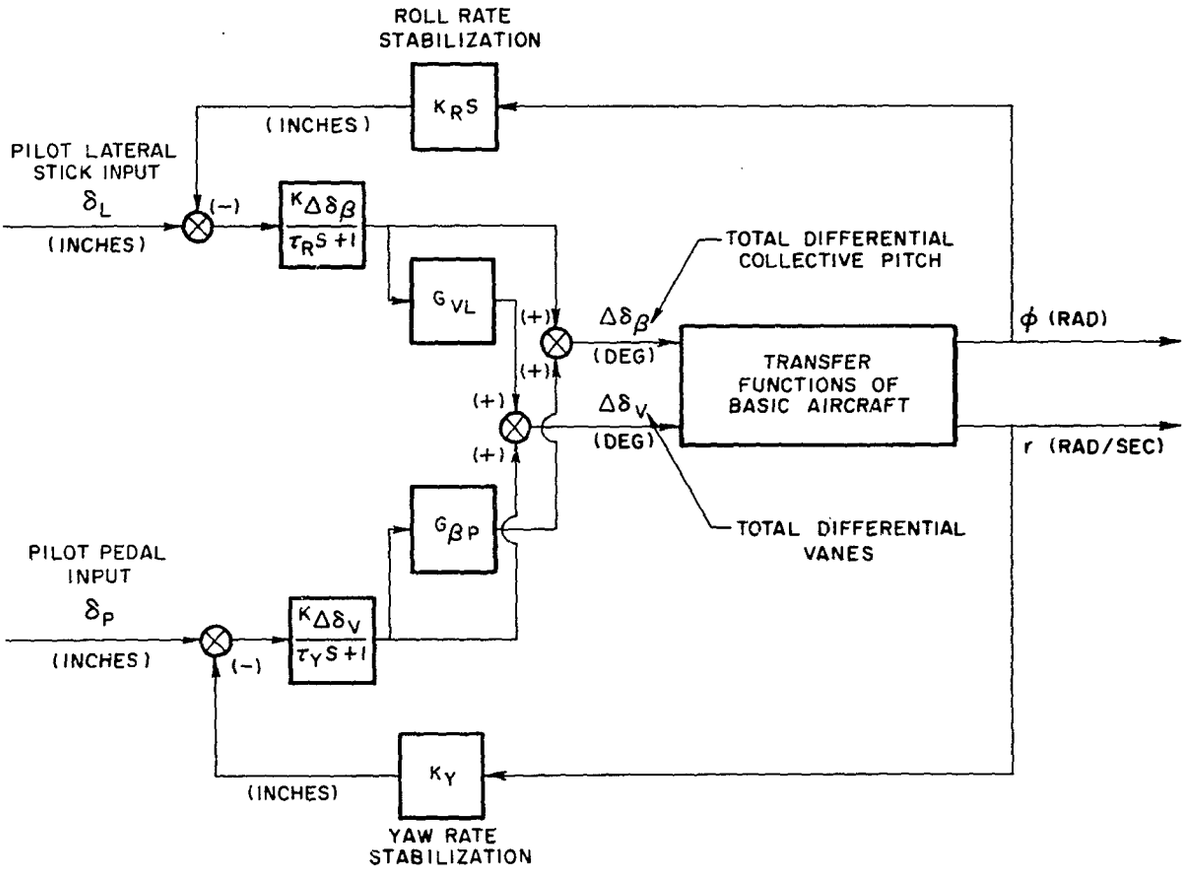

EFFECT OF LAGS IN STABILITY AUGMENTATION SYSTEM ON

STEADY LEVEL FLIGHTS AT 40 KT

COMBINED τ_Y AND τ_R LAGS

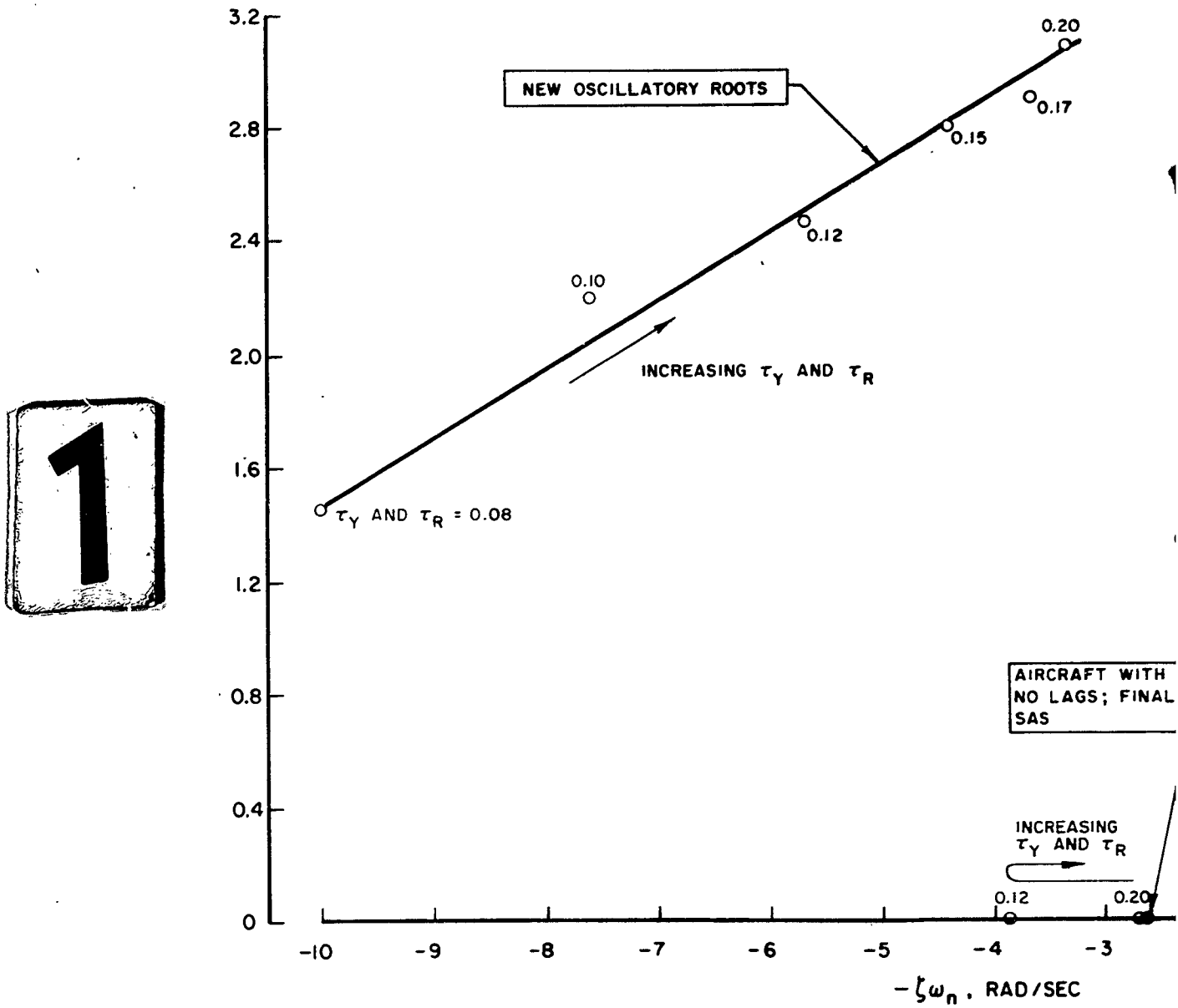

FIG. 31

GMENTATION SYSTEM ON LATERAL-DIRECTIONAL DYNAMICS

DY LEVEL FLIGHTS AT 40KTS

:OMBINED τ_Y AND τ_R LAGS

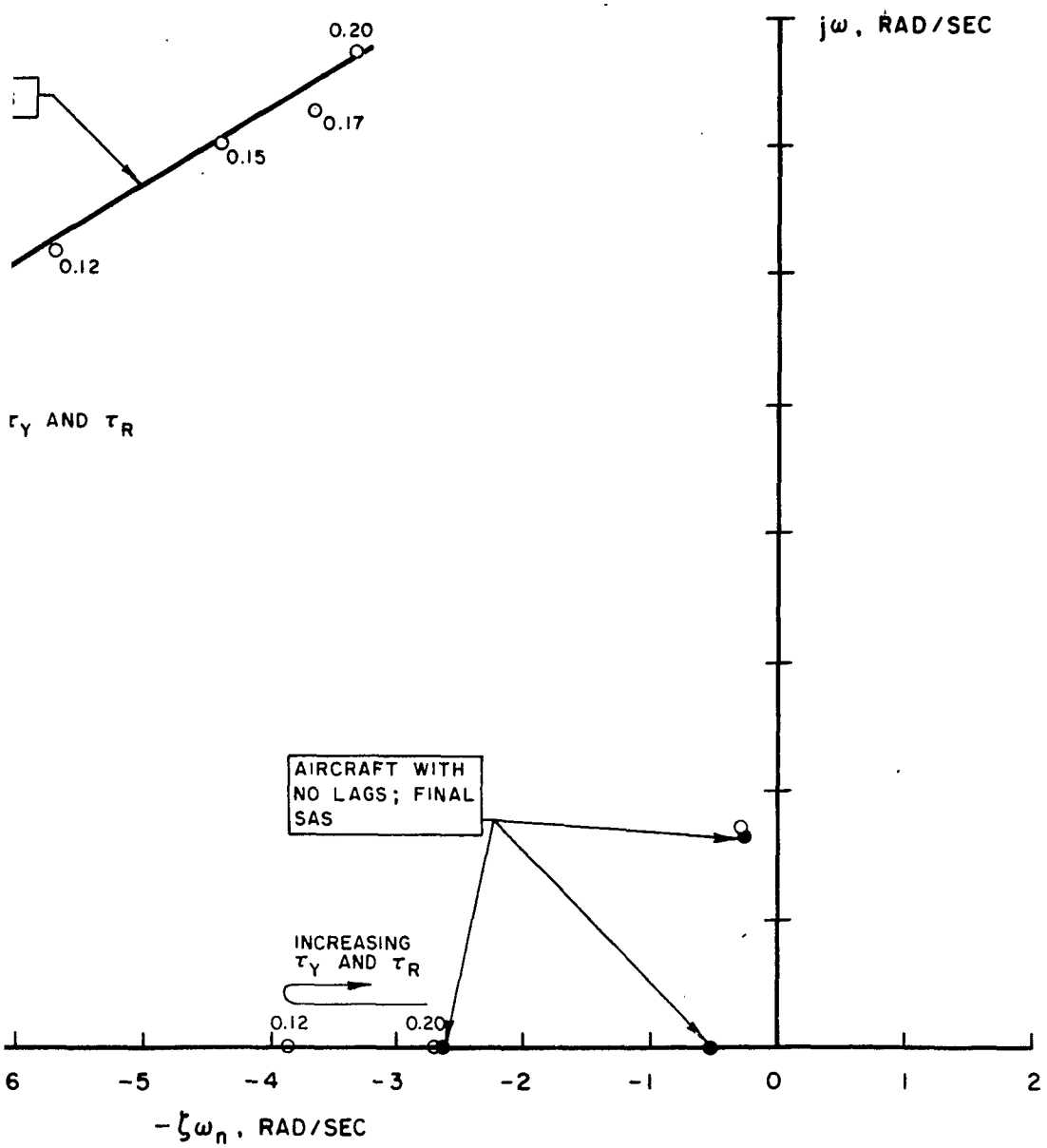

τ_Y AND τ_R

2

FIG. 32

BLOCK DIAGRAM OF LONGITUDINAL CONTROL AND STABILITY AUGMENTATION SYSTEM

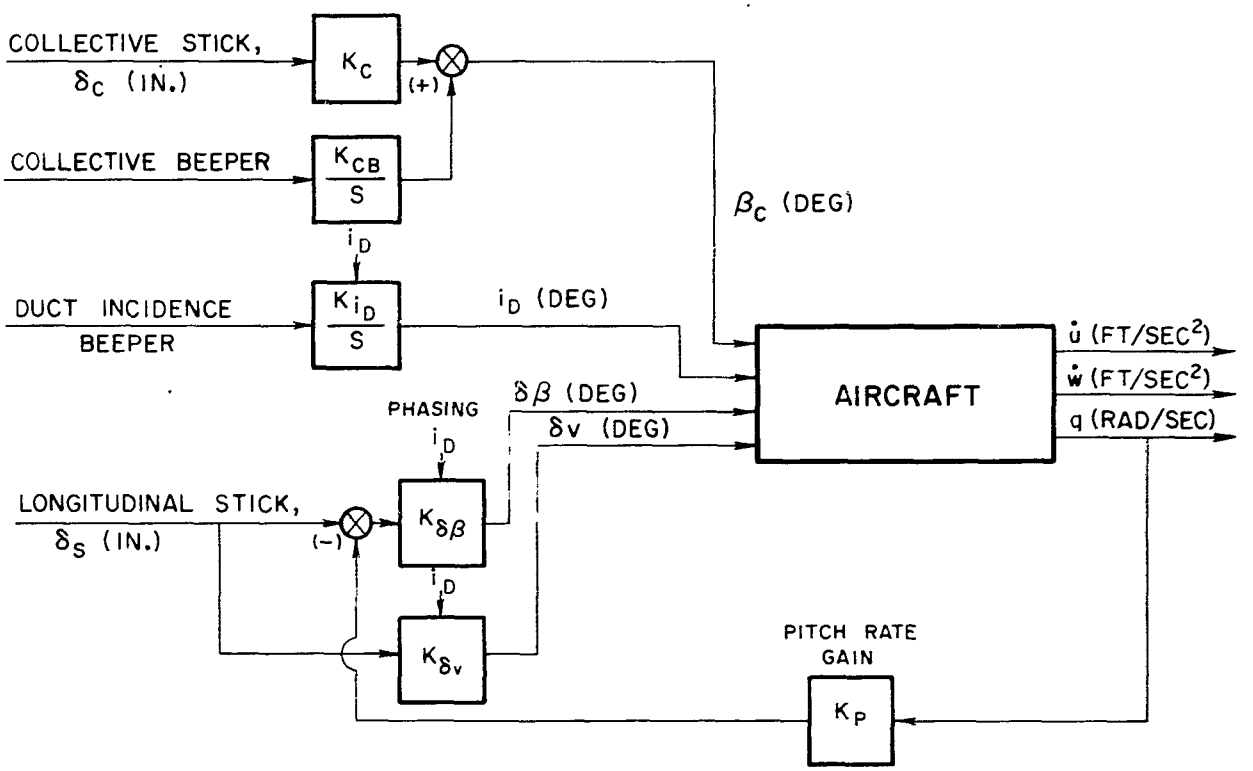

SCHEMATIC OF INITIAL LONGITUDINAL CONTROL AND STABILITY AUGMENTATION SYSTEM

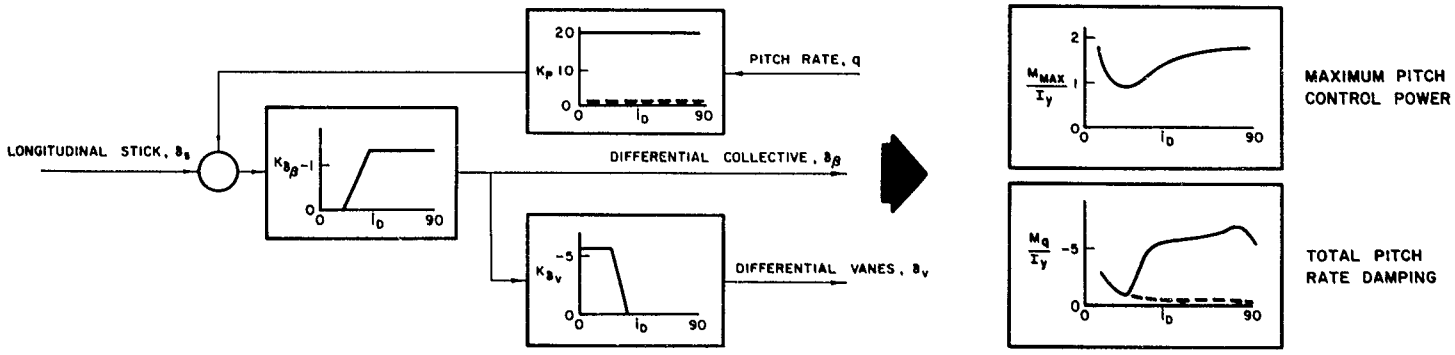

FIG. 33

BLOCK DIAGRAM OF LATERAL-DIRECTIONAL CONTROL AND STABILITY AUGMENTATION SYSTEM

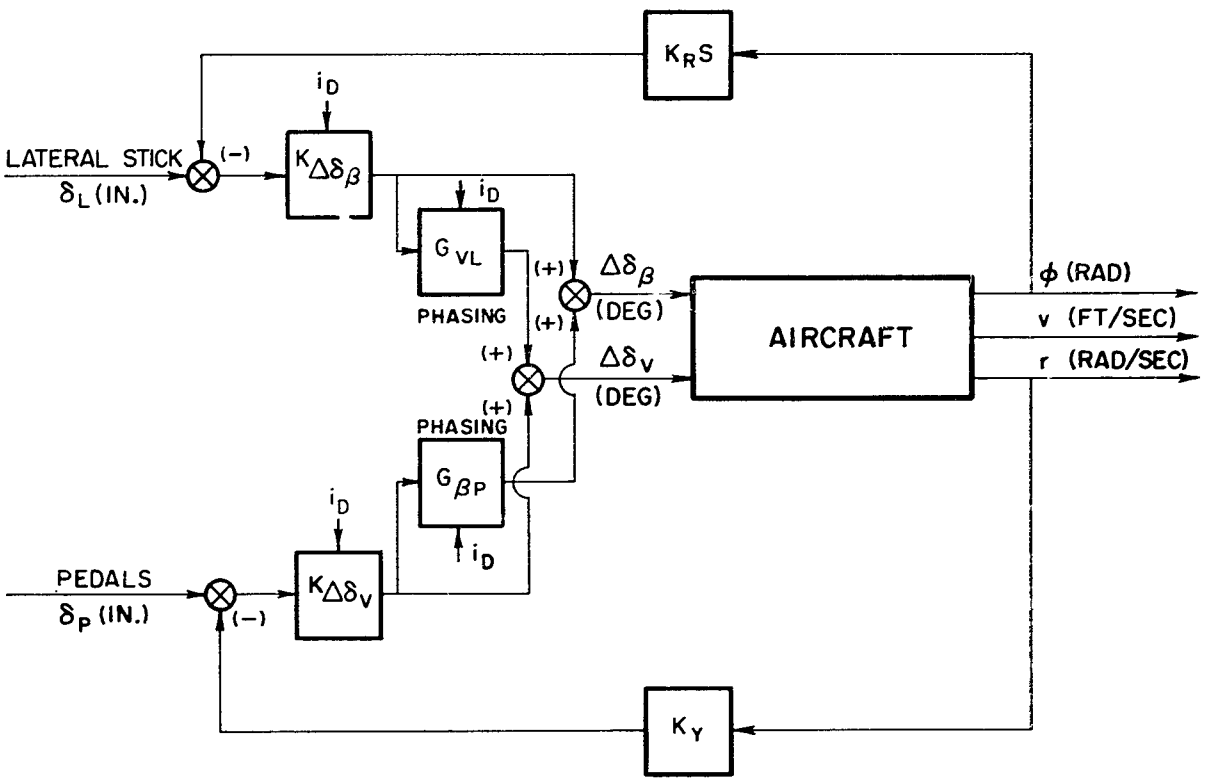

SCHEMATIC OF INITIAL LATERAL-DIRECTIONAL CONTROL AND STABILITY AUGMENTATION SYSTEM

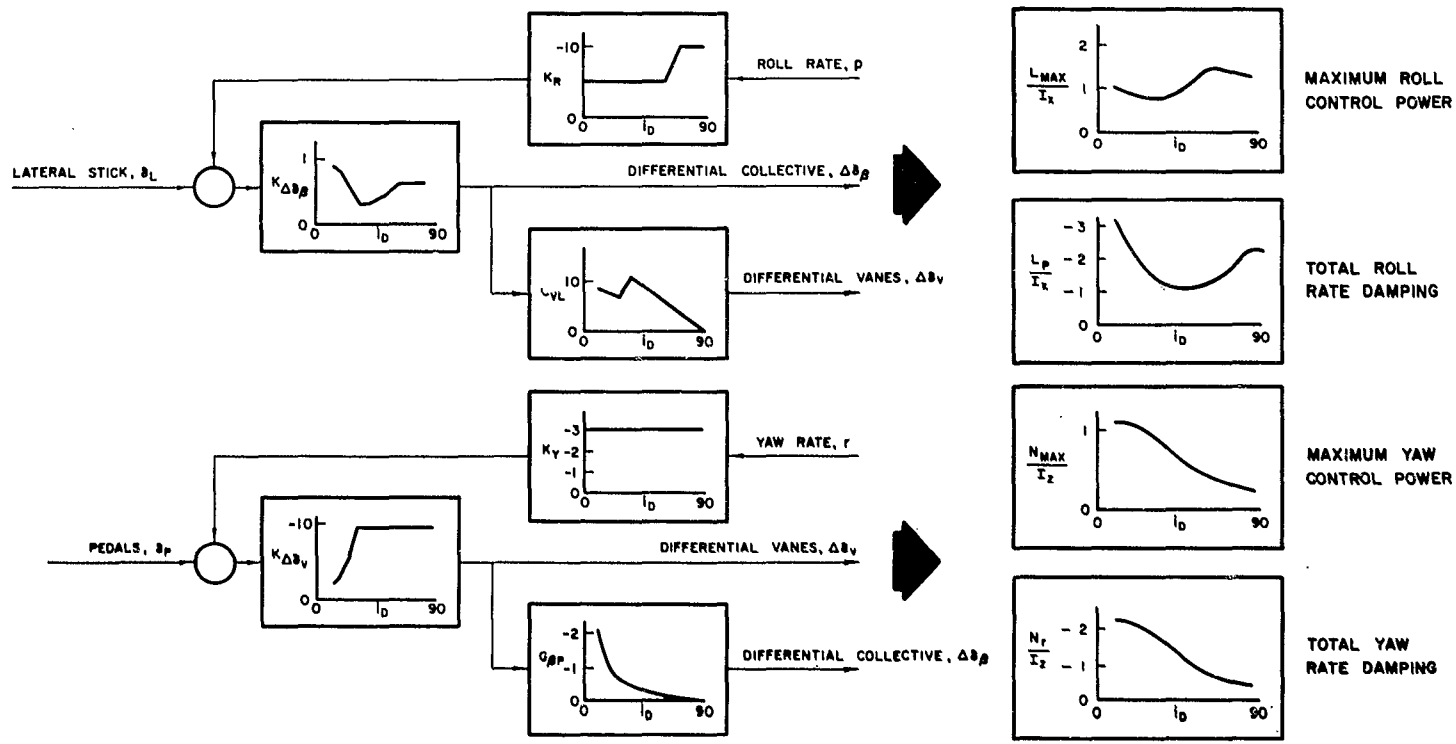

FIG. 35

FIG. 36

VARIATION OF LONGITUDINAL CONTROL STICK SENSITIVITY WITH DUCT INCIDENCE ANGLE

STEADY LEVEL FLIGHT

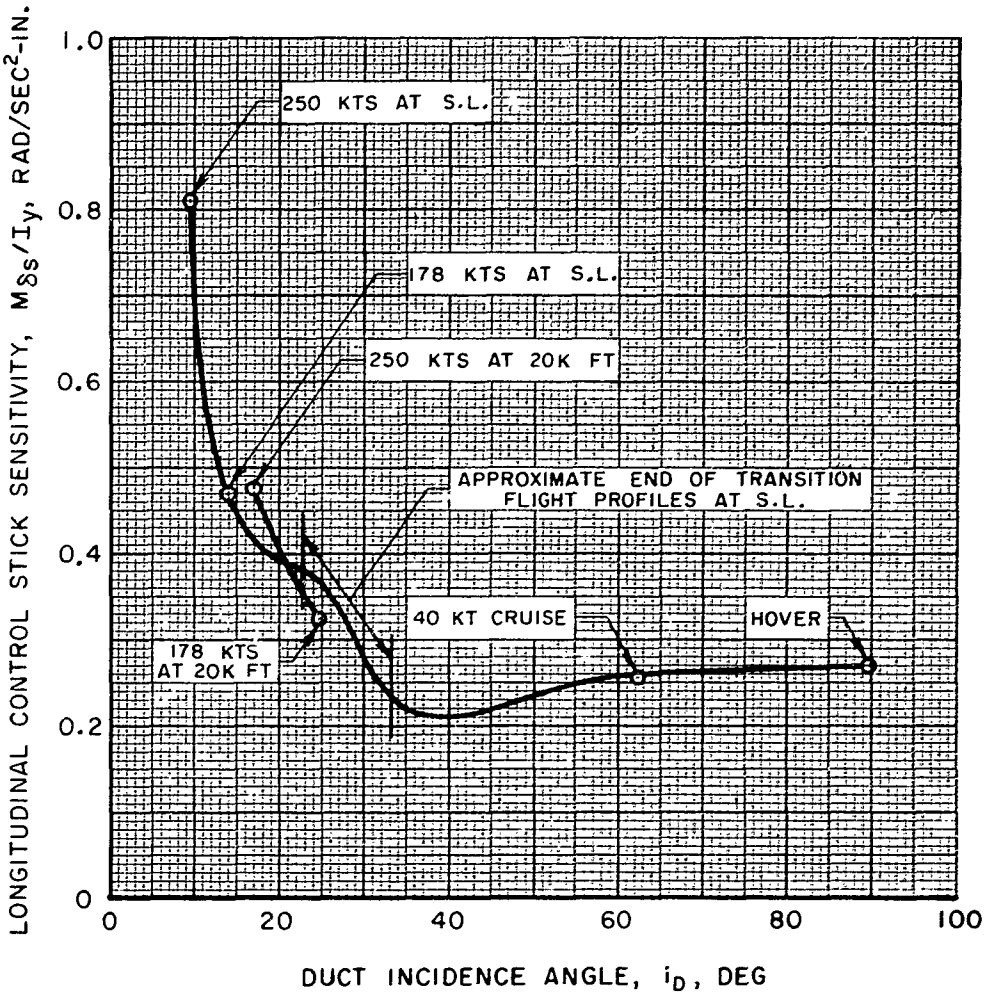

FIG. 37

VARIATION OF PITCH RATE DAMPING WITH DUCT INCIDENCE ANGLE

STEADY LEVEL FLIGHT

K_p = CONSTANT = 7.5 IN.– SEC/RAD

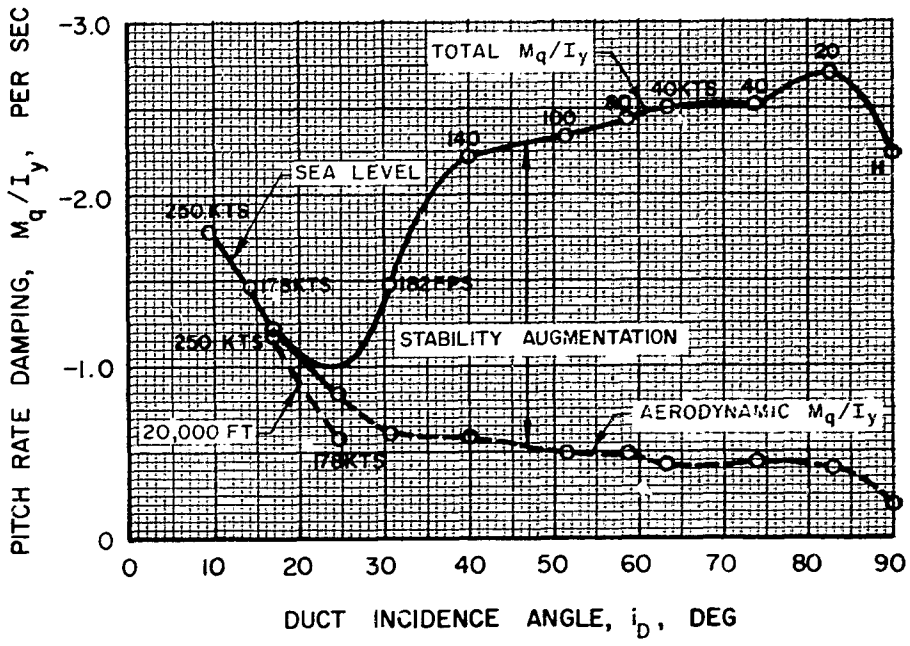

VARIATION OF MAXIMUM LONGITUDINAL CONTROL POWER WITH DUCT INCIDENCE ANGLE

STEADY LEVEL FLIGHT

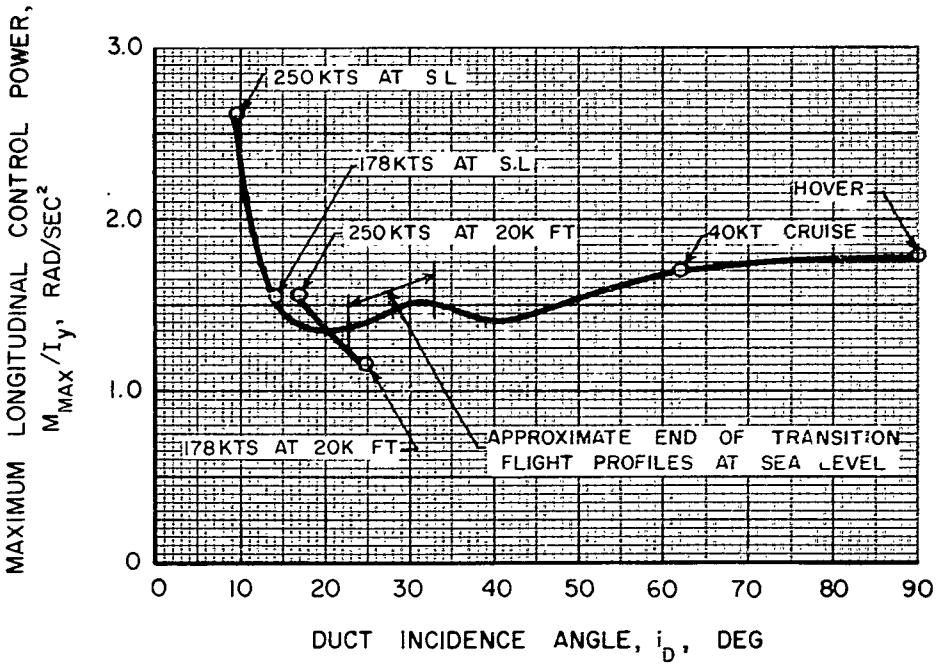

FIG. 39

COMPARISON OF SELECTED LEVELS OF LONGITUDINAL CONTROL SENSITIVITY AND PITCH RATE DAMPING WITH RESULTS OF BELL STUDY

NOTE: 1. M_q/I_y AND M_{δ_s}/I_y ARE VALUES AT HOVER
2. PILOT RATING BOUNDARIES FROM BELL REPORT NO. 2023-917002

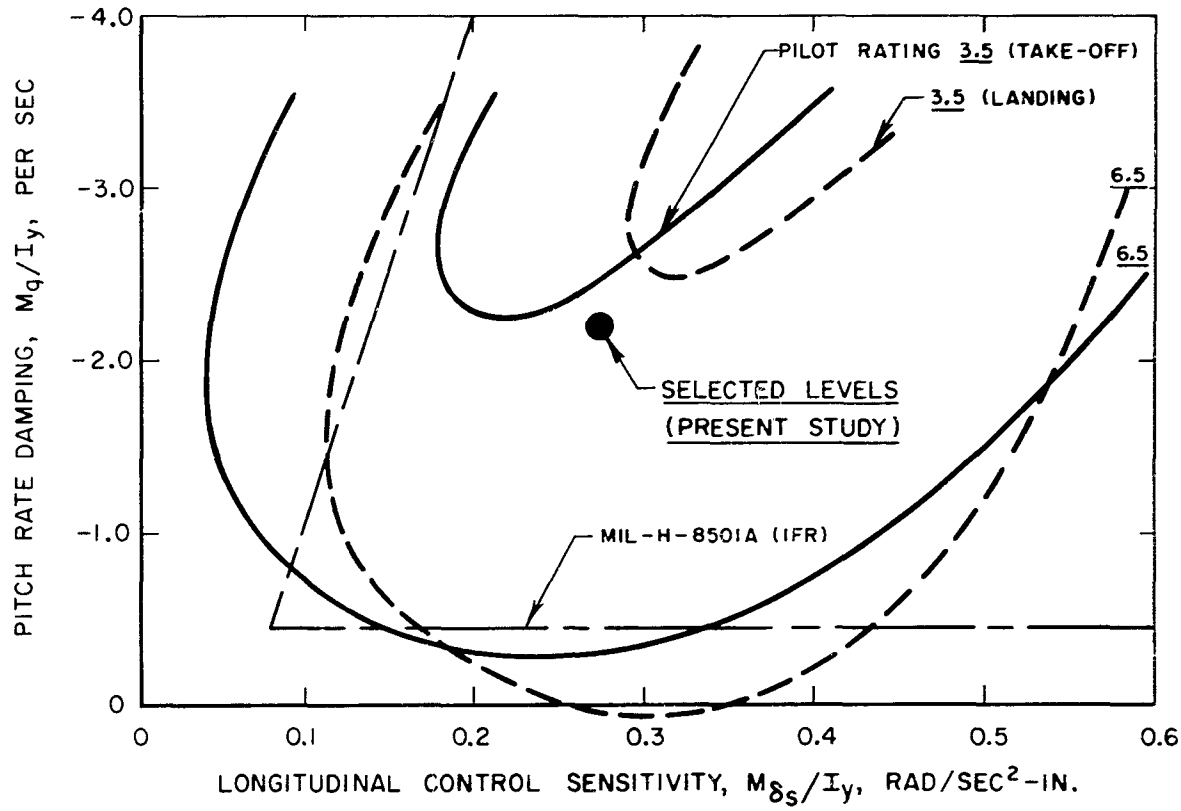

SUMMARY OF LONGITUDINAL ROOT LOCATION
FLIGHT AT SPEEDS FROM -30KTS
WITH STABILITY AUGMENTAT

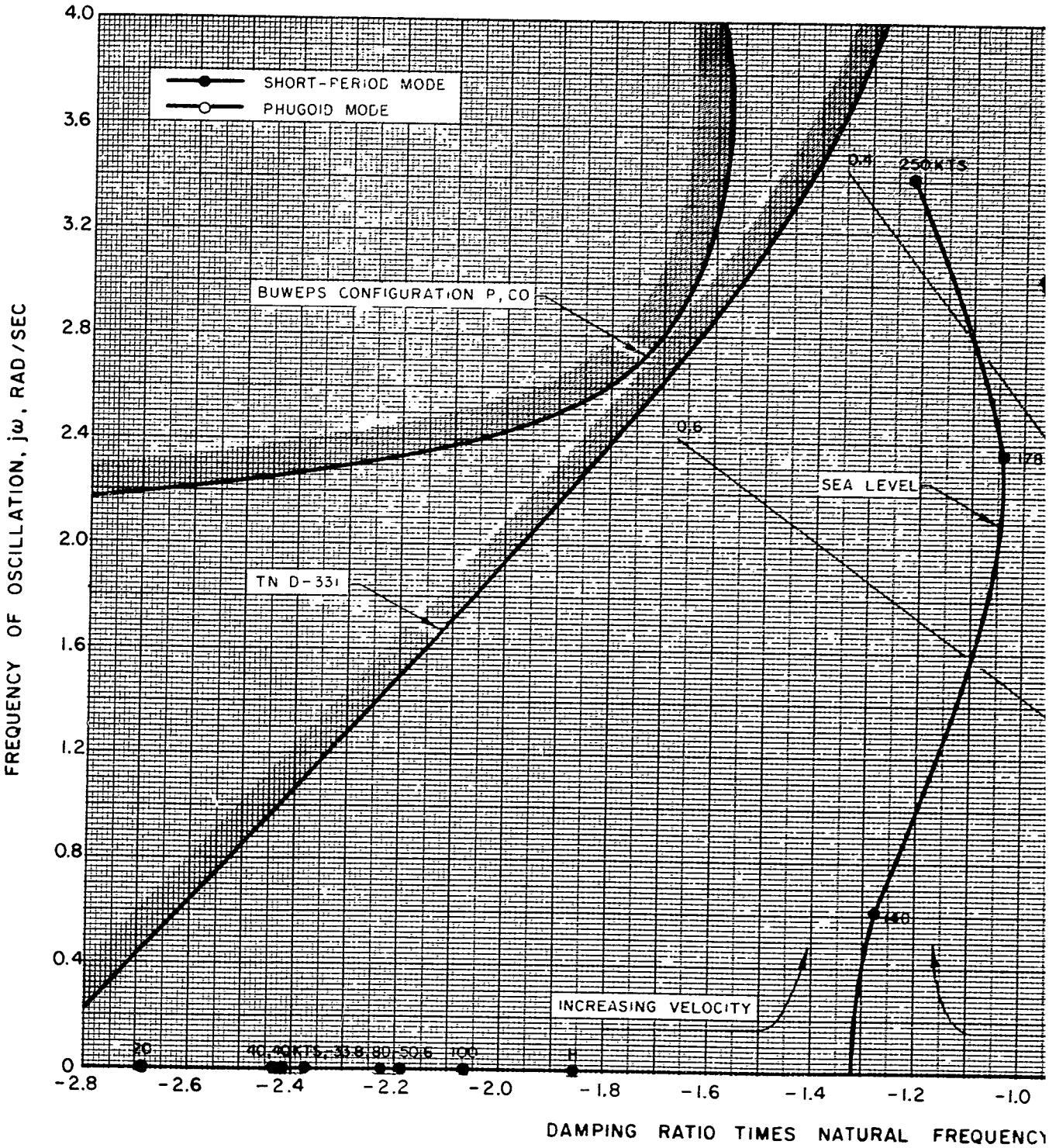

FIG. 40

)INAL ROOT LOCATIONS FOR STEADY LEVEL
EEDS FROM -30KTS TO +250KTS
1 STABILITY AUGMENTATION

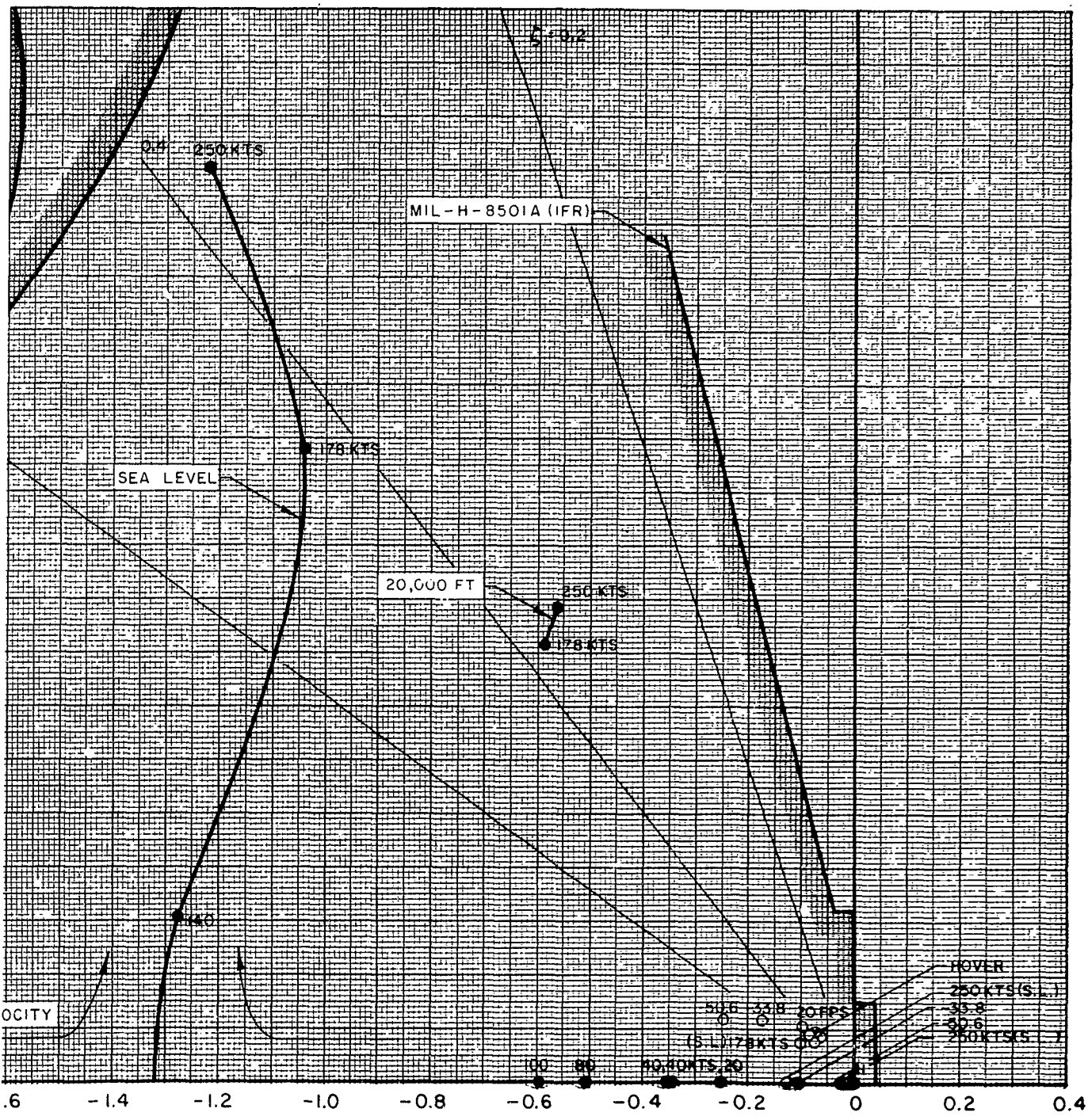

2

)O TIMES NATURAL FREQUENCY, $-\zeta\omega_n$, RAD/SEC

LONGITUDINAL ROOT LOCATIONS FOR T/W
WITH STABILITY AUGMENTATIOI

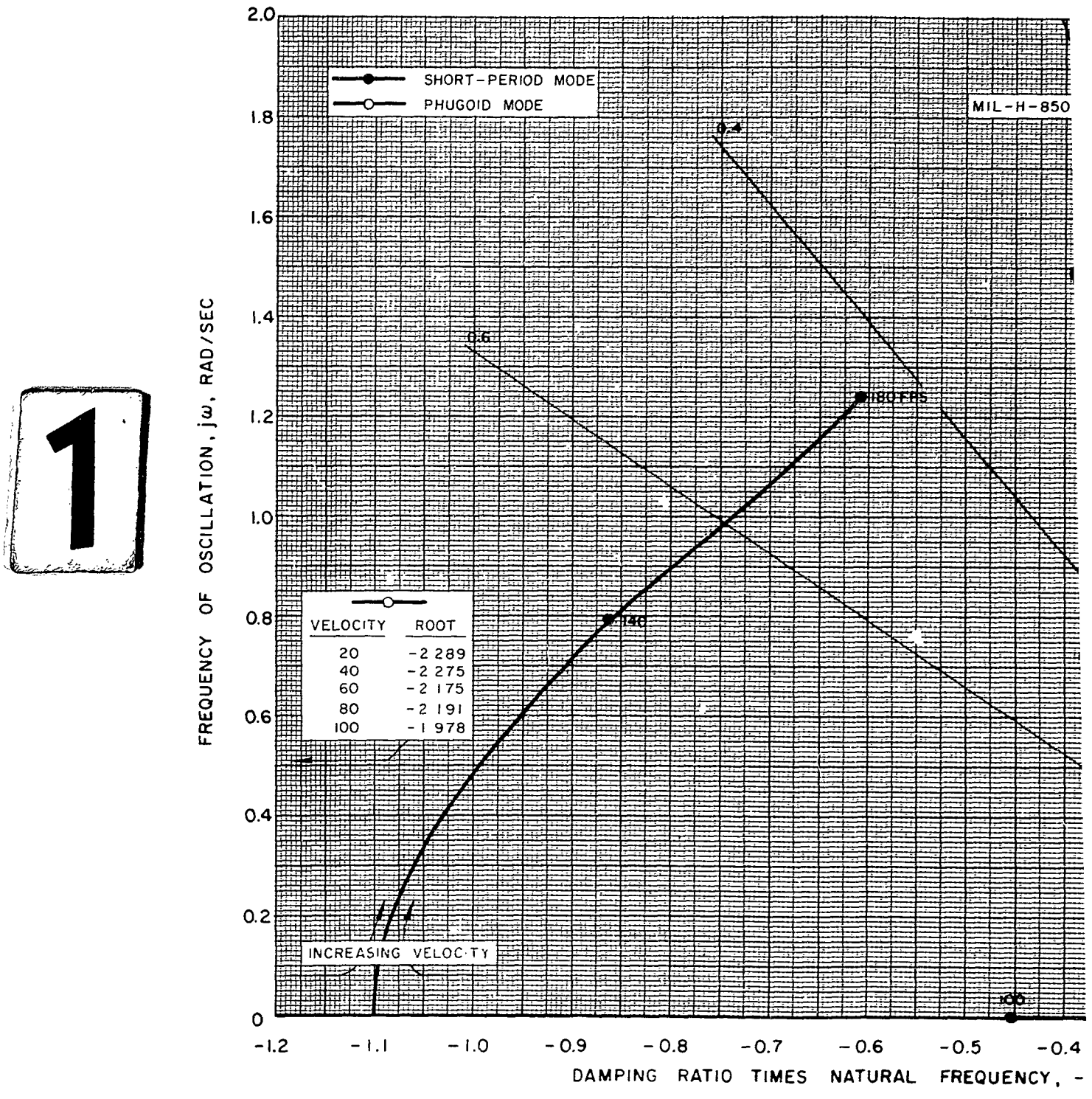

FIG. 41

OT LOCATIONS FOR T/W = 1.35 TAKE-OFF
TH STABILITY AUGMENTATION

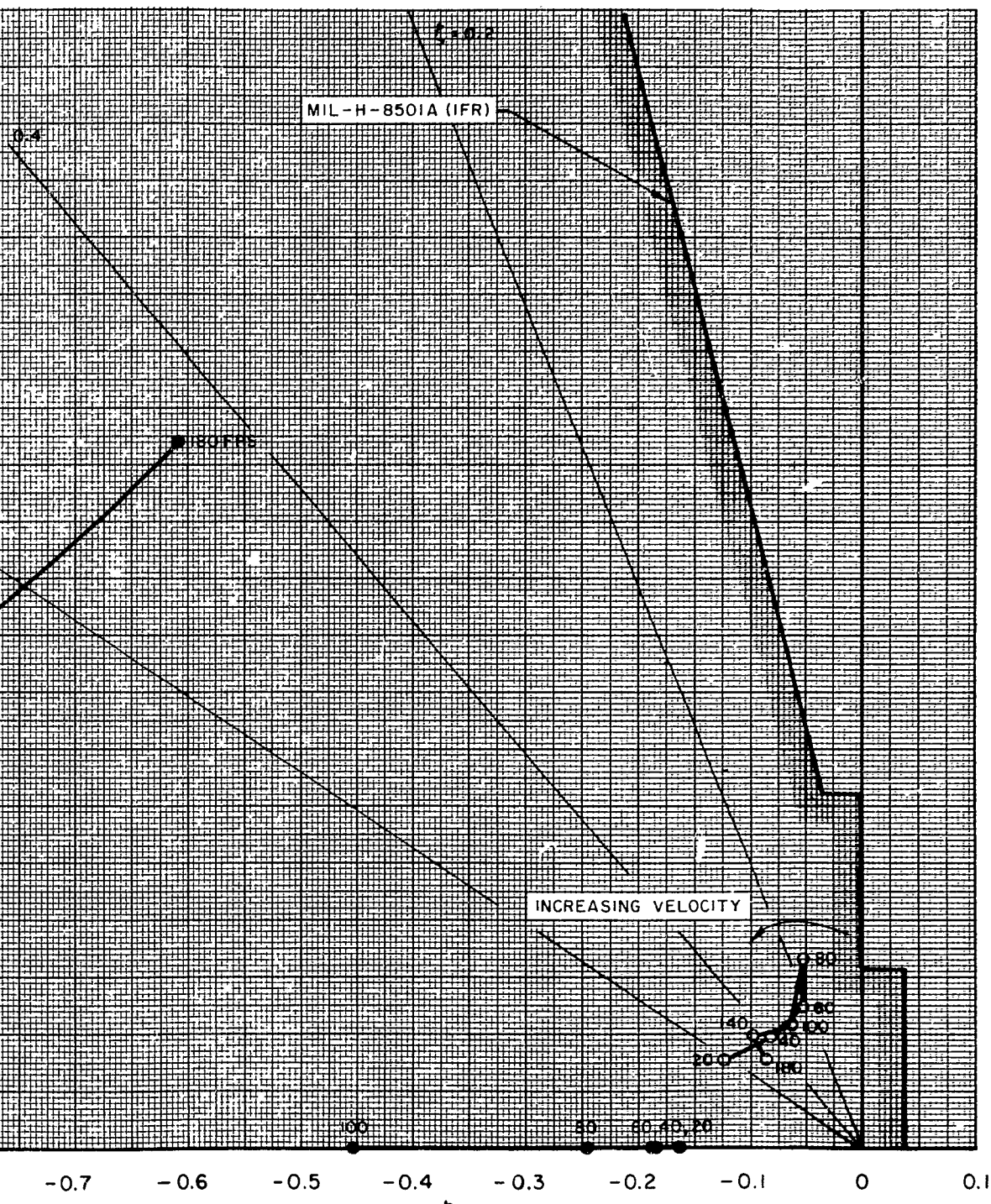

2

FIG. 42

ALTITUDE DAMPING AND COLLECTIVE STICK SENSITIVITY IN HOVER

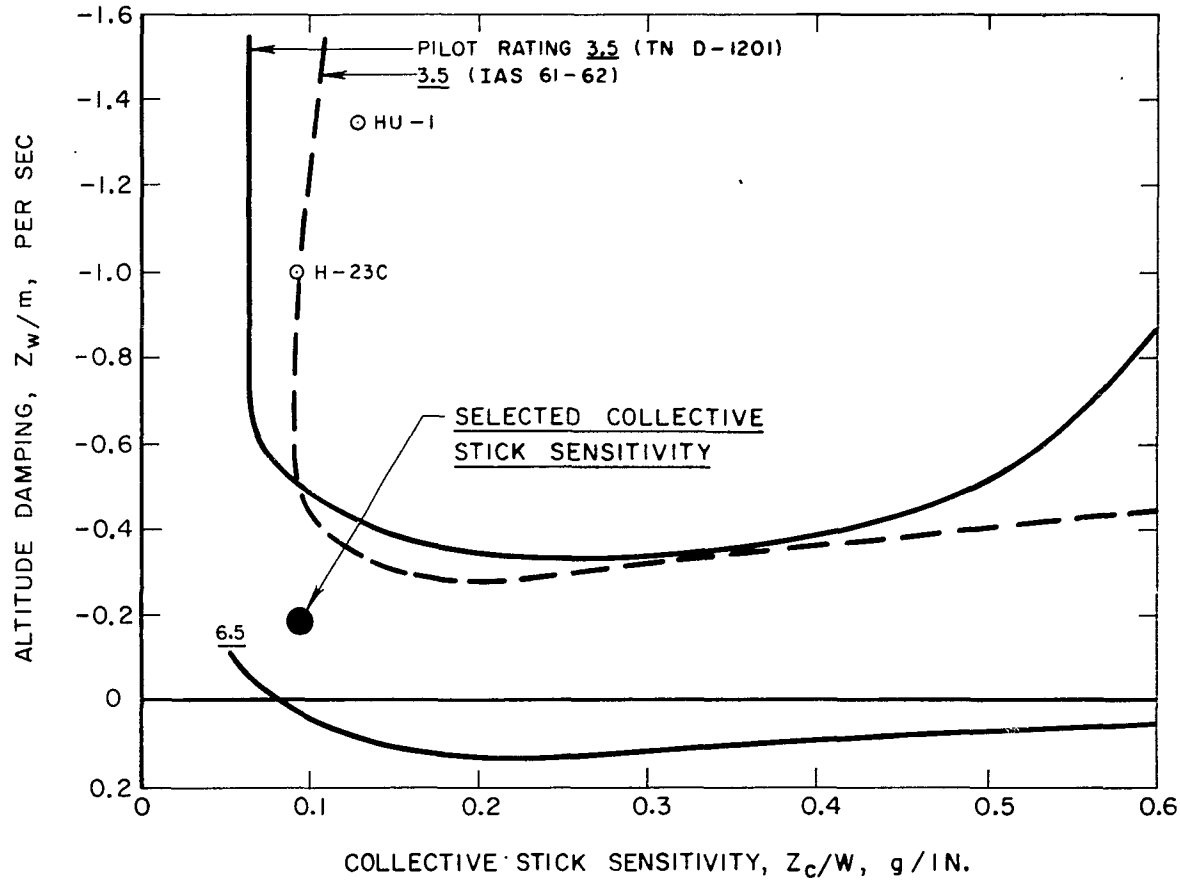

FIG. 43

VARIATION OF LATERAL CONTROL STICK SENSITIVITY WITH DUCT INCIDENCE ANGLE

STEADY LEVEL FLIGHT

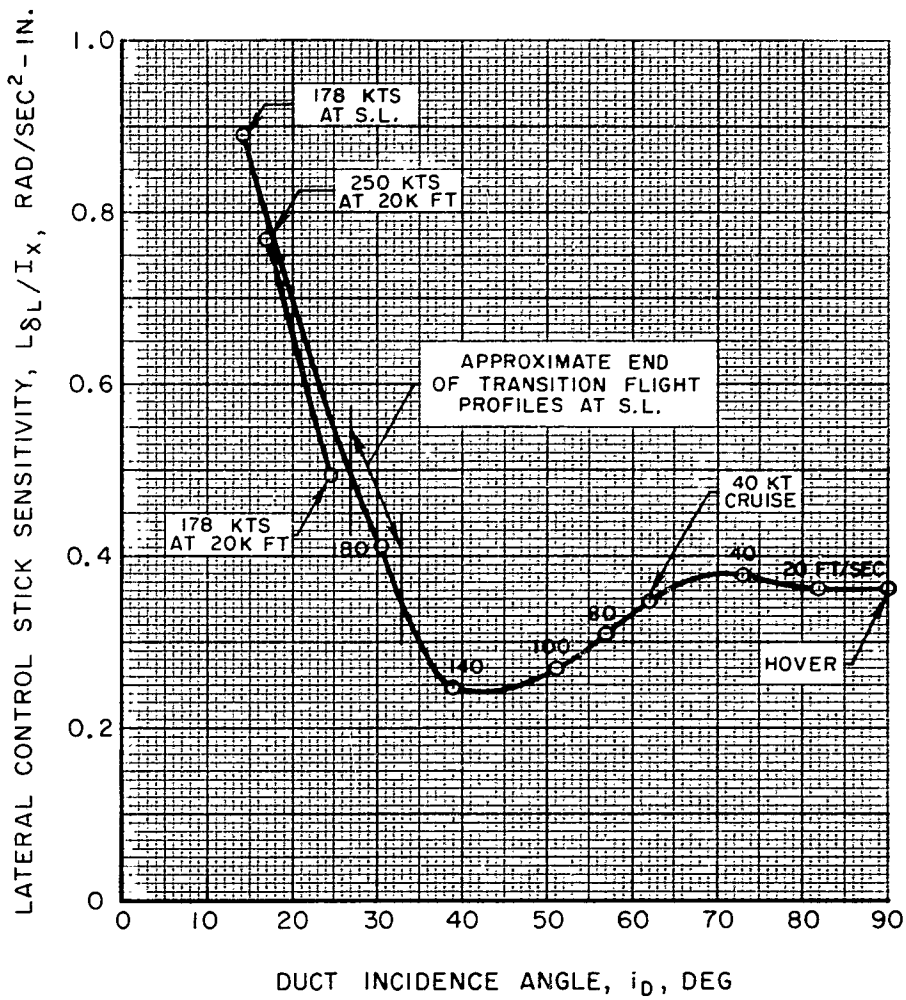

FIG. 44

VARIATION OF ROLL RATE DAMPING WITH DUCT INCIDENCE ANGLE

STEADY LEVEL FLIGHT

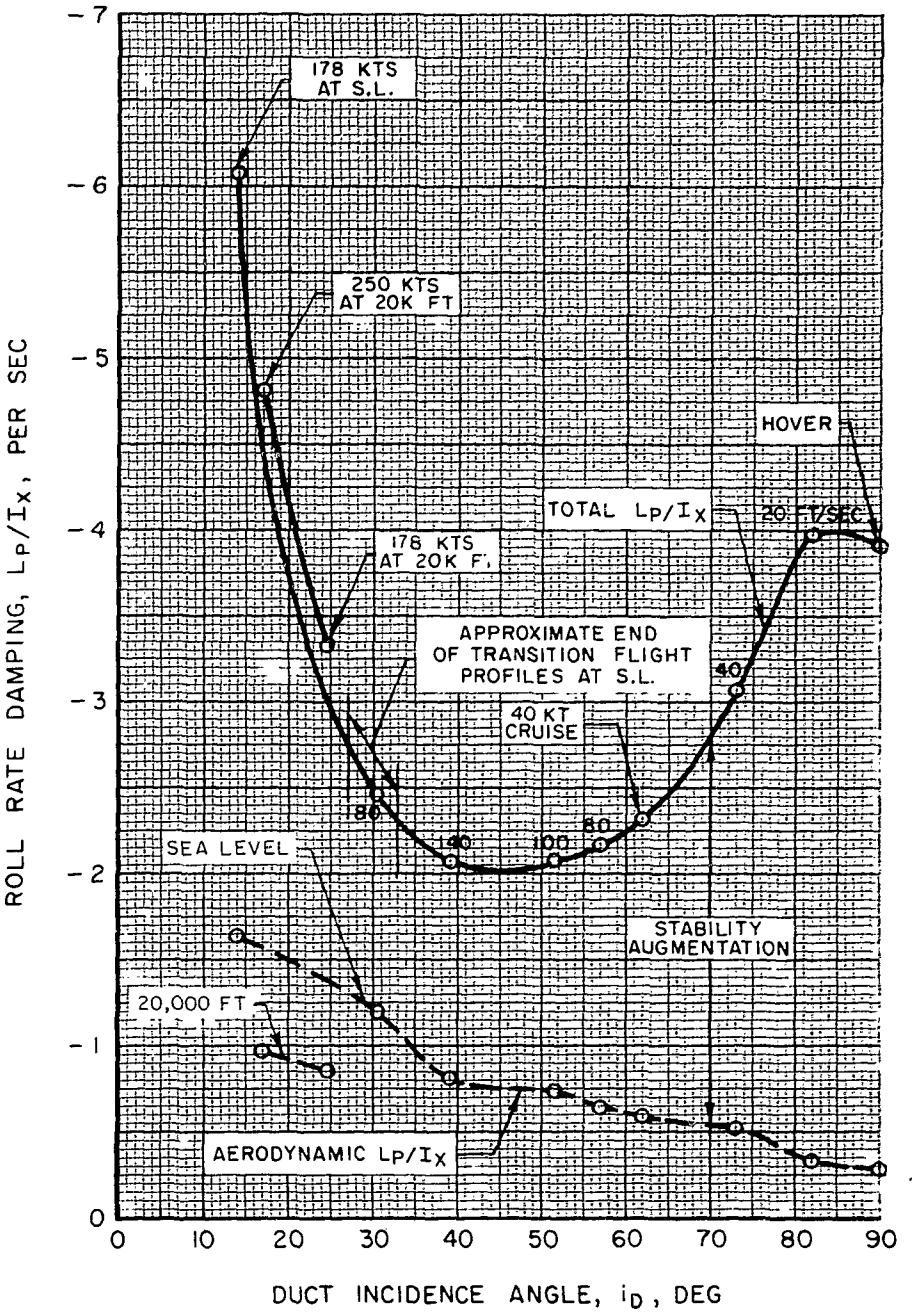

FIG. 45

VARIATION OF MAXIMUM LATERAL CONTROL POWER WITH DUCT INCIDENCE ANGLE

STEADY LEVEL FLIGHT

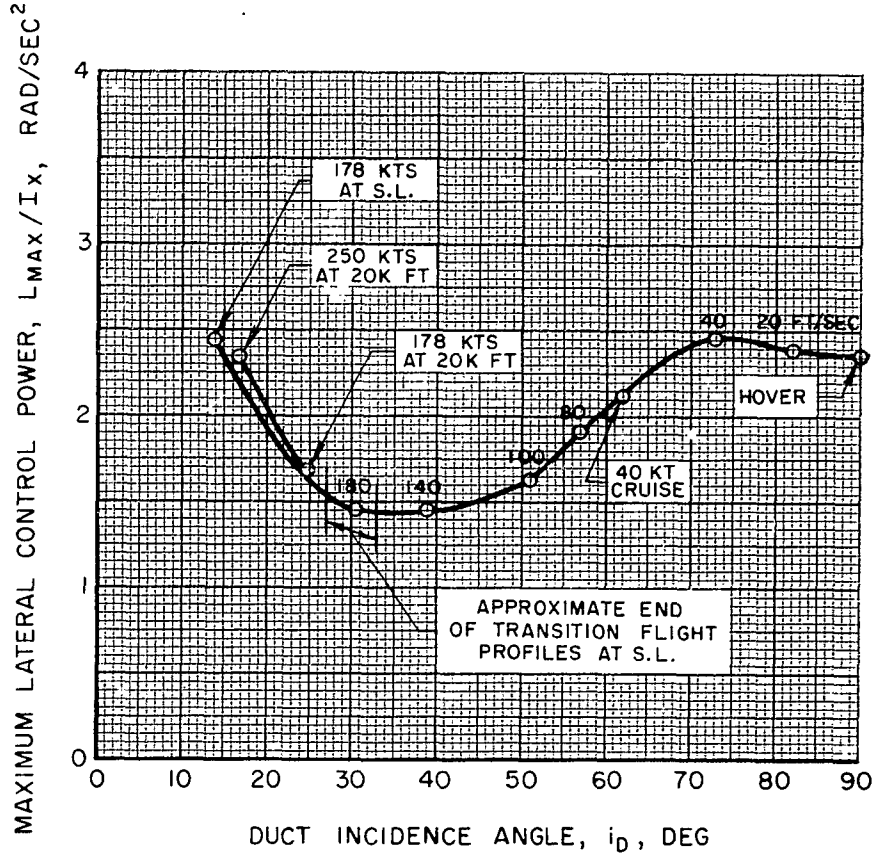

FIG. 46

VARIATION OF PEDAL SENSITIVITY WITH DUCT INCIDENCE ANGLE

STEADY LEVEL FLIGHT

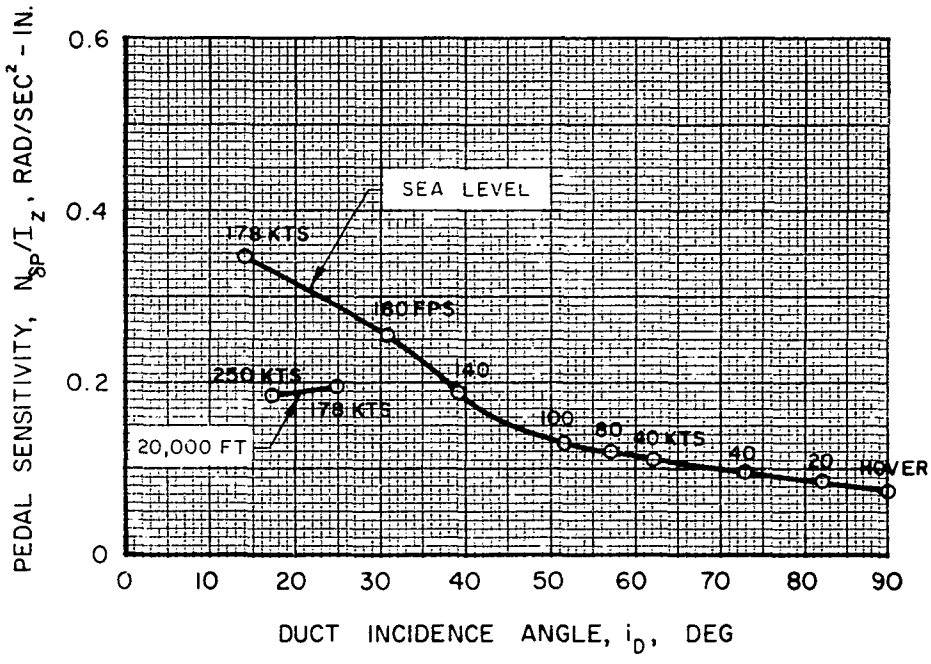

FIG. 47

VARIATION OF YAW RATE DAMPING WITH DUCT INCIDENCE ANGLE

STEADY LEVEL FLIGHT

K_Y = CONSTANT = − 3.0 IN. − SEC/RAD

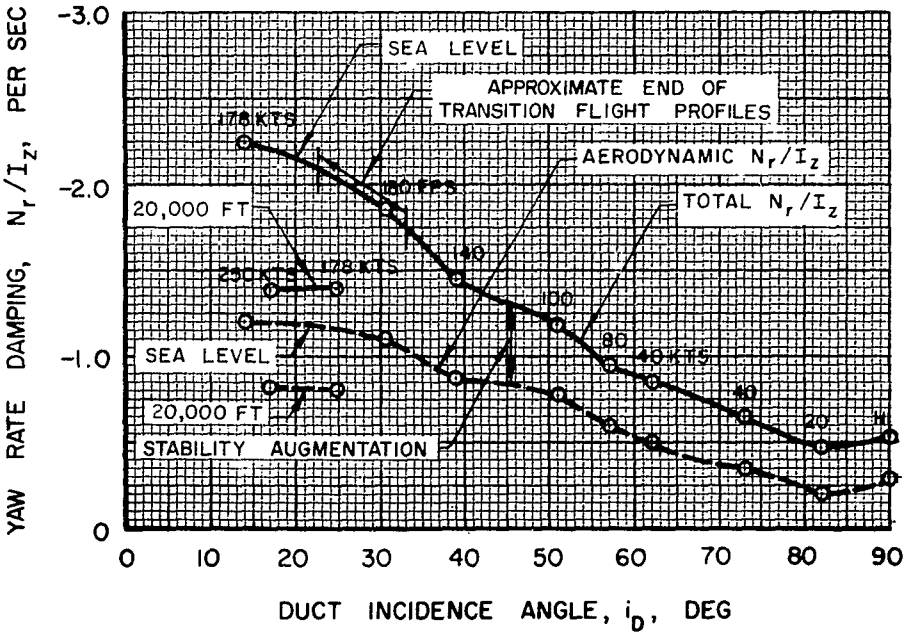

FIG. 48

VARIATION OF MAXIMUM YAW CONTROL POWER WITH DUCT INCIDENCE ANGLE

STEADY LEVEL FLIGHT

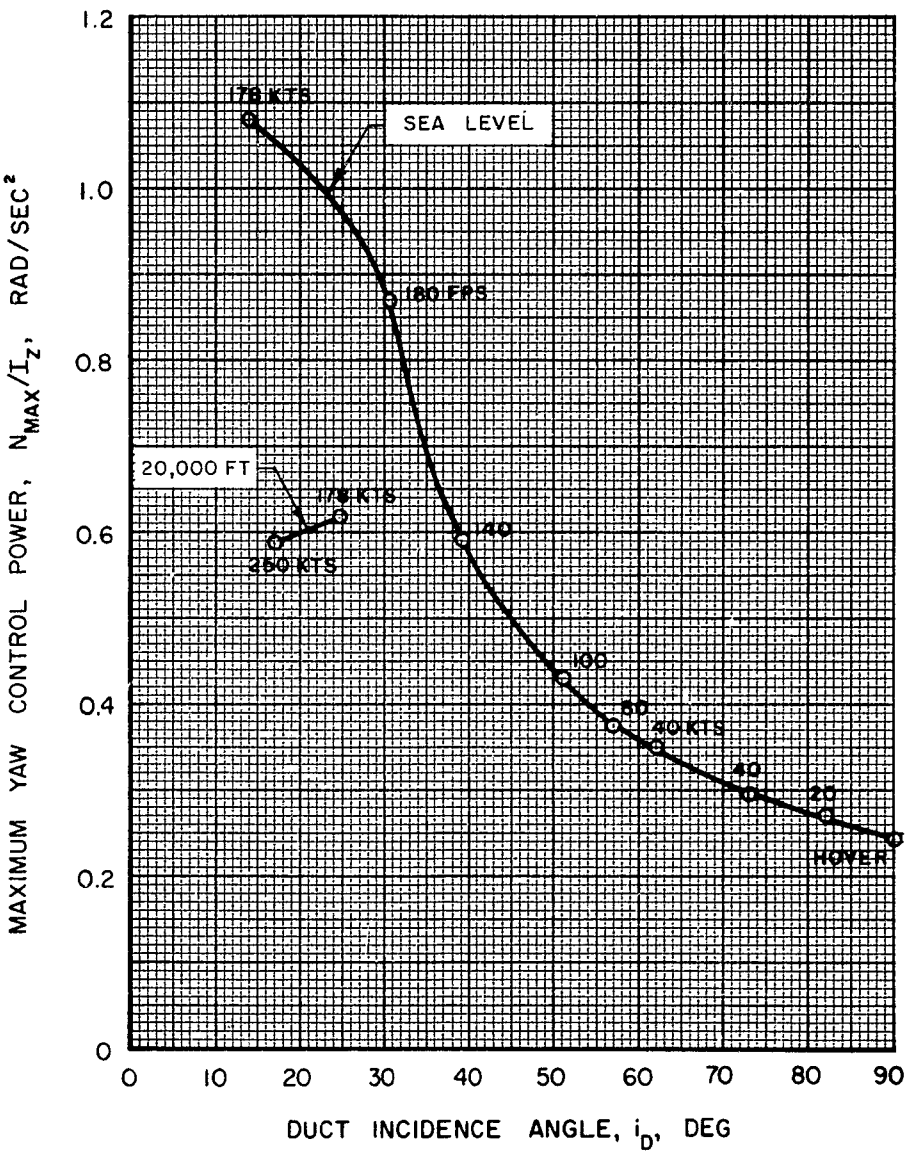

PILOT RATINGS FOR FLIGHT IN PARTIALLY-CONVERTED CONFIGURATIONS

RATINGS BASED ON CONTINUATION OF FLIGHT AT INDICATED SPEED, TRANSITION, AND VTOL-TYPE LANDING

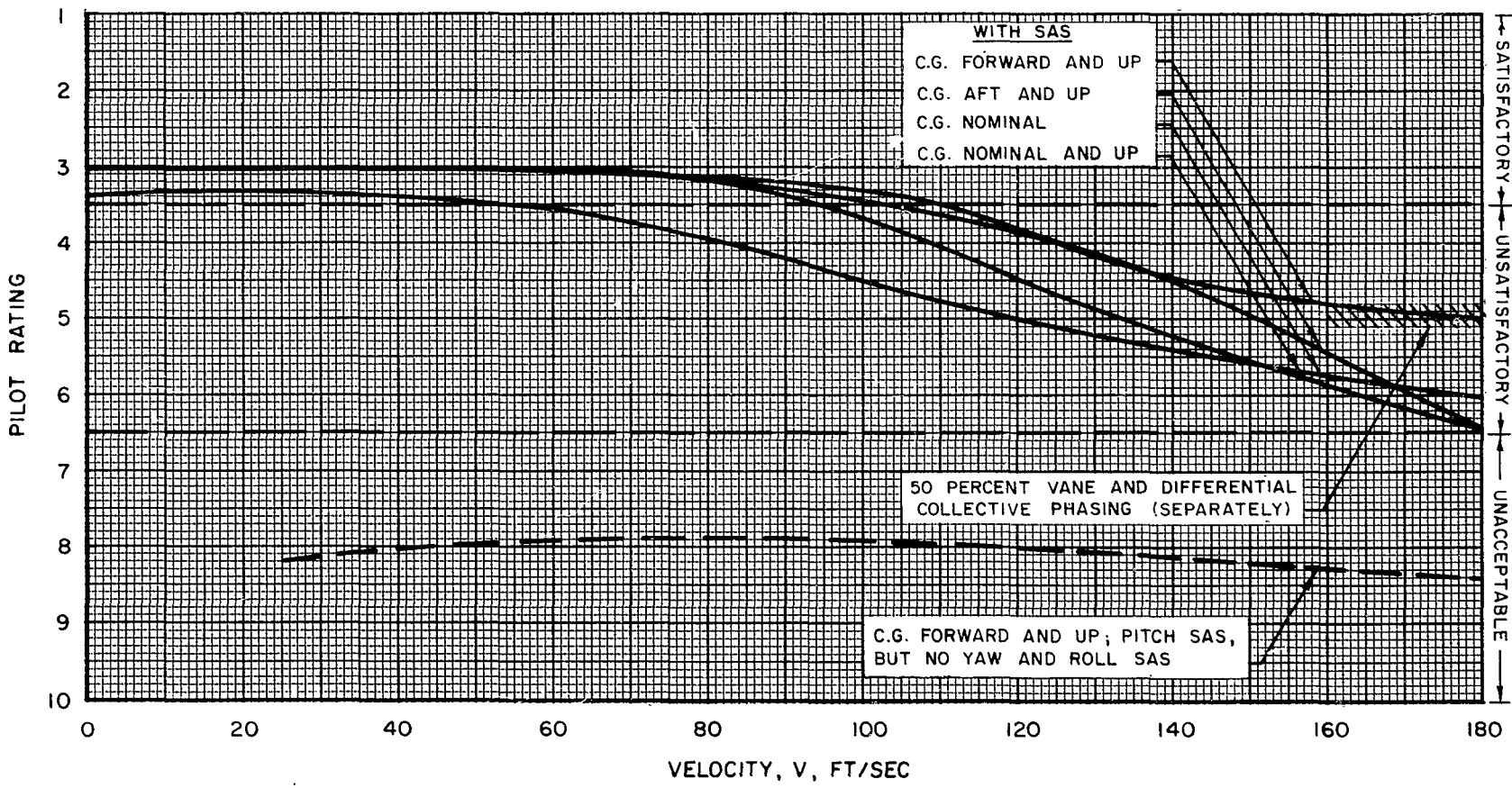

FIG. 49

R-1624-5

SUMMARY OF LATERAL-DIRECTIONAL ROO
STEADY LEVEL FLIGHT AT SPEEDS FROM
WITH STABILITY AUGMENTATI

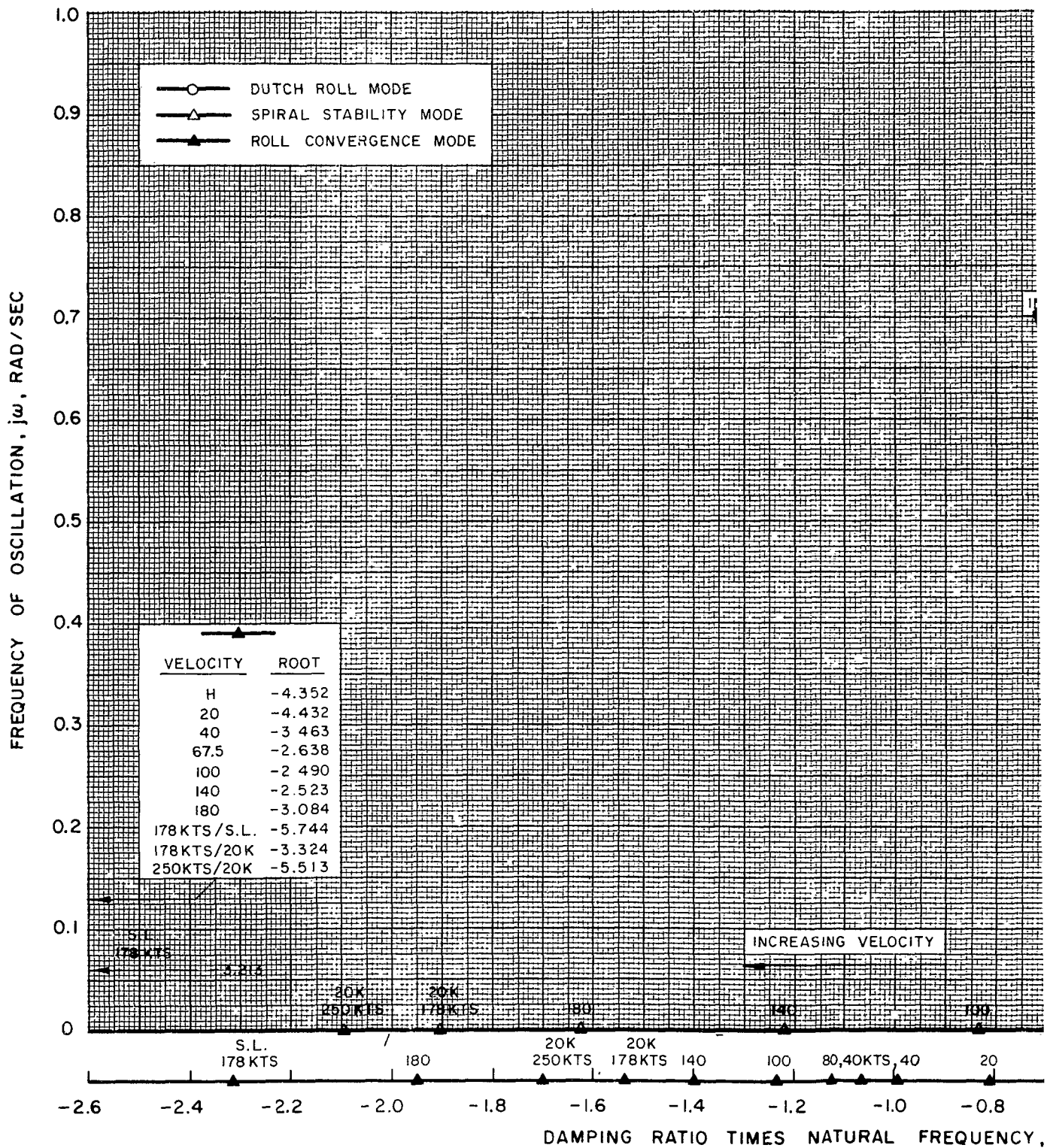

FIG. 50

TERAL-DIRECTIONAL ROOT LOCATIONS FOR GHT AT SPEEDS FROM HOVER TO 250 KTS TH STABILITY AUGMENTATION

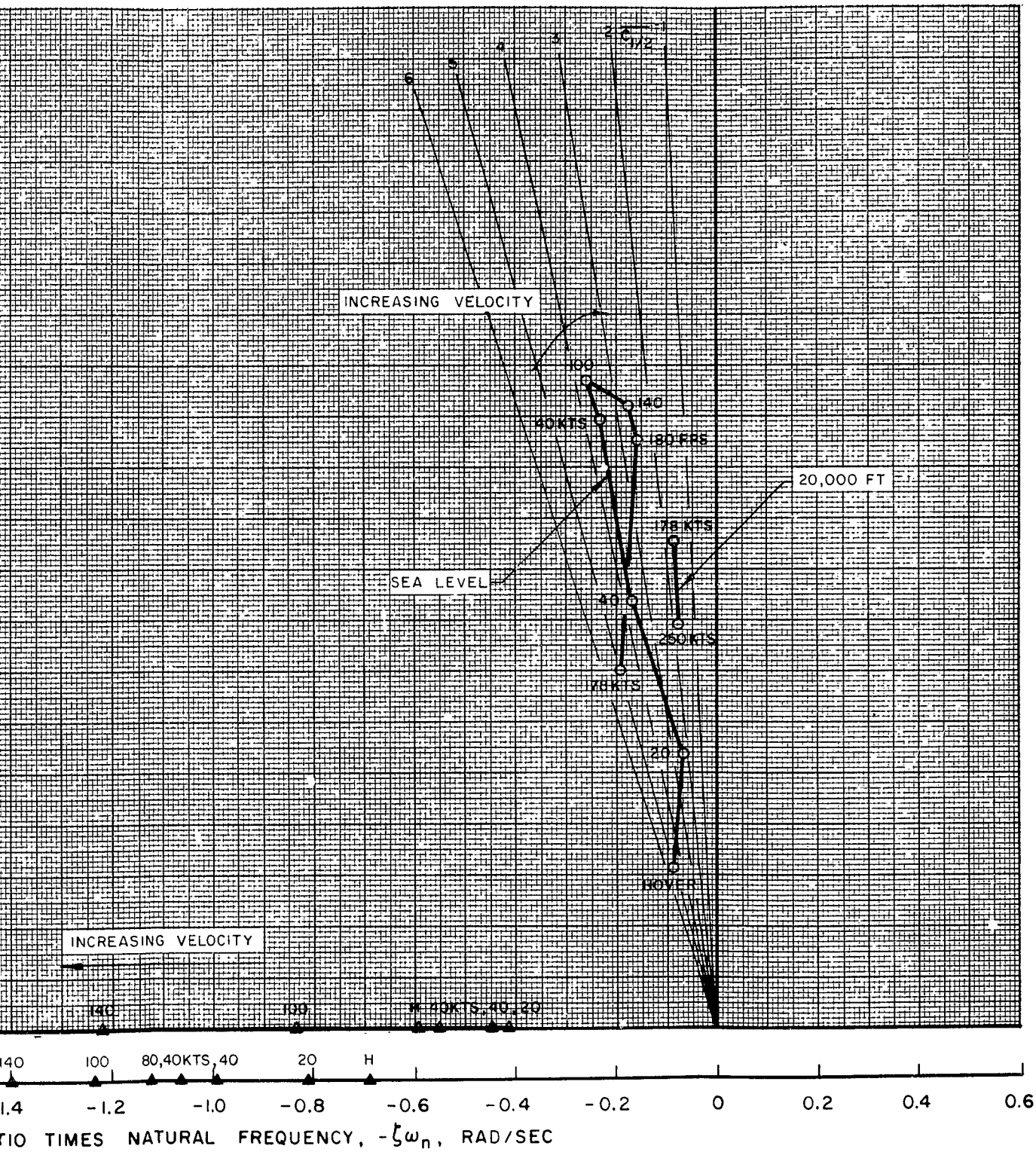

2

R-1624-5

LATERAL-DIRECTIONAL ROOT LOCATIONS F
WITH STABILITY AUGMENT

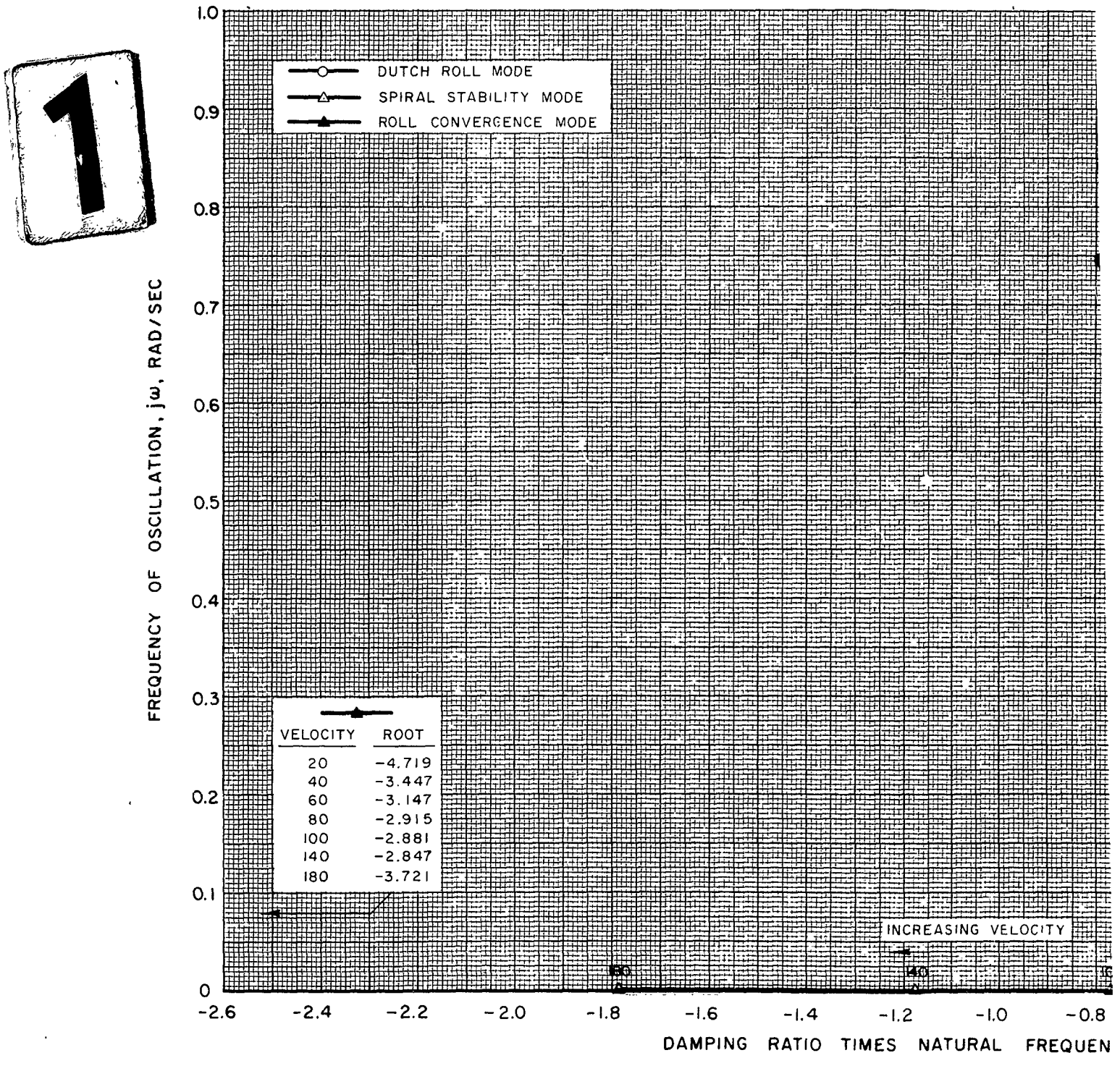

FIG. 51

ROOT LOCATIONS FOR T/W = 1.35 TAKE-OFF
H STABILITY AUGMENTATION

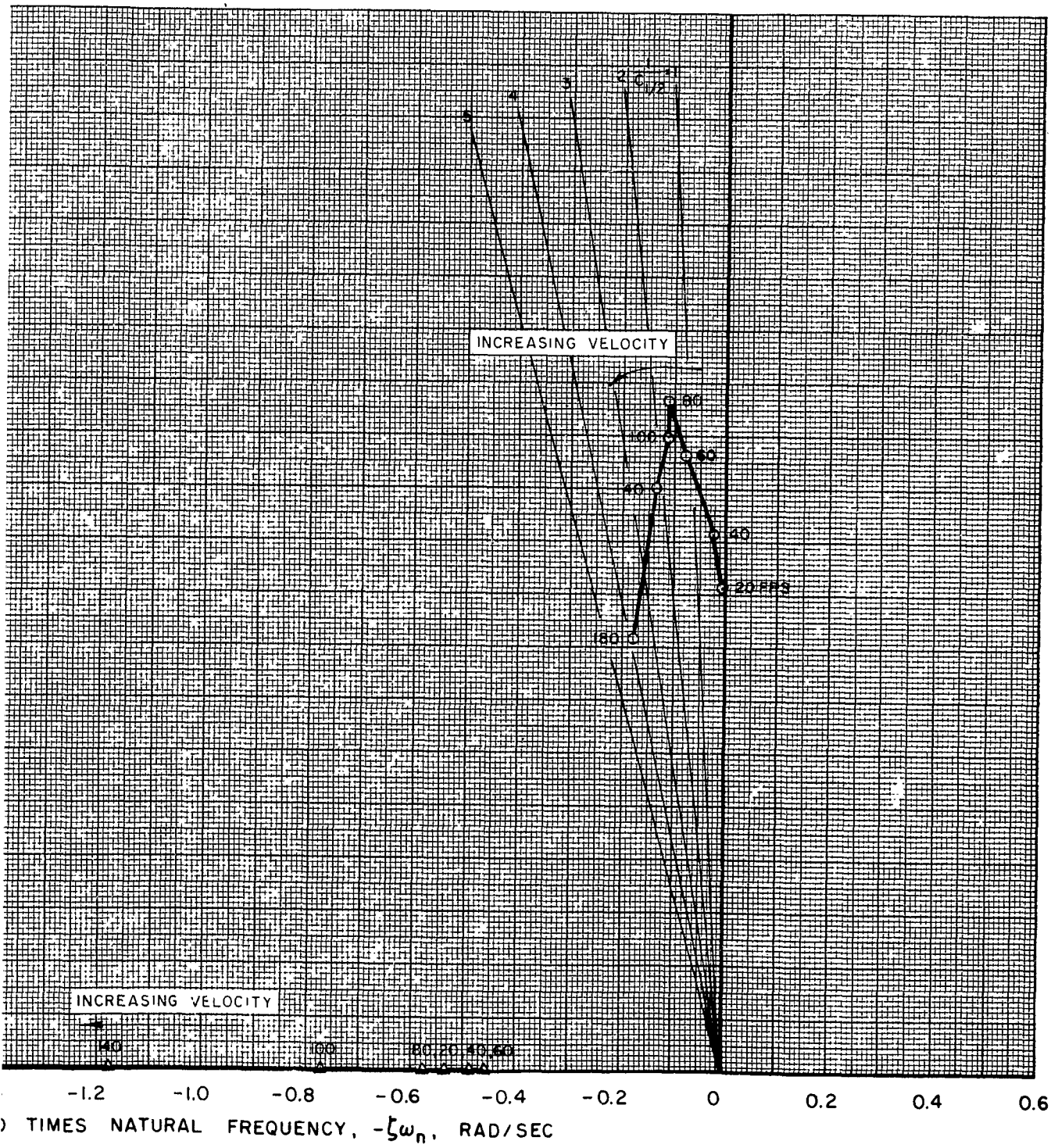

2

FIG. 51

ROOT LOCATIONS FOR T/W = 1.35 TAKE-OFF
H STABILITY AUGMENTATION

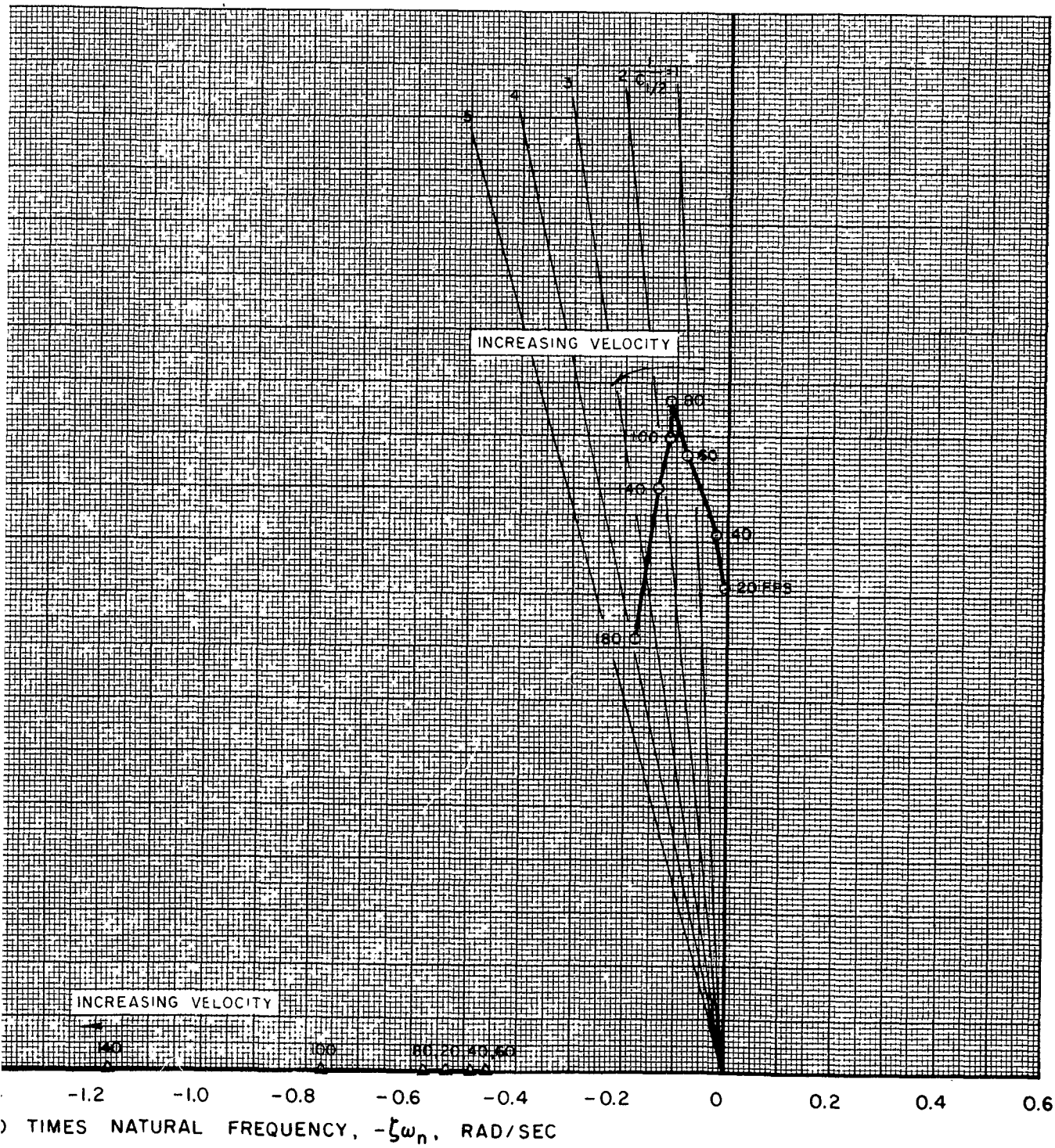

ROLLING PARAMETER VS RECIPROCAL OF CYCLES TO DAMP TO HALF AMPLITUDE FOR STEADY LEVEL FLIGHT

WITH STABILITY AUGMENTATION

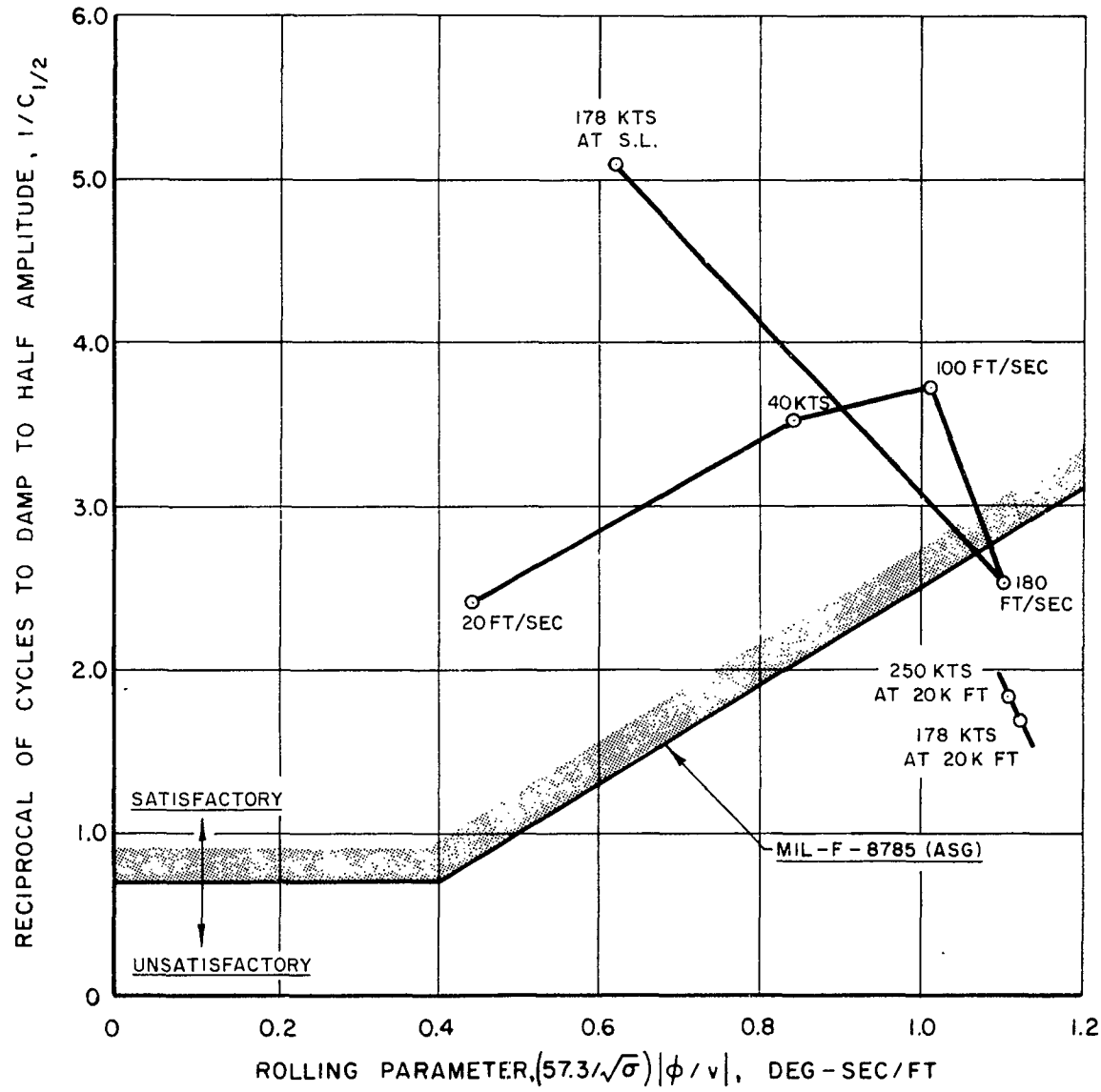

FIG. 53

PHASING GAINS REQUIRED TO ELIMINATE YAWING MOMENT DUE TO LATERAL CONTROL STICK INPUTS

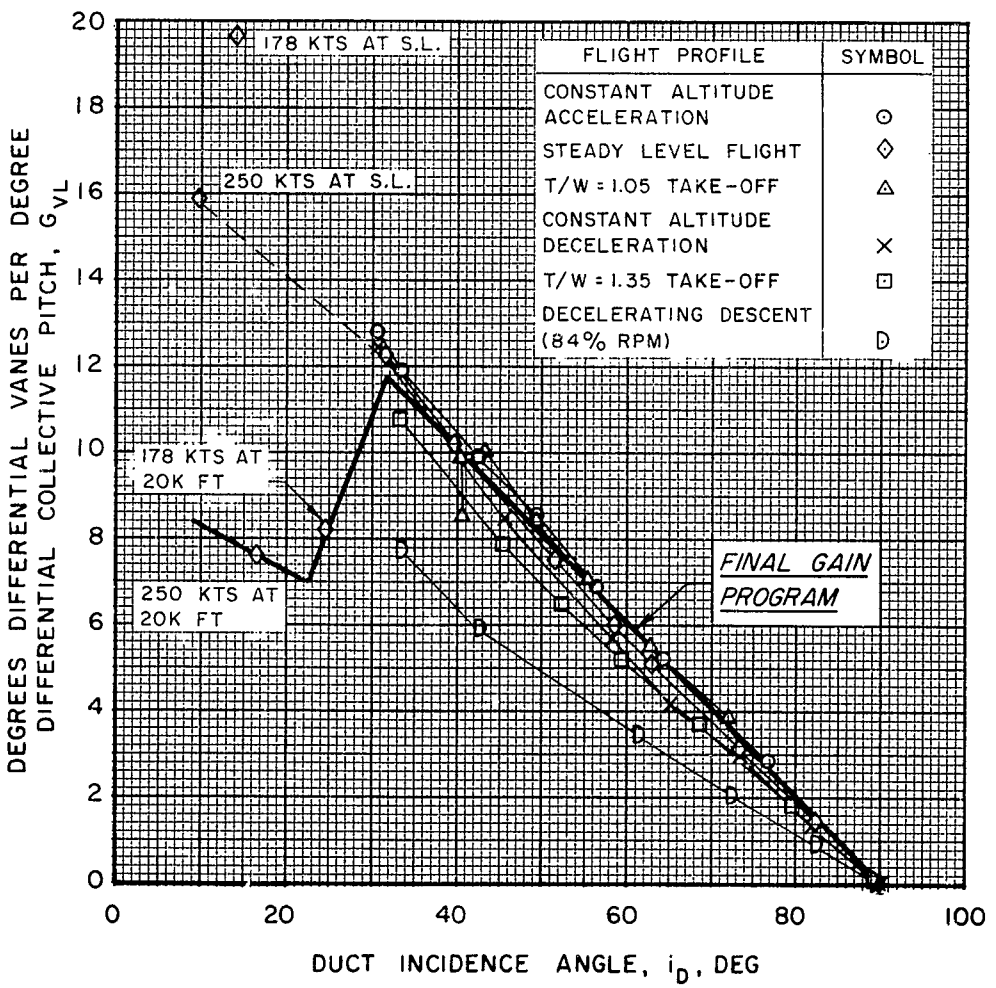

FIG. 54

PHASING GAINS REQUIRED TO ELIMINATE ROLLING MOMENT DUE TO PEDAL INPUTS

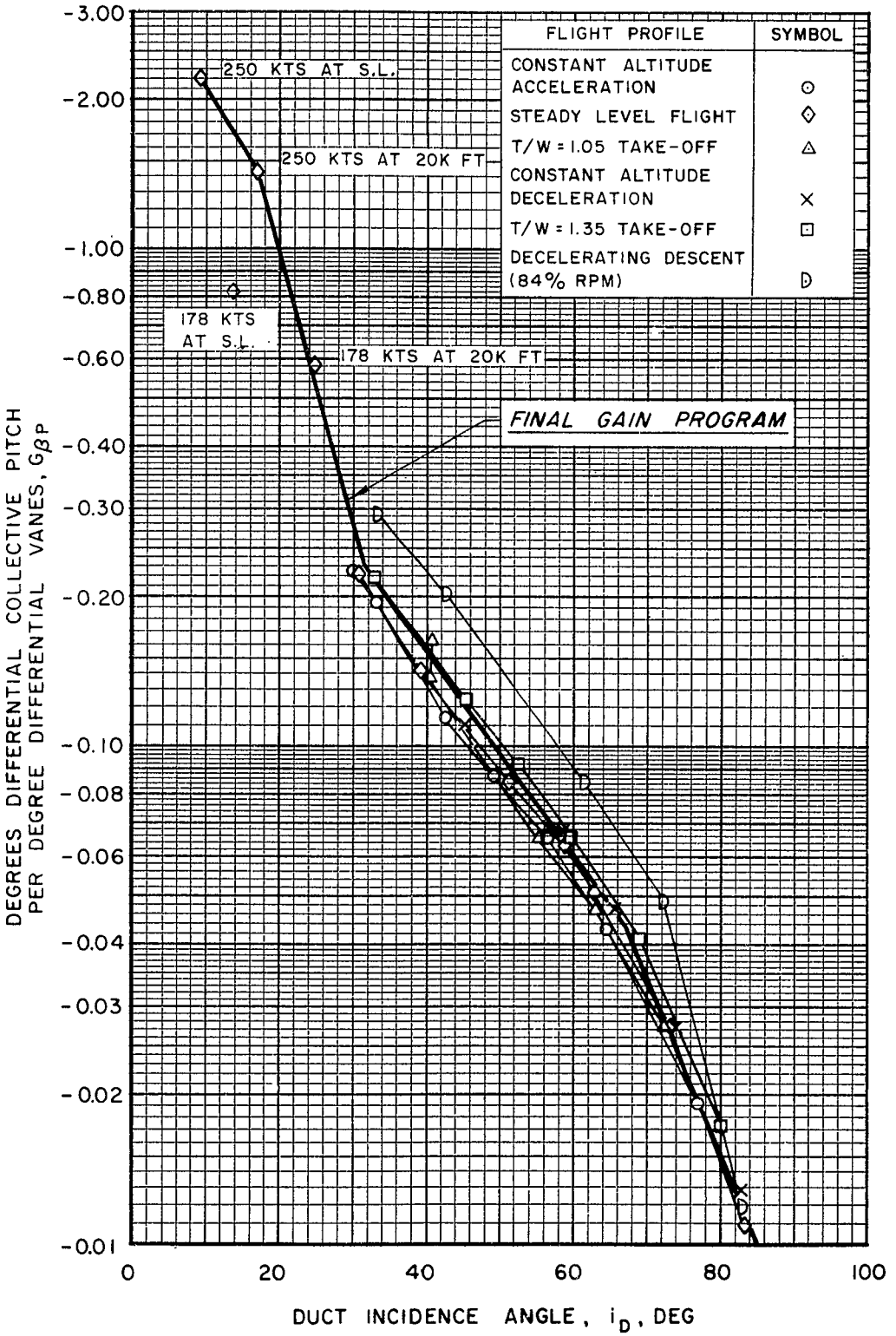

FIG. 55

EFFECT OF $M_u g/Iy$ STABILITY DERIVATIVE ON PILOT RATING FOR HOVER AND LOW SPEEDS

V = 0 TO 20 FT/SEC

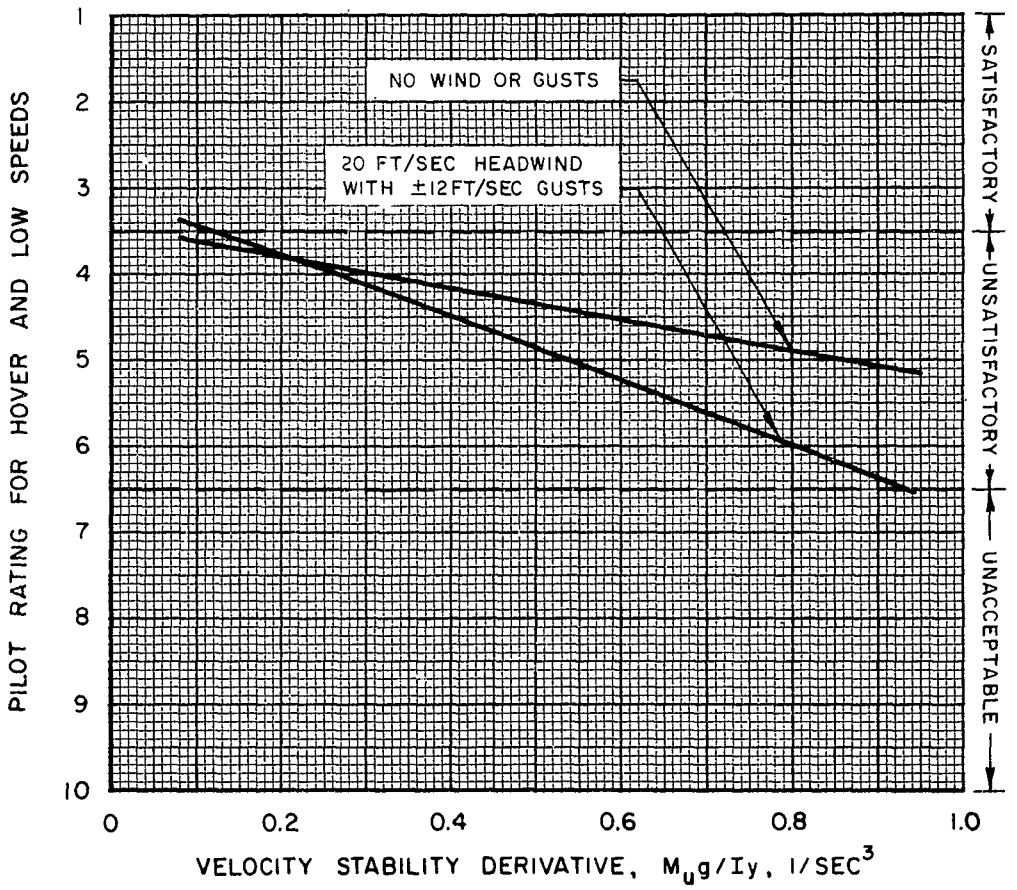

FIG. 56

EFFECT OF LAG IN PITCH CONTROL SYSTEM ON OVER-ALL PILOT RATING FOR SPEED RANGE FROM HOVER TO 106 KTS

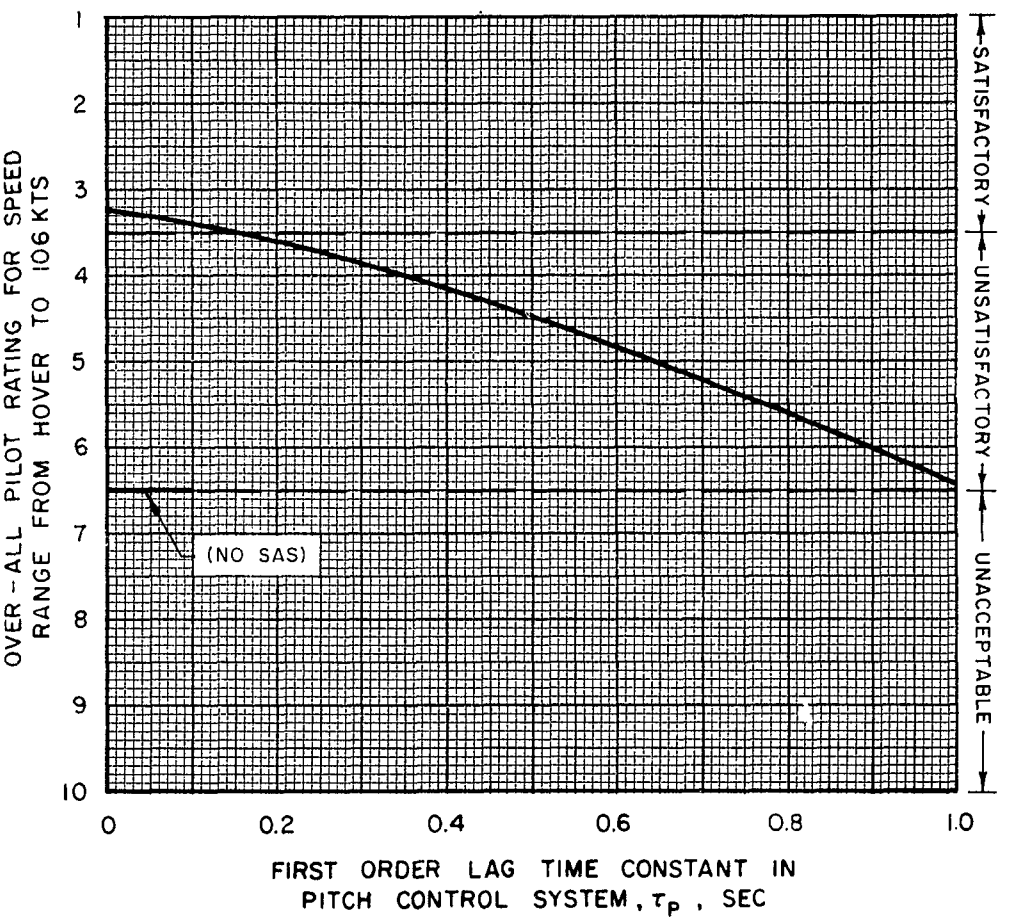

EFFECT OF LAGS IN LATERAL-DIRECTIONAL CONTROL SYSTEM ON OVER-ALL PILOT RATING FOR SPEED RANGE FROM HOVER TO 106 KTS

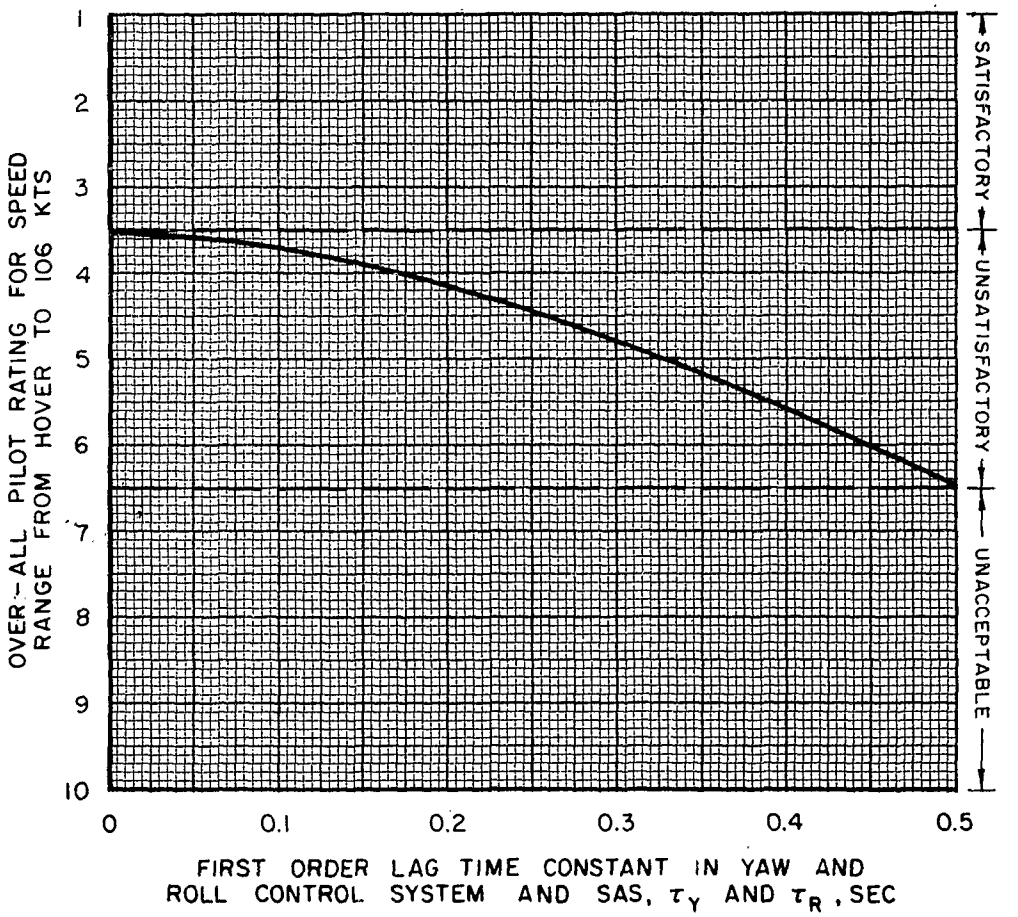

EFFECT OF LAG IN COLLECTIVE PITCH CONTROL ON PILOT RATING FOR HOVER

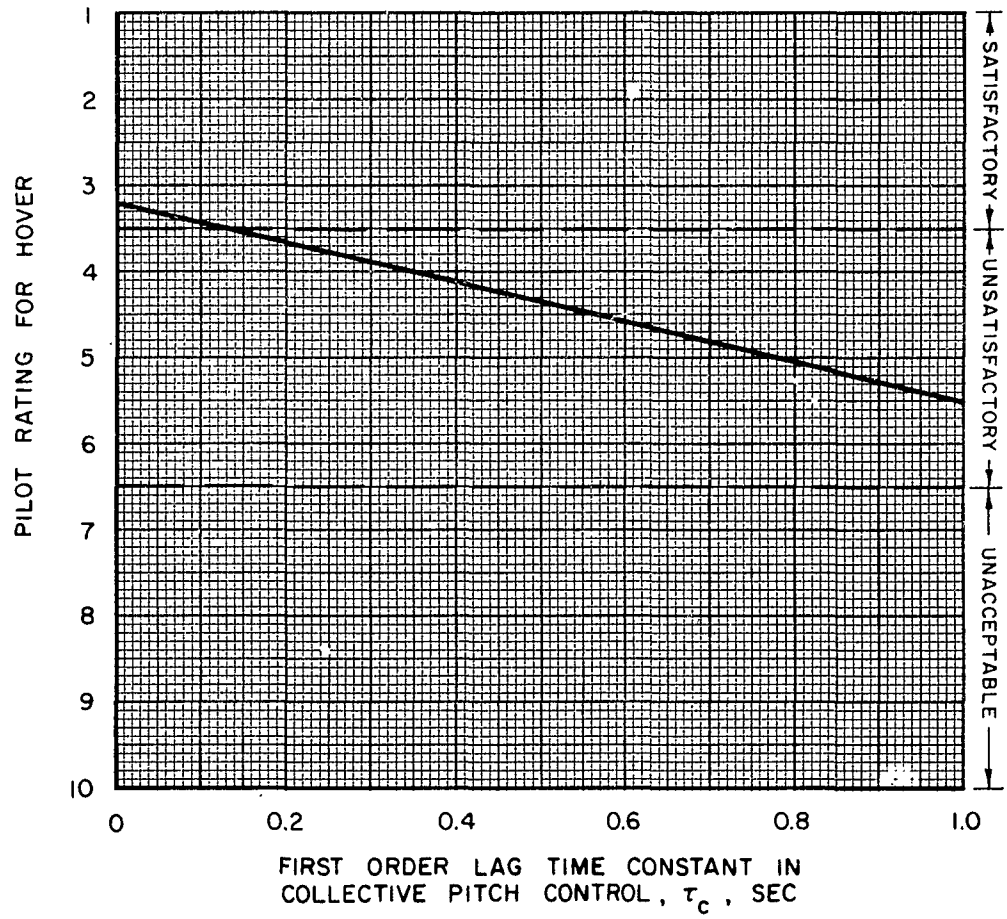

EFFECT OF CROSSWIND AND GUSTS ON PILOT RATING FOR APPROACH AND STOL TOUCHDOWN

STEADY WIND OF 20 FT/SEC FROM 0 DEG
RATE OF DESCENT OF 600 FT/MIN

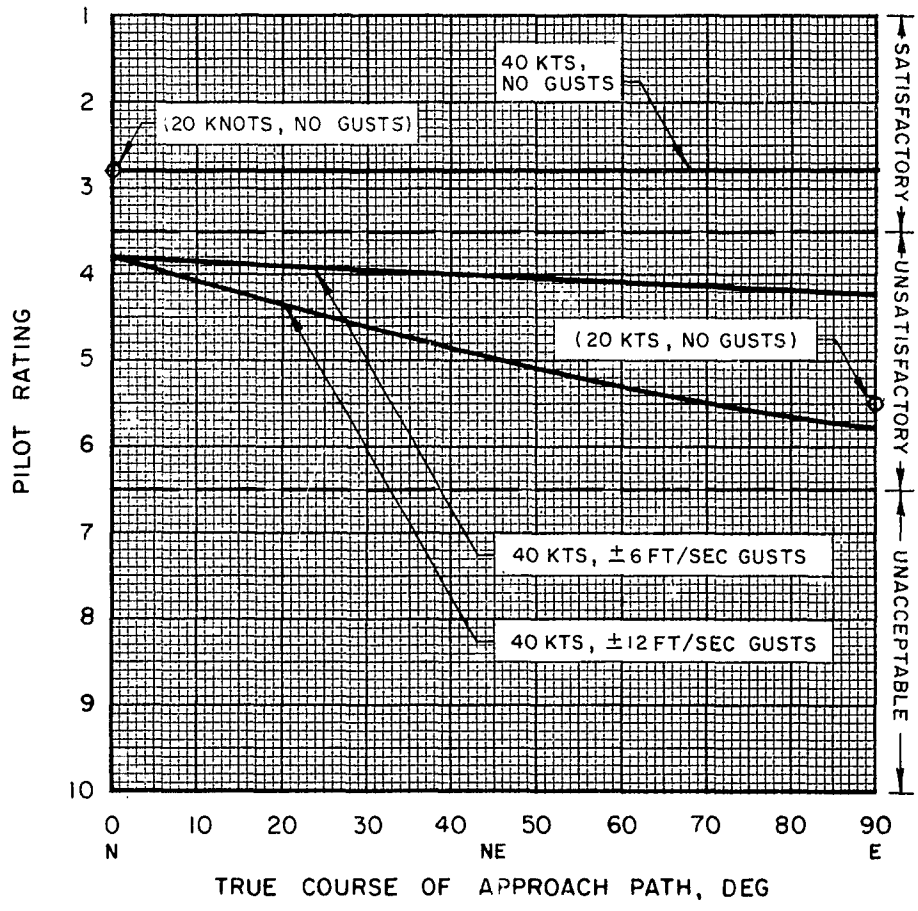

COMPARISON OF WEIGHTS OF ALTERNATE STABILITY AUGMENTATION SYSTEMS

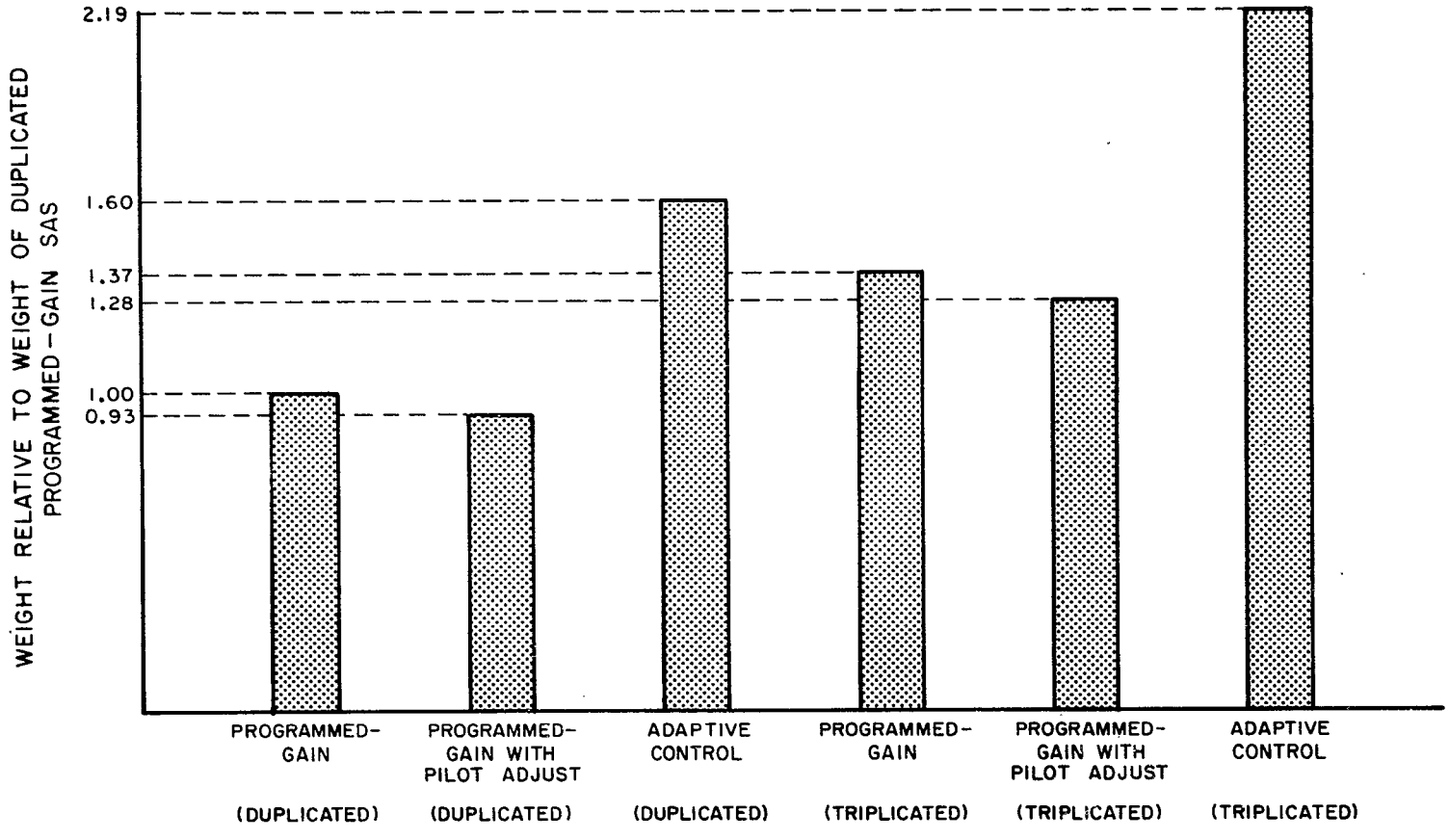

FIG. 60

COMPARISON OF COSTS OF ALTERNATE STABILITY AUGMENTATION SYSTEMS

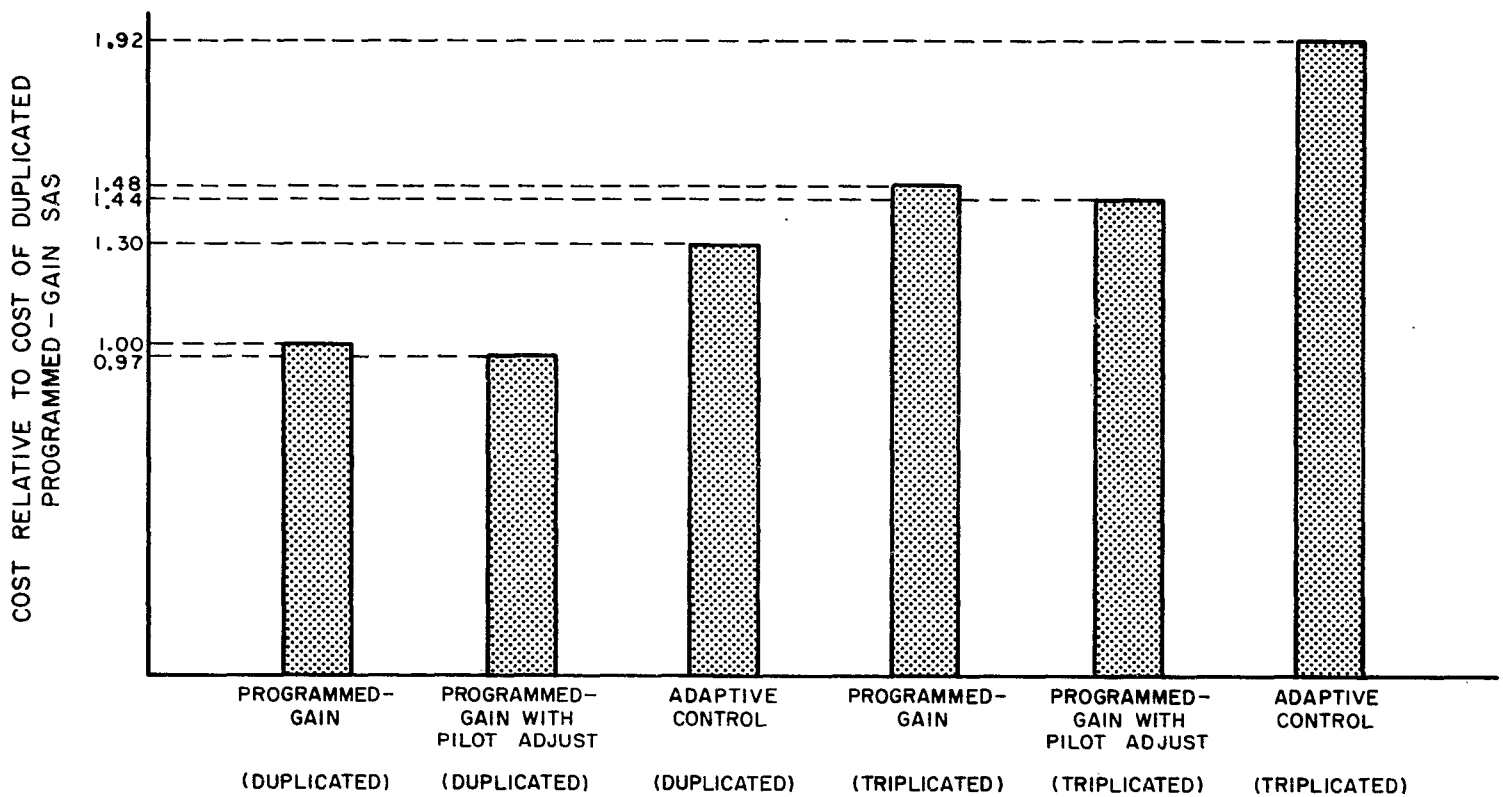

FIG. 61

FIG. 62

DETAILS OF DUCTED PROPELLER AND CONTROL VANE

ALL DIMENSIONS IN FEET

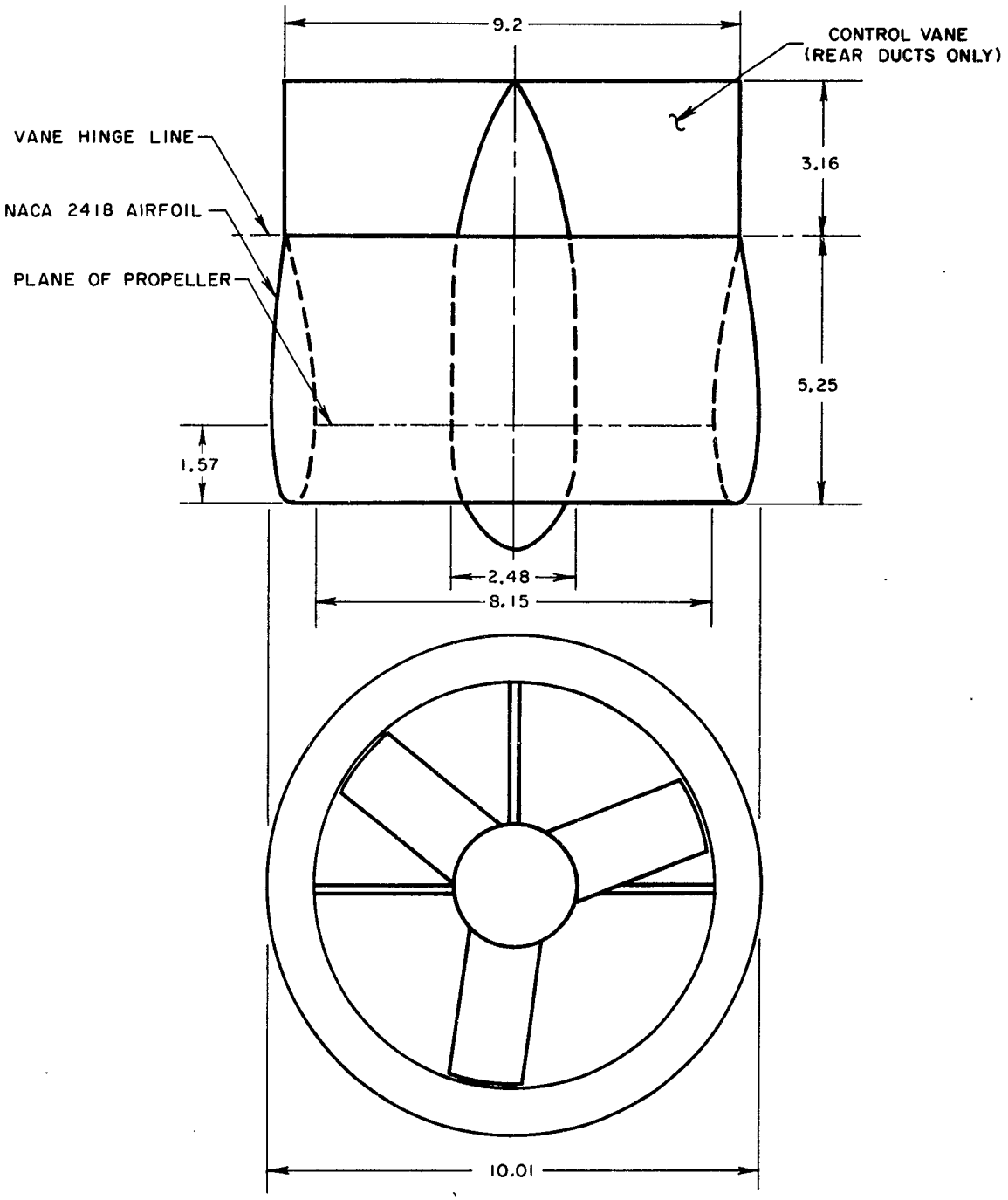

FIG. 63

DUCT LIFT COEFFICIENT FUNCTION

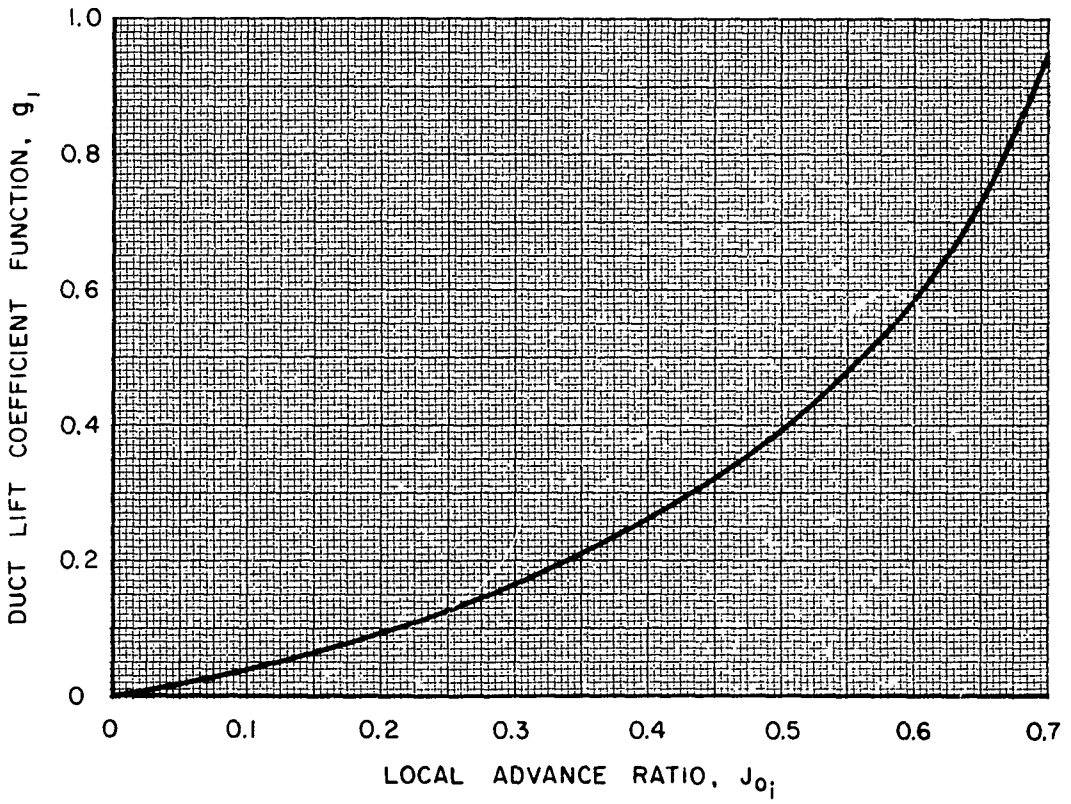

FIG. 64

VARIATION OF LIFT COEFFICIENT WITH ANGLE OF ATTACK FOR ONE DUCTED PROPELLER

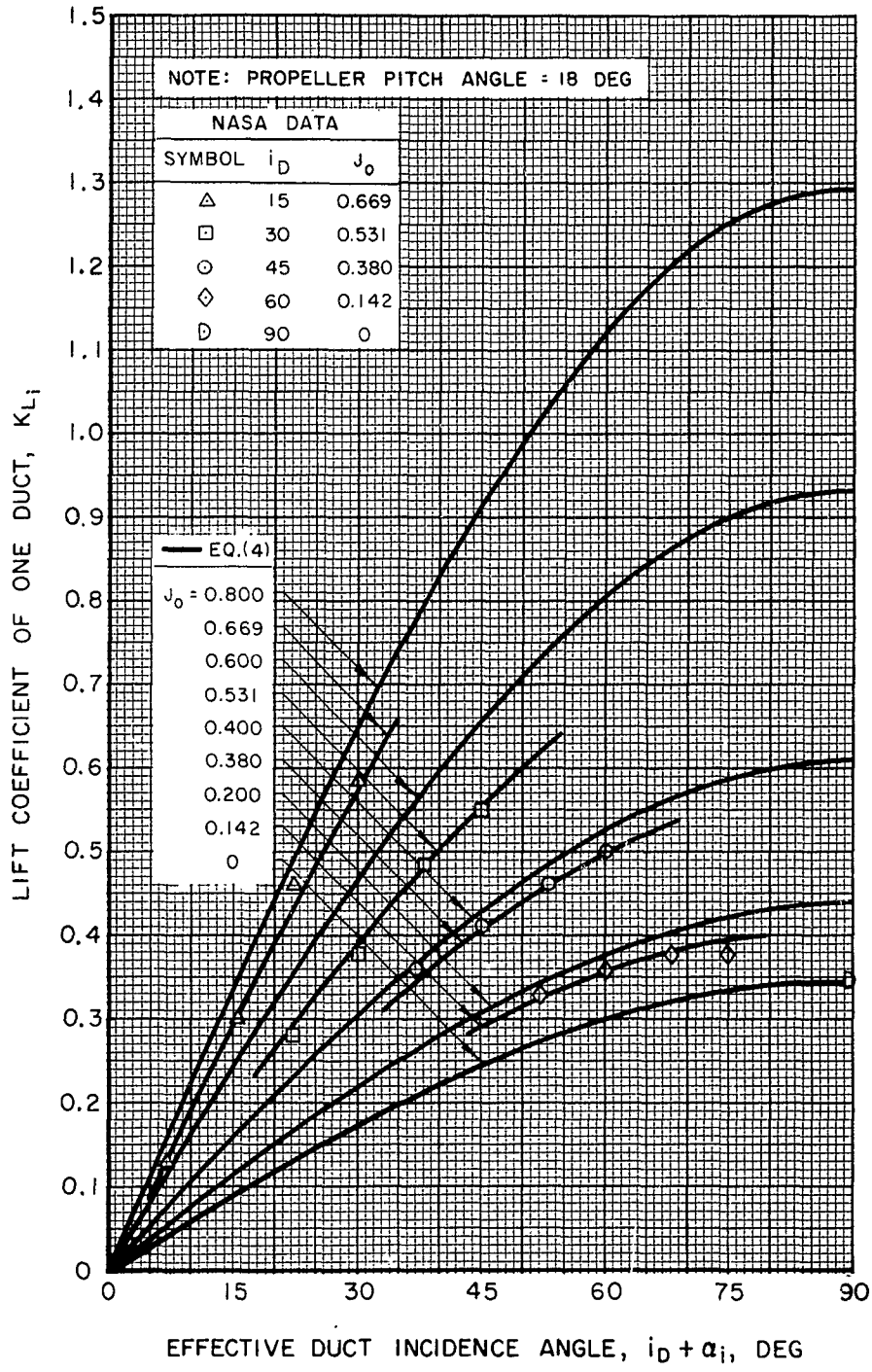

FIG. 65

DUCT DRAG COEFFICIENT FUNCTIONS

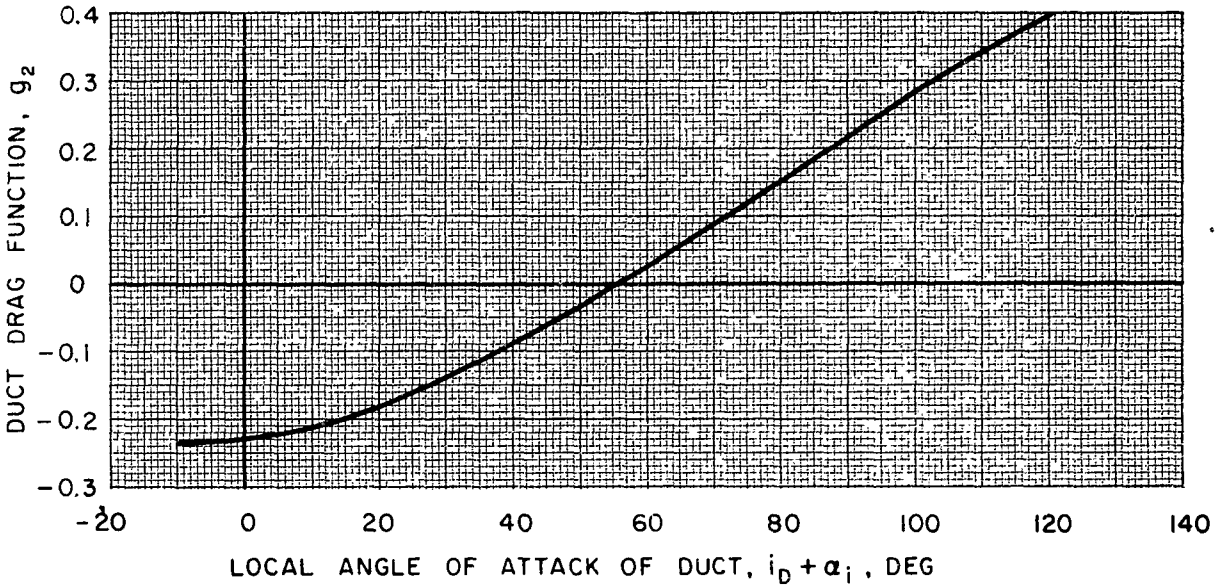

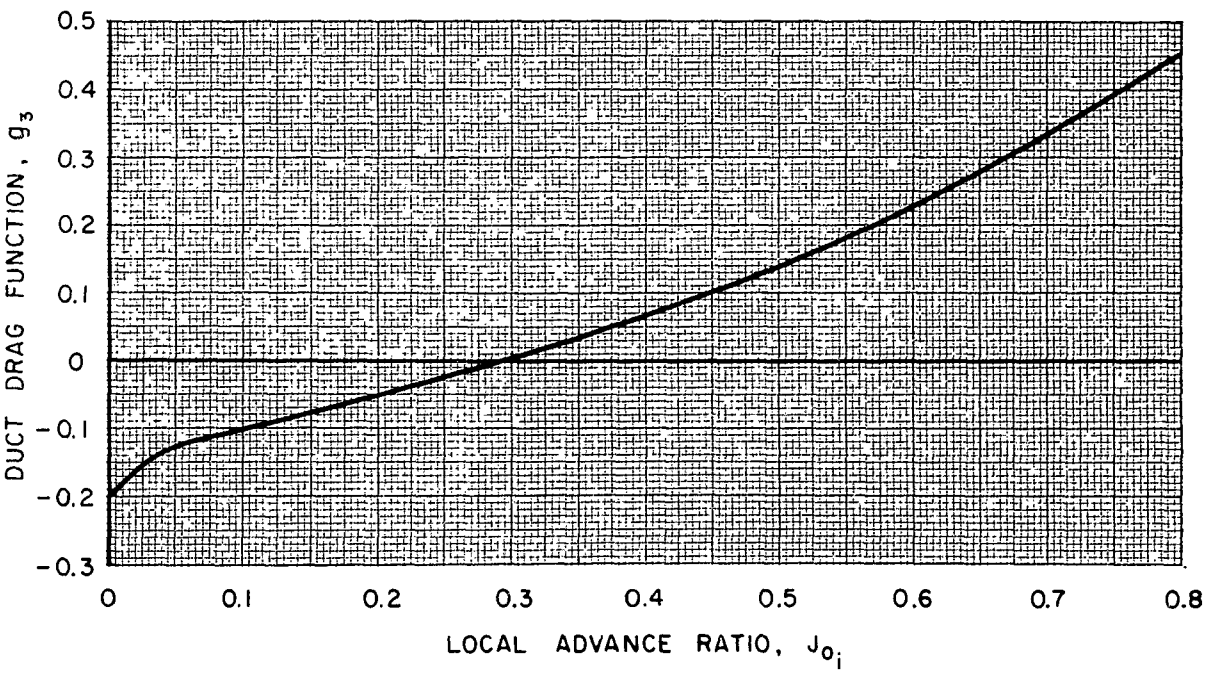

FIG. 66

SIDE FORCE COEFFICIENT SLOPE FOR ONE FORWARD DUCTED PROPELLER

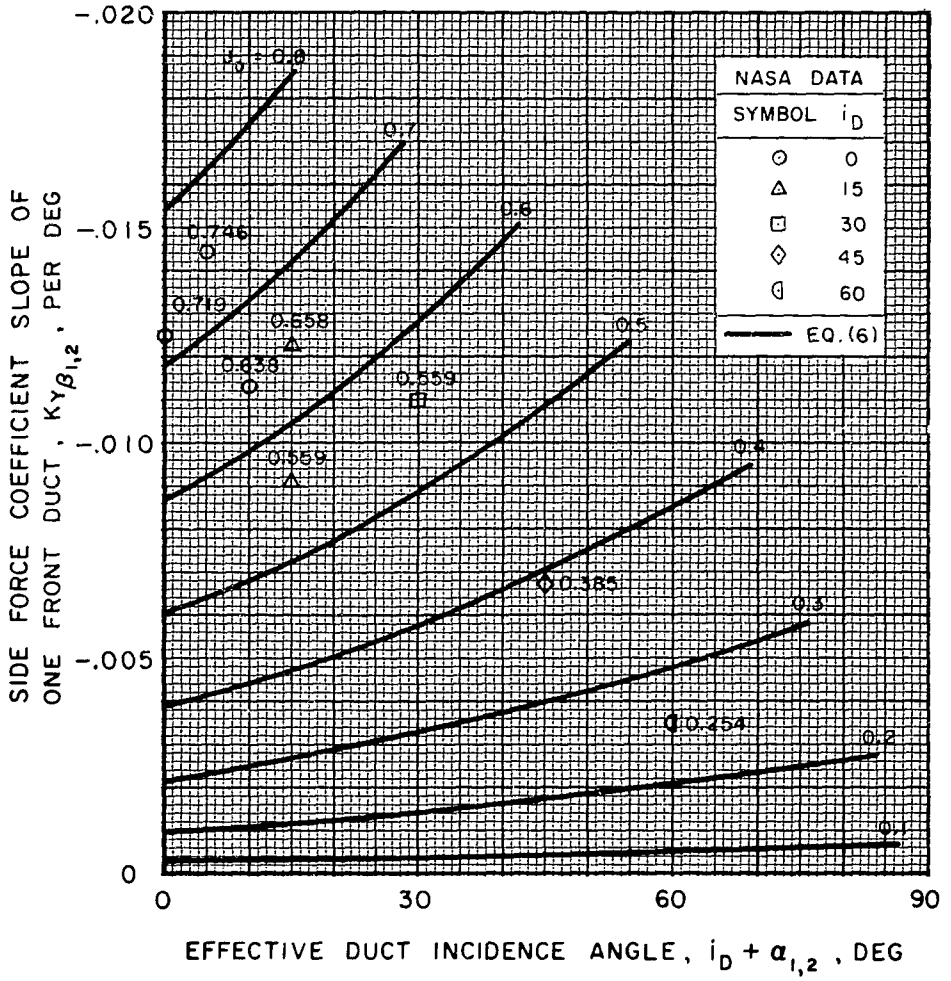

FIG. 67

CORRECTION FACTOR FOR SIDE FORCE OF REAR DUCTS

$$\eta = \eta_{\alpha} + \eta_{i_D}$$

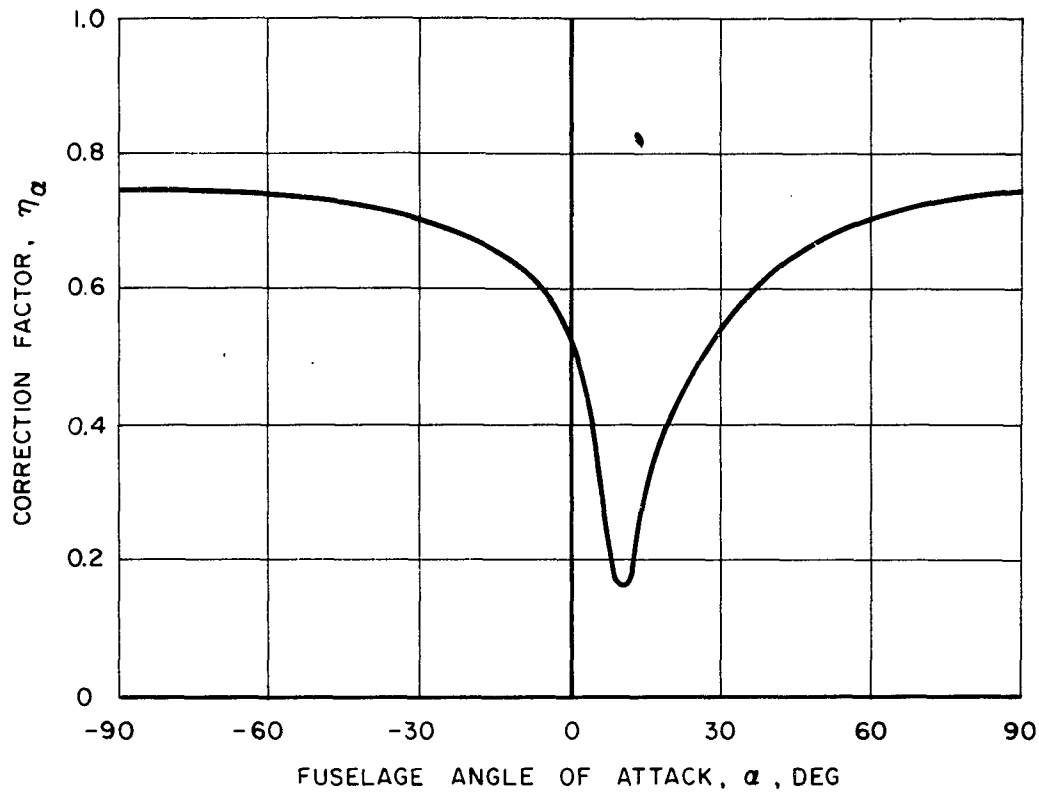

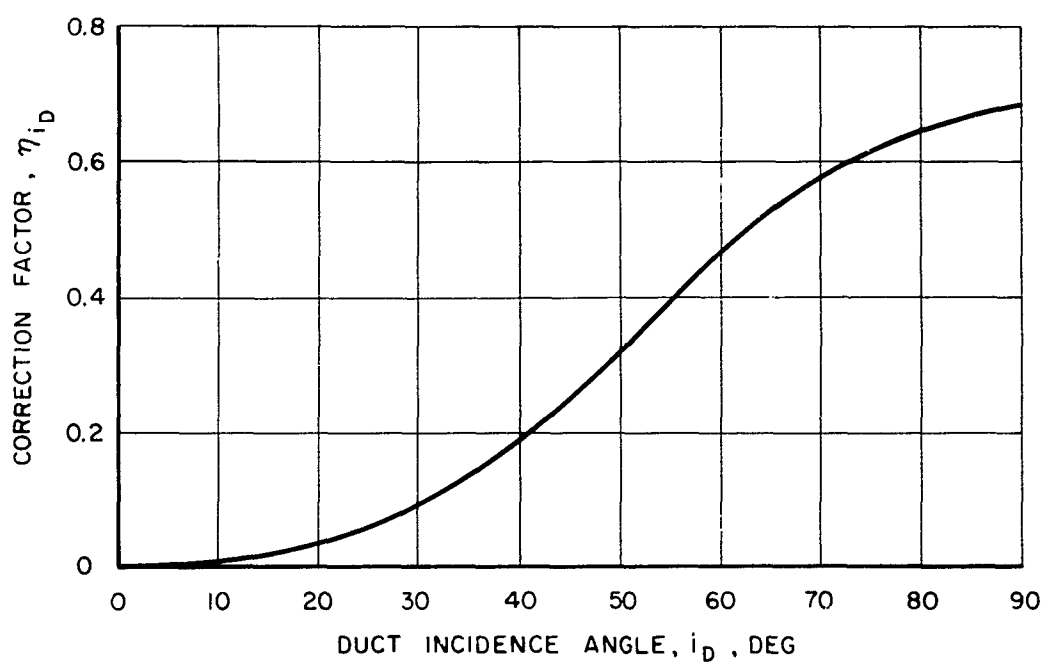

FIG. 68

CORRECTION FACTOR FOR PITCHING MOMENT

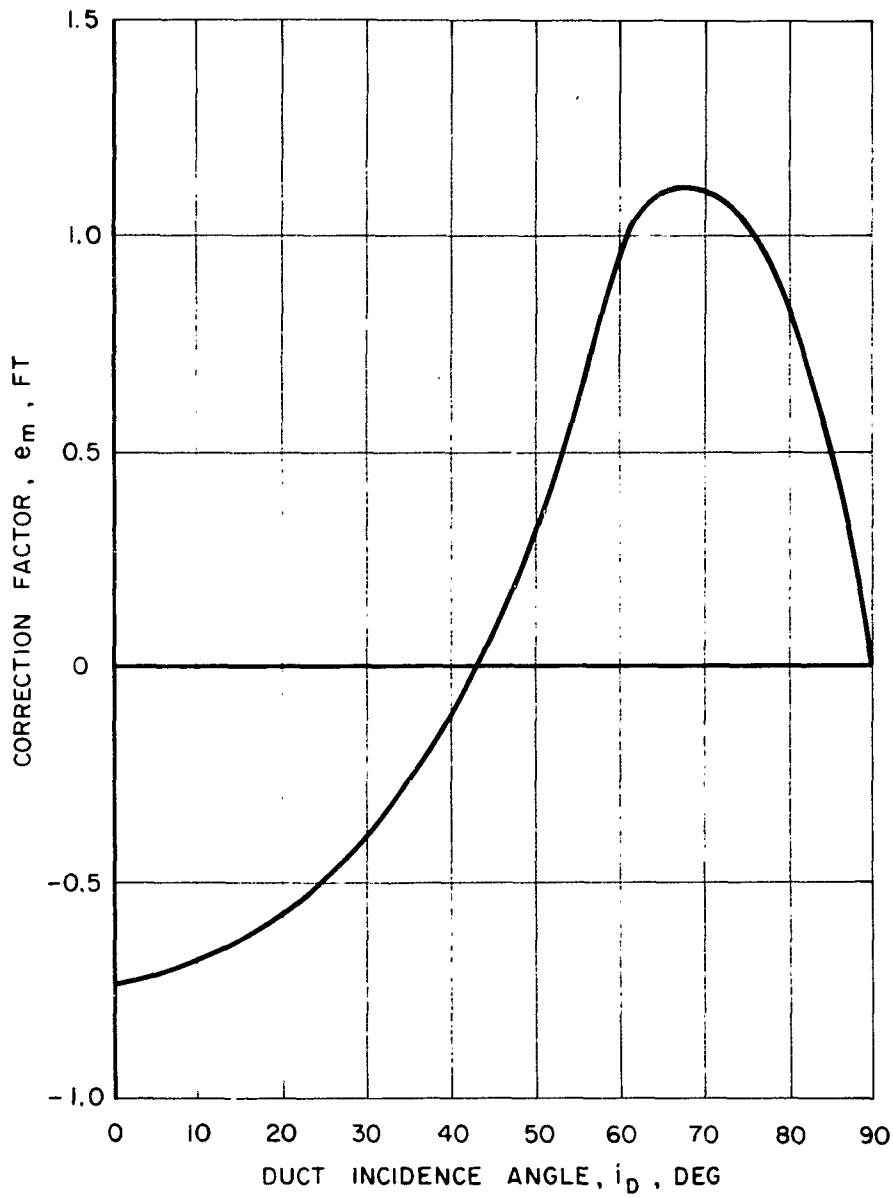

FIG. 69

VARIATION OF PITCHING MOMENT REQUIRED TO TRIM WITH VELOCITY FOR NASA WIND TUNNEL MODEL

MODEL 1/7 FULL SCALE

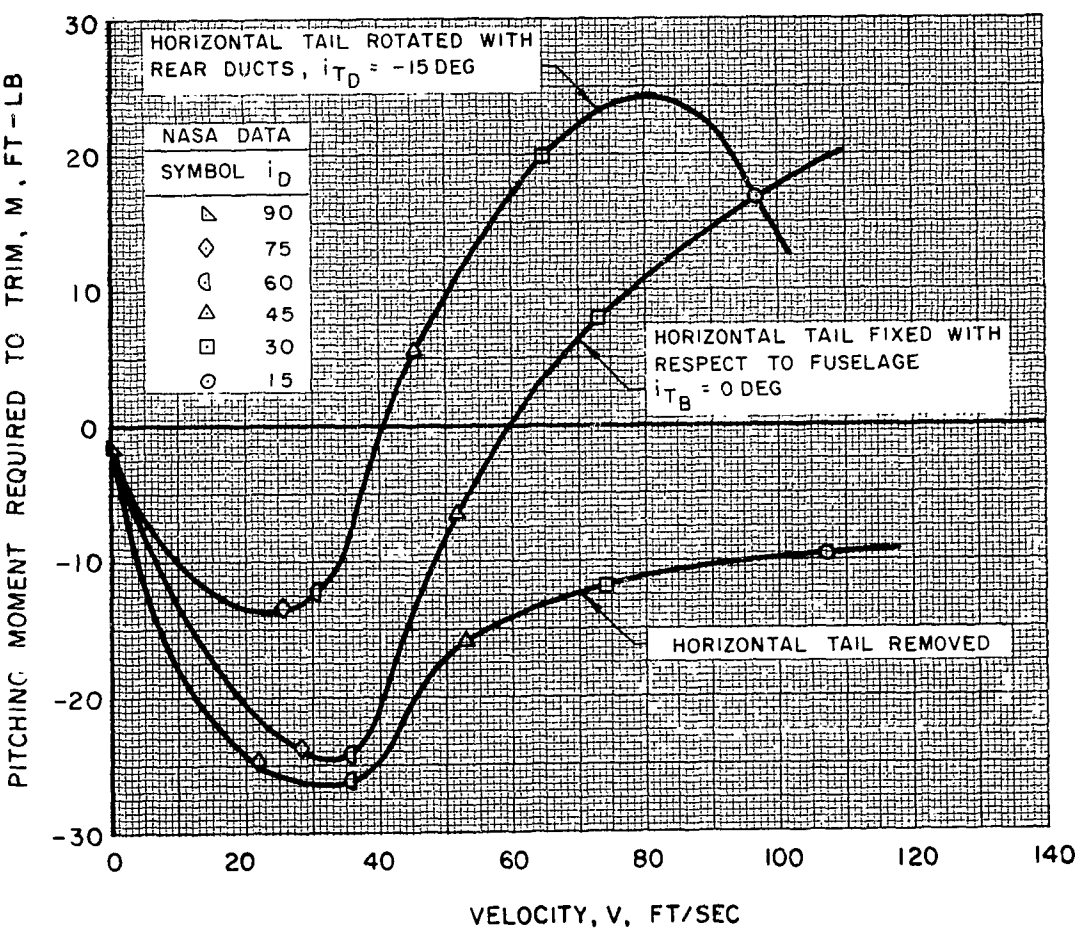

FIG. 70

VARIATION OF ROLLING MOMENT COEFFICIENT SLOPE OF DUCTS WITH DUCT INCIDENCE ANGLE

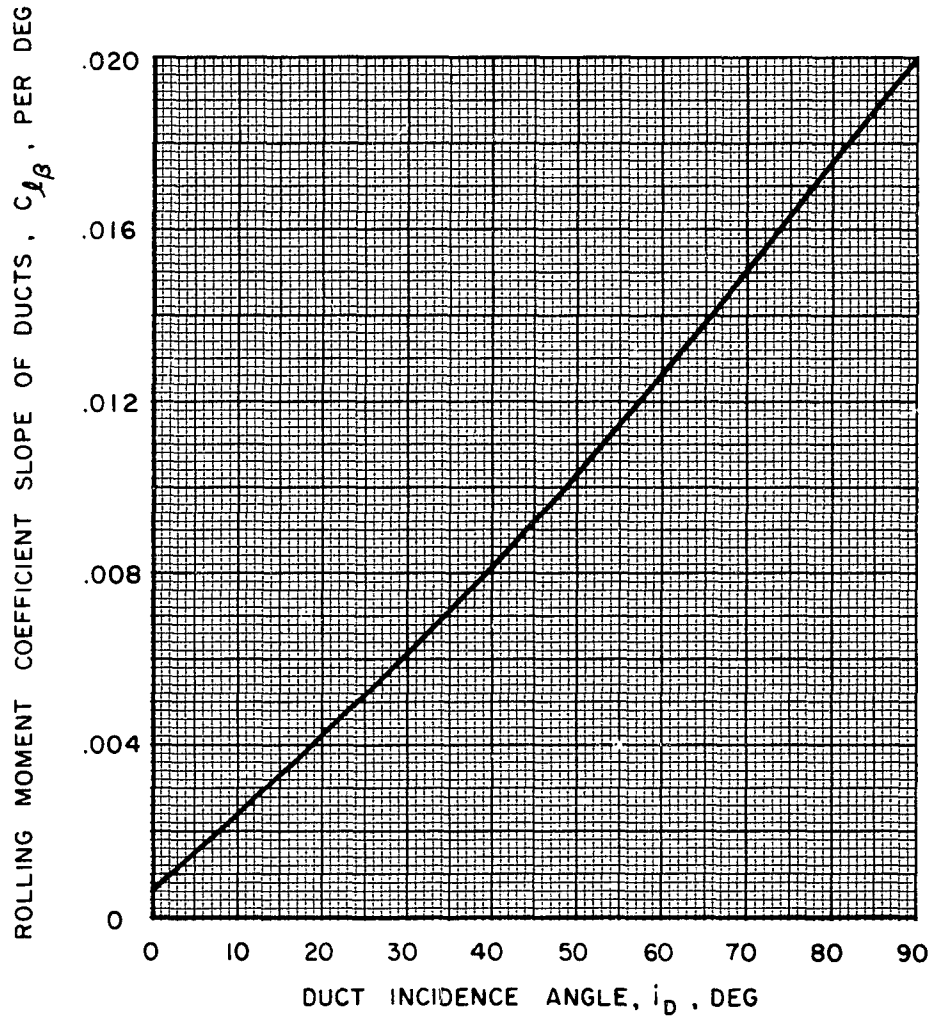

FIG. 71

CONTROL EFFECTIVENESS OF DUCTED PROPELLERS IN STEADY LEVEL FLIGHT

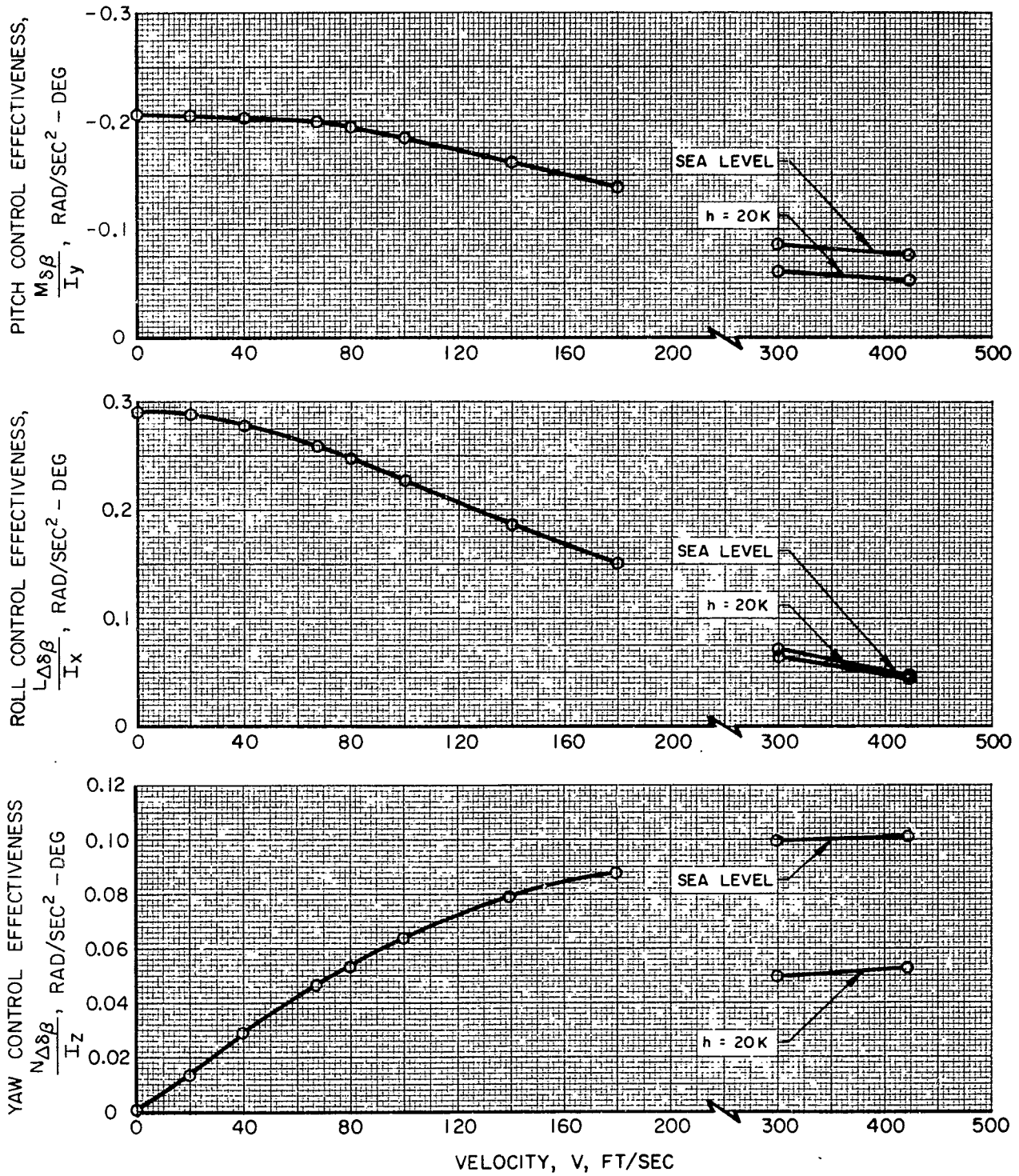

FIG. 72

CONTROL EFFECTIVENESS OF DUCT EXIT VANES IN STEADY LEVEL FLIGHT

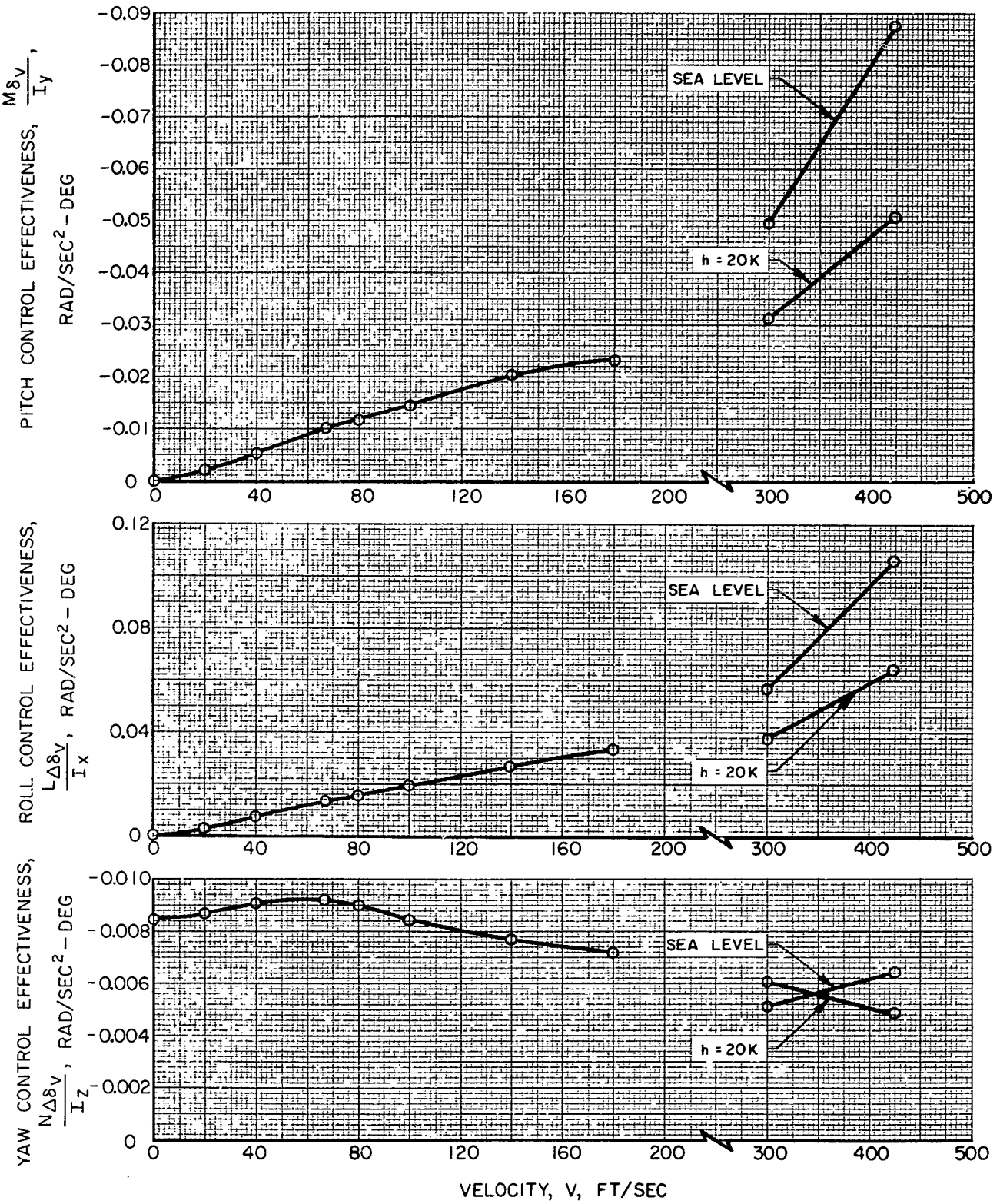

FIG. 73

VARIATION OF LIFT AND DRAG COEFFICIENTS OF FUSELAGE WITH ANGLE OF ATTACK

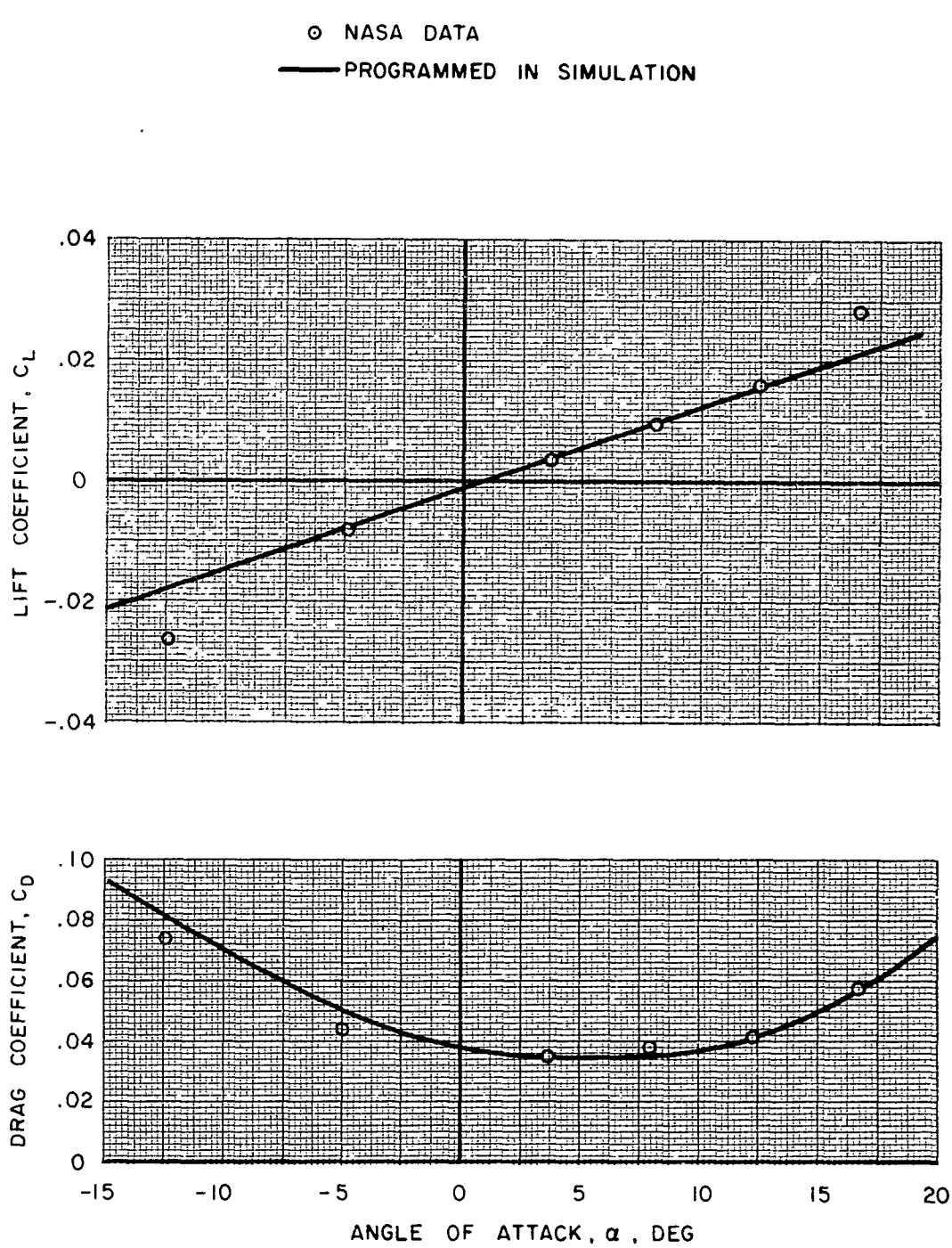

FIG. 74

VARIATION OF SIDE FORCE COEFFICIENT SLOPE OF VERTICAL TAIL WITH DUCT INCIDENCE ANGLE

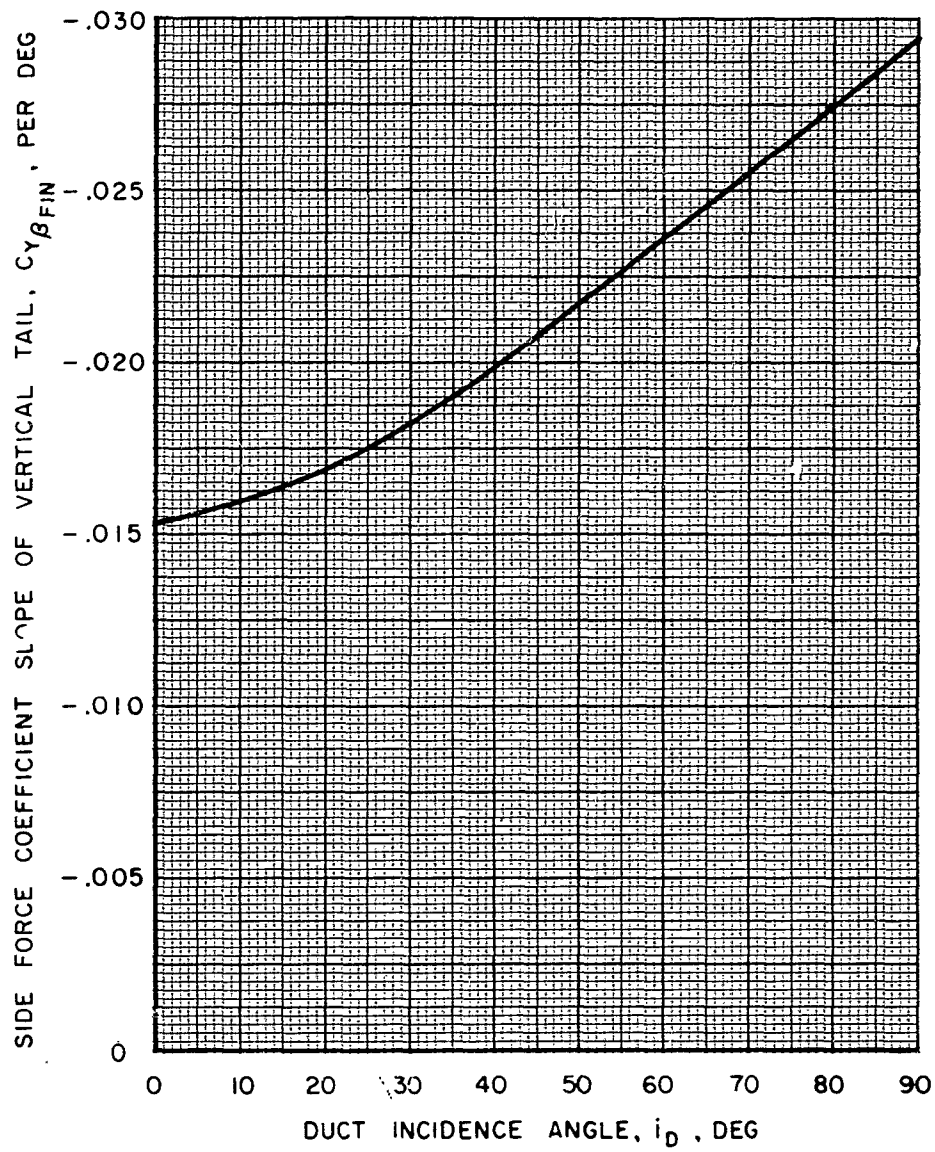

FIG. 75

STABILITY-AXIS SYSTEM FOR ANALYSIS OF LONGITUDINAL DYNAMICS

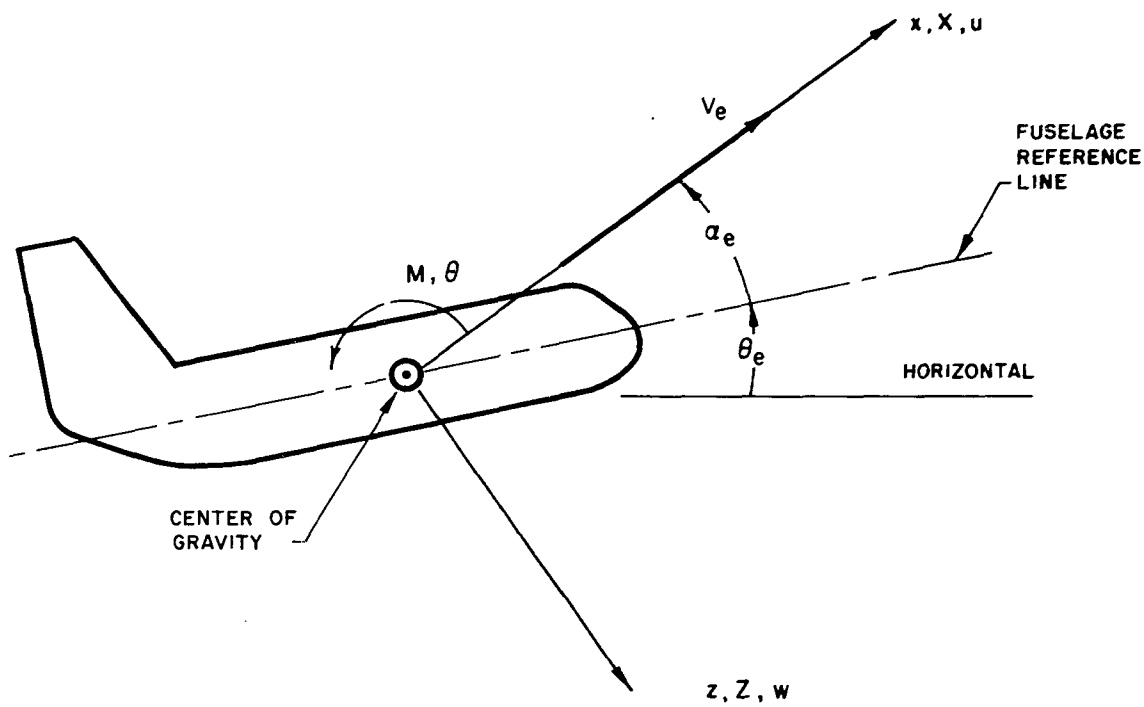

SKETCH OF ROOT-LOCUS DIAGRAM SHOWING SIGNIFICANT INFORMATION FOR LONGITUDINAL STABILITY ANALYSES

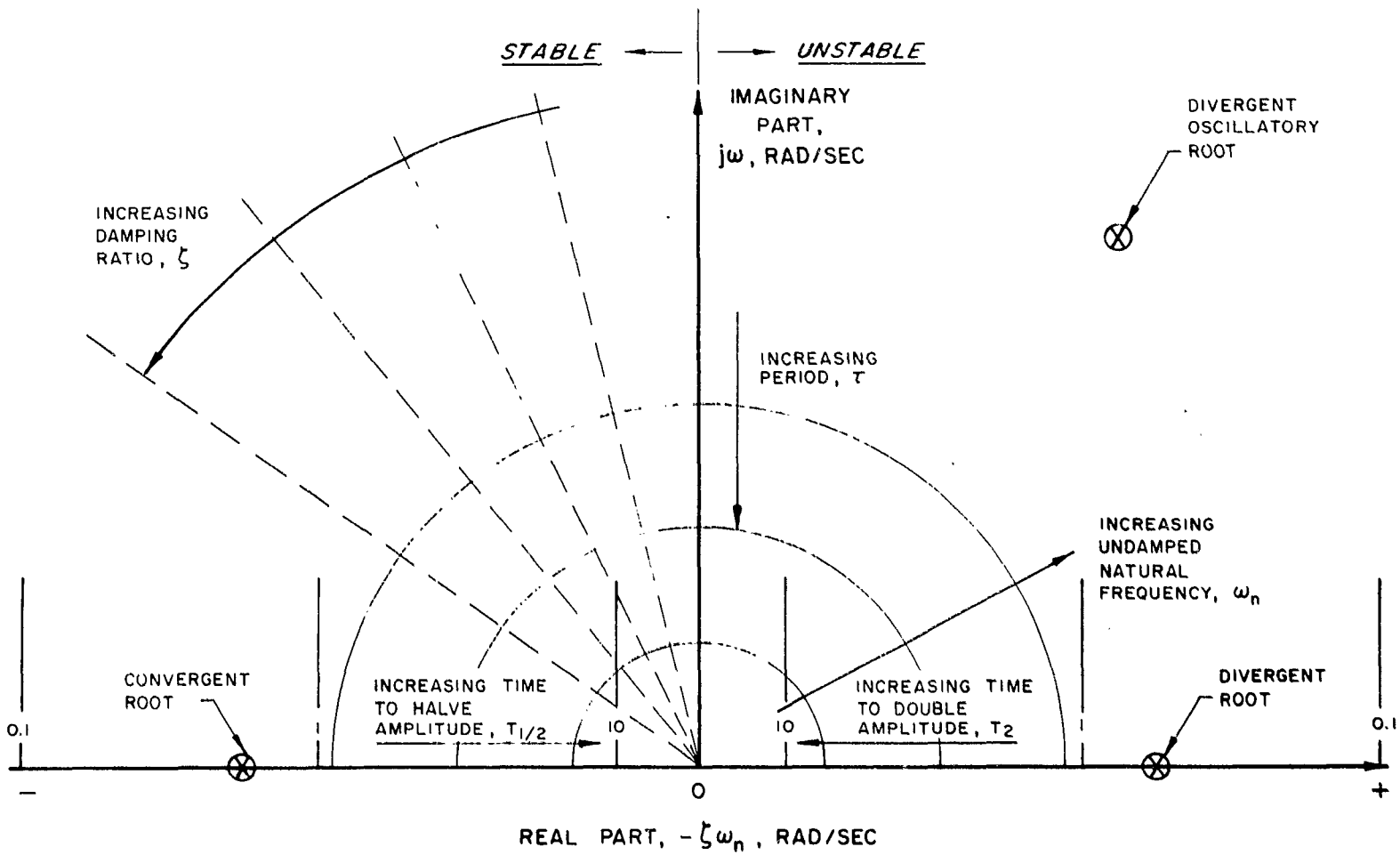

FIG. 76

FIG. 77

SKETCH OF ROOT-LOCUS DIAGRAM FOR STEADY LEVEL FLIGHT

NO STABILITY AUGMENTATION

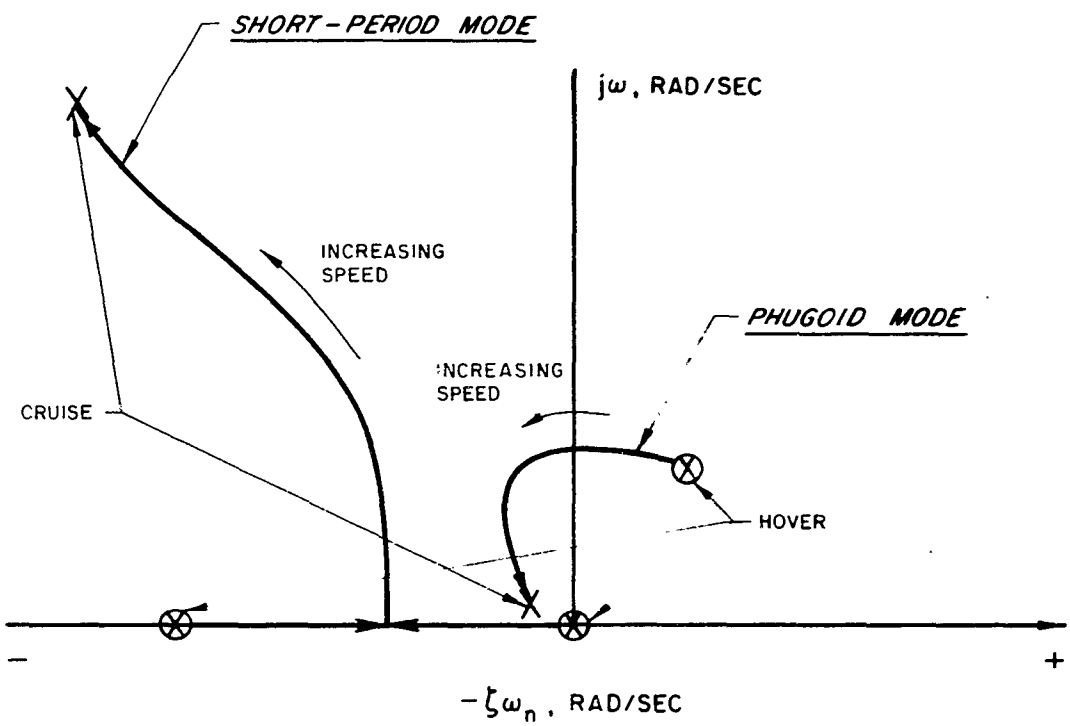

FIG. 78

AXIS SYSTEM FOR ANALYSIS OF LATERAL - DIRECTIONAL DYNAMICS

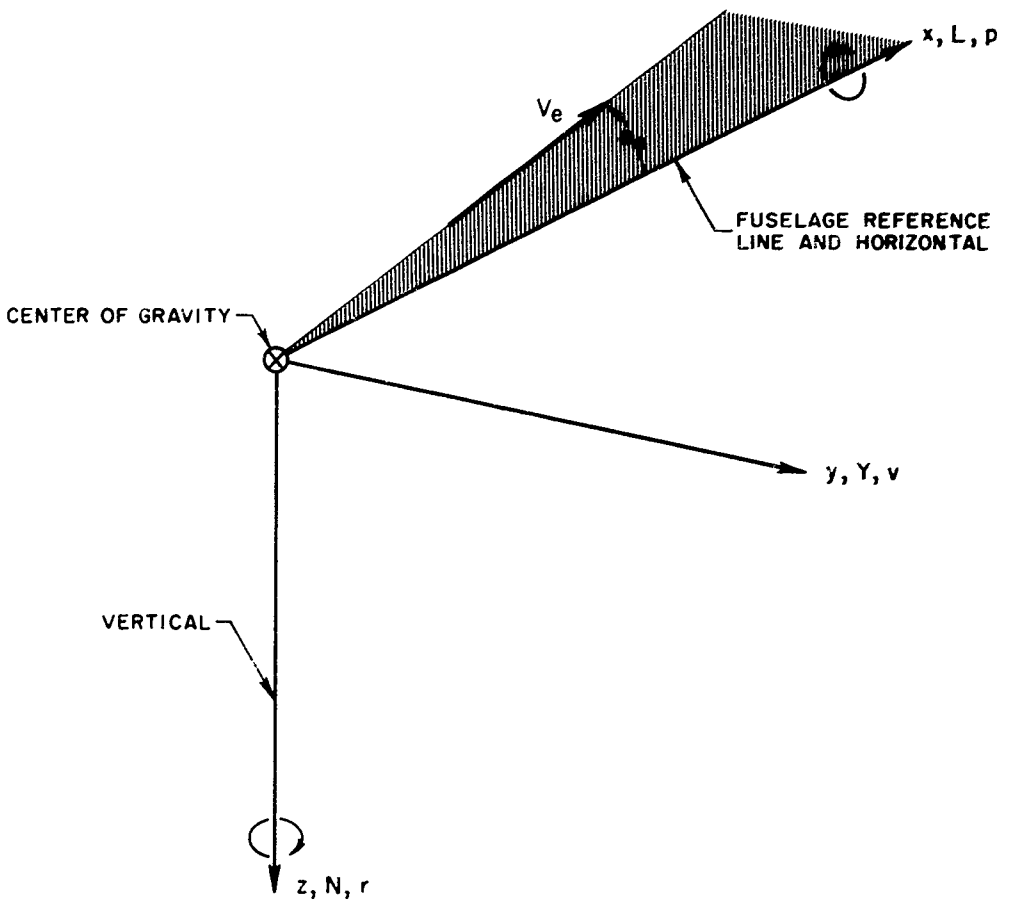

FIG. 79

SKETCH OF ROOT-LOCUS DIAGRAM FOR STEADY LEVEL FLIGHT

NO STABILITY AUGMENTATION

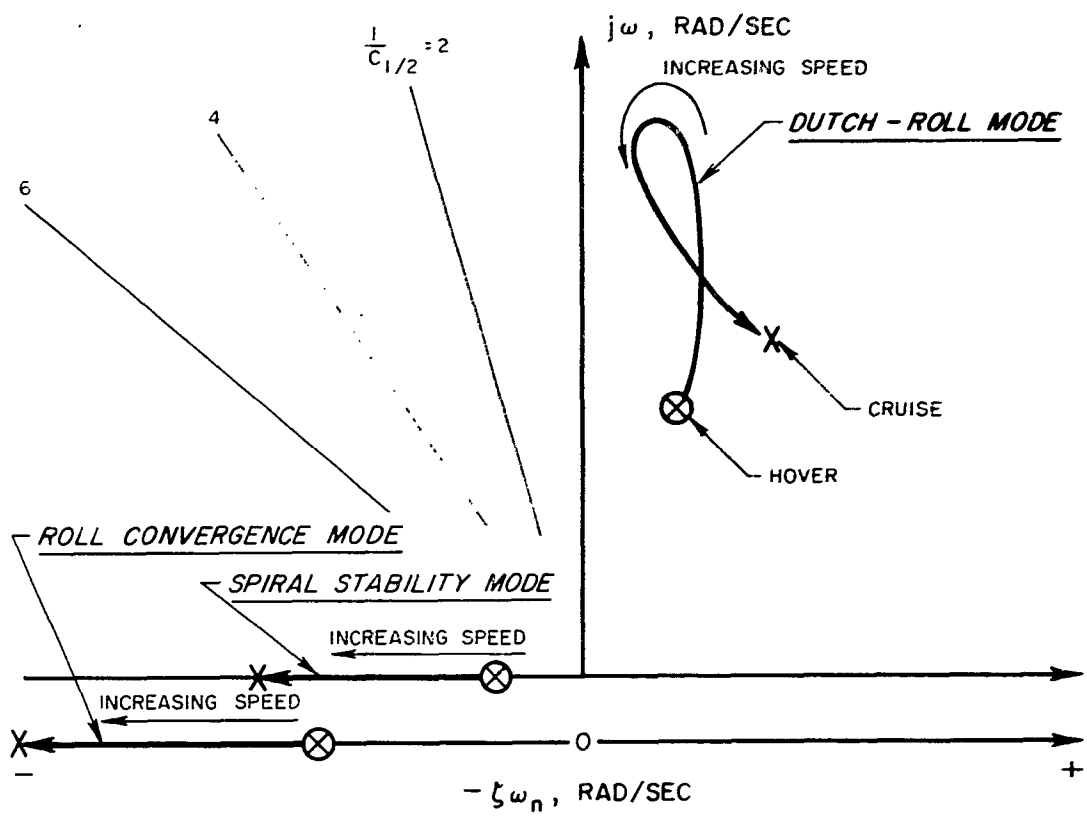

FIG. 80

EFFECT OF INCORRECT PHASING ON LATERAL-DIRECTIONAL DYNAMICS IN STEADY LEVEL FLIGHT AT 40 KTS

50% STABILITY AUGMENTATION
NOMINAL CENTER OF GRAVITY LOCATION

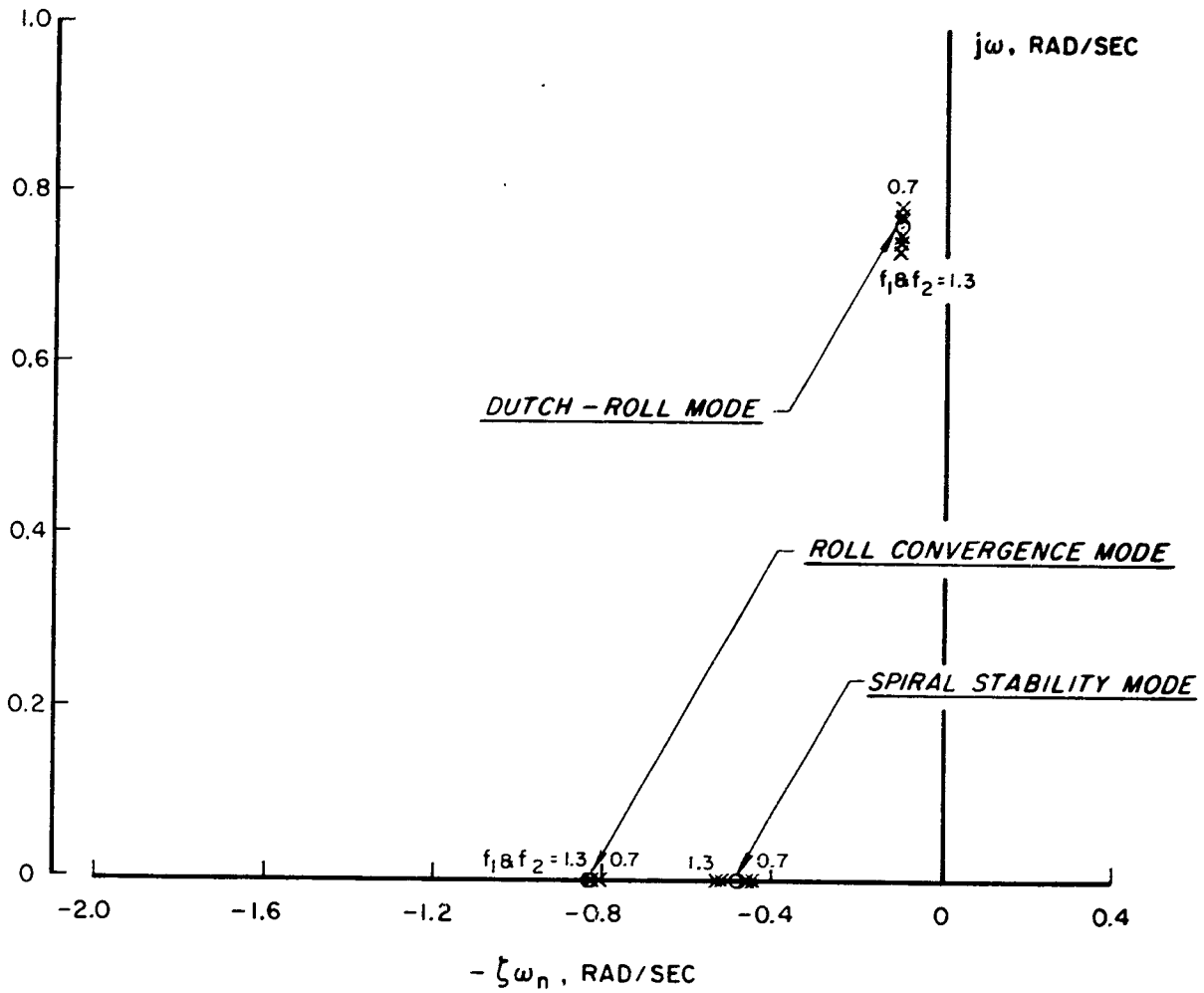

FIG. 81

GAIN PROGRAM FOR LATERAL CONTROL STICK

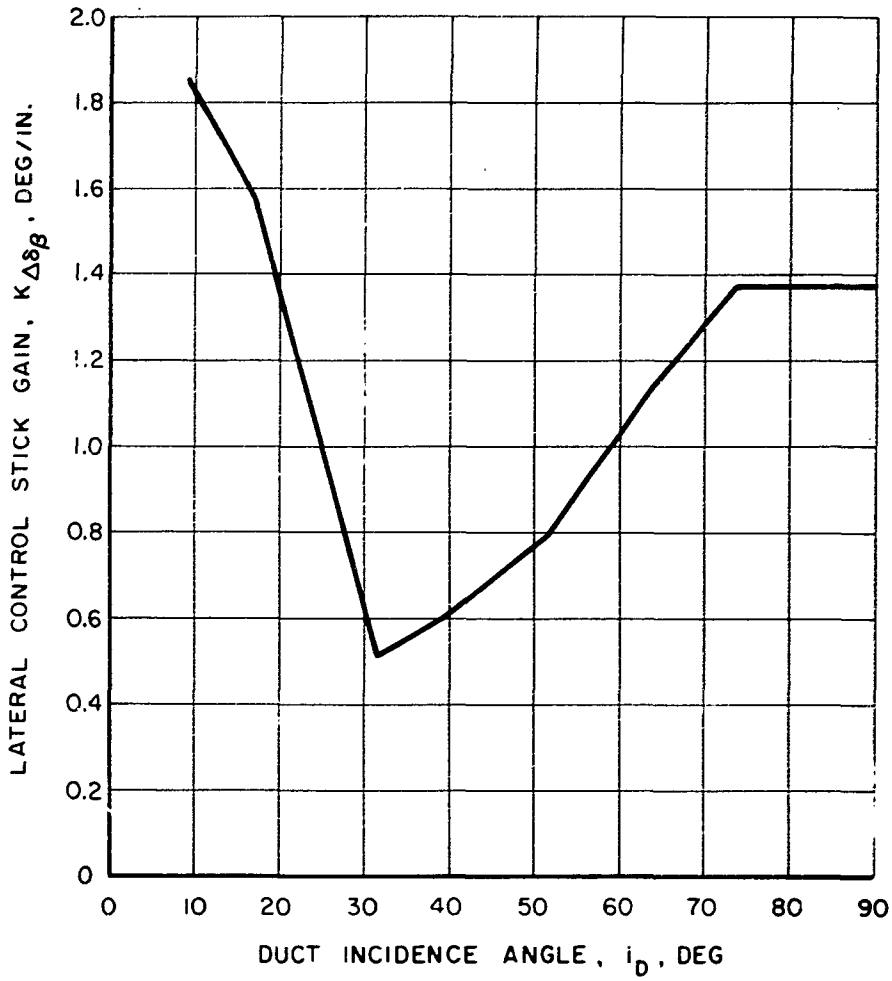

PHASING GAIN PROGRAM FOR LATERAL CONTROL STICK

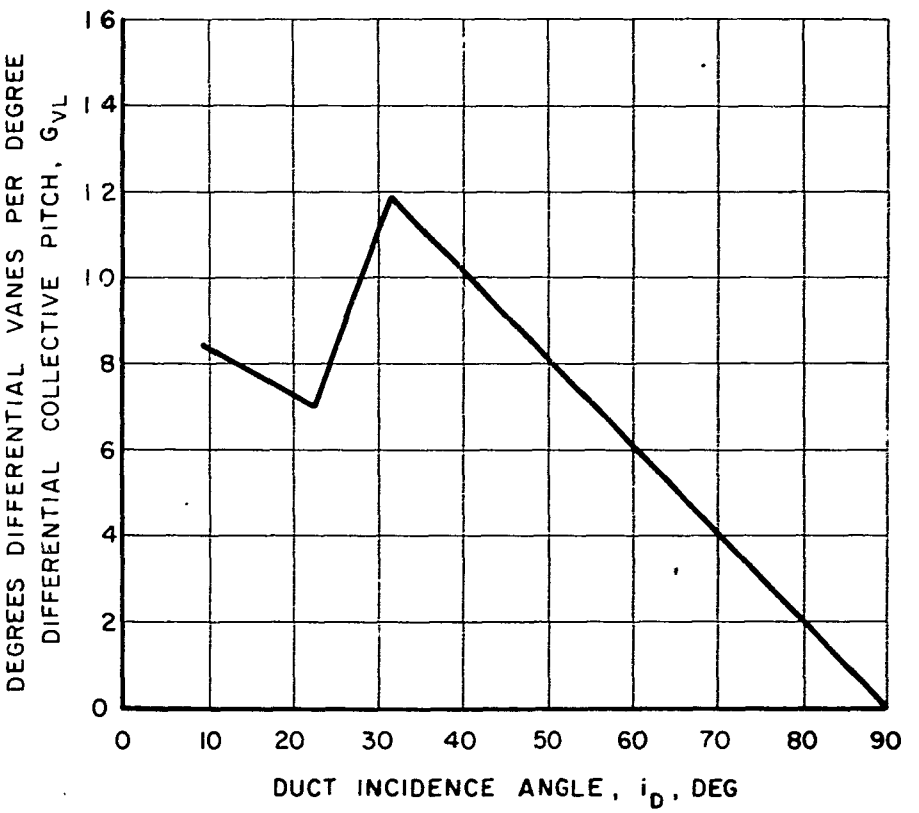

FIG. 83

GAIN PROGRAM FOR ROLL RATE STABILIZATION

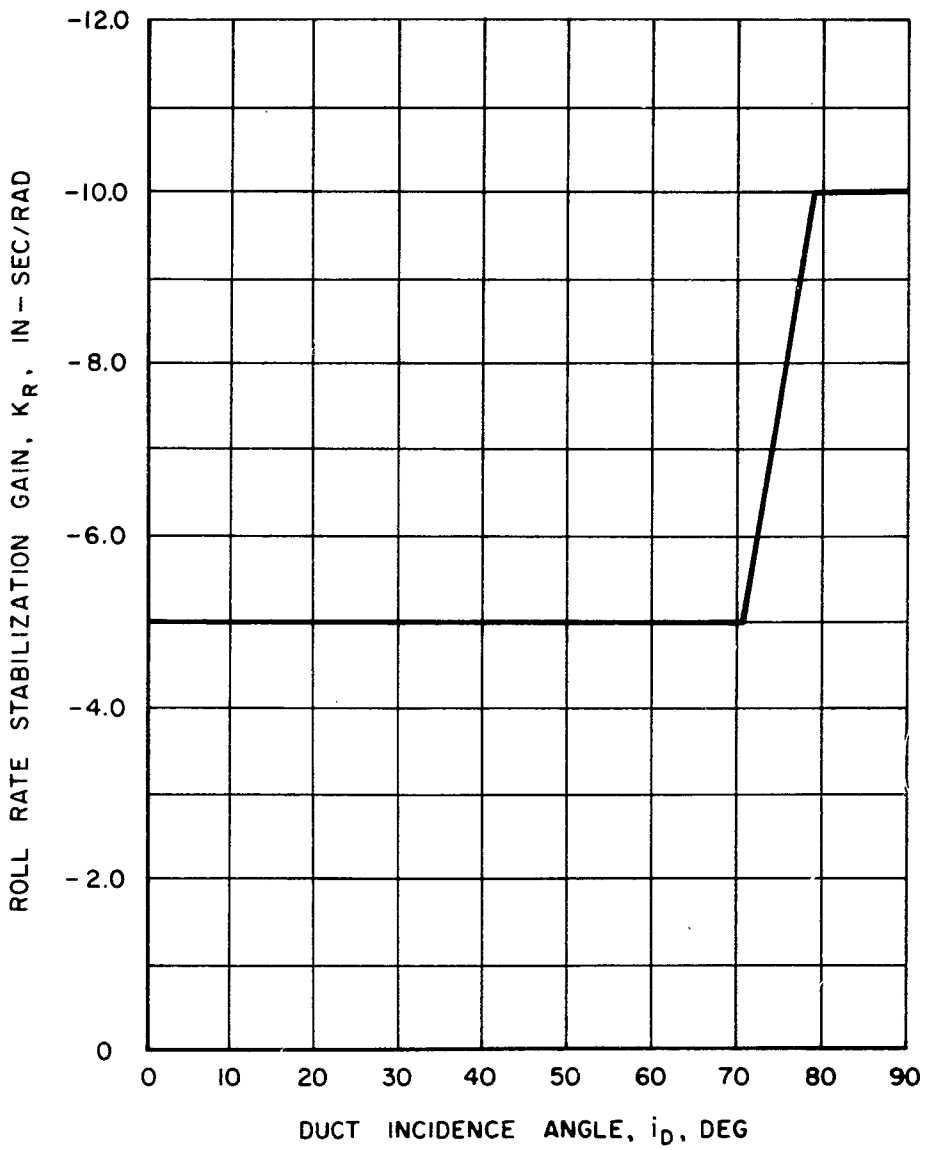

FIG. 84

GAIN PROGRAM FOR PEDALS

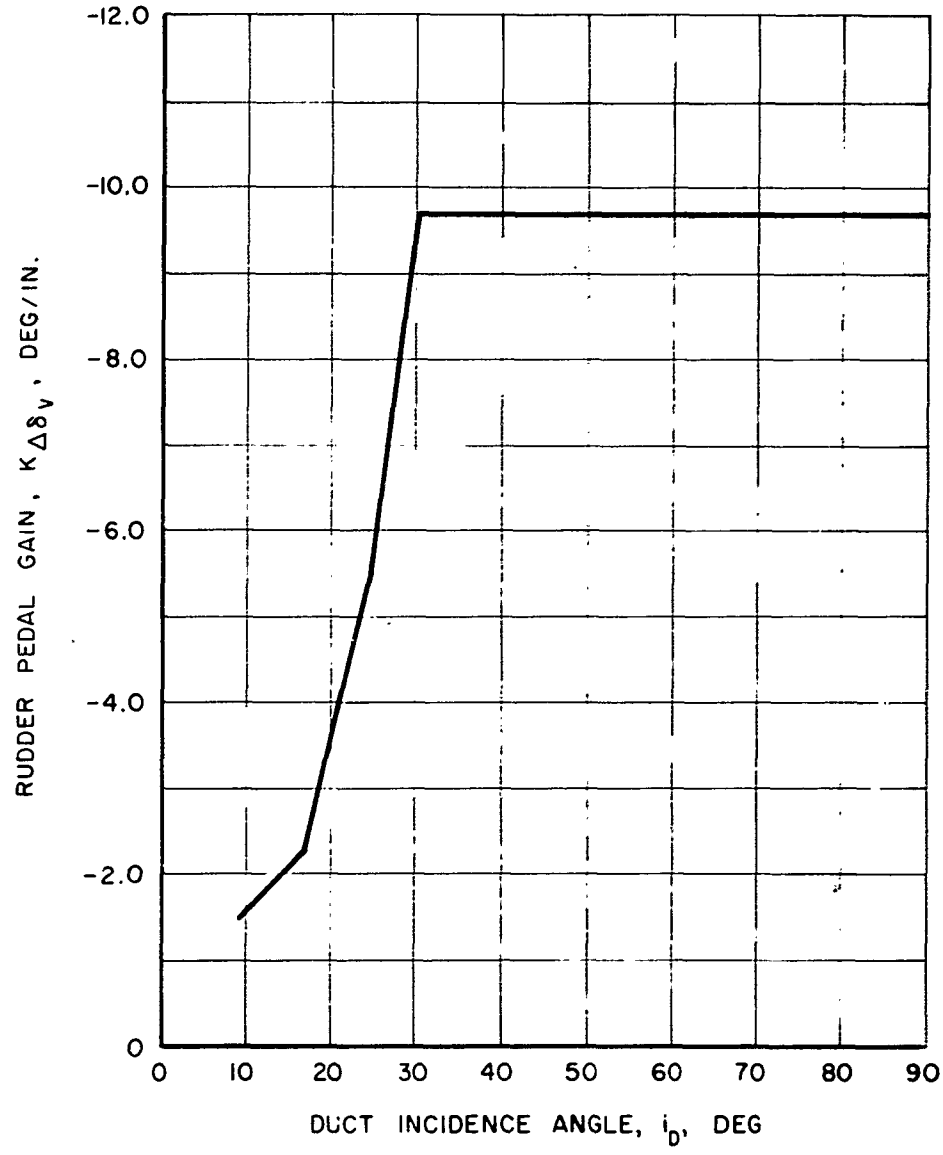

FIG. 85

PHASING GAIN PROGRAM FOR PEDALS

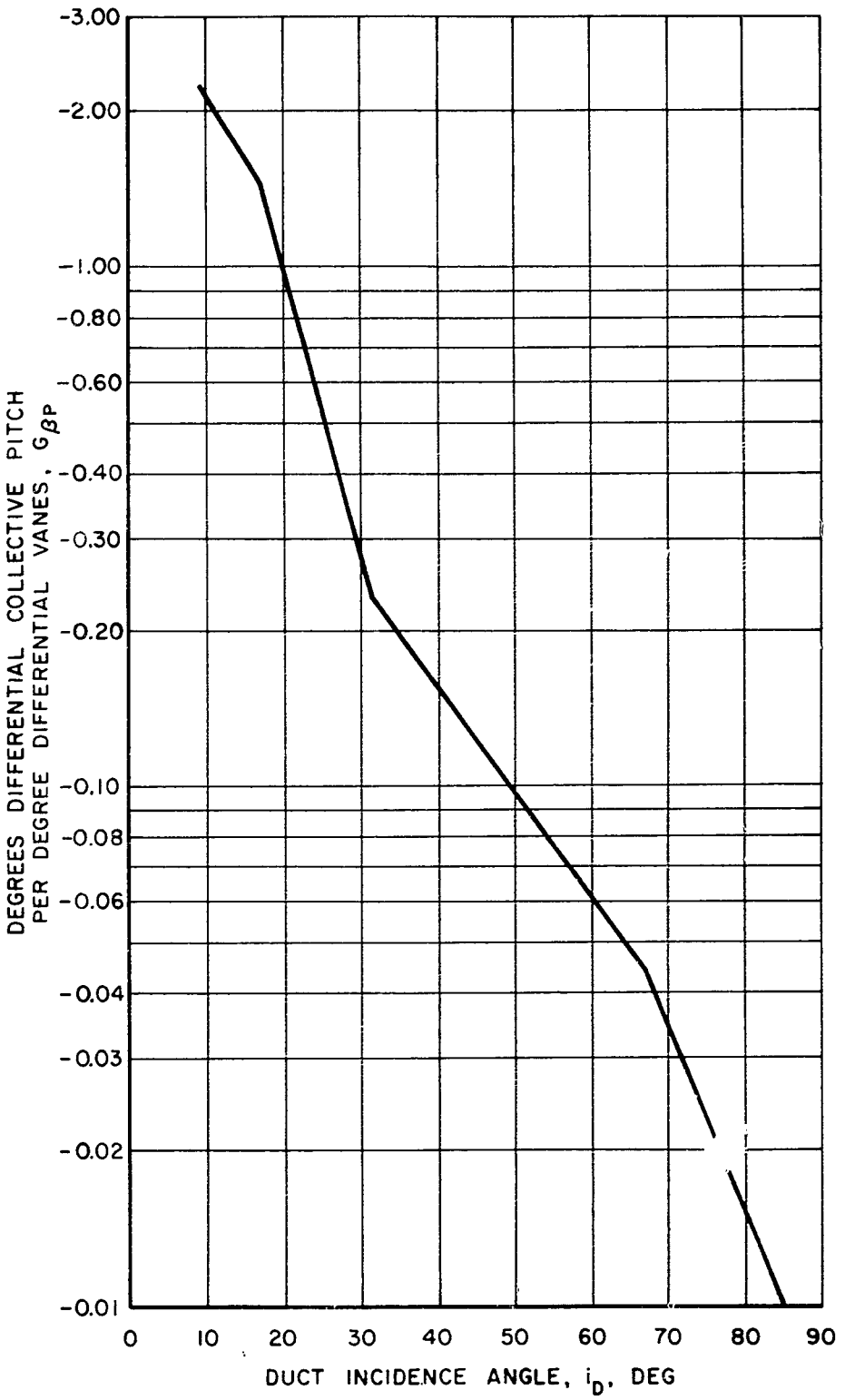

R-1624-5

FIG. 86

VIEW OF INTERIOR OF SIKORSKY V/STOL AIRCRAFT SIMULATOR WITH CONTACT ANALOG DISPLAY

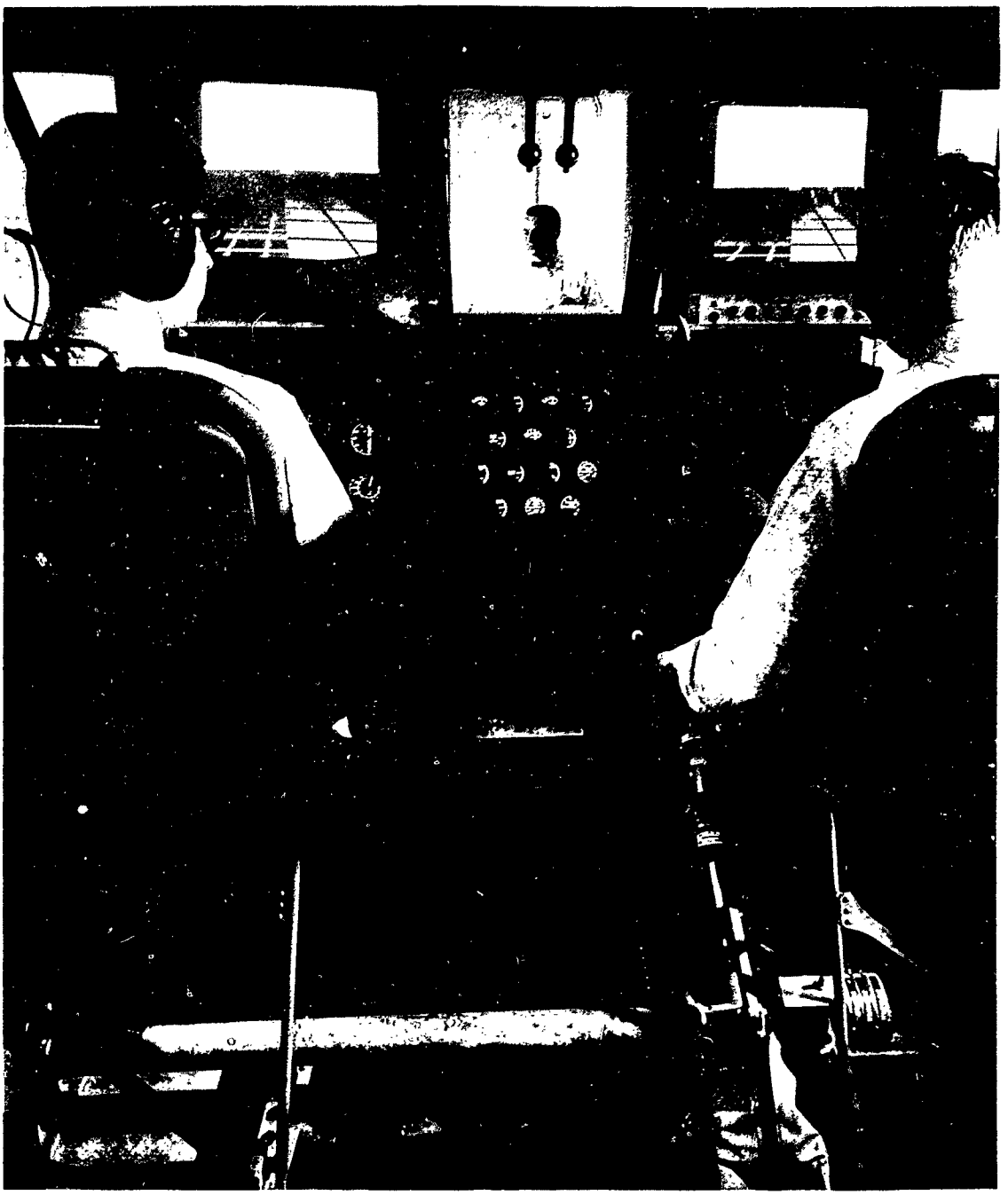

RL-62-393A

FLIGHT INSTRUMENT PORTION OF SIKORSKY V/STOL SIMULATOR CONTROL PANEL

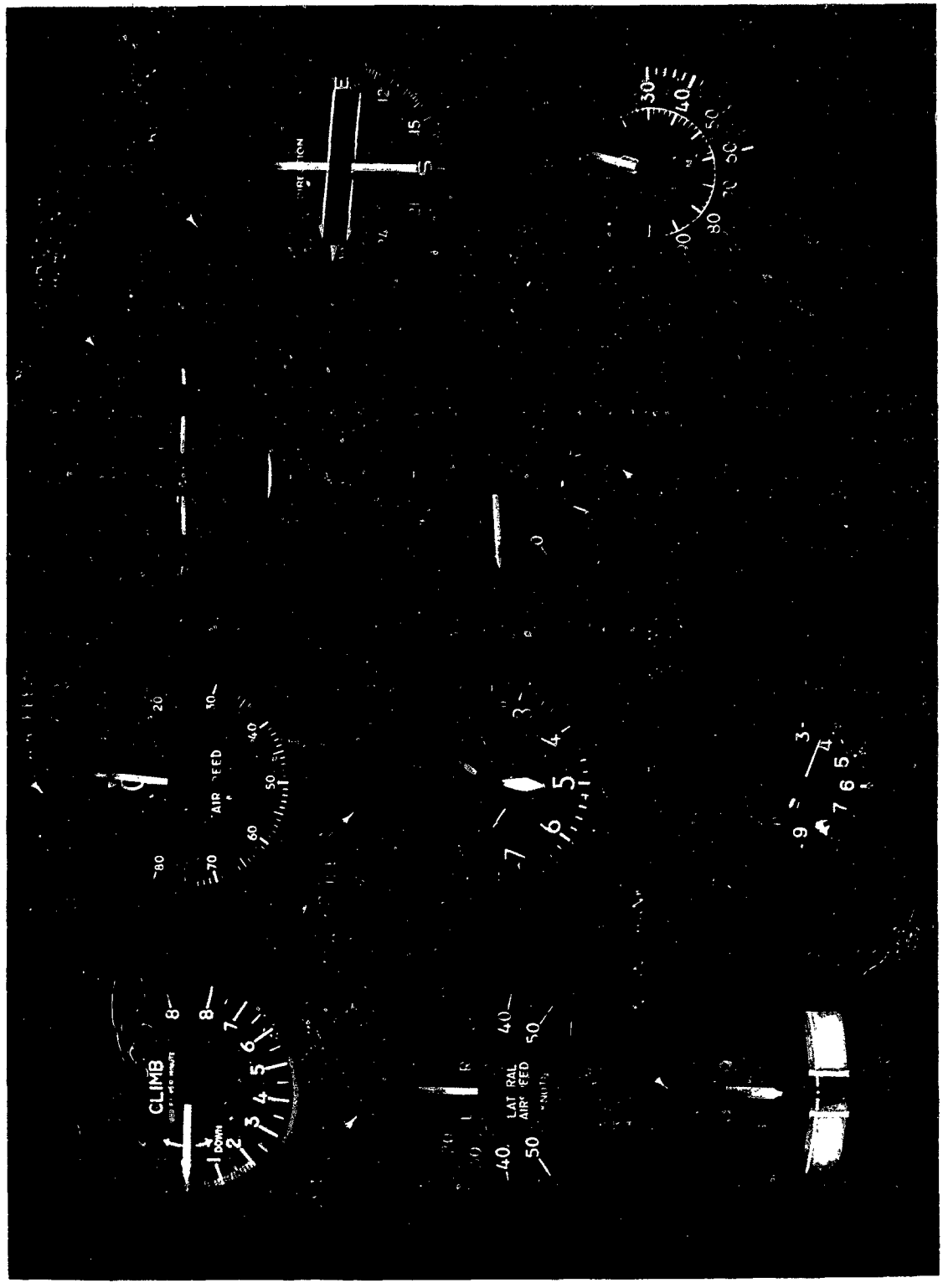

RL-62-381F

RL-62-381D

CONTROL INSTRUMENT PORTION OF SIKORSKY V/STOL SIMULATOR CONTROL PANEL

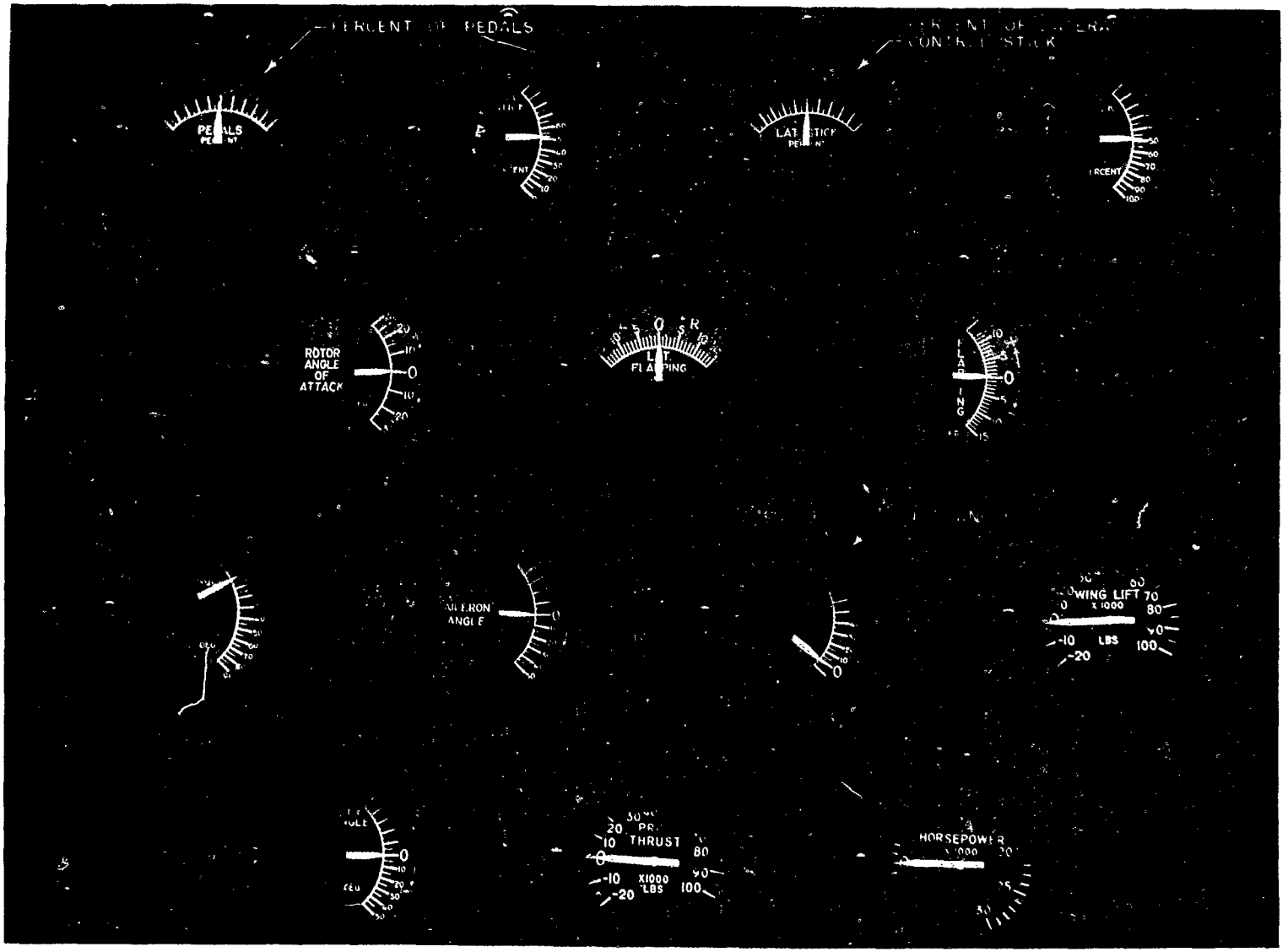

R-1624-5

FIG. 88

PHOTOGRAPHS OF CONTACT ANALOG DISPLAY

(a.) RIGHT TURN AT 50 FT ALTITUDE

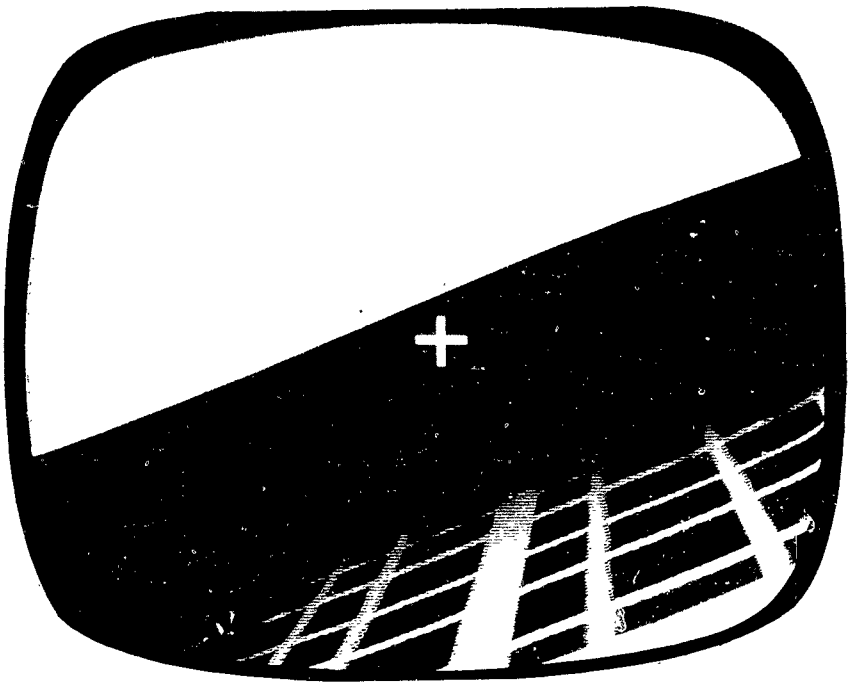

(b.) LEVEL FLIGHT AT 85 FT ALTITUDE

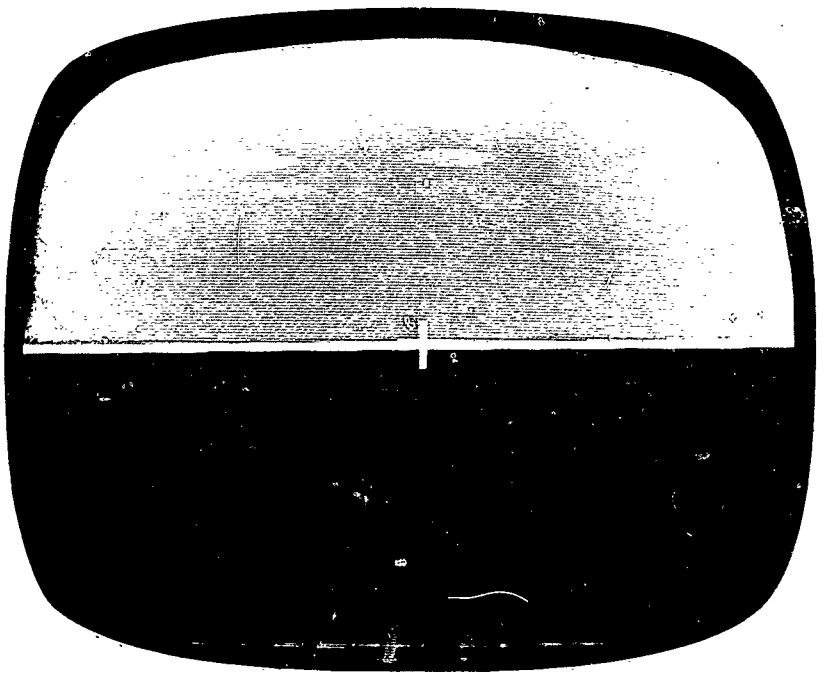

RL-62-381

RL-62-381B

R-1624-5

DISPLAY ELEMENTS USED IN SIMULATION OF TANDEM TILTING DUCTED PROPELLER VTOL AIRCRAFT

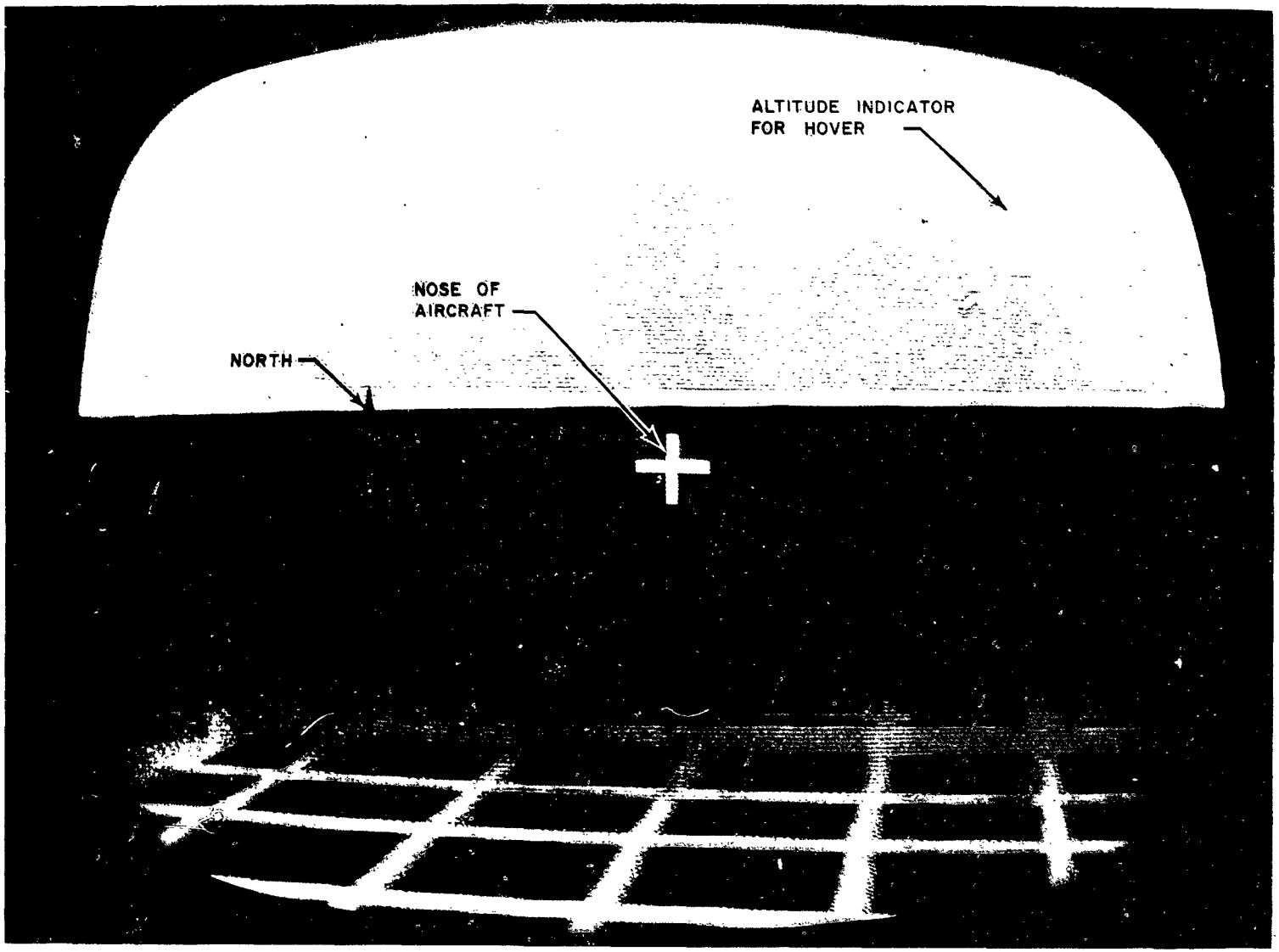

FIG. 90

R-1624-5

PROGRAMMED-GAIN STABILITY AUGMENTATION S

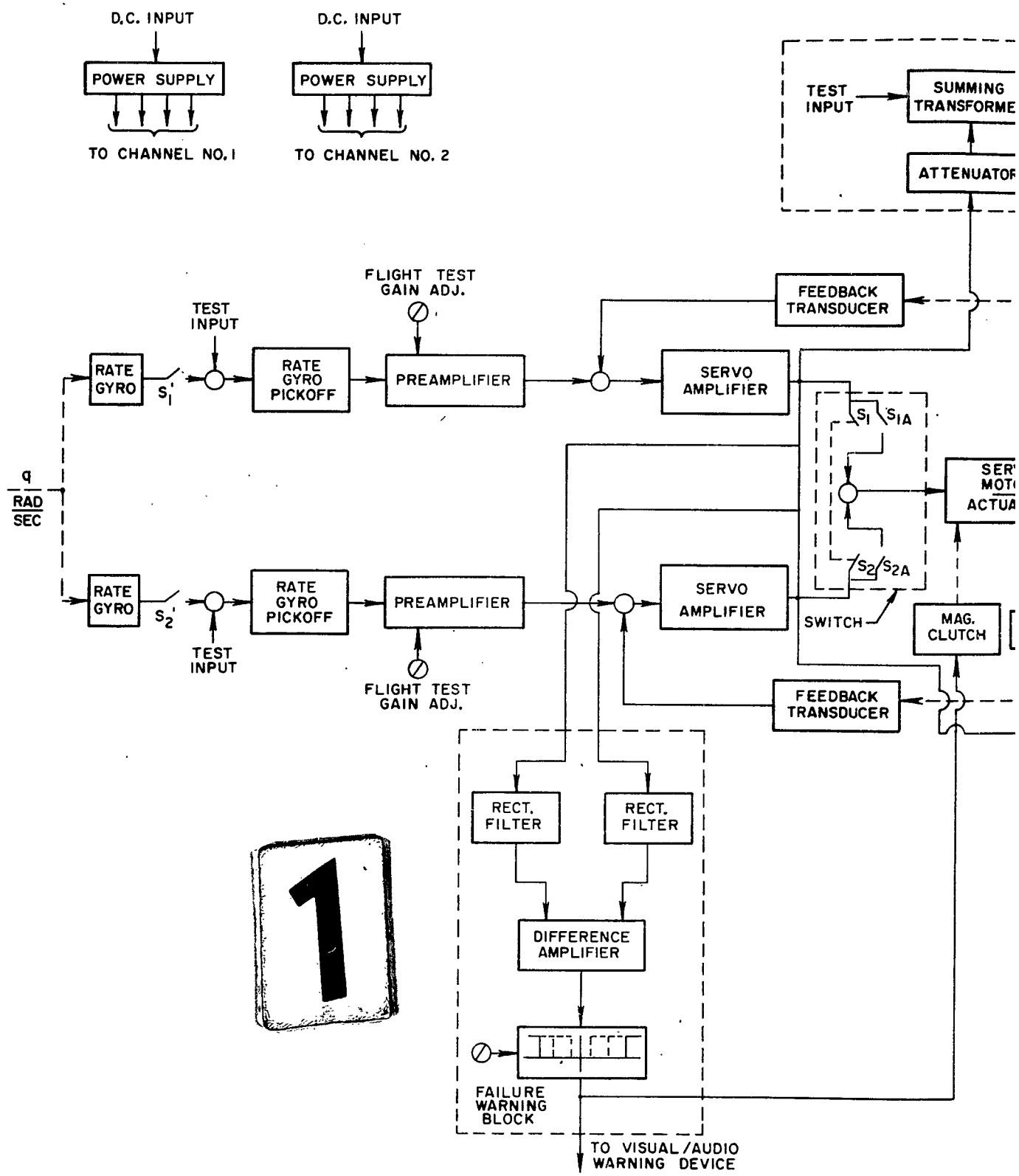

FIG. 91

UGMENTATION SYSTEM FOR PITCH AND ALTITUDE, MODES

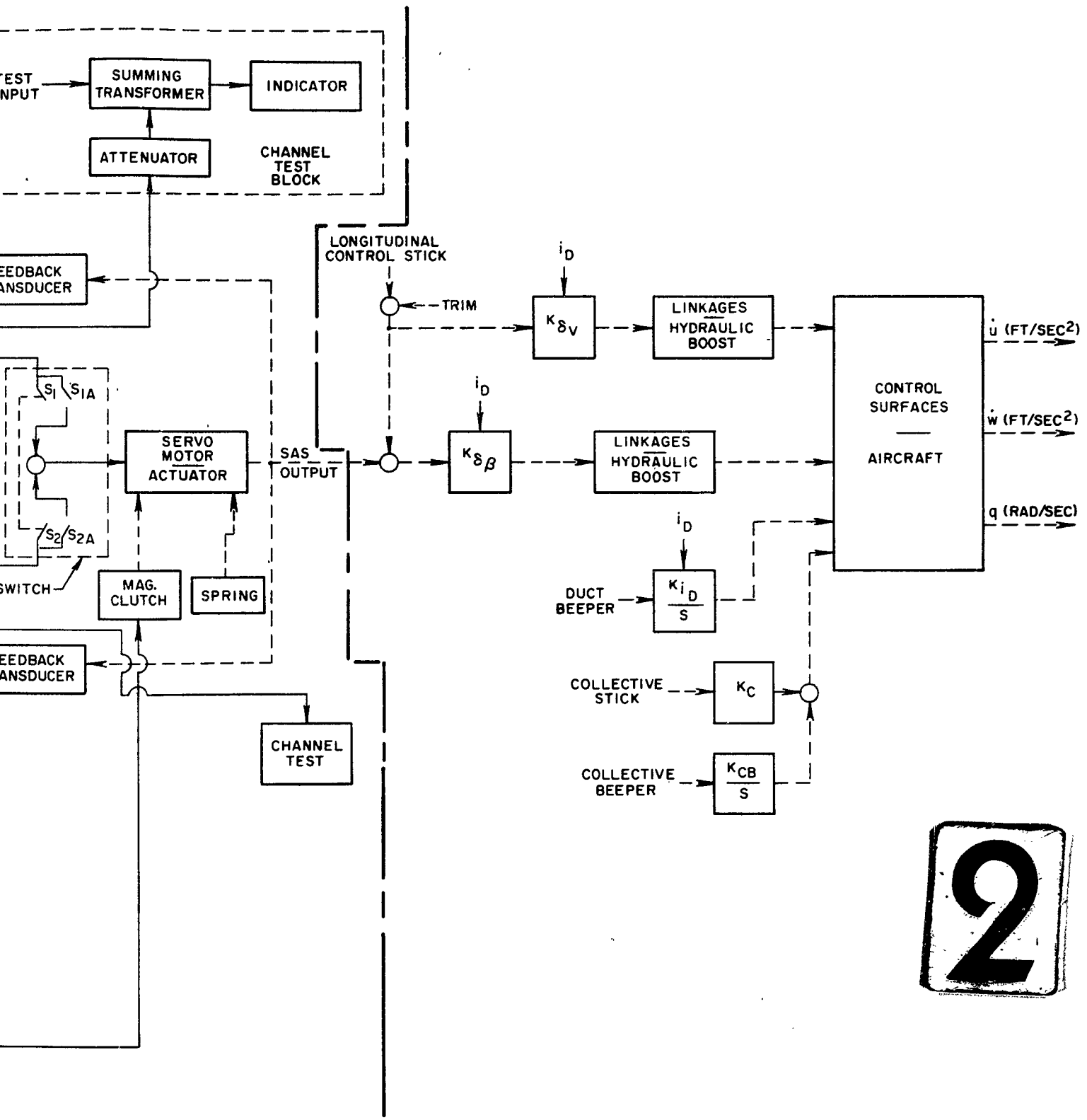

2

PROGRAMMED-GAIN STABILITY AUGMENTATION SYSTEM F(

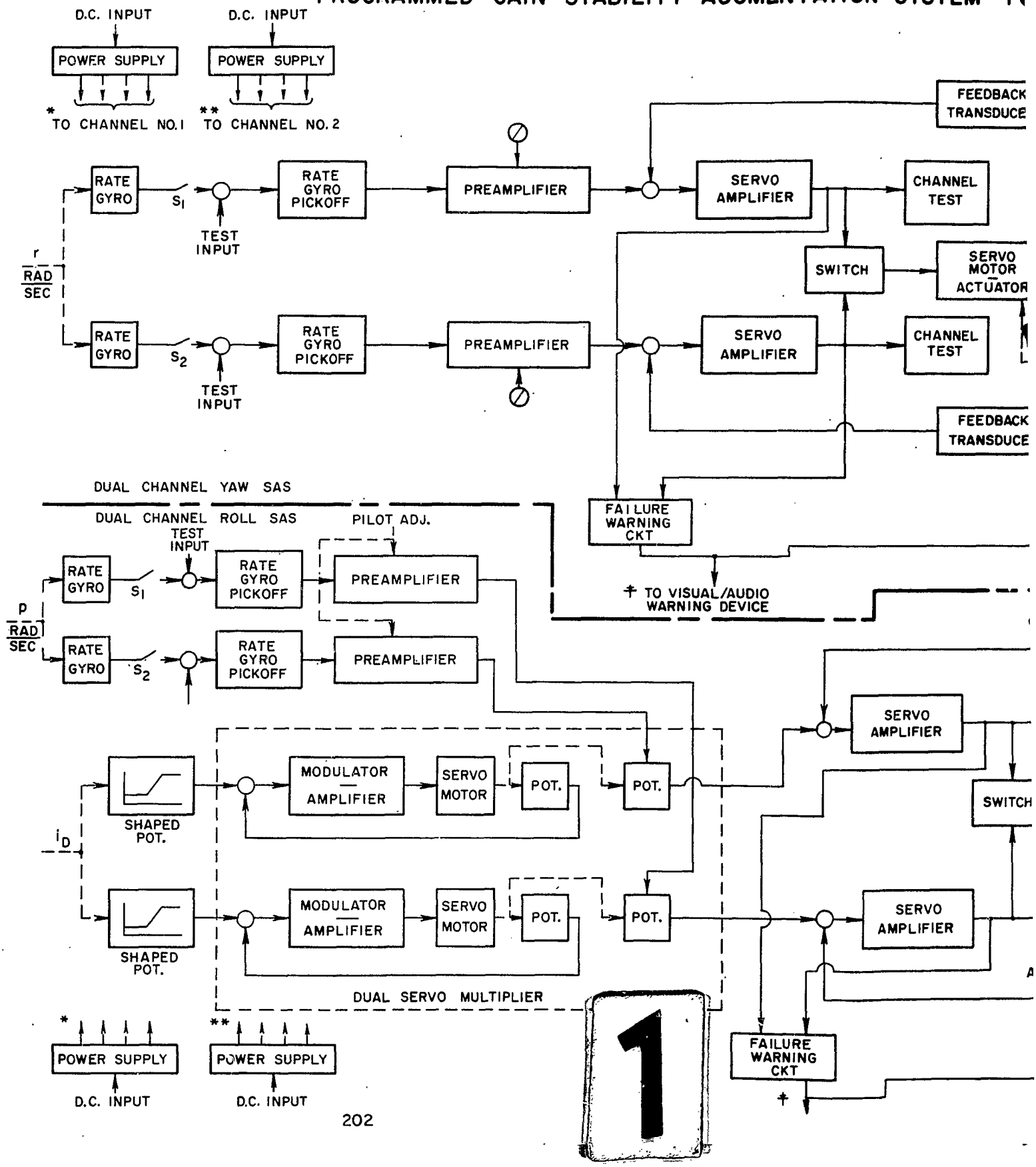

FIG. 92

GMENTATION SYSTEM FOR LATERAL - DIRECTIONAL MODES

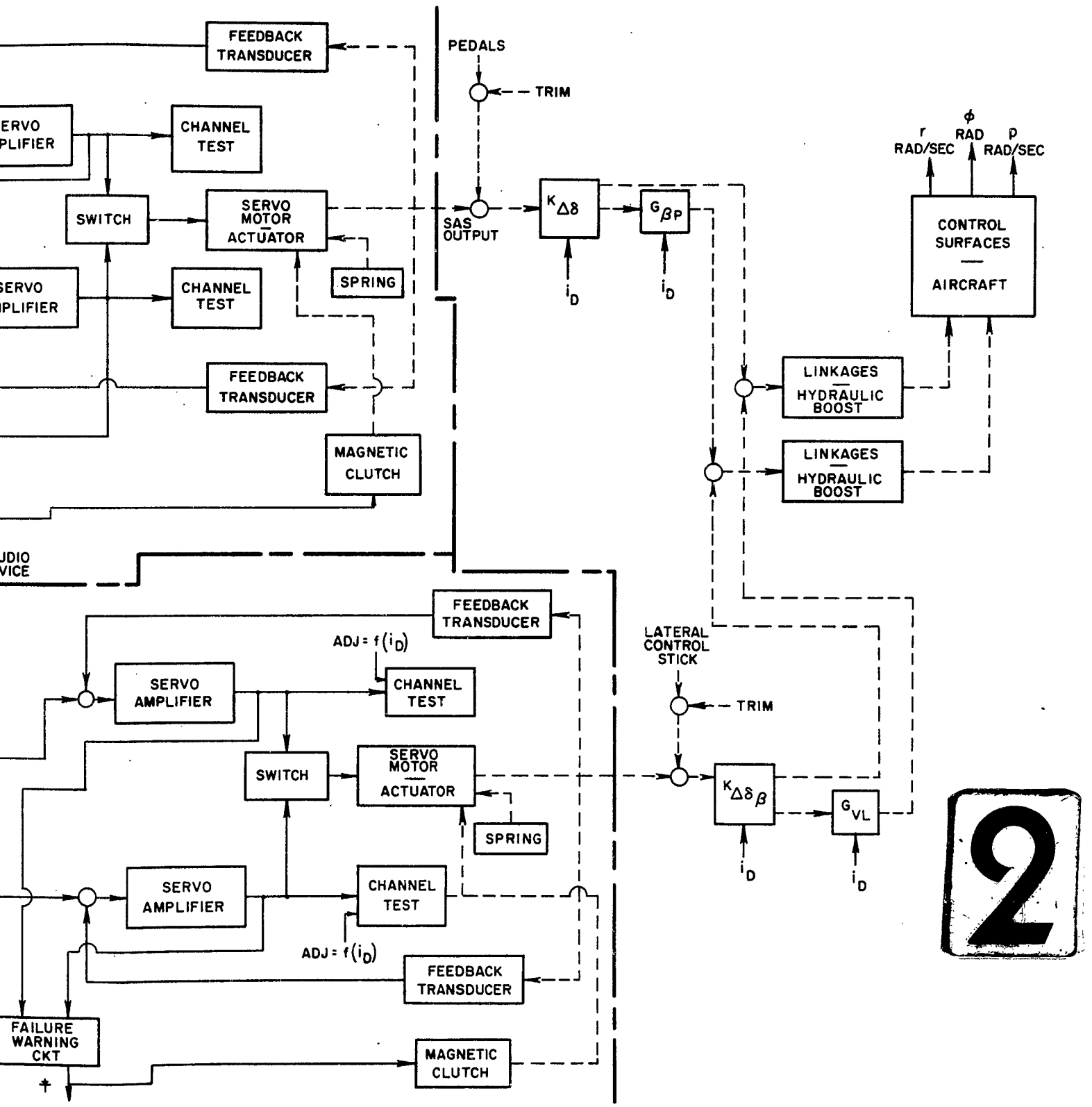

PITCH CHANNEL OF DUPLICATED ADAPTIVE CONTROL SYSTEM

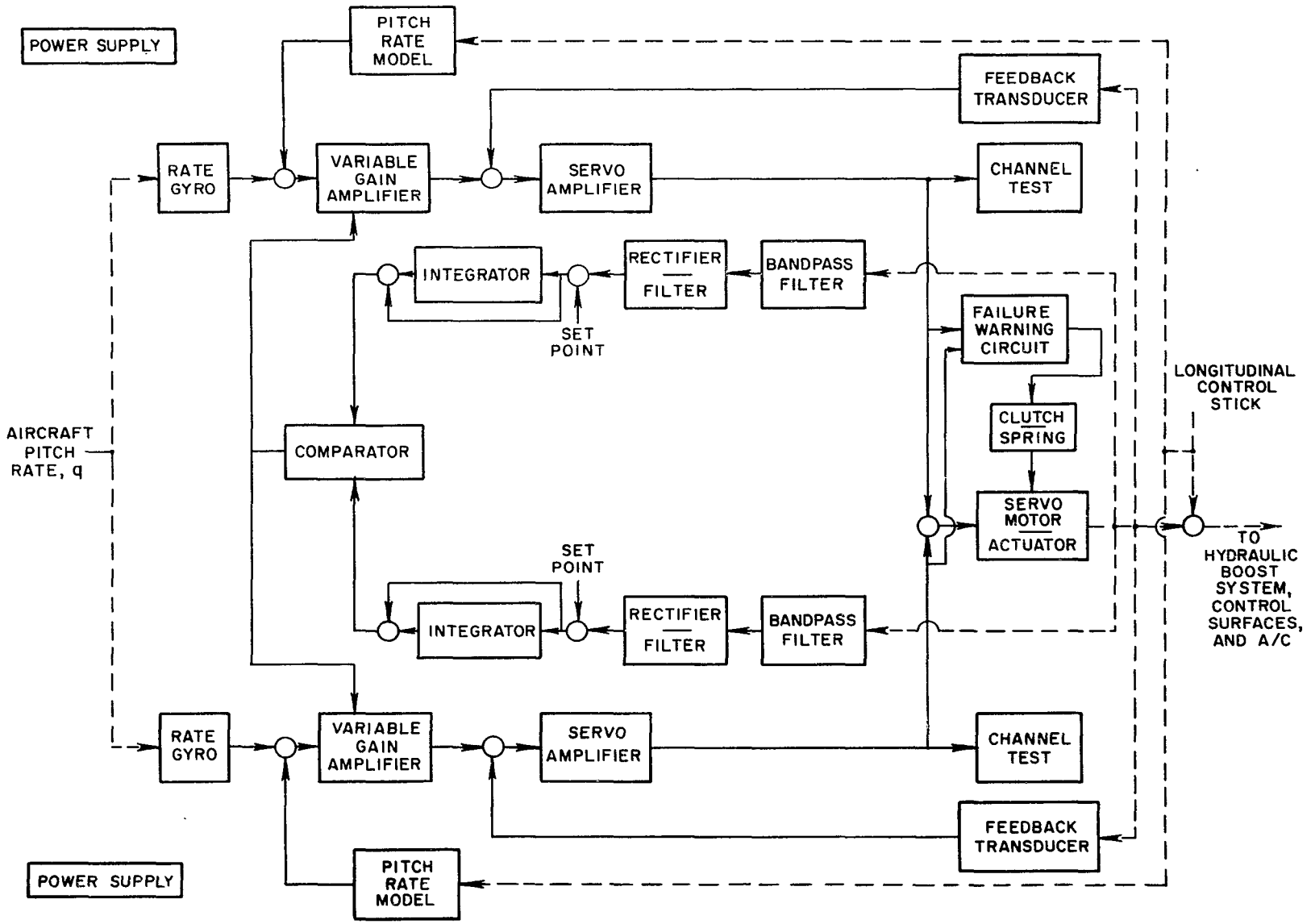

FIG. 93

PITCH CHANNEL OF TRIPLICATED PROGRAMMED-GAIN STABILITY AUGMENTATION SYSTEM

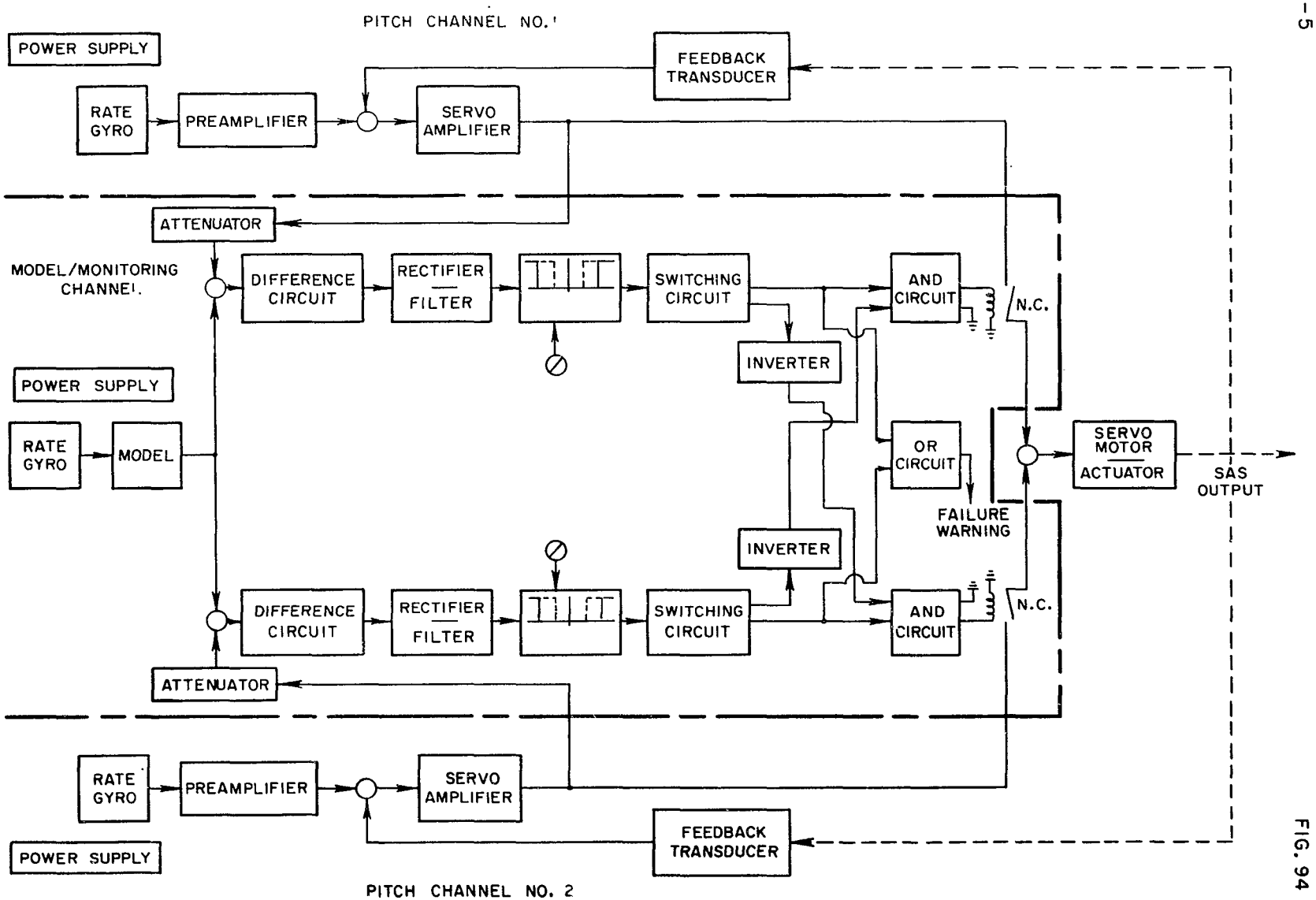

R-1624-5

FIG. 94

SUMMARY OF LONGITUDINAL ROOT LOCATIONS FO
15,000-LB AIRCRAFT WITHOUT STABILITY

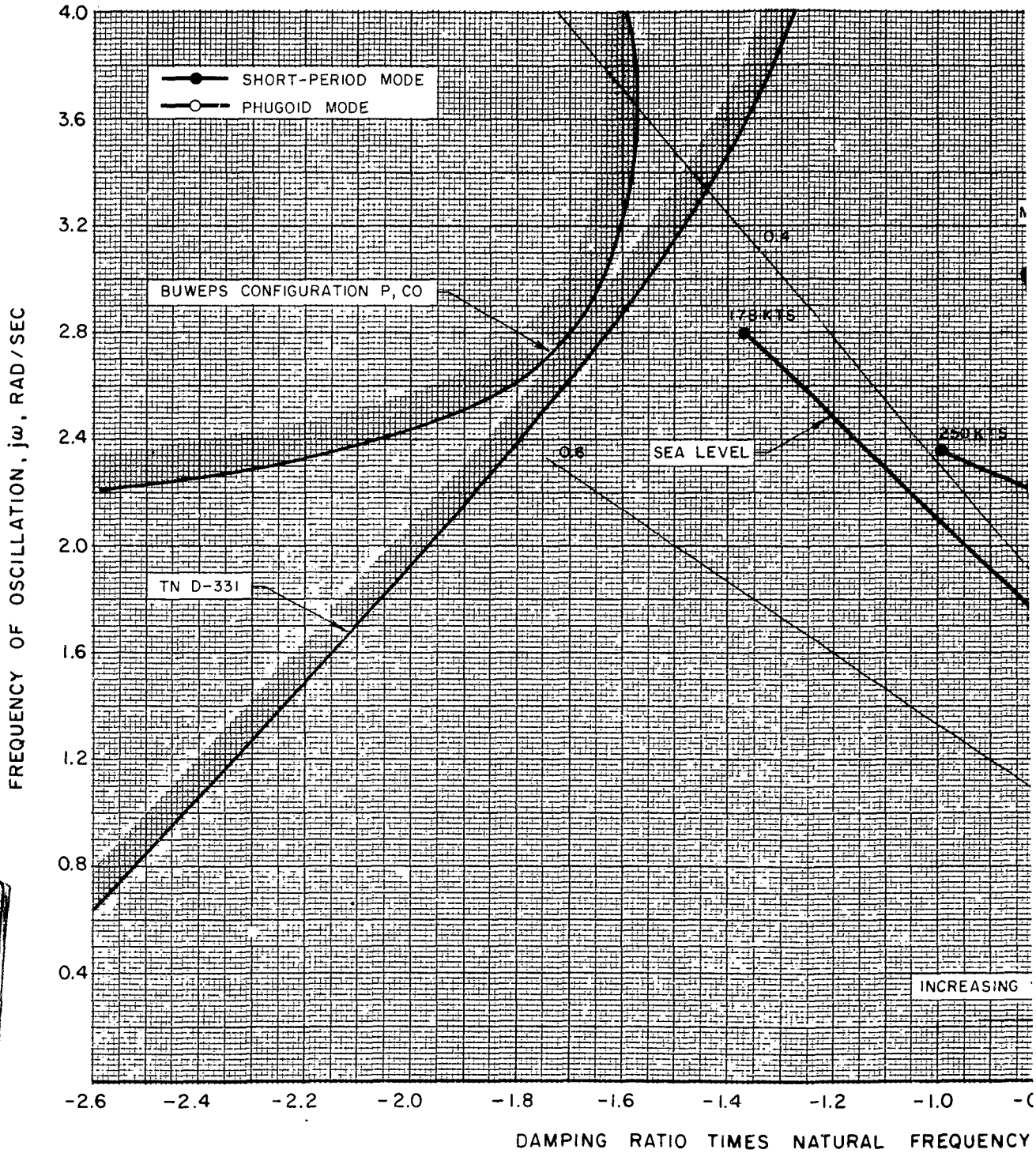

FIG. 95

AL ROOT LOCATIONS FOR STEADY LEVEL FLIGHT
CRAFT WITHOUT STABILITY AUGMENTATION

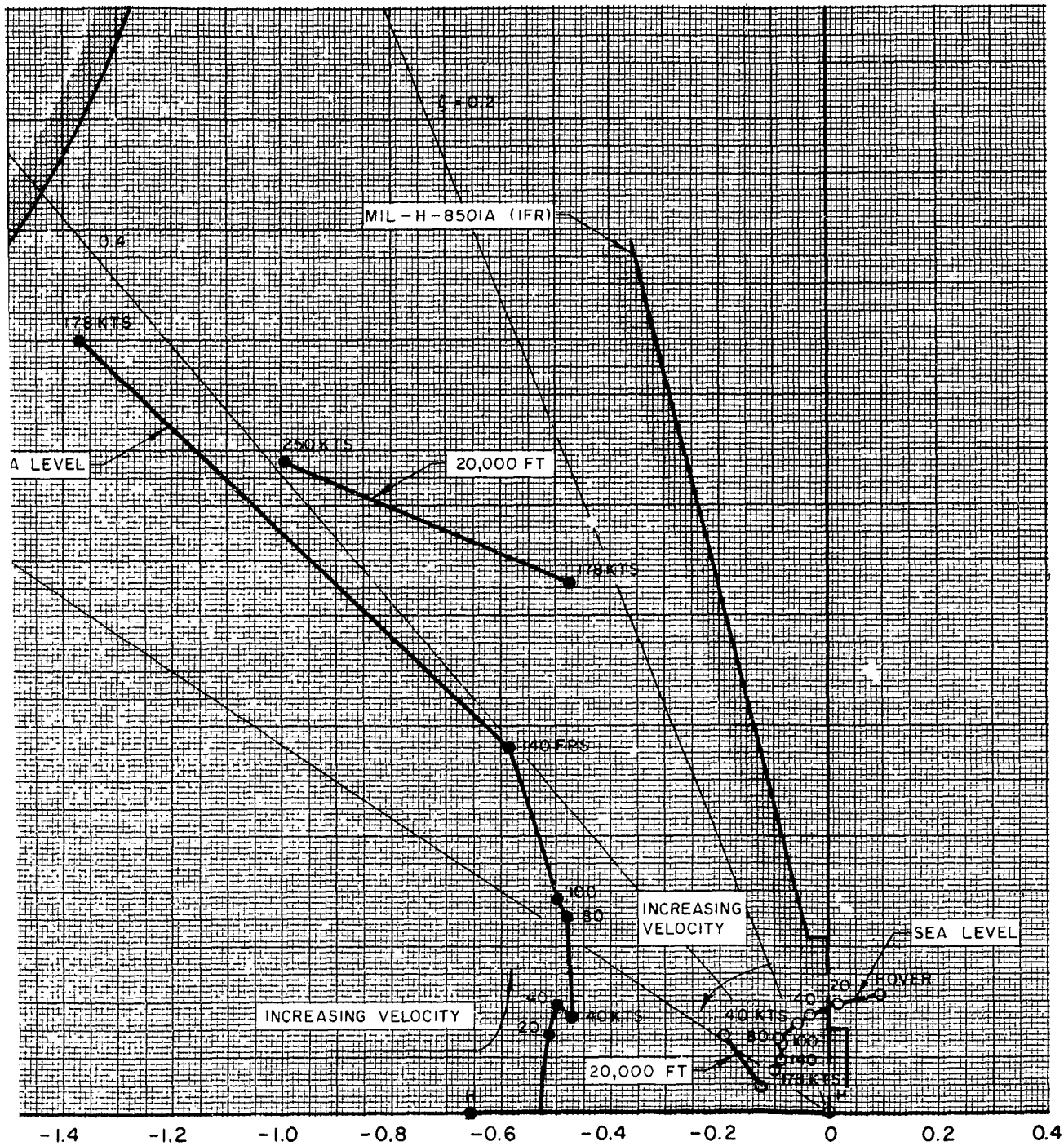

TIMES NATURAL FREQUENCY, $-\zeta\omega_n$, RAD/SEC

2

SUMMARY OF LATERAL-DIRECTIONAL ROOT LOCATIO
15,000-LB AIRCRAFT WITHOUT STABILI

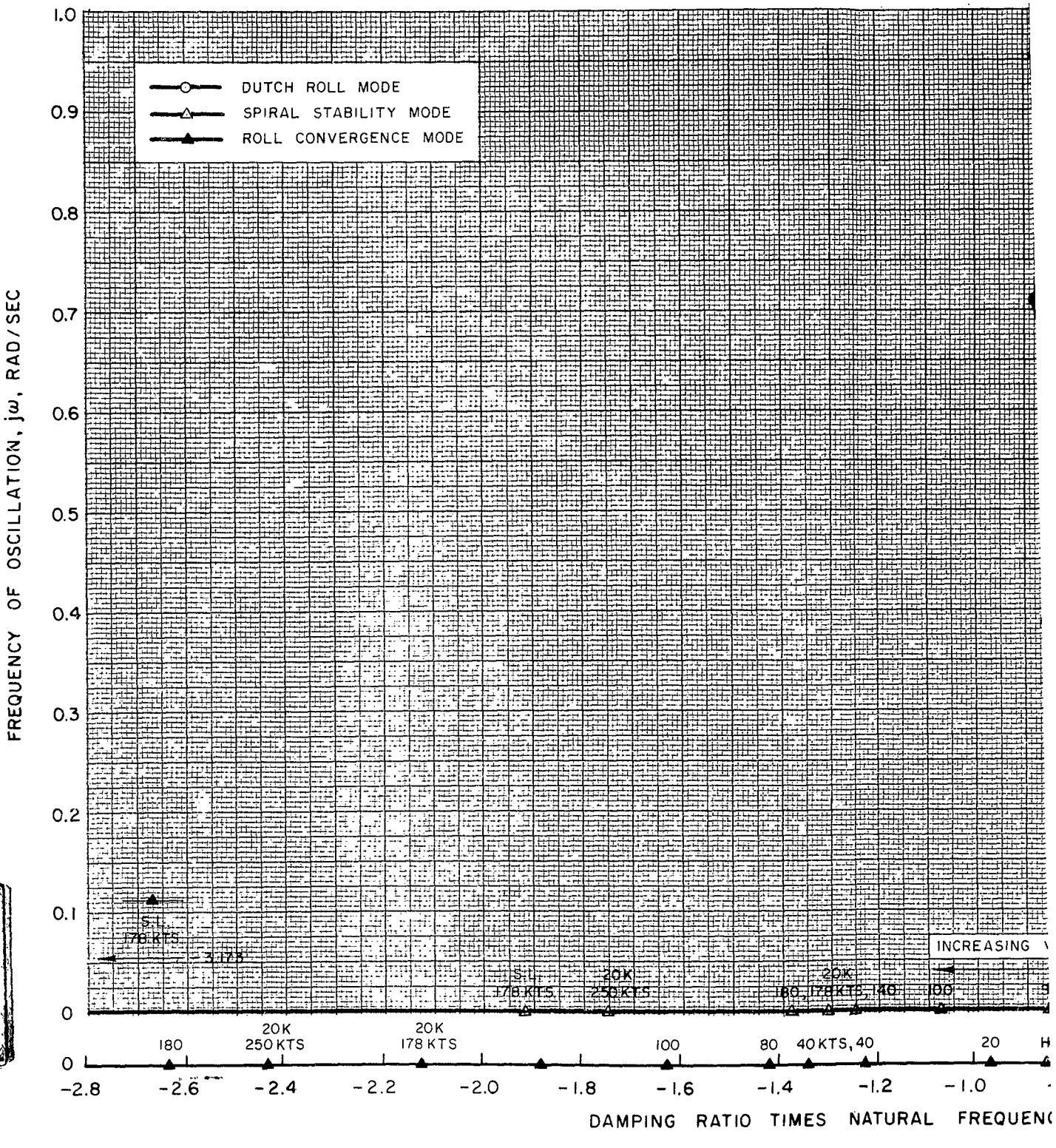

FIG. 96

TIONAL ROOT LOCATIONS FOR STEADY LEVEL FLIGHT
CRAFT WITHOUT STABILITY AUGMENTATION

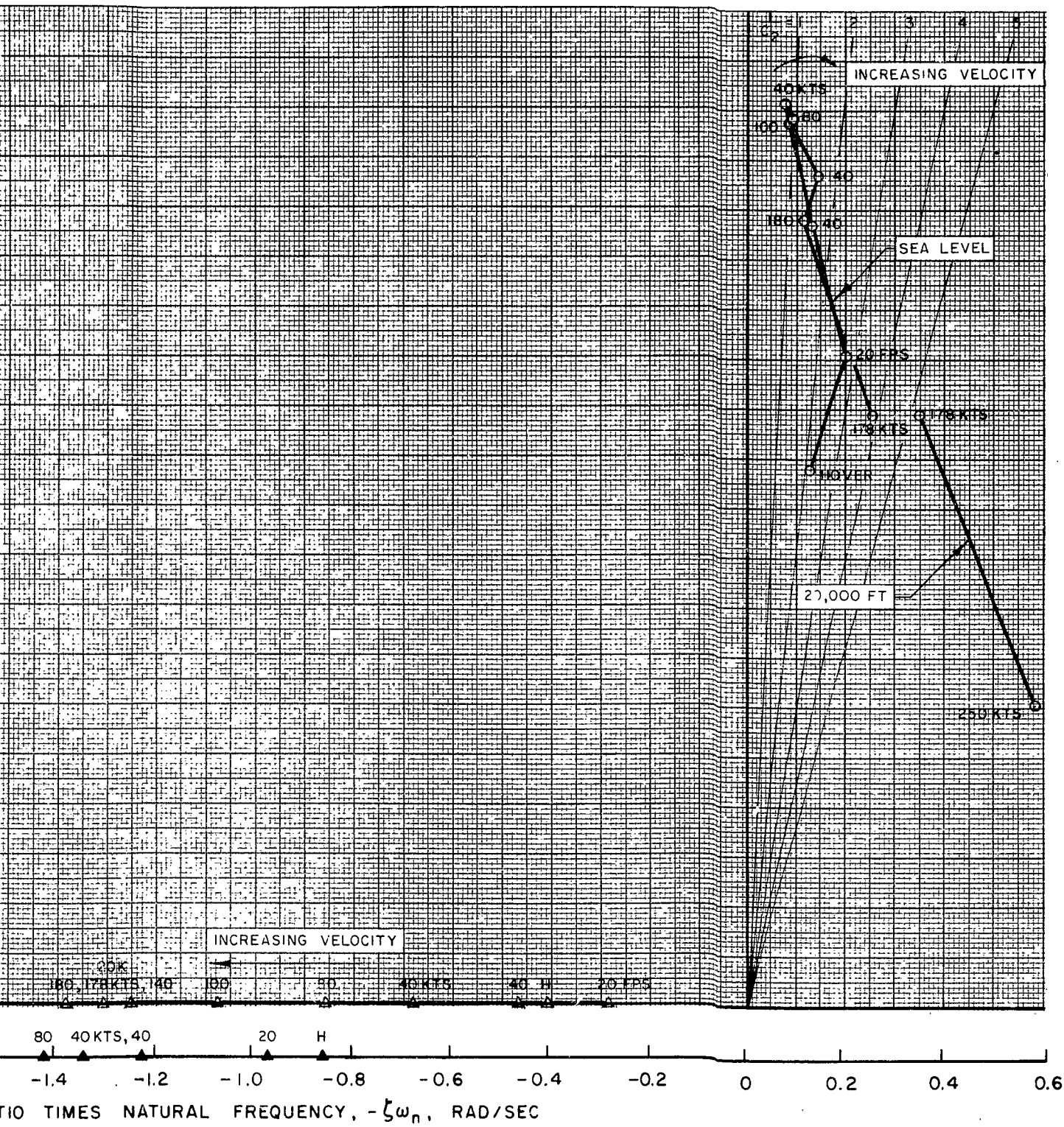

TIO TIMES NATURAL FREQUENCY, $-\zeta\omega_n$, RAD/SEC

FIG. 97

EFFECT OF ROLL RATE STABILIZATION ON LOCATION OF DUTCH ROLL ROOTS

15,000-LB AIRCRAFT